Dual role of IFT57 in cilia and nucleus in Paramecium

Lei Shi

UNIVERSITE PARIS-SUD

ÉCOLE DOCTORALE : *Gènes Génomes Cellules*
Laboratoire de Centre de Génétique Moléculaire,
CNRS, avenue de la Terrasse
91198 Gif-sur-Yvette

***DISCIPLINE** Cell Biology*

THÈSE DE DOCTORAT

soutenue le 20/09/2013

par

Lei SHI

DUAL ROLE OF IFT57 IN CILIA AND NUCLEUS IN *PARAMECIUM*

Directeur de thèse :	Jean Cohen	**DR2 CNRS**
Composition du jury :		
Président du jury :	Roland Pérasso	**professeur Paris 11 Vice-Doyen**
Rapporteurs :	Philippe Bastin,	**DR2 INSERM**
	Eric Meyer	**DR1 CNRS**
Examinateurs :	Jean Cohen	**DR2 CNRS**

Ackonwledgements

This work presented here was down at the Centre de Génétique Moléculair, CNRS under the supervision of Dr.Jean COHEN.
Foremost, I would like to express my deepest appreciation to my advisor Dr. Jean COHEN for the continuous support for my thesis throughout my studies in France. In particular, I am grateful to Madam France KOLL for her comments on the thesis and precious suggests about my project.I would also express my sincere thanks to my dear colleagus : Anne AUBUSSON-FLEURY, Michel LEMULLOIS, Martine LE GOUAR and Janine BEISSON for their kindly help for my thesis and my life.
Thanks to my friends for the wonderful time we were together in France.
Last but not least, thanks to my parents: Xianfeng SHI and Caixia Wang, my girlfriend: Yuan SHEN for their understanding and accompany that powered me going on.

CONTENTS

INTRODUCTION

The eukaryotic cell structure differs from prokaryotes by the apparition of cell compartments during evolution, including a nucleus separated from the rest of the cytoplasm by a double membrane. In the same scale of time appeared another eukaryote-specific organelle, the cilium, an extension of the cytoplasm supported by a cytoskeletal structure, the axoneme, itself anchored at the surface by a so-called basal body, structurally and functionally related to the centriole. Recent evidences showed a relationship between the evolutionary origin of nuclei and cilia in the first eukaryotes (Jekely & Arendt 2006), with similar signaling in import pathways still detectable today (Dishinger et al., 2010). When I started my thesis work on the *Paramecium* model, I wanted to look for functional links between cilia and nuclei, and I first looked at the protein kinase NM23 gene family, whose products have been detected in proteomics of cilia in several species including *Paramecium* and which are also known to be involved in carcinogenesis and to be translocated to the nucleus (Jarrett et al., 2012). However, my first functional studies of NM23 on *Paramecium* by protein depletion did not reveal any phenotype, so that I decided to rapidly move on a subject arising with IFT57, another ciliary protein having also nuclear functions in mammals (Banerjee et al., 2010) that I was using as a marker, and which displayed interesting dual localization in cilia and nuclei, within the scope of my initial project. The rest of my work presented here concerned essentially this protein. I will first introduce the cilia, their structure, their function and associated pathologies, their biogenesis with particular emphasis on the intra-flagellar transport (IFT), and then, I will present the cell model I used in my work, *Paramecium tetraurelia*.

I.1. Eukaryotic cilia and flagella

I.1.1 Structure of cilia

Eukaryotic cilia, also called flagella in certain cell types, are membrane-bound cytoskeletal structures protruding from the cell surface, with a length of the range of a few micrometers, generally around 10 µm and a diameter around 0.5 µm. They are absent organelles present in the first eukaryotes and lost in some phyla such as land plants and some fungi. Although the length, the morphology and the number of cilia per cell show high diversity between different organisms, from protozoa to mammals (Fig. I-1), the basic protein composition and ultrastructure are conserved through evolution. Cilia are organized as a microtubular cylinder-shaped backbone, the axoneme, surrounded by an extension of plasma membrane with differentiated protein and lipid composition, and elongate from a centriolar derivative, the basal body. The nine-fold symmetry of the basal body is transmitted to the axoneme, therefore composed of nine doublets of microtubules, either with a central pair of microtubules (configuration 9+2), or without this pair (configuration 9+0).

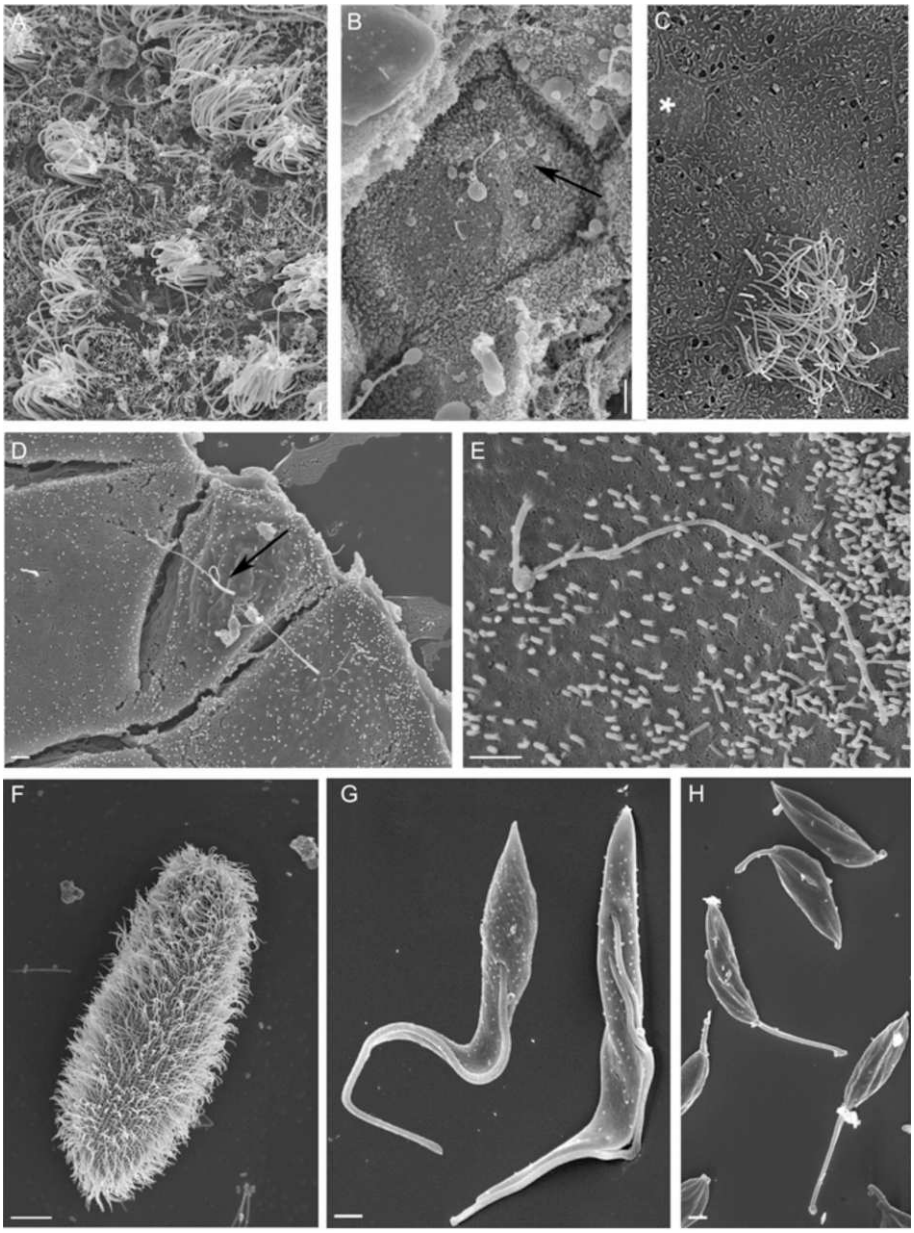

Figure I-1. Diversity of cilia number, length and disposition. *Scanning electron micrographs of the epithelium lining the ventricles of a mouse brain (4 days old) (**A**), collecting tubules from mouse kidneys visualized after mechanical cryofracture (**B**), mucociliary epithelium of Xenopus epidermis including a ciliated cell, a small secretory cell (marked by an asterisk) and several large goblet cells (**C**), cultured inner medullary collecting duct cells (IMCD) (**D**), cultured Madin Darby canine kidney cells (MDCK) (**E**), Paramecium tetraurelia (**F**), Trypanosoma brucei procyclic form (**G**) and Leishmania donovani promastigote stage (**H**). Scale bar: 1 um, except for Paramecium, 10 µm. (Vincensini et al., 2011)*

Although they all seem to display a sensory function, cilia can be classified in two types, motile and immotile cilia. Motile cilia are involved in cell locomotion and fluid movement. Generally they have a typical 9+2 configuration. Immotile cilia are restricted to sensory and signaling functions. Immotile cilia generally display the 9+0 configuration. However, the classification is simplistic and we can also find 9+0 motile cilia, like mammalian embryo nodal cilia, or 9+2 immotile cilia, like the kinocilium of auditory hair cells in mammals (McGrath et al., 2003).

Cilia are anchored at the cell surface by a basal body through an intermediate zone called transition zone, which may represent a barrier for sorting cytoplasmic components destined to reach the cilium (Fig. I-2).

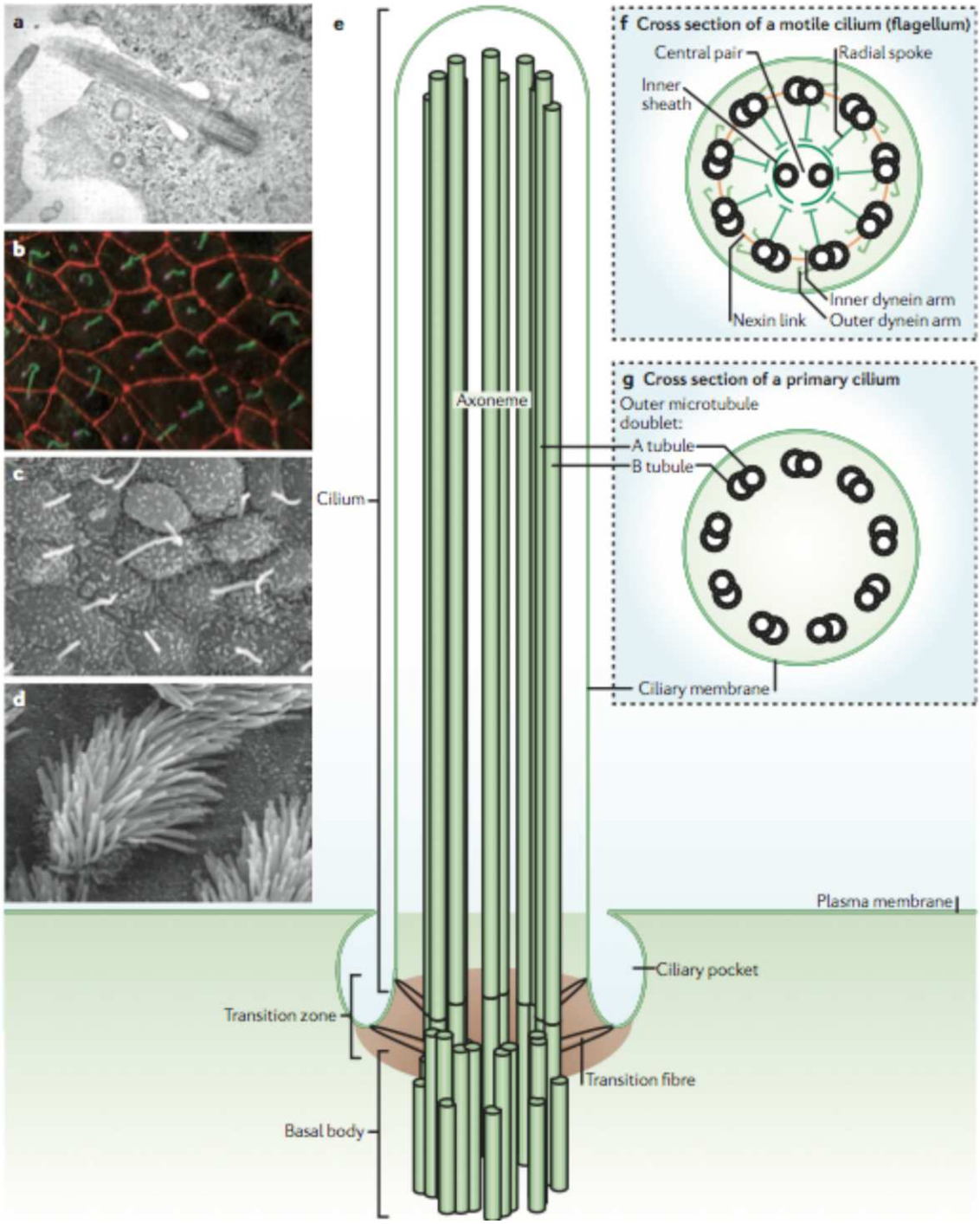

Figure I-2. The architecture of cilia. ***a*** *Transmission electron micrograph of the primary cilium of retinal pigment epithelial (RPE1) cells.* ***b*** *Immunofluorescence image of primary cilia in inner medullary collecting duct (IMCD3)cells. The primary cilium (green) is produced once per cell and extends from the basal body (magenta). Cell–cell junctions are shown in red.* ***c***,***d*** *| Scanning electron micrographs of mouse nodal cilia (****c****) and mouse tracheal motile cilia (****d****).* ***e*** *| Schematic diagram of the primary cilium.* ***f***,***g*** *Cross-section diagrams of a typical motile cilium (which is identical to a flagellum) (****f****) and a non-motile primary cilium (****g****). (Ishikawa and Marshall, 2011)*

I.1.1.1. Ciliary basal body

The basal body is a centriolar anchored at the cell surface and is responsible for nucleation of ciliary biogenesis. It is composed of nine triplets of microtubules (A, B, C). The microtubule A is complete and composed of 13 protofilaments, connected to an incomplete microtubule B composed of 10 protofilaments, itself connected to 10-protofilament incomplete microtubule C. In addition to nucleating a cilium, the basal body can have a function of microtubule-organized centre (MTOC), with γ-tubulin as a major actor in the formation of MTOC and microtubule nucleation.

I.1.1.2. Ciliary gate: Transition fibers and transition zone

Recent studies found more and more functional evidence for a 'cilia gate' like organelle between basal body and axoneme. It usually includes two parts, transition fibers (TF) and transition zone (TZ) (Reiter et al., 2012). The basal body can anchor to the plasma membrane and provides, through the TF, a docking site for intraflagellar transport (IFT) particles, which are involved in a bi-directional movement along the axoneme to control ciliogenesis (Deane et al., 2012; Williams et al., 2011). TZ terminates the distal region of basal bodies where the microtubules C end up. TZ is characterized by the presence of multiple rows of Y-shaped linkers projecting out from the outer doublets and attaching to special membrane zone called necklace (Reiter et al., 2012). The protein CEP290 is a major protein for the structure and function of TZ. It has been identified as an integral component of TZ in *Chlamydomonas*. The internal domain of CEP290 is associated with the Y-shaped linkers and mutations in CEP290 cause the absence of Y-shaped linkers, which indicates that CEP290 is required to form microtubule-membrane linkers which tether the membrane to the microtubule in TZ (Craige et al., 2010). In addition, human CEP290 mutations induce a various cilia-relate disorders including blindness and perinatal lethality (Valente et al., 2006). A thorough study in *C.elegans* showed that some MKS (Meckel-Gruber syndrome) and NPHP (nephronophthisis) proteins localized in the TZ (Williams et al., 2011), which indicates a direct relationship between proteins in TZ and ciliopathies. In *Paramecium*, Centrins 2 and 3, as well as FOR20 have also been shown to be important elements in basal body anchoring at the plasma membrane (Aubusson-Fleury et al., 2012).

TF and TZ represent a diffuse barrier situated at ciliary base to control proteins entry in or exit from the cilium compartment. Recent research proposes a relationship between the cilia gate and the nuclear pore complex (NPC) that is essential for protein entry into the nucleus (Obado & Rout, 2012) (Fig. I-3). Functional similarities have been found between ciliary gates and NPC: the small GTPase Ran was found in its RanGTP form in the cilia and in its RanGDP form in the cytoplasm as a requirement for ciliary import (Dishinger et al., 2010), as it was already known for nuclear import. Moreover, another study found that cilia localization signal sequences (CLS) resembled nuclear localization signal sequences (NLS) and could be recognized by one karyopherin-like present at ciliary gate, Importin β2 (Nachury et al., 2010). In addition, a NPC component, septin, was shown to localize at the ciliary base and participate in the regulation of the diffusion of ciliary membrane proteins in and out of cilia (Hu et al., 2010). In other work, we still can find some proteins have both ciliary and nuclear localization, like kinesin in sea urchin embryo (Morris et al., 2004), hippi/IFT57 in mammal (Houde et al., 2006; Banerjee et al., 2010), BUG22 in mammals (Ishikawa et al., 2012) in *Paramecium* (Laligné, Ph.D. thesis) and in Drosophila (Maia, Ph.D. thesis), OFD1 in mammal (Giorgio et al., 2007). These works together suggest that there should be an evolutionary functional link between ciliary and nuclear import.

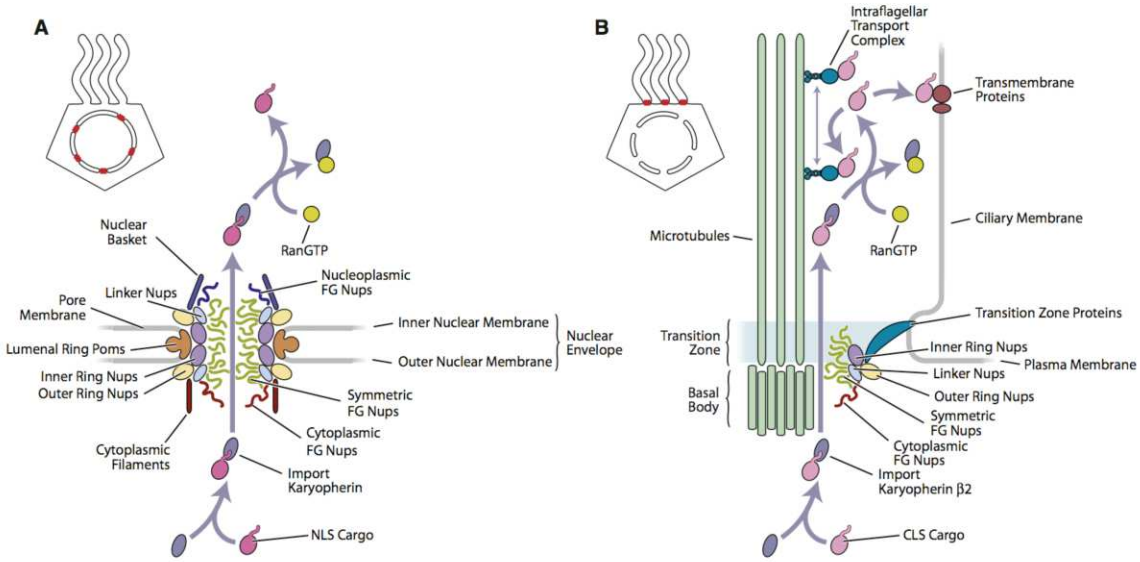

Figure I-3. Structural and Transport Features of the Nuclear and Ciliary Pore Complexes. *Highlights of the similarities between the nuclear pore complex (A) and the ciliary barrier (B) showing the hypothetical route of a cargo protein through each type of barrier. (Position of each shown in inset diagram of ciliated eukaryotic cell.) FG Nups (containing Phenylalanine-Glycine repeats) provide docking sites for transport factors called karyopherins, which bind cargo containing nuclear or ciliary localization signals (NLSs and CLSs, respectively) and facilitate nuclear and ciliary transport. So-called transition zone proteins in cilia connect the plasma membrane and the region between the microtubules and the basal body. The ciliary pore complex is thought to be located in this zone (Obado and Rout, 2012).*

In addition, ciliary proteins have been found to have a role in transcription, thus in the nuclear compartment, such as Spag16 in male germ cells (Nagarkatti-Gude et al., 2011).

I.1.1.3. The ciliary cytoskeletal backbone: the axoneme

The axoneme, with its nine outer doublets of microtubule surrounding or not a central pair of microtubules makes the structural part of the cilium. Using electronic microscopy observation, some appending structures are detected, such as outer dynein arms (ODA), inner dynein arms (IDA), radial spokes and nexin in motile cilia, all necessary for coordinated ciliary beating, while they are not found in immotile cilia. Cilia or flagella motility is based on the relative sliding of outer doublet microtubules associated with the accessory structure (Huitorel. 1988; Gadelha et al., 2007; Nicastro et al., 2006; Sui & Downing et al., 2006; Lin et al., 2012).

Besides that, at the tip of cilia or flagella, there is a carrot-shaped plug named flagella cap complex. It connects to the central pair microtubule and membrane with special filaments (Dentler. 1980). Recent work reviewed by Fisch and Dupuis-Williams (2011) indicates that the tip complex may be involved in the regulation of microtubular growth and shortening. In vitro experiments showed that the central MT cap could block MT assembly (Dentler & Rosenbaum, 1977) and a MT-plus-end-binding protein named EB1 was found to localized at the flagellar tip of *Chlamydomonas*. (Pedersen et al., 2003; Sloboda & Howard, 2007).

Ciliary proteins are substrate for various posttranslational modifications, including phosphorylation, acetylation, polyglycylation, polyglutamylation, and methylation. Among of them, acetylation, polyglycylation and polyglutamylation are specific for ciliary tubulin (Sloboda. 2009). Posttranslational modifications are not only participating in tubulin diversity but are also important for the function of motility. For example, phosphorylation was found to exist in many ciliary structures including α-tubulin, ODA, radial spokes and nexin (Sloboda, 2009), and to be important for flagellar activity (Bloodgood, 1992). Depletion of three β-tubulin polyglycylation sites in *Tetrahymena* caused the loss of central pair microtubules, which induce the motility defects (Xia et al., 2000). Tubulin polyglutamylation appears to be important in either axoneme assembly or stability (Gaertig & Wloga, 2008).

I.1.1.4. The ciliary pocket, a membrane structure associated to cilia

Ciliary pocket is a membrane structure that was found at the base of mammalian primary cilia (Molla-Herman et al., 2010) and of flagella in *Trypanosoma*. Electron microscopy studies made in *Trypanosoma* showed that the orientation and function of flagellar pocket required normal flagella elongation (Absalon et al., 2008; Field & Carrington, 2009). More recently, it has been shown that the ciliary pocket starts from the docking site of the basal body, at transition fibers, and that its membrane is almost perpendicular to the axoneme but rapidly folds and lies along the cilium to surround its proximal part (Benmerah, 2013). The ciliary pocket shows morphology diversity in different kinds of cells and it is not randomly positioned (Molla-Herman et al., 2010). Moreover, recent research about the hair follicle (a ciliary pocket-like structure) in mouse skin suggests that ciliary pockets play a role in the sensory function (Delmas al., 2011).

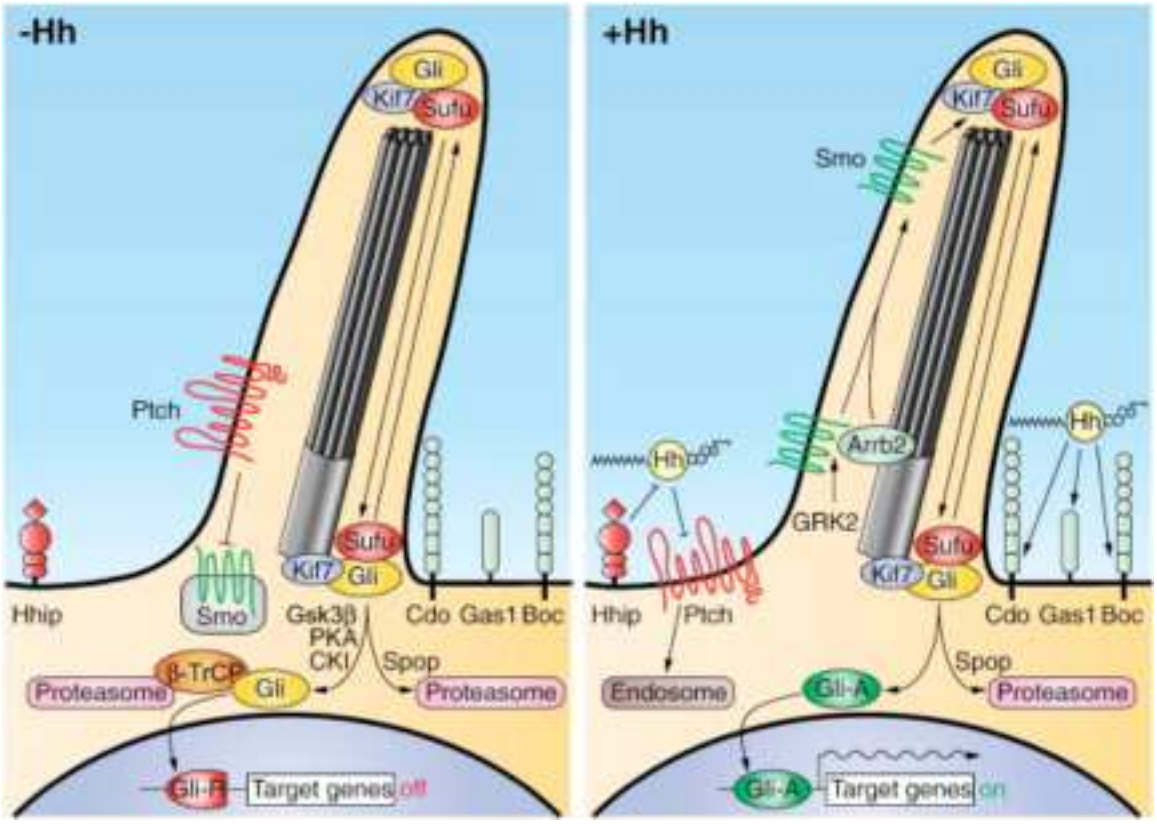

Figure I-4. A schematic model depicting the Hh signaling pathway in mammals. *In the absence of Hh ligands (left panel), the Ptch receptor at the base of the primary cilium suppresses the function of Smo by preventing its entry into the cilium. Full-length Gli proteins (Gli, yellow), mainly Gli3, are converted to a C-terminally truncated repressor form (Gli-R, red). Formation of the Gli-R is promoted by sequential phosphorylation of full-length Gli by GSK3β, PKA, and CKI, which creates binding sites for the adapter protein β-TrCP. Then, the Gli/β-TrCP complex becomes subject to ubiquitination mediated by the Cul1-based E3 ligase, which results in partial Gli degradation by the 26S proteasome and formation of the Gli-R. The Gli-R mediates transcriptional repression of Hh target genes. Whether Gli, Sufu, and Kif7 exist in a complex that traffics the cilium in the absence of Hh signaling remains to be resolved. Instead of partial Gli degradation, full-length Gli may also be completely degraded by the 26S proteasome, in this case facilitated by Spop-mediated Cul3-based E3 ligase ubiquitination. In the presence of Hh ligands (right panel), binding inhibits Ptch's function, which results in the movement of Smo from intracellular vesicles to the primary cilium. Upon binding, the Hh/Ptch complex becomes internalized in endosomes and later degraded. Smo trafficking is promoted by GRK2 phosphorylation, thereby recruiting β-arrestin (Arrb2), which interacts with the anterograde IFT motor kinesin-II and this may facilitate the movement of Smo along the cilia microtubule. Smo becomes activated and promotes the activation of full-length Gli proteins (Gli, green), mainly Gli2, which enters the nucleus and promotes transcription of target genes. The cell surface protein Hhip competes with binding of the Hh ligands and limits their range of action while the Hh-binding GPI-linked Gas1 and the Ig/Fn repeat-containing Cdo and Boc cell surface proteins positively affect the Hh signaling outcome (Teglund and Toftgard, 2010).*

I.1.2. Sensory functions of cilia

In addition to the motility function found in many cilia, governed by the ATPase activity of dynein arms, all cilia, be they motile or immotile, have a sensory function, which concerns the perception of an extracellular signal (luminous, mechanical, chemical) and the transduction of the signal into an intracellular pathway that triggers particular cell function (regulation of ciliary activity, action potential, membrane traffic, gene transcription, cell division…). The diversity of the extracellular signals and cellular responses is carried out by different sorts of differentiated cells. The primary cilia that exist in almost every kind of mammalian cell can transduce signals through the hedgehog (Hh) od Wnt signaling pathways. Specialized sensory cilia reside in certain sensory organ, which have a special structure dedicated to sensory function. The most famous examples are found in rod and cone cells of the retina (light sensing) or in the olfactory epithelium (odorant sensing) (Vincensini et al., 2011). Here, I present two examples of signal transduction performed by primary cilia, hedgehog signaling and Wnt signaling.

I.1.2.1. Hedgehog signaling.

The hedgehog signaling (Hh) pathway plays a crucial role in mammal embryo development and adult stem cell function. Defect of this signaling can cause disorders at birth and cancer development. Important Hh pathway components are enriched in primary cilia, including two key member proteins, Patched (Ptch1), a Hh receptor, and smoothened (Smo), a downstream partner of Ptch1. In the absence of Hh ligand, Ptch1 is localized at the base of the cilium and inhibits the accumulation of Smo on the ciliary membrane. PKA and Kif7 promote proteolytic processing of the transcription factor Gli3 by the proteasome into a repressor form (GliR) that suppresses Hh target gene expression in the nucleus. Besides that, Sufu stabilizes the Gli proteins and inhibits the transcriptional activity of Gli2, while PKA prohibits the accumulation of full-length Gli2 (GliFL) in the cilium. The Hh pathway is silent without the ligand. After exposure to the ligand, Ptch1 binds to it and releases Smo into the cilium. Smo accumulates in the ciliary membrane through both lateral transport and the secretory pathways. Phosphorylation of Smo abrogates the inhibiton of PKA and promotes the movement of Sufu–Gli2/3 complexes and Kif7 to the ciliary tip and perhaps the dissociation of Gli2/3 from Sufu. In this process, the accumulation of Gli2/3 at the ciliary tip is associated with the production of Gli activators (GliA) that dissociated from the full-length Gli proteins. GliA translocates to the nucleus and activates several Hh target genes including Ptch1, Gli1 and Hhip1(Nozawa et al., 2013) (Fig. I-4). In addition, the transport of these proteins requires the intraflagellar transport system in the primary cilium (Huangfu et al., 2003). When the retrograde process from tip to the base is disrupted, Smo would be accumulated at the tip of cilium. Beside that, some basal body proteins like talpid3 in chicken is also essential for Hh signaling (Davey et al., 2007).

I.1.2.2. Wnt signaling.

The Wnt signaling pathway is carried out by a protein network that transduces different signals from receptors on the cell surface through control the linking between the cytoplasm and cell's nucleus. The activity of this signaling cascade leads to the expression of target genes. The Wnt genes were both found in vertebrate and invertebrate (*Drosophila*). Wnt signaling can be divided in two-antagonism mechanism, canonical Wnt (or β-catenin dependent) and non-canonical Wnt (or β-catenin independent). Recent research on Kif3a, IFT88 (ciliary proteins) and OFD1 (basal body protein) mutant mice shows that primary cilia and basal bodies regulate the Wnt signaling pathway (Corbit et al., 2008). This study also described that Inversin (Inv) and BBS4 are implicated in both β-catenin dependent and β-

catenin independent Wnt signalling. β-catenin levels were increased in Kif3a or BBS4 mutated cells. Kif3a prevents β-catenin dependent Wnt signalling by restricting the casein kinase I (CKI)-dependent phosphorylation of Dishevelled (Dvl) in a non-ciliary mechanism and through a separate ciliary mechanism (Corbit et al., 2008). In addition, another study in zebrafish shows that a duboraya (dub) mutant clone has a ciliogenesis defect and that dub phosphorylation requires Frizzled, a noncanical Wnt signaling component, which indicates that Wnt signaling also plays a role in ciliogenesis (Oishi et al., 2006) (Fig. I-5).

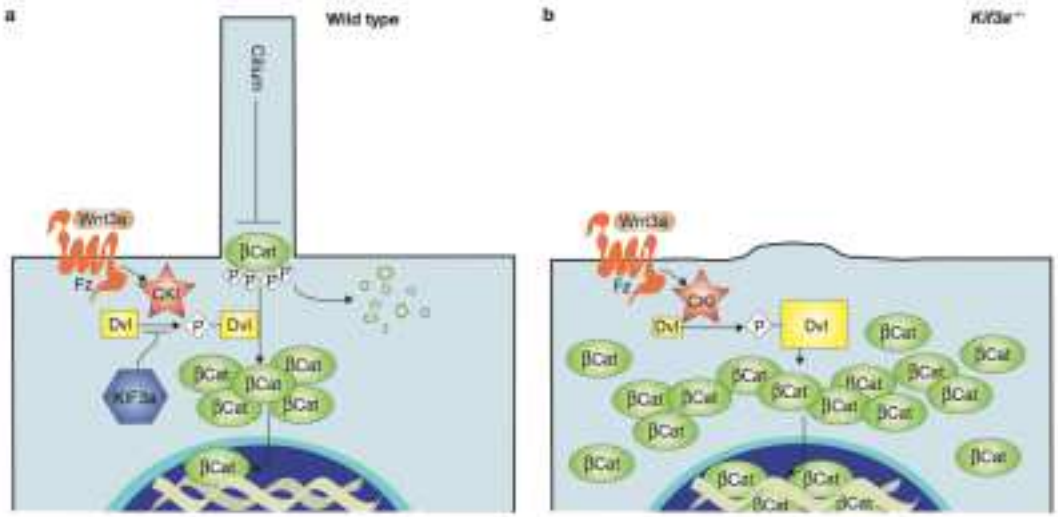

Figure I-5. Ciliated and unciliated cells respond differently to Wnt stimulation. *(**a**) Kif3a inhibits CKI phosphorylation of Dvl, providing a brake to the Wnt3a-induced stabilization of β-catenin. (**b**) In the absence of Kif3a, this brake is lost and CKI shifts Dvl to the phosphorylated form. An additional ciliary brake on Wnt signaling is also lost. Consequently, β-catenin is stabilized and, in the presence of Wnt3a, accumulates in the nucleus where it over activates the Wnt transcriptional program (Corbit et al., 2008).*

I.1.2.3. Light receptors in retina.

Vertebrate retina uses photoreceptors to detect light. This kind of cells is composed an inner and an outer segment linked by a structure derived from a primary cilium called connecting cilium. Photopigments are synthesized in the inner cell body and then transported to the distal outer segment through the connecting cilium. Defect of this cilium leads to retina degeneration and induces blindness (Boldt et al., 2011).

I.1.2.4. Olfactory sensory cilia.

Another kind of sensory cilia are found in olfactory receptor neurons. Each neuron cell has an apical dendritic knob containing several basal bodies and cilia. Depletion of some cilia-associated proteins would reduce the ciliary layer, which leads to complete or partial anosmia (McEwen et al., 2007; Kulaga et al., 2004).

I.1.3. Biogenesis of cilia.

The biogenesis of cilia is performed in two steps, first the biogenesis and anchoring at the cell surface of the basal body, second the assembly of the cilium itself (Kim & Dynlacht, 2013).

I.1.3.1. Basal body biogenesis

Basal body generally maturates from a centriole that migrates towards the surface and anchor to the plasma membrane (Azimzadeh & Marshall, 2010). Several proteins have been demonstrated to be essential for their duplication and anchoring, SAS-4, SAS-6, BLD10 for early steps of duplication, with SAS-6 being a key element in the establishment of the nine-fold symmetry (Nakazawa et al., 2007, van Breugel et al., 2011, Mizuno et al., 2012), γ-tubulin and other divergent tubulins for microtubule nucleation and elongation (Guichard et al., 2010), and centrins and FOP-like proteins for anchoring at the membrane (Aubusson-Fleury et al., 2012). As well dissected in the *Paramecium* model, basal body assembly can be divided in four successive steps: nucleation of microtubules, elongation, maturation of microtubular scaffold and docking at the cell surface (Aubusson-Fleury et al., 2012). (Fig. I-6).

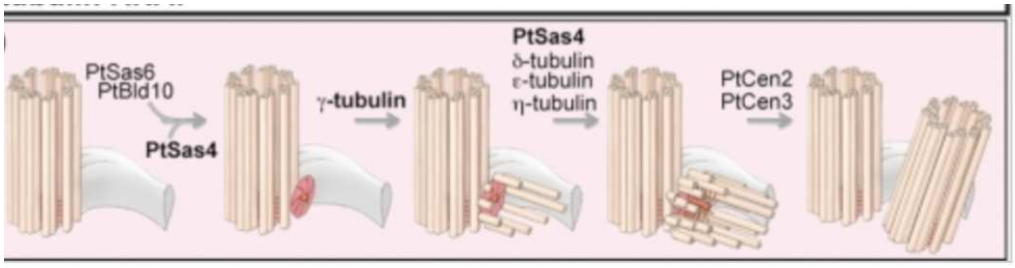

Figure I.6. Model for basal body duplication in Paramecium. *PtSas4, together with PtSas6 and PtBld10, seems to be involved in the early steps of basal body duplication for the assembly and stabilization of the germinative disk and cartwheel. γ-Tubulin allows the nucleation of the first microtubular singlets. The addition of the other microtubules seems to require PtSas4, δ-tubulin (Garreau de Loubresse et al., 2001), η-tubulin (Ruiz et al., 2000), and ε-tubulin (Dupuis-Williams et al., 2002). PtCen2 and PtCen3 act at the last step of duplication, in the tilting and positioning of the newly assembled basal body (Ruiz et al., 2005). Image from Gogendeau et al., 2011.*

I.1.3.1.1. Basal body nucleation

Recent studies of PtSas4, PtSas6 and PtBld10 in *Paramecium* revealed that they are involved in the early step of the new basal body assembly (Gogendeau et al., 2011; Jerka-Dziadosz et al., 2010). Other work in man and *Xenopus* also showed that the nucleation process requires the coordination between Plk4/Zyg-1 and Asterless/Cep152 (Hatch et al., 2010). Sas-6 was also identified as the structural source of the nine-fold symmetry of the centriolar scaffold (Avidor-Reiss & Gopalakrishnan, 2013).

I.1.3.1.2. Microtubule elongation in basal body duplication

γ-tubulin is an essential actor in microtubule nucleation involved in basal body duplication. γ-tubulin has first been shown to recruit α-tubulin and β-tubulin for microtubule nucleation through the γTuRC complex (Moritz et al., 1998; Oegema et al., 1999; Detraves et al., 1997), but this role was also found for centriole/basal body microtubule assembly. Depletion of γ-tubulin in *Paramecium* caused the loss of new basal body assembly (Ruiz et al., 1999). Study in *Tetrahymena* revealed that γ-tubulin plays an important function in the initial process of basal body duplication by nucleotide binding domain (Shang et al., 2005). However, the role of γ-tubulin in basal body nucleation concerns only the A-tubule (Guichard et al., 2010).

Other divergent members of the tubulin family, more or less conserved in other eukaryotes, were also found to be involved in basal body biogenesis.

δ-tubulin was first identified in *Chlamydomonas* as a mutation in the *UNI3* gene, which causes a defect in flagella number. The observation by electron microscopy of *Chlamydomonas* uni3 mutants and of *Paramecium* depleted for δ-tubulin showed that this protein is important for the formation and maintenance of C-tubule in triplet (Dutcher et al., 1998; Garreau de Loubresse et al., 2001).

ε-tubulin was identified in human genome using a genetic approach and it localized at mammalian centrosomes (Shang et al., 2000). Studies in mammals and in *Paramecium* showed that complete loss of ε-tubulin was lethal and caused defects in centriole or basal body duplication (Dupuis-Williams et al., 2002; Shang et al., 2003). In addition, partial depletion of ε-tubulin was also found to causes the loss of B-tubule and C-tubule in *Chlamydomonas* and *Paramecium*, which indicate that B-tubule and C-tubule are needed for the formation and maintenance of new basal body (Dupuis-Williams et al., 2002; Dutcher et al., 2002).

η-tubulin has only been found in four organisms (*Trypanosoma*, *Chlamydomonas*, *Ciona* and *Xenopus*) (Dutcher, 2003). Mutations of η-tubulin in *Paramecium* inhibit basal body duplication and causes delocalization of γ-tubulin (Ruiz et al., 2000). Another study also identified an interaction between η-tubulin and β-tubulin (Ruiz et al., 2004). These results together suggest that η-tubulin is important for binding other tubulins to the basal body that is required for correct basal body duplication.

I.1.3.1.3. Basal body anchoring

Centrin was first identified in *Chlamydomonas* and it is essential for calcium sensitive striate flagellar roots and for basal body assembly (Salisbury et al., 1984; Koblenz et al., 2003). A study of centrin homologs in mammal, *Marsilea*, *Leishmania*, *Tetrahymena* and *Paramecium* showed the conserved function of centrin in basal body or centriole formation (Middendorp et al., 2000; Salisbury et al., 2002; Klink et al., 2001; Selvapandiyan et al., 2004; Stemm-Wolf et al., 2005; Ruiz et al., 2005). Moreover, study in *Paramecium* found that centrin is responsible for basal body positioning at the surface rather than duplication (Ruiz et al., 2005), which is different from the observation in *Tetrahymena* (Stemm-Wolf et al., 2005). Another research on PtFor20 revealed that this protein is participates in the late step of basal body duplication, like PtCen2 and PtCen3, and is important for the transition zone maturation. The presence of PtCen2 is necessary to recruit PtFor20, itself necessary for PtCen3 recruitment. These proteins are needed for transition zone formation and for new basal body docking (Aubusson-Fleury et al., 2012). In mammalian cells, the centrosomal protein CEP164 was found to mediate the vesicular docking to the mother centriole during early steps of ciliogenesis, which is important for the initial establishment of ciliary membrane at distal end of centriole (Schmidt et al., 2012). Similar conclusions on a role in basal body anchoring

could be obtained by analysis of mutants for other genes such as talpid (Stephen et al., 2013) and OFD1 (Thauvin-Robinet et al., 2013).

I.1.3.2. Assembly of the cilium

Generally, the cilium is nucleated at the basal body and built from proteins synthesized in the cytoplasm that transit through the transition zone and are delivered to the distal part of the growing cilium by a so-called intraflagellar transport (IFT). This transport machinery was first observed in green alga *Chlamydomonas*, with two motile flagella, using differential interference contrast microscopy (Kozminski et al., 1993; Kozminski et al., 1995). The IFT ultrastructure was refined at the electronic microscopy level by identifying train-like particles moving along the axoneme microtubule in cilium (Pigino et al., 2013). Then, IFT was also identified in other organisms such as *Caenorhabditis elegans* (Cole et al., 1998), sea urchin (Morris, 2004), zebra fish (Tsujikawa M, et al., 2004) and mammals (Pazour et al., 2000), proving that the system is evolutionarily conserved in eukaryotes. Since then, the intraflagellar transport mechanism has been dissected at the molecular level. The IFT particle, carrying cargos along the axoneme, can be grouped in two sub-complexes with different motors during ciliogenesis, IFTA and IFTB. The IFTB sub-complex contains sixteen proteins connected to a kinesin-II motor responsible for the anterograde transport in ciliary building. The IFTA sub-complex contains six proteins connected to a dynein motor responsible for the retrograde transport form the ciliary tip to the base of the cilia during recycling processes (Table I-1; Fig. I-7).

IFT polypeptide	Chlamydomonas	C. elegans	H. sapiens
Kinesin-2			
Heterotrimeric	FLA10	KRP85/ KLP-20	KIF3A
	FLA8	KRP95/ KLP-11	KIF3B
	FLA3	KAP/KAP-1	KAP
Homodimeric	?	OSM-3	KIF17
Cytoplasmic dynein 2			
	DHC1b	CHE-3	DYNC2H1/ DHC2
	D1bLIC	D2LIC/ XBX-1	DYNC2LI1/ D2LIC
	FAP133	?	WD34
	LC8/FLA14	?	?
Complex A			
IFT144	FAP66	DYF-2	WDR19
IFT140	IFT140	CHE-11	IFT140
IFT139	FAP60	ZK328.7	THM-1
IFT122A	XP_001700201.1	DAF-10	IFT122/ WDR10
IFT122B	IFT122B	IFTA-1	WDR35
IFT43	FAP118	?	?
Complex B			
IFT172	IFT172	OSM-1	IFT172
IFT88	IFT88	OSM-5	IFT88/Polaris
IFT81	IFT81	F32A6.2	IFT81
IFT80	IFT80	CHE-2	IFT80
IFT74/72	IFT74/72	C18H9.8	IFT74/72
IFT57	IFT57	CHE-13	IFT57/Hippi
IFT52	IFT52	OSM-6	IFT52/NGD5
IFT46	IFT46	DYF-6	C11orf60
IFT27	IFT27	?	RABL4
IFT20	IFT20	Y110A7A.20	IFT20
New putative IFT proteins			
	FAP259	DYF-1	TPR30A
	FAP22	DYF-3	CLUAP1
	XM_001698717.1	DYF-13	TTC26
	FAP116	DYF-11	MIP-T3

Table I-1. Main components of IFT conserved in Chlamydomonas, C .elegans and human. *The table presents the IFT proteins known in different organisms with specific names, as well as the motor proteins. The complex A corresponds to the retrograde transport IFT driven by cytoplasmic dynein and the complex B to the anterograde IFT driven by kinesin II (Pedersen & Rosenbaum, 2008).*

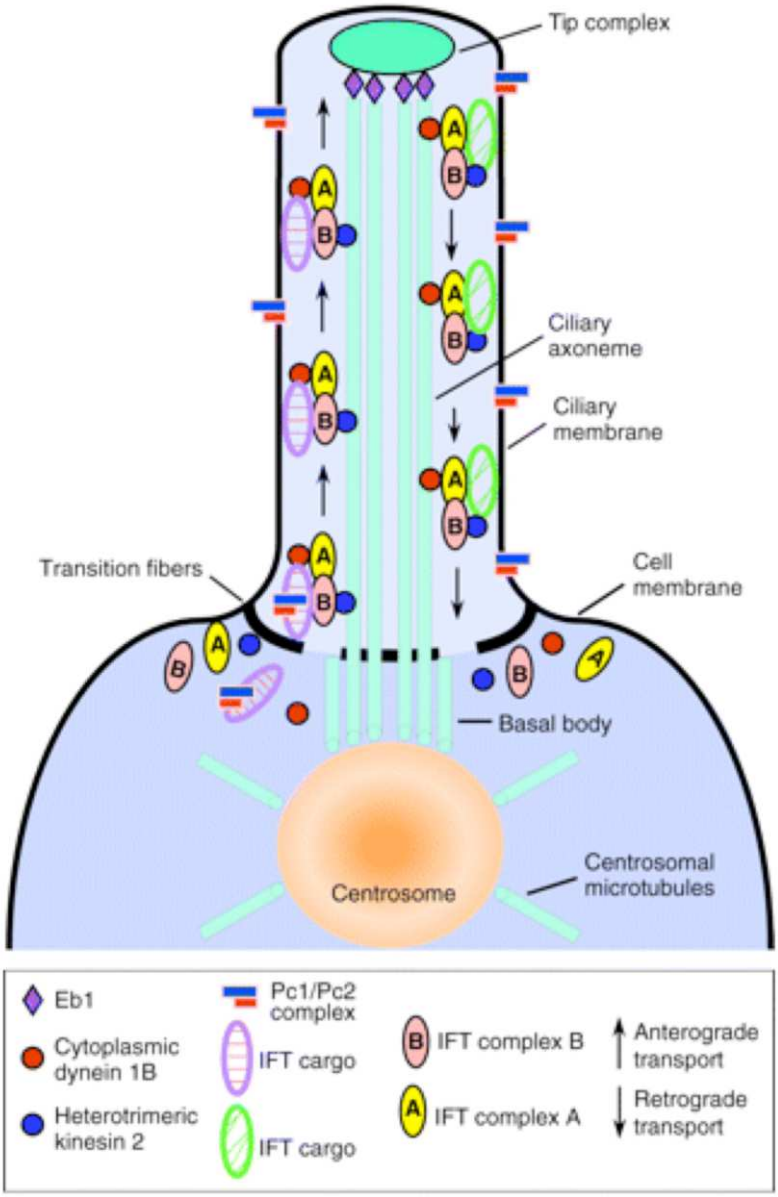

Figure I-7. Intraflagellar Transport (IFT) in cilium. *Ciliary assembly and maintenance is accomplished by intraflagellar transport (IFT), which relies on the microtubule motor proteins kinesin 2 and cytoplasmic dynein to transport IFT protein complexes and their associated cargo up and down the length of the cilium (depicted in A). Abbreviations: Eb1, end- binding protein 1; Pc1 and Pc2, polycystin 1 and polycystin 2. (Bisgrove & Yost, 2006)*

I will first give details about the motors that drive IFT particle motion, then about the IFT itself, the components of the IFTB and IFTA sub-complexes, and I will finish this part by showing some evidences about diversification of roles of IFT proteins in processes other than ciliary biogenesis.

I.1.3.2.1. Motors.

I.1.3.2.1.1.Kinesin-II.

The kinesin-II complexes, first discovered in sea urchin embryo (Morris et al., 1997), were found to exist in two forms and to play functions in anterograde transport of IFT particles along the axoneme: the first one is the heterotrimeric kinesin-II (also known as FLA-10-

kinesin-II or KIF3A/KIF3B/KAP), which was found in most studied models from *Chlamydomonas* to mammals (Cole et al., 1998) and the second one the homodimeric kinesin-II (also named Osm-3-kinesin-II or KIF17) found in the sensory cilium of *Caenorhabditis elegans* (Khan et al., 2000; Snow et al., 2004; Pan et al., 2006).
The heterotrimeric kinesin is composed of two distinct subunits named KIF3A and KIF3B, containing a 35-nm long coiled-coiled tail linking the kinase head to an accessory third partner named KAP (Khan et al., 2000). First evidence about the function of heterotrimeric kinesin-II in IFT came from temperature-sensitive mutant of FLA-10 in *Chlamydomonas*. The FLA-10 gene encodes one of the subunits of kinesin-II. Under restrictive temperature, fla-10 mutant cannot form the flagella and IFT particles are no longer transport along the axoneme. In addition, when fla-10 mutants, which have full grown flagella at permissive temperature, were shifted to restrictive condition, the flagella would be lost by graduate shortening, which indicate that kinesin-II is essential not only for ciliogenesis but also for ciliary maintenance (Walther et al., 1994; Kozminski et al., 1995). Similar results based on mutant clone or RNAi experiments were found in other organisms, suggesting that the function of kinesin-II in IFT machinery is conserved (Cole et al., 1998; Krock et al., 2008; Sarpal et al., 2003; Yang et al., 2001a; Yang et al., 2001b).
The homodimeric kinesin-II contains two N-terminal domains linked to each other by a 26-nm long coiled-coiled rod. Using GFP fusion in *Caenorhabditis elegans* sensory cilium, the moving speed of IFT particle along the axoneme could be detected. In wild-type animals, IFT particles in the middle segment of the amphid channel cilia are driven by both OSM-3-kinesin-II and heterotrimeric kinesin-II at the velocity of 0.7 µm/s. After the IFT particles have reached the portion of the cilium where outer doublets stop and leave outer singlets of microtubules, the IFT is driven by the sole OSM-3-kinesin-II at the velocity of 1.2 µm/s. In a dyf-5 mutant, in which OSM-3-kinesin-II and heterotrimeric kinesin-II are no longer associated, IFT particles, driven by heterotrimeric kinesin-II alone in the middle segment, are moving at the velocity of 0.5 µm/s, and then driven by OSM-3-kinesin-II alone at the velocity of 0.6 µm/s, significantly lower than the normal 1.2 µm/s (Brust-Mascher et al., 2013).

I.1.3.2.1.2. Cytoplasmic dynein.

The motor for retrograde IFT movement is a dynein, which was first discovered in sea urchin embryos as one kind of cytoplasmic dynein (Gibbons et al., 1994). This dynein is composed of heavy chains (Porter et al., 1999), intermediate chains (Rompolas et al., 2007), light intermediate chains (Hou et al., 2004) and light chain (Pazour et al., 1998). Evidences about the role of dynein in IFT comes from mutations in genes encoding dynein heavy chains, CHE-3 in *Caenorhabditis elegans* or DHC-1b in *Chlamydomonas* (Signor et al., 2007; Wicks et al., 2000; Porter et al., 1999), light chain, LC8 in *Chlamydomonas* (Pazour et al., 1998) and light intermediate chains, D2LIC in *Chlamydomonas* (Perrone et al., 2003). These mutants, with normal anterograde IFT transport, often display short flagella or sensory cilium and their IFT particles accumulate at tip, an indication that the pathway of retrograde transport is blocked (Wicks et al., 2000; Porter et al., 1999; Yang et al., 2009; Perrone et al., 2003). However, another research on the IFT motors show that dynein-2 (IFT retrograde motor) regulates cilia length but is not necessary for cilia assembly (Rajagopalan et al., 2009).

I.1.3.2.2. IFT particles

By comparison of protein composition of the flagella of the fla-10 mutant of *Chlamydomonas* at restrictive temperature and permissive temperatures, most IFT particle proteins could be purified and identified. Firstly a 17S complex containing at least thirteen peptides was discovered. Soon after, another study using two-dimensional gel electrophoresis showed that a complex containing fifteen subunits dissociated in two sub-complexes. Functional studies

revealed that these two sub-complexes play different roles during IFT and were named IFTA and IFTB respectively. IFTB mutants often lead to the phenotype of loss or significant size reduction of cilia, whereas IFTA mutants mostly form cilia with a bulge contain IFT particle accumulation at the tip. Generally, IFT proteins are named by their molecular weight displayed in SDS-PAGE. Now, six IFTA proteins (IFT139, IFT144, IFT121, IFT122, IFT140 and IFT43) and thirteen IFTB proteins (IFT172, IFT88, IFT81, IFT80, IFT72/74, IFT55/57, IFT46, IFT20, IFT27, IFT52, IFT70/Dyf-1, IFT25, IFT54/Elipsa/Dyf-11, IFT22/IFTA-2/RabL5) are known. The homologs of *Chlamydomonas* IFT genes were successively identified in other organisms and they show similar functions, which indicate the highly conservation of IFT system in different species.

In association with the IFT machinery, a cytoplasmic complex of proteins associated with the ciliary membrane called BBSome has been found to regulate IFT transport in the cilium. In *C. elegans*, BBS-7 and BBS-8 are required for the ciliary localization and motility of IFT proteins such as OSM-5 (IFT88) and CHE-11 (IFT144). The depletion of BBS7 or BBS8 breaks down the IFT complex, which indicates that BBS proteins are essential for the assembly and function of IFT particles (Blacque et al., 2004). Further research revealed that BBSome associates with the small GTPase Rab8 at the ciliary base and then enters the cilium to promote ciliary membrane biogenesis in mammals (Nachury et al., 2007). Another study showed that the BBSome subunit BBIP10 regulates microtubule stability through its function in tubulin acetylation (Loktev et al., 2008). In addition, a more recent work illustrated the roles of BBSome in controlling the ITF assembly and turnaround. Mutations of BBS-1 and DYF-2 (IFT144) cause a defect of the retrograde transport while the anterograde transport is normal (Wei et al., 2012).

I.1.3.2.3. IFTB components

According to the resistance to dissociation in 300 mM NaCl concentration, IFTB can be divided into a “core” ITFB containing the IFT88, IFT81, IFT80, IFT72/74, IFT46, IFT52 and IFT70 proteins and a “peripheral” IFTB containing the IFT20, IFT54, IFT57 and IFT172 proteins (Pederson and Rosenbaum, 2008).

I.1.3.2.3.1. Core IFTB proteins.

The core complex of IFTB is itself composed of different subcomplexes (Fig. I-18).

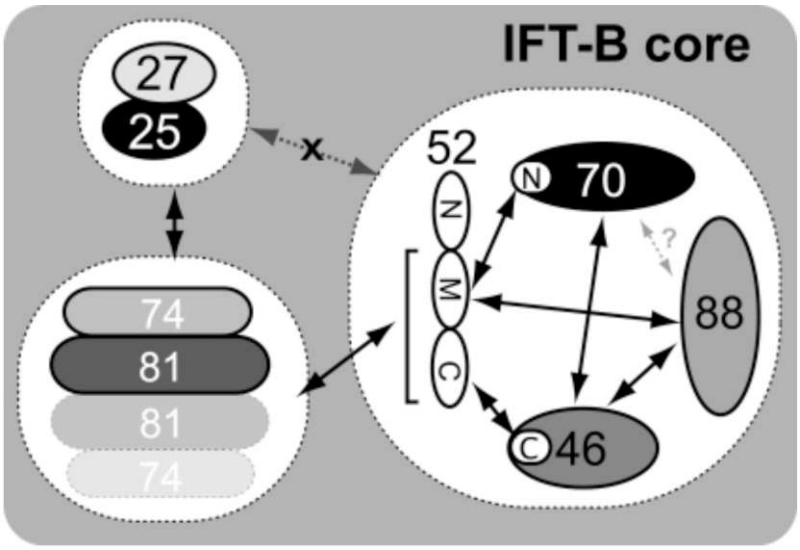

Figure I-8. Interaction map of the IFT-B core complex. *IFT27/25 form a stable heterodimer that interacts directly with another subcomplex containing IFT81/74. IFT88/70/52/46 form a stable heterotetramer in which the central part of IFT52 (IFT52(281–381), IFT52*M*) binds to both IFT70 and IFT88, and the C-terminal part of IFT52 (IFT52(382–454), IFT52*C*) binds to IFT46. IFT52 also binds to the IFT81/74/27/25 tetramer thus providing a physical link between the IFT88/70/52/46 and IFT81/74/27/25 sub-complexes. Because the N-terminal 281 residues of IFT52 do not bind IFT81/74/27/25, the C-terminal half (*M *plus* C*) of IFT52 is shown to bind IFT81/74 in the figure. Other known but still unmapped interactions within the IFT88/70/52/46 tetramer are shown with* black arrows*, and a potential interaction between IFT88 and IFT70 is shown with a* gray*,* dashed arrow*. No direct interaction was observed between the IFT88/70/52/46 and IFT27/25 sub-complexes. (Taschner et al., 2011).*

IFT88

The homolog of IFT88 in mouse, Tg737 was first identified as a gene responsible for Polycystic Kidney Diseases: mutant mice have severe kidney defects and die within a few weeks after birth (Schrick et al., 1995). Later research in *Chlamydomonas* and mouse showed that IFT88 is required for assembly of cilia and flagella. Flagella were absent in mutant *Chlamydomonas* and mice mutants have short primary cilium in the kidney (Pazour et al., 2000). Other studies also revealed that IFT88 is essential for vertebrate photoreceptor assembly and maintenance (Pazour et al., 2002). Studies in human HeLa cells showed that IFT88 is a centrosome protein and that it regulates the cell cycle G1-S transition in non-ciliated cells (Robert et al., 2007). In addition, IFT88 has been identified as a regulator of Hedgehog signaling in primary cilium of chondrocytes (Huangfu et al., 2003).

IFT70

IFT70 was first identified in *C. elegans* as named DYF-1. It is an essential activator of the anterograde motor OSM-3 (Ou et al., 2005; Starich et al., 1995). The zebra fish fleer/IFT170 mutant showed the importance of this protein for tubulin polyglutamylation and polyglycylation (Pathak et al., 2007). A work in *Tetrahymena* showed that IFT70 is required for either assembly or stability of the entire axoneme (Dave et al., 2009). Recent study in *Chlamydomonas* revealed that IFT70 is a core component of IFTB and that it interacts directly with IFT46, another IFTB protein (Fan et al., 2010).

IFT46

IFT46 was first identified in *C. elegans* as DYF-6, then in *Chlamydomonas* (Bell et al., 2006; Hou et al., 2007). A study in *Chlamydomonas* showed that IFT46 is essential for the transport of the outer dynein arms into flagella, based on the fact that the mutant flagella lack the axonemal outer dynein arms and can not beat (Hou et al., 2007). Later, it was shown that the outer dynein arm adaptor ODA16 directly links to IFT46 (Ahmed et al., 2008). Moreover, using western blots immunological assays, it was found that the levels of some other IFTB proteins (including IFT52, IFT70 and IFT88) are significant reduced in IFT46 mutant compared to wide type. This indicates that IFT46 is important for the stability of the IFTB sub-complex and these researches also provide evidence of the direct interaction between IFT46, IFT52, IFT70 and IFT88 in IFTB core complex (Fan et al., 2010; Lucker et al., 2010; Taschner et al., 2011).

IFT74 and IFT81

A study in *Chlamydomonas* shows that IFT72/IFT74 (two proteins encoded by a single gene that differ by post-translational modifications) and IFT81 share a similar structural organization with a predicted coil-coil domain. Yeast-based two-hybrid experiments suggest that IFT72/IFT74 and IFT81 directly interact with each other to form a tetrameric complex (Lucker et al., 2005). Another study in *C. elegans* confirmed the conservation of this interaction. A more recent study using protein purification and a proteolysis method confirmed that two stable sub-complexes, respectively composed of IFT81/74/25/27 and IFT88/70/52/46, are present in IFTB (Taschner et al., 2011).

IFT52

As part of sub-complex IFT88/70/52/46, IFT52 was identified to play key roles in the assembly of cilia in *C. elegans* (OSM-6), *Chlamydomonas*, *Trypanosoma*, and mammals (NGD5) (Collet et al., 1998; Brazelton et al., 2001; Absalon et al., 2008, Wick et al., 1995). Furthermore, a research in *Chlamydomonas* showed that IFT52 localized at basal body transitional fibers and that it serves as the docking site for IFT particles (Deane et al., 2001). In addition, mouse Ngd5 mutants show abnormal Hedgehog signaling and defects in embryogenesis, which indicates the important function of IFT in signaling pathways of vertebrates (Liu et al., 2005).

IFT25 and IFT27

IFT25 and IFT27 constitute another interacting pair in the IFTB core complex, discovered in *Chlamydomonas* (Wang et al, 2009). IFT25 was not found in early study, but identified later in green alga and mouse by *in silico* database analysis (Lechtreck et al., 2009; Follit et al., 2009). A study in *Chlamydomonas* revealed that IFT25 is a phosphoprotein localized in cilia, transition zone and basal body, that overlap with IFT27 (Wang et al., 2009). IFT27 is a Rab-like small GTPase involved in membrane traffic regulation. The complete depletion of IFT27 in *Chlamydomonas* reduces the level of both IFTA and IFTB proteins, leading to cell death. Furthermore, this study also showed that partial knockdown of IFT27 resulted in defects in cytokinesis and in the elongation of the cell cycle. This indicates that IFT27 may play more functions in the cell-cycle control (Qin et al., 2007).

IFT22

IFT22 is also a core IFTB protein that was not found in initial studies but was identified later in *C. elegans* as IFTA-2 and in *Trypanosoma* as RABL5 (Schafer et al., 2006; Adhiambo et al., 2009). Interestingly, the depletion of RABL5 in *Trypanosoma* induces a phenotype of short cilia with accumulation of IFT particle at tip that usually correspond to an IFTA defect, which indicates that IFT22 may participate to retrograde transport (Adhiambo et al., 2009). A

subsequent study in *Chlamydomonas* showed that the depletion of IFT22 causes a smaller pool of both complexes A and B leading to an increased amount of IFT particles in flagella. An over-expression of IFT22 leads to the accumulation of IFT particles in flagella. Both results indicate that IFT22 regulates the cellular levels of the complexes A and B, thus that it plays an important role in determining the cellular availability of IFT particles (Silva et al., 2012).

I.1.3.2.3.Peripheral IFTB proteins

Peripheral IFTB proteins act as linkers between the kinesin motor and the core of IFTB (Fig. I-9).

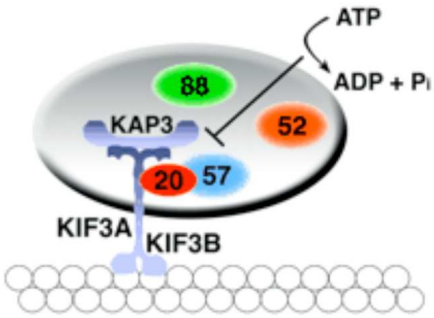

Figure I-9. Schematic view of the main IFTB peripheral proteins interacting with the molecular motor Kinesin-II. *White balls schematizes a microtubule along which the kinesin motors walk, in direct connection with the peripheral IFT proteins IFT20 and IFT57.*

IFT172

IFT172 is the largest IFT protein, which contains several putative domains, with predicted N-terminal WD-40 repeats and C-terminal α-helical TPR motifs. IFT172 is encoded by *FLA-11* in *Chlamydomonas* and a study of the fla-11 mutant showed that IFT172 is required for the localization of the microtubule end-binding protein1 (CrEB1) to the flagellar tips (Pedersen et al., 2005). Another study showed that the fla-11 mutant produces a defect in IFT particles turnaround at flagellar tips (Iomini et al., 2001). In addition, a recent study revealed that IFT172 is required for the flagellar entry of the IFT-dynein complex that drives the retrograde transport (Williamson et al., 2012). A study in *Tetrahymena* also showed that partial truncation of the IFT172 RPD domain caused the accumulation of other IFT protein at the tip of cilia (Tsao et al., 2008b). These results together suggest that IFT172 mediates IFT complex disassembly/reassembly at cilia/flagella tips. In zebra fish, IFT172 is essential for the assembly of photoreceptor outer segment (Sukumaran et al., 2009). In mouse, IFT172 is needed for the primary cilium formation and normal Hedgehog signaling (Huangfu et al., 2003).

IFT80

Pioneer study of the WD40 repeats-containing IFT80/CHE-2 protein in *C. elegans* showed that it is required for the assembly of sensory cilium in neuron (Fujiwara et al., 1999). Depletion of IFT80 in *Tetrahymena* produced shortened or absent cilia. In zebra fish, knock down of IFT80 resulted in cystic kidney and abnormal Hedgehog signaling. Moreover, this study also showed that IFT80 mutations underlie a subset of Jeune asphyxiating thoracic dystrophy (JATD) cases, which indicated that IFT80 play roles in the pathways of some human disease (Beales et al., 2007).

IFT54

IFT54, named DYF-11 in *C. elegans*, is an orthologue of the mammalian MIP-T3 protein that contains a microtubule α- and β-tubulin-binding domain at its N-terminal region and a coiled-coiled polypeptide at its C-terminal region, involved in binding to IFT20 (Kunitomo et al., 2008; Omori et al., 2008). IFT54 is essential for sensory cilium formation in *C. elegans*. Study on Elipsa (IFT54 homolog in zebra fish) showed that this protein localized to cilia and interacted with Rabaptin5, a regulator of endocytosis through the binding to the small GTPase Rab8. Knock out of Elipsa causes cilia and kidney defect (Omori et al., 2008). This research suggests that IFT54 play a function of linking IFT particle to ciliary membrane proteins.

IFT20

IFT20 is the smallest IFT protein. A study in mouse revealed that IFT20 is associated with the Golgi complex, besides its localization in the cilium and the basal body, and is required for cilium formation (Follit et al., 2006). A subsequent study confirmed that the Golgi protein GMAP210/TRIP11 recruits IFT20 to the Golgi complex in mammals (Follit et al., 2008). Another research of mammal photoreceptor outer segments (a modified sensory cilium) showed that IFT20 links the anterograde motor kinesin II to the IFTB complex (Baker et al., 2003) (Fig. I-10). In mouse retina, IFT20 is required for opsin trafficking and photoreceptor outer segment development (Keady et al., 2011). These works together indicate that IFT20 play an important role in the IFT trafficking from cytoplasm to the cilium. IFT20, together with IFT57 and IFT88, was also found at a regulator of immune synapse assembly in T-lymphocytes (Finetti et al., 2009).

IFT57

IFT57, also found as a 55kDa IFT55 protein because of post-translational modifications, is another peripheral IFTB protein first discovered in *C. elegans* as CHE-13, linking the IFT to the kinesin motor. It was found to be essential for cilia formation in cooperation with other IFT proteins (Haycraft et al., 2003; Houde et al., 2006; Krock et al., 2008; Sukumaran et al., 2009) (Fig. I-10). Mutation in IFT57 in zebra fish cause morphological defects of photoreceptor outer segment. (Krock et al., 2008; Sukumaran et al., 2009). In mouse, IFT57 also called HIPPI is essential for node cilia assembly and Sonic hedgehog signaling. Mutant mice show left–right asymmetry developmental defects, failure in establishing normal nervous system and embryonic lethality (Houde et al., 2006).

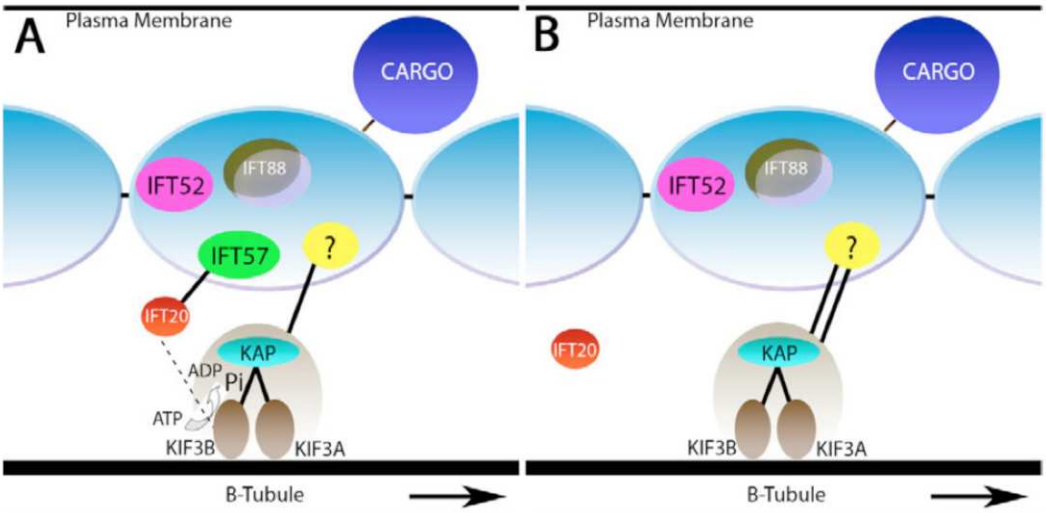

Figure I-10. IFT57 and IFT20 mediate the ATP-dependent dissociation of kinesin. *(A) A model describing the nature of protein interactions within the IFT complex. IFT57 tethers IFT20 to the IFT particle, while kinesin binds to the IFT particle through an unknown entity. IFT20 physically interacts with KIF3B and mediates the ATP-dependent dissociation of kinesin. (B) In the absence of IFT57, IFT20 can no longer associate with the IFT particle. However, the interaction of kinesin with the IFT particle is stabilized by loss of IFT57 and IFT20 from the IFT particle. (Krock et al., 2008)*

Interestingly, another function of IFT57/HIPPI resides in the nucleus through its interaction with proteins involved in the human Huntington's disease, a neurodegenerative genetic disorder that affects muscle coordination and leads to cognitive defects and psychiatric problems. Hippi acts as a partner of HIP-1 (Huntington protein interacting protein 1) binding to it through a C-terminal pDED domain in the cytoplasm, allowing the HIP-1-HIPPI heterodimer to enter the nucleus and to interact with the putative promoters of caspase-1, caspase-8 and caspase-10. This increases their expressions and induces apoptosis, which is important in the pathogenesis of Huntington's disease (Gervais et al., 2002; Majumder et al., 2007a; Majumder et al., 2007b). Some research provides direct evidence for the interaction between HIPPI and capase-1 and the amino acid R393 of HIPPI was found to be important for this interaction (Banerjee et al., 2010). An increased release of cytochrome C and of the apoptosis inducing factor (AIF) from mitochondria and nuclear fragmentation were also observed in GFP-Hippi expressing HeLa and Neuro2A cells. The same research also showed that the overexpression of HIPPI induces an activation of caspase-3 and caspase-9/6, later than the activation of caspase-1 and caspase-8 (Majumder et al., 2006). In addition, a recent study using microarray data obtained from the brains of HD patients showed that HIPPI binds sites of some transcription factors like CREB, P300, SREBP1, SP1 and significantly over-expresses genes altered in Huntington's disease patients, which suggests that HIPPI is an important transcriptional regulator in Huntington's disease (Datta et al., 2011a; Datta et al., 2011b) (Fig. I-11).

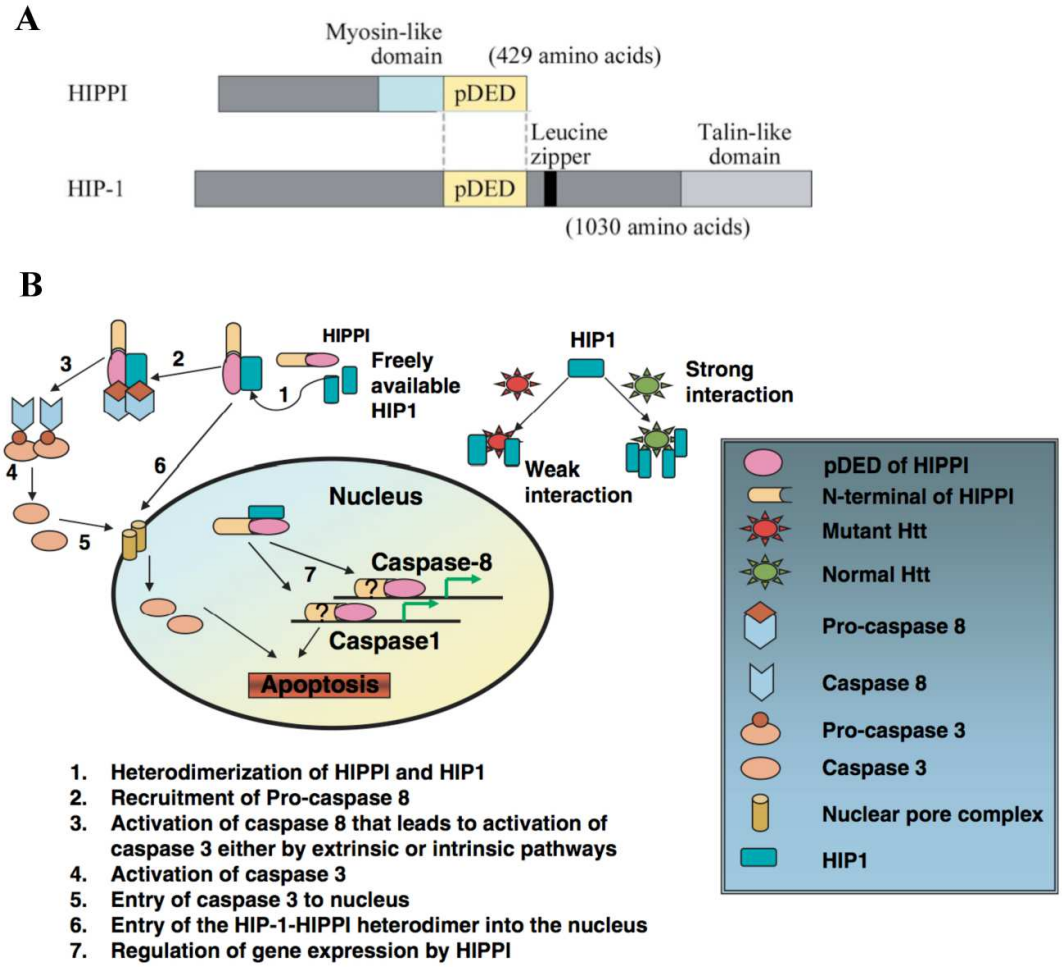

Figure I-11. Possible mechanisms of regulation of transcription and apoptosis by HIPPI and HIP-1 in Huntington's disease*. A. Schematic diagram showing the organization of HIPPI and HIP-1. The pDED domain in HIPPI and HIP-1 is shown in yellow and labelled, while the other domains are in different colours (Manisha et al., 2006). B.Interaction of HIP-1 with the wild-type Htt allele is stronger than that of the mutated Htt. In Huntington's disease, one of the alleles of Htt is mutated and thus likely to release free HIP-1. Free HIP-1 then interacts with HIPPI through its C-terminal pDED domain and recruits caspase-8, and activates caspase-8 and its downstream effector proteins, resulting in apoptosis. On the other hand, HIPPI–HIP-1 heterodimer may translocate to the nucleus, interact with the putative promoters of caspase-1, caspase-8 and caspase-10, and increase their expressions. In turn, increased pro-caspase-8 is recruited to HIPPI–HIP-1 (Bhattacharyya et al., 2008).*

I.1.3.2.4. IFTA components

Until now, there is not much evidence to illustrate the detailed interactions of six IFTA proteins within the complex. Most IFTA proteins have a large molecular weight and complicated protein motifs. Four IFTA (IFT140, IFT144, IFT122, IFT121) are predicted to have WD-repeats in the N-terminal regions and WAA (degenerate TPR-like repeats) in the C-terminal regions. IFT139 does not contain the WD-repeats domain but has the TPR repeats motif in C-terminal. The last member, IFT43 does not contain any predicted protein domain already known. A recent study in *Chlamydomonas* revealed that all IFTA subunits are

associated in a 16S complex in both cell bodies and flagella, but that a faction of IFT43 is unassociated with the complex and found to sediment at 2S. The same study also identified a 12S sub-complex constituted of IFT122, IFT140 and IFT144 and yeast two-hybrid results confirmed an interaction between IFT121 and IFT43 (Behal et al., 2012) (Fig. I-12).

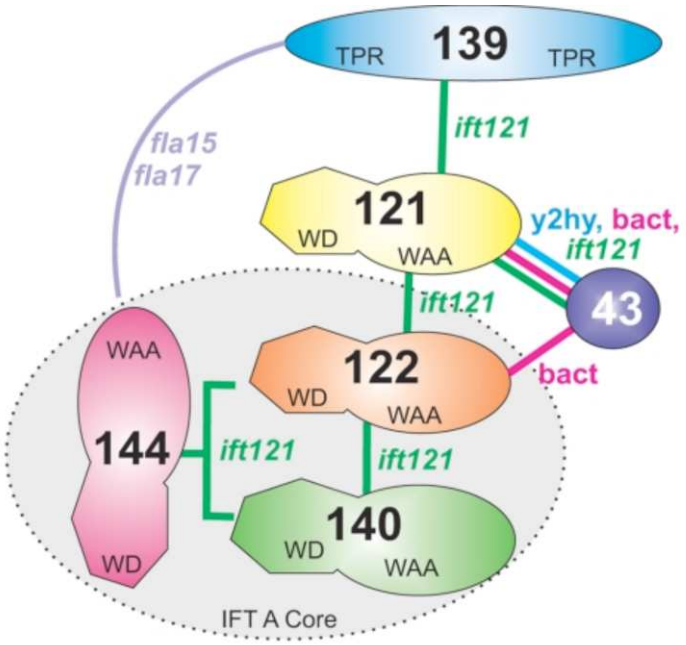

Figure I-12. Interaction model within the Chlamydomonas IFTA complex. *The model shown summarizes the IFTA subunit interactions that have been directly visualized, such as IFT121-IFT43, or implied, such as IFT139-IFT121. Based on biochemical analysis of the ift121 mutant, it is proposed that IFT122, IFT140, and IFT144 assemble to create a heterotrimeric stable core complex. The interactions of IFT121 with both IFT139 and IFT43 are supported by the observation that loss of IFT121 completely removes IFT139 and IFT43 from complex A. Last, IFT139 and IFT144 demonstrate a complex genetic interaction that suggests a functional association (Behal et al., 2012).*

IFT139

IFT139 was first identified in *Chlamydomonas* as FLA17. The mutant produced flagella with characteristic bulge and significant defects in retrograde transport when they were transferred to the restrictive temperature (Piperno et al., 1998). Another study showed that IFT139 and IFT144 are essential for the exit of IFT-dynein from the flagellum, since the cellular amount of IFTA complex is significantly reduced in the mutant (Williamson et al., 2012). Aln, a mouse mutant devoid of THM1 /Ttc21b (homolog of IFT139), produces abnormal primary cilia, which have bulb-like structures at their tips and in which IFT proteins are sequestered. This mutant also shows the over-activation of sonic hedgehog signaling, which indicates that the IFTA play a role in signaling pathways (Tran et al., 2008; Stottmann et al., 2009).

IFT121 and IFT122

IFT121 and IFT122 display a similar protein organization, both of them having predicted β-propellers at their N-terminus and low-confidence TPR repeats at their C-terminus. In *Tetrahymena*, IFT122 is not essential for ciliary assembly, but is important for IFT particle turnaround at tips (Tsao et al., 2008a). A study in mouse showed that IFT122 regulates Sonic Hedgehog signaling and controls the ciliary localization of components of the pathway (Qin

et al., 2011). Mutations in IFT121 or IFT122 in *Chlamydomonas* induce severe ciliogenesis defects (Behal et al., 2012). A *C. elegans* IFT121 (IFTA-1) mutant displays chemosensory abnormalities and shortened cilia with the accumulation of IFT particles (Blacque et al., 2006). In man, mutations in WDR35, the homolog of IFT121, cause the Sensenbrenner syndrome (Gilissen et al., 2010).

IFT140

IFT140/CHE-11 was shown to be involved in the IFT movement in *C. elegans* (Qin et al., 1998). A study in zebra fish showed that the depletion of IFT140 did not induce ciliary defect similar to the ones produced by the depletion of IFTB proteins (Tsujikawa et al., 2004). In contrast, a more recent study in mouse showed that the deletion of the *IFT140* gene causes cystic kidney (Jonassen et al., 2012). Moreover, resent research identified the Mainzer-Saldino syndrome in human as a ciliopathy caused by IFT140 mutations, which establish a link between IFTA and human disease (Perrault et al., 2012).

IFT144

IFT144 is encoded by the FLA-15 gene in *Chlamydomonas*. The disruption of IFT144 produces abnormal flagella with a bulge containing IFTB proteins (Iomini et al., 2009). Recent studies separately in mouse and human confirmed that mutations in IFT144 (WDR19) cause two ciliopathies (Sensenbrenner syndrome and Jeune syndrome) with skeletal anomalies and renal insufficiency phenotypes including short ribs and limps, polydactyly and craniofacial defects (Bredrup et al., 2011; Ashe et al., 2012).

IFT43

IFT43 is the smallest IFTA protein. It was not purified in initial studies and was then identified in *Chlamydomonas* mutant FLA-15 using two-dimensional electrophoresis of 35S-labeled polypeptides (Piperno et al., 1998). A recent study revealed that one fraction of IFT43 is apart from the 17S IFTA complex and interacts with IFT121 (Behal et al., 2012). Similarly to IFT121, mutations in human IFT43 cause Sensenbrenner syndrome with skeletal and kidney defects (Arts et al., 2011; Gilissen et al., 2010).

I.1.3.2.5. IFT accessory proteins

Besides the individual IFT proteins I introduced above, recent work also revealed that some other proteins including CrFAP22/CeDyf-3/Ceqilin/HsCLUAP1 and CeDyf-13/TbBIFTC3 participate in the IFT and are regarded as IFT accessory proteins (Murayama et al., 2005; Ou et al., 2005; Takahashi et al., 2004; Blacque et al., 2005; Franklin & Ullu. 2010).

I.1.3.2.6 IFT cargos

The obvious function of the IFT in cilia is supposed to be the transport of cargos (precursors) essential for ciliary building and maintenance. First evidence about the composition of cargos came from a study in *Chlamydomonas*, which showed that the ciliary localization of inner dynein arm, a part of axonemal components, required the activity of kinesin (Piperno et al., 1996). Other studies also showed that the IFT controls the tubulin balance in flagella (Marshall & Rosenbaum, 2001) and that the transport of outer dynein arms into flagella also needs IFT (Hou et al., 2007). In *Chlamydomonas*, some flagellar components can be preassembled in the cell body before entering the flagella. They can form a 12S complex transported by anterograde IFT from basal body to tip and then reassemble a 20S complex that turns around from tip to base by retrograde IFT (Qin et al., 2004; Behal et al., 2012). In addition, in mammalian retina, the photopigments, which are important for animal light

detection, are synthesized in the inner cell body and then transported to the distal outer segment by the IFT system through the connecting cilium (Insinna & Besharse, 2008).

I.1.3.3. Diverse functions of IFT proteins beyond ciliary transport.

As I presented above, the IFT plays a crucial role in cilium assembly through a conserved motile mechanism in various organisms. However, recent studies in ciliate and non-ciliate cells provide more and more evidence to reveal that some IFT proteins also perform functions in other cellular compartments than the cilium. This indicates that IFT proteins are more complicated than people firstly imagined. For example, IFT88 (IFTB) was shown to localize at centrosomes in actively proliferating cells and that it can regulate the G1-S transition in the cycle of non-ciliated cells (Robert et al., 2007). Research in human HeLa cells also showed that IFT88 is required for spindle orientation and chromosome segregation during mitosis (Delaval et al., 2011). As already mentioned, IFTB members such as IFT20, IFT57 and IFT88, were found to take part in immune synapse organization (Finetti et al., 2009).

I.1.4. Ciliopathies: pathologies related to ciliary dysfunction.

Due to the diverse roles of cilia during development and in various organs at the adult stage, ciliopathies can be very diverse in symptoms and very pleiotropic. They can be associated with a wide range of human disorders, including obesity, polydactyly, kidney and liver disease, brain and nervous system defect, retina degeneration, anosmia, etc. Each syndrome can be caused by a mutation in several genes, and each ciliopathy gene can cause different syndromes according to the nature of the mutation, which makes the study of ciliopathies very complex (Gerdes et al., 2009).

I.1.4.1. Polycystic kidney disease (PKD).

Kidney is the most commonly affected organ in ciliopathies. Pathological structure changes in kidney are displayed in several kinds of illness including PKD, Nephronophthisis (NPHP) and Bardet-Biedl syndrome (BBS). ADPKD (Autosomal Dominant Polycystic Kidney disease) and ARPKD (Autosomal Recessive Polycystic Kidney disease) represent the largest proportion of PKD. Mutation of PKD1 (encoding polycystin-1) and PKD2 (encoding polycystin-2) were identified in ADPKD patients and are believed to cause the disease. ARPKD are more common in childhood, while mutations of PKHD-1 (encoding fibrocystin/polyductin) are confirmed in ARPKD patients (Harris & Torres, 2009).

I.1.4.2. Nephronophthisis (NPHP).

Similar to PKD, NPHP is a recessive inherited renal cystic disease that more often happens in young adults. Eleven mutated genes (NPHP1- NPHP11) have been identified during patient genome scanning and they were gathered in one group whose coding products are named nephrocystins and they are also confirmed to play roles in the pathology of other ciliopathies including Bardet-Biedl syndrome (BBS), Meckel Gruber syndrome (MKS) and Joubert syndrome (JBTS) (Shiba & Yokoyama, 2012; Hurd & Hildebrandt, 2011).

I.1.4.3. Bardet-Biedl Syndrome (BBS)

BBS represent one wide range of human multisystemic developmental disorders including obesity, retina defect, polydactyly and learning obstacle. Until now, 14 genes (BBS1-BBS14)

have been identified, which encode proteins localized to the primary cilium, basal body or centrosome. Recent studies showed that some BBS proteins (BBS1, BBS2, BBS4, BBS5, BBS7, BBS8, BBS9) form a complex named BBSome, which associates to RAB8, and regulate vesicle travel from cytoplasm to cilium, an important step for ciliogenesis and ciliary maintenance. In addition, the other three BBS proteins, BBS6, BBS10 and BBS12 form a second group that regulate the assembly of the BBSome. In addition, recent studies revealed that the BBSome is involved in intraflagellar transport (IFT) in the cilium, in *Chlamydomonas*. The BBSome has been found to control IFT assembly at cilia base and turnaround at flagella tip. A study in *Caenorhabditis elegans* also showed that two BBS proteins (BBS7 and BBS8) are required for the stabilization of IFT particles (Blacque et al., 2004).

I.1.4.4. Meckel Gruber syndrome (MKS)

Polydactyly, dysplastic kidney and occipital encephalocele constitute the characteristic clinic phenotype of MKS. The MKS causal genes known so far include MKS1, MKS2 (TMEM216), MKS3 (TMEM67), MKS4 (CEP290), MKS5 (RPGRIP1L), MKS6 (CC2D2A), MKS7 (NPHP3), MKS8 (TCTN2), MKS9 (B9D1), MKS10 (B9D2), TMEM237, C5orf42, EVC2, EXOC4 and TMEM231. Mutations of MKS1 or MKS3 in human and rat are responsible for ciliary and centrosomal defects (Tammachote et al., 2009; Weatherbee et al., 2009).

I.1.4.5. Joubert syndrome (JBTS)

JBST is a recessive human disorder affecting brain. Patients often have abnormal eye movements, abnormal weakness, neonatal breathing difficulties, clumsiness, mirror movements, varying degrees of mental retardation, and often autistic-like behaviors. Now mutation of seven genes, NPHP1, AHI1, CEP290, RPGRIP1L, MKS3 (TMEM67), ARL13B, MKS2 and CC2D2A are confirmed to be the genetic cause for this syndrome (Paprocka and Jamroz, 2012). CEP290 is also an important component of cilia transition zone, which localizes at the ciliary base, and NPHP1 is also a gene responsible for another ciliopathy, Nephronophthisis.

I.1.4.6. Other ciliopathies.

Besides these common ciliopathies, since primary cilium in mammal is essential for several signaling that control the cell cycle, other research also try to detect putative relationships between cancer and cilium. For example, two cancer-promoting proteins, Aurora A and HEF1, were found to induce ciliary disassembly (Plotnikova et al., 2008). Cilium acted as a cellular watchtower, whose absence can be an initiating event in neoplastic growth (Mans et al., 2008). However, further research is still needed to understand the putative linking between cilia and cancer.

I.1.5. Important models for ciliary studies.

It is important to introduce here the various models that were irreplaceable for the progress in understanding the structure, biogenesis and function of cilia. These are unicellular organisms such as *Chlamydomonas reinhardtii*, *Trypanosoma brucei*, *Paramecium tetraurelia* and *Tetrahymena thermophila*, or multi cellular organisms such as *Caenorhabditis elegans*, *Danio rerio* and *Mus musculus.*

I.1.5.1. Chlamydomonas reinhardtii

Chlamydomonas reinhardtii is a unicellular green alga of ~10µm in length, with a chloroplast, a pyrenoid, a senses light 'eyespot' and two anterior flagella of 10~12µm in length. During vegetative growth, the two flagella beat, which provokes cell swimming. Cell can direct their movements in response to various light stimuli. In the early stage of mating process, flagella are also required for gamete adhesion. During mitosis, the flagella are not essential and are disassembled, allowing the two centrioles (basal bodies) to migrate and organize the spindle pole to contribute to mitosis.

Several advantages of *Chlamydomonas* make it a good model for research on flagella. First, it is possible to grow them synchronously in a medium and large amounts of flagella can be easily purified for biochemical analyses. Secondly, *Chlamydomonas* has a clear genetic background, all three genomes (nucleus, chloroplast, mitochondrion) are sequenced and there are standard biological protocols that can be applied for the genetic and cellular research. Further more, a large number of mutants have been screened and identified.

Over 500 proteins have been detected by proteomics to be components of the flagella. Many of them have homologs in mammals, which make *Chlamydomonas* an interesting model for some human cilium-related disease. In addition, a conserved mechanism essential for ciliogenesis, intraflagellar transport (IFT), was first discovered in *Chlamydomonas*. Most IFT proteins were first purified in *Chlamydomonas*, and then found in other organisms.

I.1.5.2. Trypanosoma brucei

Trypanosoma brucei is a parasite with a flagellum. It causes sleeping sickness in human and nagana in animals. It is also an attractive model for flagellar research because of the unique biological flagellar feature, that it assembles a new flagellum while keeping the old one (Absalon, et al., 2008). Therefore, it is possible to study both flagellum construction and maintenance in one individual cell, using the gentical and molecular tools provided by this organism. In addition, the morphology of flagella is changed according to different life cycle and this differentiation can be reproduced in vitro, that provide us a wonderful model for researching the regulation mechanism of flagellar assembly. Recent works in *Trypanosoma brucei* provide some supplement evidence about IFT recycling process (Buisson, et al., 2013).

I.1.5.3. Paramecium tetraurelia and Tetrahymena thermophila

Ciliates such like *Paramecium* and *Tetrahymena* represent models harboring a huge number of cilia. In ~50µm long *Tetrahymena* cell, there are ~750 cilia and basal body while there are ~4000 cilia and basal body in ~120µm long *Paramecium* cell. Specific cilia arrangement over the cell surface allowed for long morphogenetic studies at the cell level by following basal body duplication pattern. Using GFP-fusion and gene depletion method, localization and function of basal body and ciliary proteins can be easily detected.

Ciliates are also excellent models for studying tubulin post-translational modifications, which are important processes for tubulin diversity and for ciliary function. Since almost all known tubulin members were found in *Paramecium* or *Tetrahymena*, it has been possible to approach the roles of the different post-translational modifications in cilia and other microtubule-based organelles. Elimination of β-tubulin polyglycylation in *Paramecium* or *Tetrahymena* induces various phenotypes including lethality, slow swimming, and division defects. Mutant clones produce non-motile cilia lacking the central pair or abnormally short cilia. Polyglycylation is also required for maintenance of length of already assembled cilia. Basal bodies in mutant cells show redundant number of microtubule (Thazhath et al., 2004). Another post-translational modification, polyglutamylation, was also identified in *Paramecium* and found

to be important in the interactions of tubulin with microtubule-associated proteins and calcium, essential for microtubule dynamics (Edde et al., 1990). *Tetrahymena* is also a tool often used for IFT research in ciliogenesis (Beals et al., 2007; Dave et al., 2009).

I.1.5.4. Caenorhabditis elegans

Caenorhabditis elegans is a nematode that contains sensory immotile cilia at the tip of specialized neurons in the adult hermaphrodite. *Caenorhabditis elegans* need these neurons to detect changes of environment. Using different kinds of environmental stimuli including chemosensory (CHE) and osmosensory (OSM), a series of worm mutant clones with various ciliary defects have been obtained. Many important discoveries about cilium and IFT come from *Caenorhabditis elegans*. Sensory cilia are easy to observe in vivo because of their immotility, which allows the observation of the bi-directional IFT complex movements.
The roles of several IFT proteins and cargos were also refined in *Caenorhabditis elegans*. For example, the homolog of human CLUAP1 protein qilin was identified as associating with the IFT complex (Ou et al., 2005). BBSome proteins were found to move in association with the IFT complex and to be important for the stability of IFT particles. TRP-type channels OSM-9 and OCR-2 represent IFT cargos, which play important roles in chemosensory responses (de Bono et al., 2002). Mutations in TUB-1, a *Caenorhabditis elegans* homolog of the Tubby mammalian protein, which is also an IFT cargo, causes an extension of life span and an increased fat storage (Mukhopadhyay et al., 2005; Inglis et al., 2009).

I.1.5.5. Danio rerio

Danio rerio or zebra fish represents a vertebrate model in which immotile and motile cilia can be found. Several zebra fish mutants with cystic kidneys provided evidence for a link between the formation of renal cysts and ciliary dysfunction (Sun et al. 2004). Similarly to mammals, the depletion or inactivation of some ciliary proteins in zebra fish induces various organic defects including photoreceptor cell death, randomization of left–right asymmetry, and degradation of photoreceptors and hydrocephalus. All this makes this animal to be a excellent material to study human disease (Brand et al., 1996, Drummond et al., 1998, Sun et al., 2004; Zhao & Malicki, 2007).

I.1.5.6. Mus musculus

Because of the high degree of homology with human, the mouse is often regarded as “the” mammalian model for medical research. Concerning ciliary research, the pioneer work on the mutant Tg737 with severe kidney defect linked the IFT protein IFT88 to a genetic disease (Schrick et al., 1995). Mouse is also a good model for primary cilium research, such as the study of signaling pathways (hedgehog) that follows the IFT route in primary cilium; mutants in IFT or other ciliary proteins cause a wide range of phenotype like blindness by retinal degeneration (Zhang et al., 2013); left-right asymmetry defects (Manning et al., 2013) and male infertility by abnormal spermatozoa flagellar axonemes (Zhang et al., 2012; Borg et al., 2010).

I.2. The *Paramecium* model: a powerful material for research on cilia.

The model that I used in my thesis project is *Paramecium tetraurelia*, a ciliate living freely in fresh water. This unicellular is covered with ~4000 cilia and possesses several specialized organelles making it a true differentiated organism. *Paramecium* has a full digestive track starting by the oral apparatus, a kind of funnel covered with hundreds of cilia whose coordinated beating drives food particle for phagocytosis in food vacuoles and ending at the cytoproct where undigested contents of the food vacuoles are rejected into the medium. It also possesses contractile vacuoles, which have a function close to the one of the kidney in regulation of osmotic pressure and elimination of liquid waste. *Paramecium* also possesses a regulated secretion pathway in the form of a thousand of trichocysts, which can be triggered by external stimulation. The change of conformation of trichocysts into thin needles when they are expelled into the medium make them easy to detect and make also easy to distinguish cells able from cells unable to release them, mutants or RNAi treated cells.

I.2.1. Basal bodies and cilia of *Paramecium*

The ciliate *Paramecium tetraurelia* has a highly organized cortical cytoskeleton in which the ciliary basal bodies are arranged in rows following a precise pattern (Fig I-13).

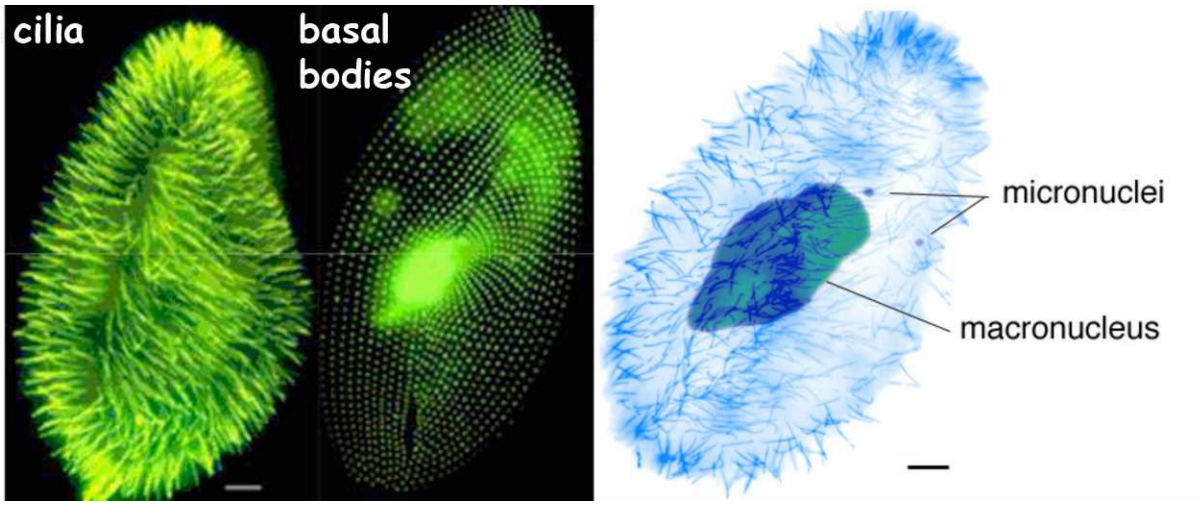

Figure I-13. Presentation of cilia, basal body and nuclear in Paramecium tetraurelia. *Left, Epifluorescence microscopic image of cilia and basal bodies of Paramecium respectively immunolabelled by an anti-paramecium cilia antibody directed against polyglycylated tubulin and the monoclonal antibody ID5 that recognizes basal bodies. Right, Illustration of the occurrence of two different kinds of nuclei in Paramecium, a macronucleus and two micronuclei stained with DAPI and superimposed on a ciliary labeling on the picture. Bar = 10µm.*

Basal bodies are duplicated during cell division similarly as the centriole duplicate by the organization and elongation of a new basal body perpendicularly to the mother one. The orientation of the site of duplication is always the same relatively to the cell axis: new basal bodies appear towards the anterior of the cell within its antero-posterior basal body row. The duplication process ends with the anchoring of the new basal body at the surface, after which ciliogenesis can start, although not all basal bodies are ciliated. The duplications of basal bodies are unequally represented at the cell surface in space and time and occur as waves (Iftode et al., 1989 and Fleury-Aubusson et al., 2003). The first wave of duplication of basal bodies starts at the division furrow, close the oral apparatus, and then extends toward the poles (Fig. I-14).

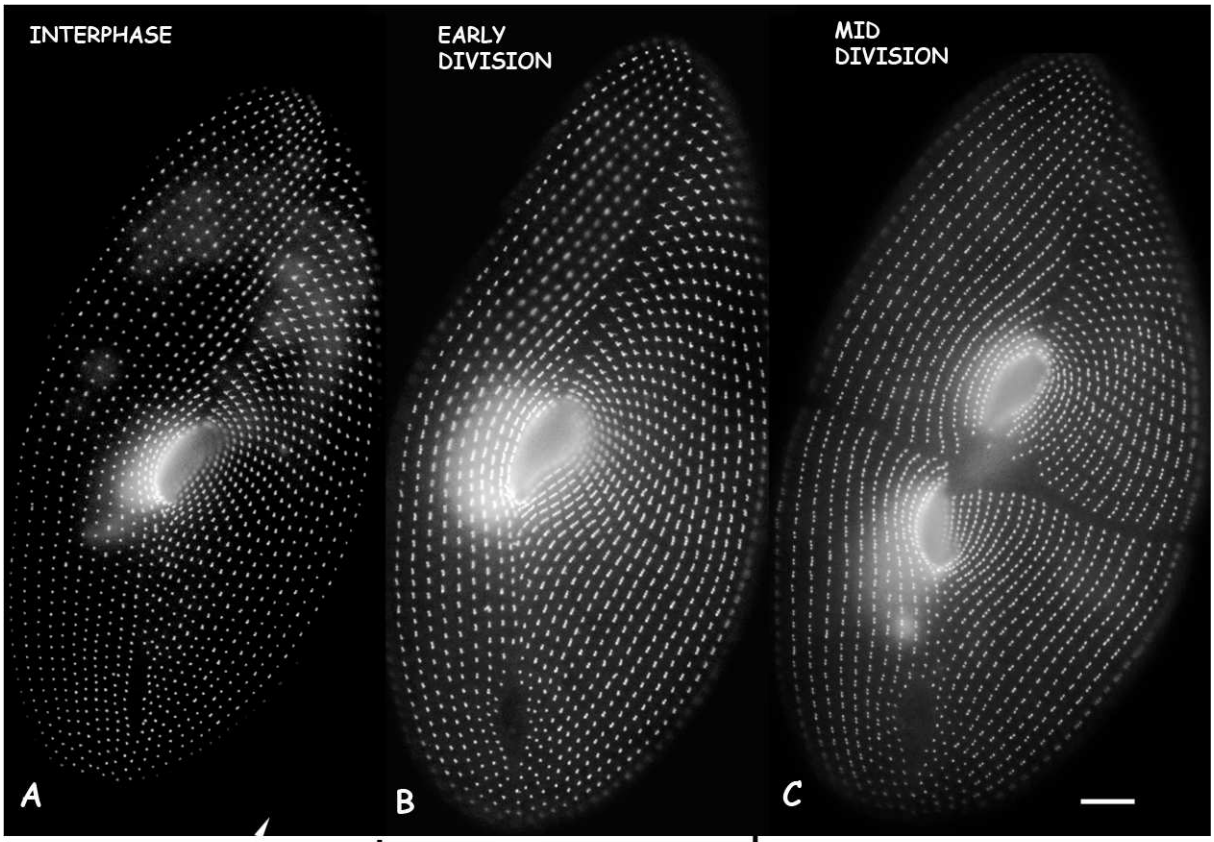
INTERPHASE
EARLY DIVISION
MID DIVISION
A
B
C

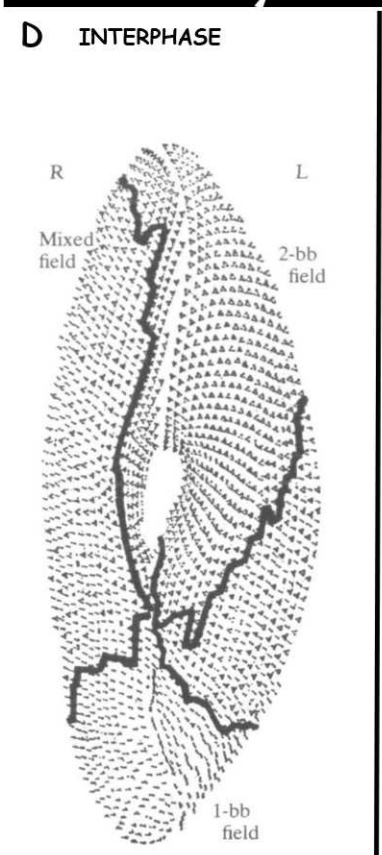
D INTERPHASE
R
L
Mixed field
2-bb field
1-bb field

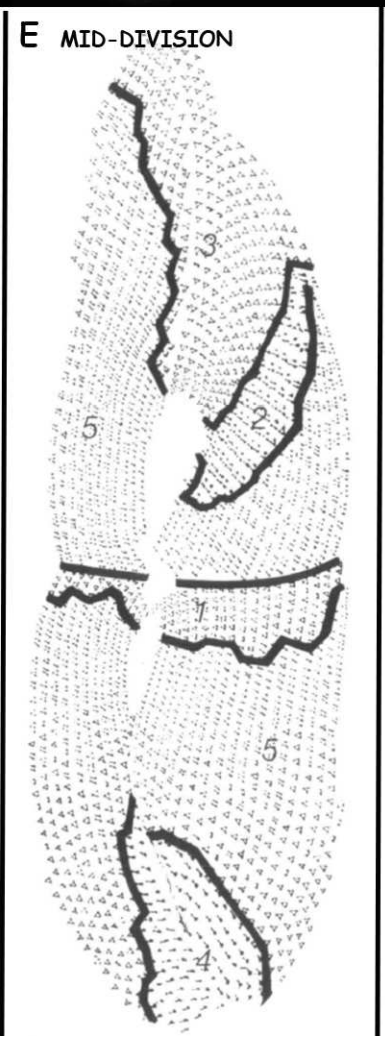
E MID-DIVISION
3
2
5
1
5
4

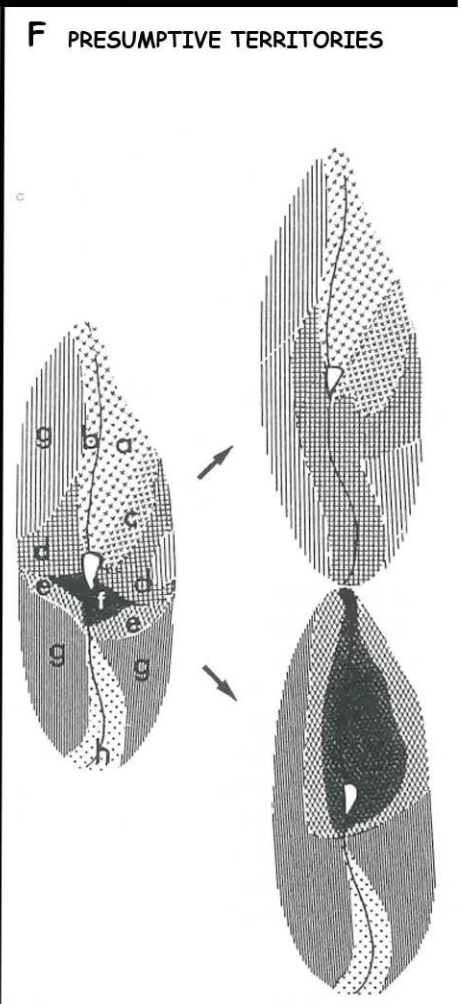
F PRESUMPTIVE TERRITORIES
g
b
a
c
d
e
f
d
e
g
g
h

Figure I-14. Organization and duplication pattern of basal bodies in Paramecium tetraurelia. *A-C: Epifluorescence microscopy fluorescence of basal bodies labeled by expression of centrin 2-GFP during the cell cycle (courtesy of F. Ruiz). A: interphase cell, B: early dividing cell, C: dell at mid division. D and E: scheme representing the different basal body fields found at the surface of Paramecium (Iftode et al., 1989). D: interphase cells in which 3 fields are found, a field in which all cortical units contain a pair of basal bodies (2-bb units) at the anterior of the cell, a field in which all cortical units contain a single basal body (1-bb units) at the posterior of the cell, and a mixed field of 1- and 2-bb units in between. E. Different fields of dividing cells. 3 and 4: invariant fields in which 2-bb and 1-bb units remain as they are throughout division. 5: fields in which basal body duplicate at least one and where all basal body will generate a new cortical unit. 2: 2-bb unit zone in which basal bodies do not duplicate but separate from each other to give two units which will be completed later into 2-bb units by a second wave of duplication. 1: zone in which a second wave of duplication will generate a future 2-bb units anterior invariant field. F: Pattern of presumptive territories from a mother cell to its daughter through division (Jerka-Dziadosz and Beisson, 1990).*

I.2.2. Nuclear duality in *Paramecium*

Paramecium, as a ciliate, is a unicellular eukaryote that contains two different kinds of nuclei, a somatic macronucleus highly polyploid (800n in *Paramecium*) and two diploid germinal micronuclei. The macronucleus is responsible for gene expression throughout the life cycle and is degraded during the sexual process (autogamy or conjugation), while the micronuclei are transcriptionally silent, but undergo meiosis and fecundation during sexual events and transmits the genome to new micro- and macronuclei to the next generation. Indeed, new macronuclei and micronuclei are derived from the mitotic copies of the zygotic nucleus (Fig. I-15).

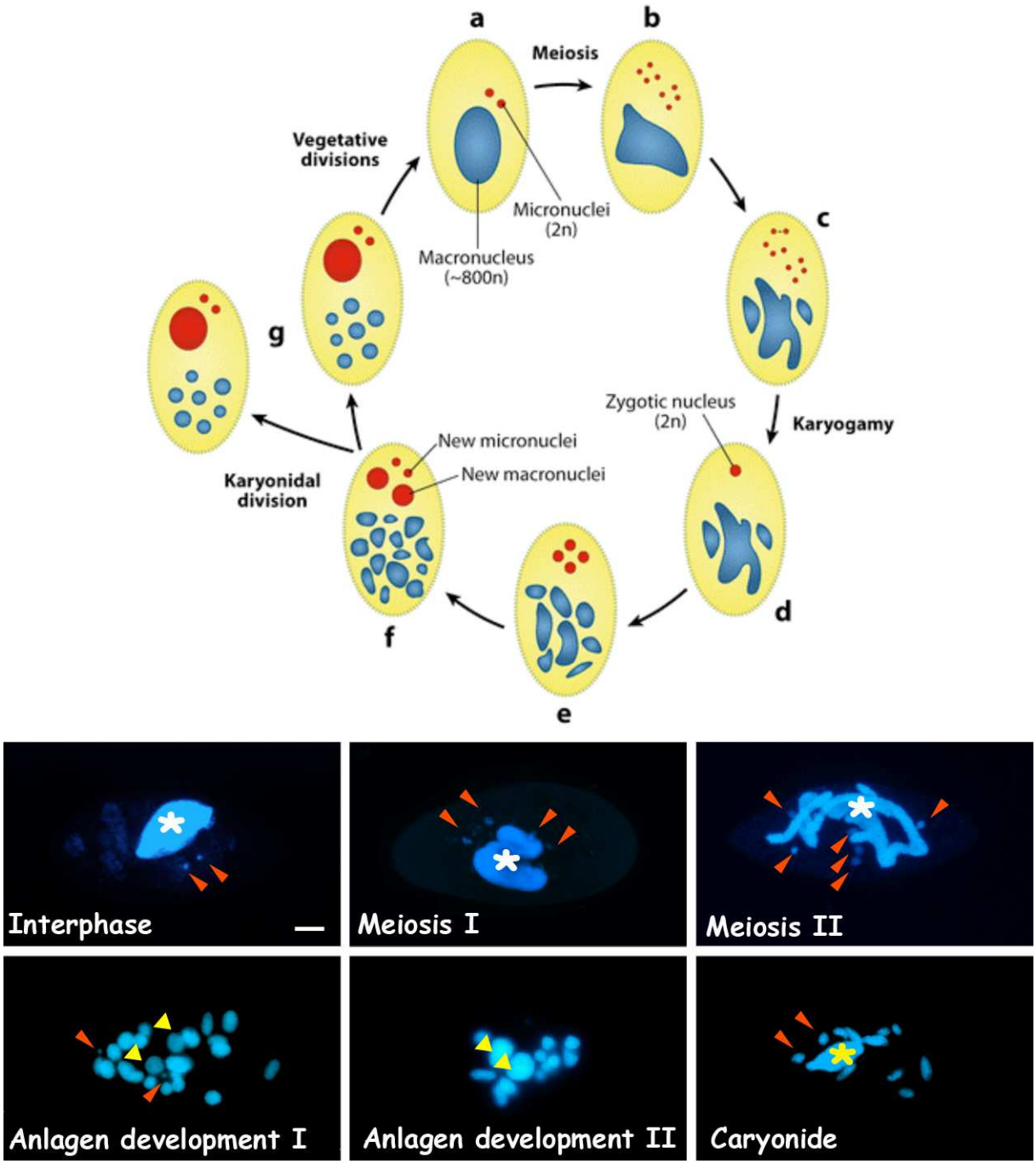

Figure I-15. The sexual cycle of Paramecium. <u>Top cartoon</u>: (a) *A vegetative Paramecium cell. (b) Meiosis of two micronuclei producing eight haploid nuclei. The macronucleus begins its fragmentation. (c) Seven out of eight haploid meiotic products degenerate; one (shown at top) divides mitotically, producing two identical gametic nuclei. During* ***conjugation****, one of the gametic nuclei is exchanged between partner cells and fuses with the resident one. In the case of* ***autogamy*** *(self-fertilization), the two identical gametic nuclei fuse together. (d) A cell that contains the zygotic nucleus. (e) The zygotic nucleus undergoes two subsequent mitotic divisions. (f) Two of the products differentiate into new macronuclei, two into micronuclei. (g) The first cell division produces two karyonidal cells, which contain each one new macronucleus, two micronuclei, and fragments of the old macronucleus. (Sperling et al., 2011).* <u>Bottom micrographs</u>*: DAPI staining of cells undergoing autogamy. The white stars label the macronucleus under disruption at the early stages. Red arrowheads point to the*

micronuclei or the meiotic products. The yellow arrowheads point to the nascent macronuclear anlagen. The yellow star in the caryonide stage labels the novel macronucleus deriving from one of the anlagen after the first cell division (courtesy of M. Bétermier).

During the sexual processes, a series of events occur in the nuclei that lead to the development of new macronuclei. First, as soon as the macronuclear anlagen are determined, a few rounds of genomic DNA replication, then DNA rearrangements occur: chromosome fragmentation with subsequent telomere addition and precise elimination of Internal Eliminated Sequences (IES). Interestingly, the pattern of DNA rearrangements in the developing macronucleus was shown to be dependent of the resident organization in the fragmenting maternal macronucleus: microinjection of certain kind of IESs in the maternal macronucleus before autogamy specifically inhibits the excision of this IES in the developing macronucleus during autogamy, which suggests an epigenetic regulation process involved in a global comparison of germ line and somatic genomes (Meyer & Duharcourt, 1996). Then a RNA-Mediated mechanism was discovered (Garnier et al., 2004), that leaded to the scanning model through scnRNA. ScnRNA are 25-nucleotide RNA molecules produced by the micronuclei at meiosis and showed to provoke homologous IES sequence elimination if they reach the developing macronucleus. Indeed, there is a subtractive comparison of RNA produced by the old macronucleus and scnRNA that allows only scnRNA with no macronuclear counterpart to enter the developing macronucleus and trigger IES excision (Lepere et al., 2008) (Fig. I-16).

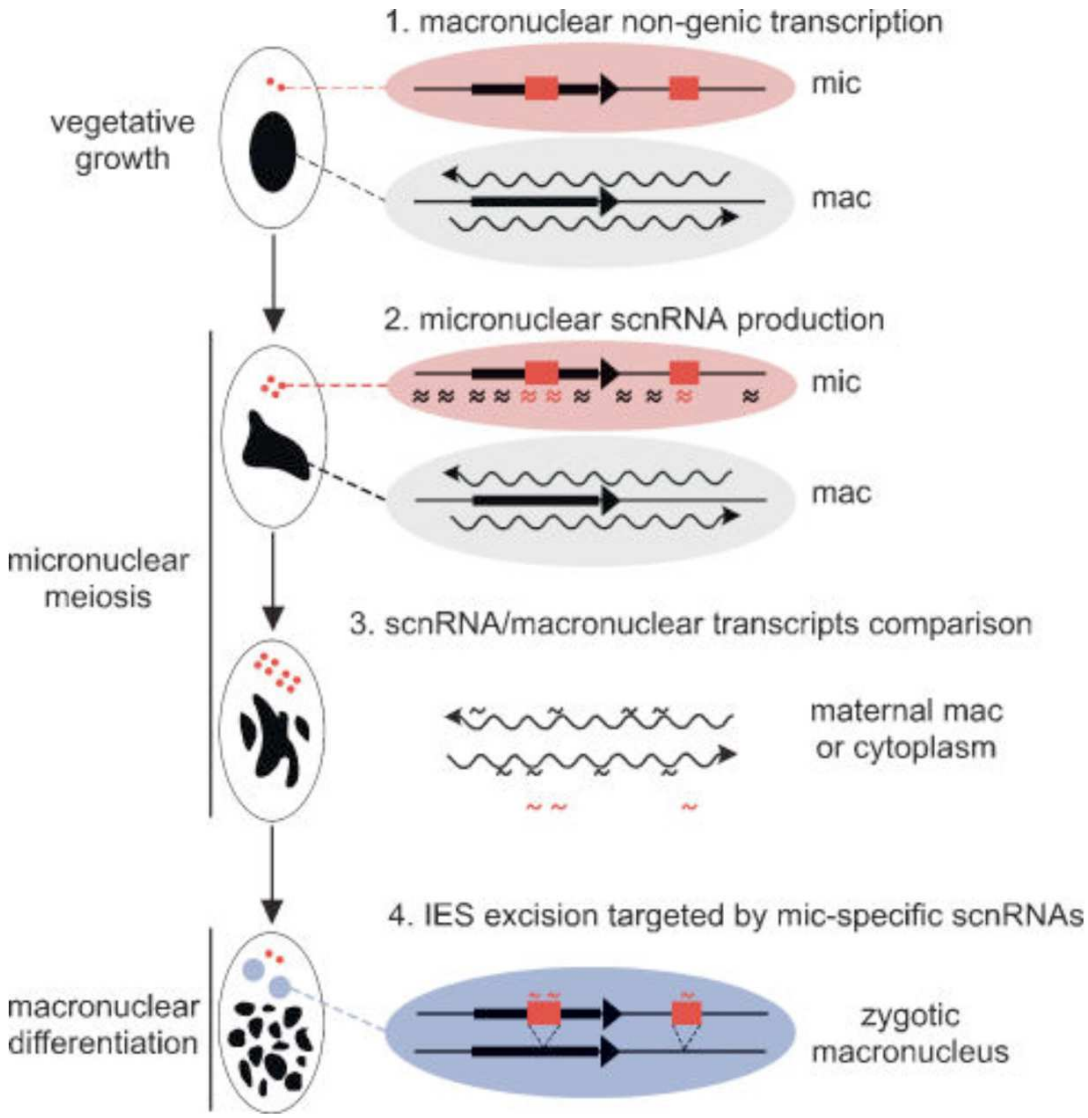
1. macronuclear non-genic transcription
vegetative growth
mic
mac
2. micronuclear scnRNA production
micronuclear meiosis
mic
mac
3. scnRNA/macronuclear transcripts comparison
maternal mac or cytoplasm
4. IES excision targeted by mic-specific scnRNAs
macronuclear differentiation
zygotic macronucleus

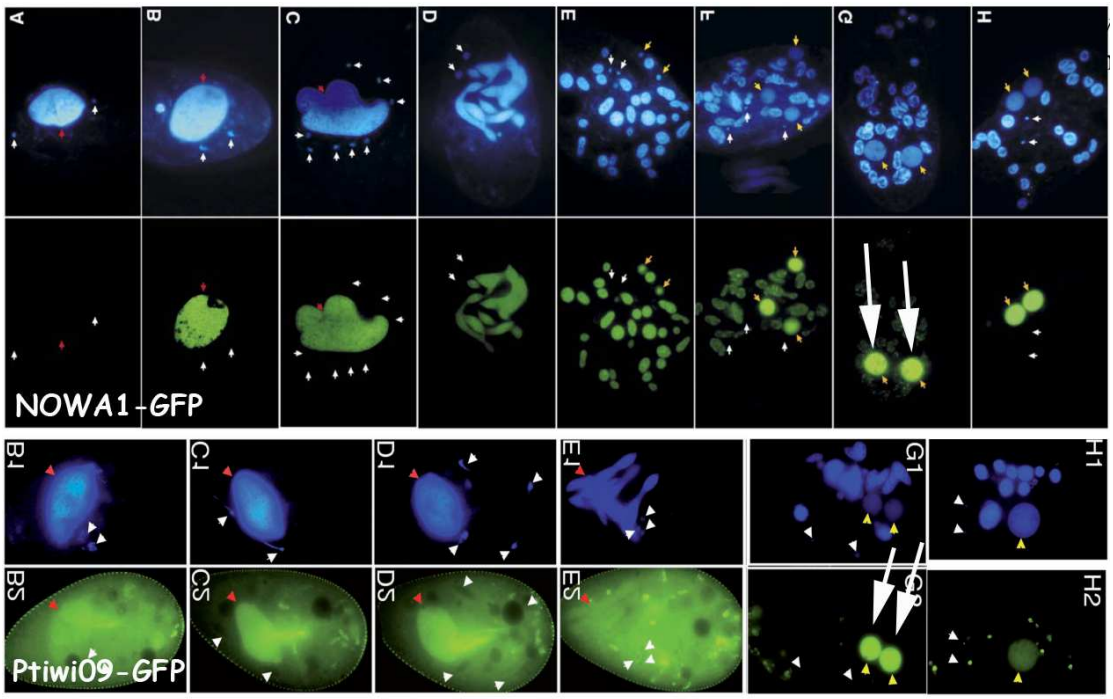
NOWA1-GFP
Ptiwi09-GFP

Fig I-16. The maternal scnRNA/macronuclear RNA scanning model. *Top cartoon: (1) During vegetative growth, a background non-genic transcription of all or most of the macronuclear genome occurs on both strands. (2) Upon initiating meiosis, short double-stranded scnRNAs from the micronuclear genome are produced by an RNAi-dependent pathway. (3) ScnRNAs scan the maternal macronuclear genome by base-pairing with non-coding macronuclear transcripts either in the maternal macronucleus or in the cytoplasm, during meiosis or soon after. (4) ScnRNAs that pair with homologous macronuclear transcripts are sequestered or destroyed, while micronuclear-specific scnRNAs pair with homologous nascent transcripts in the zygotic macronucleus and target IES excision (Lepere et al., 2008). Bottom micrographs: Illustration of the transport from the old macronucleus towards the anlagen of proteins involved in RNA metabolism during autogamy: NOWA1-GFP (Nowacki et al, 2005), Ptiwi09-GFP (Bouhouche et al., 2011).*

The scnRNA are not acting alone but are dependent on proteins for transport and action. For example, Piwi01 and Piwi09, members of the Argonaute family, were shown to be essential for IESs excision, most likely through their action in scnRNA production during the genome rearrangements (Bouhouche et al., 2011). Nowa proteins, RNA-binding proteins, were shown to be involved in the genome rearrangement upon transport from the old fragmenting macronucleus to the new macronuclear anlagen. Nowa1p/Nowa2p depletion impairs the elimination of transposons and of the IESs that are controlled by maternal effects (Nowacki et al., 2005). Another study identified a domesticated PiggyBac transposase, PiggyMac, to be required for the excision of IESs and for the imprecise elimination of several regions containing transposons or cellular genes in regions of chromosome fragmentation (Baudry et al., 2009).

I.2.3. Tools available for *Paramecium* studies.

The genome sequencing of *Paramecium tetraurelia* was completed in 2006, which shows that this species contains nearly 40000 genes arising through at least three successive whole-genome duplications (Aury et al., 2006).
A database, *Paramecium*DB, was developed to access the genome sequence results, as well as all the other resources accumulating with time, such as genetic and RNAi data, transcriptome and proteome analysis, bibliography (Arnaiz et al., 2007; Arnaiz et al, 2010; Arnaiz and Sperling, 2011).
The transformation of *Paramecium* to express exogenous DNA, for example GFP fusion genes, is easily performed by DNA microinjection into the macronucleus, in which the foreign DNA is replicated as a mini chromosome and is transcribed (Gilley et al., 1988).
An efficient homology-dependent inactivation method by RNA interference (RNAi) was developed in *Paramecium* using a method in which cells are fed with bacteria expressing double-strand RNA homologous to the sequence to inactivate (Galvani & Sperling, 2002).

I.3. Thesis project: IFT57 in cilia and nuclei in *Paramecium*.

As I explained at the beginning, my thesis project rapidly focused on the protein IFT57, then on IFT in a more general context. My motivation was the dual localization of the protein, in basal bodies and cilia on the one hand and in the macronucleus in the other hand.

However, the diverse IFT57/HIPPI functions in the cilium and the nucleus are not clearly related in the literature. From my initial interest in relationships between cilia and nuclei, I therefore started my thesis about the localization and role of IFT57 in *Paramecium*.

CHAPTER 1

IFT GENES USED IN THIS WORK

To study IFT57 in *Paramecium* on which my subject principally focusses, I also used IFT46, IFT139, IFT172 (already presented by Laligné et al. (2010) and qilin (previously studied by Houssein Chalhoub in his Master 2 project). I first looked for these IFT genes in the genome by BLAST queries. In this chapter, I compiled the general properties of the genes in a table by extraction from ParameciumDB. Then, for each gene family, I present its status according to whole genome duplications, I look for the presence of protein domains, I present the evolutionary conservation of the *Paramecium* genes based on sequence alignments, and I give expression data and results of ciliary proteomics experiments.

1.1. *Paramecium* IFT proteins used in this study.

Using *Chlamydomonas reinhardtii* IFT protein sequences as probes, we found homologous genes in the *Paramecium* genome. I extracted their properties as well as those of the encoded proteins (Table 1-1).

Locus Symbol	Synonym	Chromosome	Start	End	AA length	M W	pI
GSPATG00023787001	IFT57A	scaffold_80	138414	139799	393	45634	4,83
GSPATG00033566001	IFT57B	scaffold_138	36086	37513	402	46740	4,96
GSPATG00034629001	IFT57C	scaffold_145	208434	209826	394	45921	4,90
GSPATG00035574001	IFT57D	scaffold_152	203494	204887	394	45949	4,84
GSPATG00024708001	IFT46	scaffold_84	334502	335503	298	33869	4,37
GSPATG00011236001	IFT139A	scaffold_30	313147	316724	1157	133618	6,78
GSPATG00011426001	IFT139B	scaffold_31	121611	124911	1068	122927	6,05
GSPATG00013914001	IFT172A	scaffold_39	335500	340783	1723	197236	6,71
GSPATG00033190001	IFT172B1	scaffold_135	111662	113204	504	57905	5,98
GSPATG00033191001	IFT172B2	scaffold_135	113323	116950	1180	134762	6,98
PTETG13500002001	IFT172B	scaffold_135	111662	116950	1733	198328	6,89
GSPATG00001872001	qilinA	scaffold_4	474734	475898	352	41383	4,33
GSPATG00017664001	qilinB	scaffold_53	344814	346105	396	46679	4,39
GSPATG00005213001	qilinC	scaffold_12	278363	279651	396	46429	4,43
GSPATG00009204001	qilinD	scaffold_23	503042	504326	394	46747	4,38

Table 1-1. Chromosome position of the IFT genes used in this study and molecular weight and isoelectric point of the encoded proteins*. Data extracted from ParameciumDB. Concerning IFT172B, it appears that it has been split into 2 adjacent genes (in red in the Table) by the automatic annotation by Genoscope (Aury et al., 2006). Such errors of annotation are due to the occurrence of small indels of one or two bases along the chromosomes and can be manually corrected. The curated IFT172B gene can be retrieved as PTETG13500002001.*

1.2. IFT57 (synonyms: HIPPI; CHE-13)

Four ohnologs, GSPATG00023787001, GSPATG00033566001, GSPATG00034629001, GSPATG00035574001, called respectively IFT57A to D derive from a common ancestor through the last two whole genome duplications, WGD1 and WGD2 (Fig. 1-1).

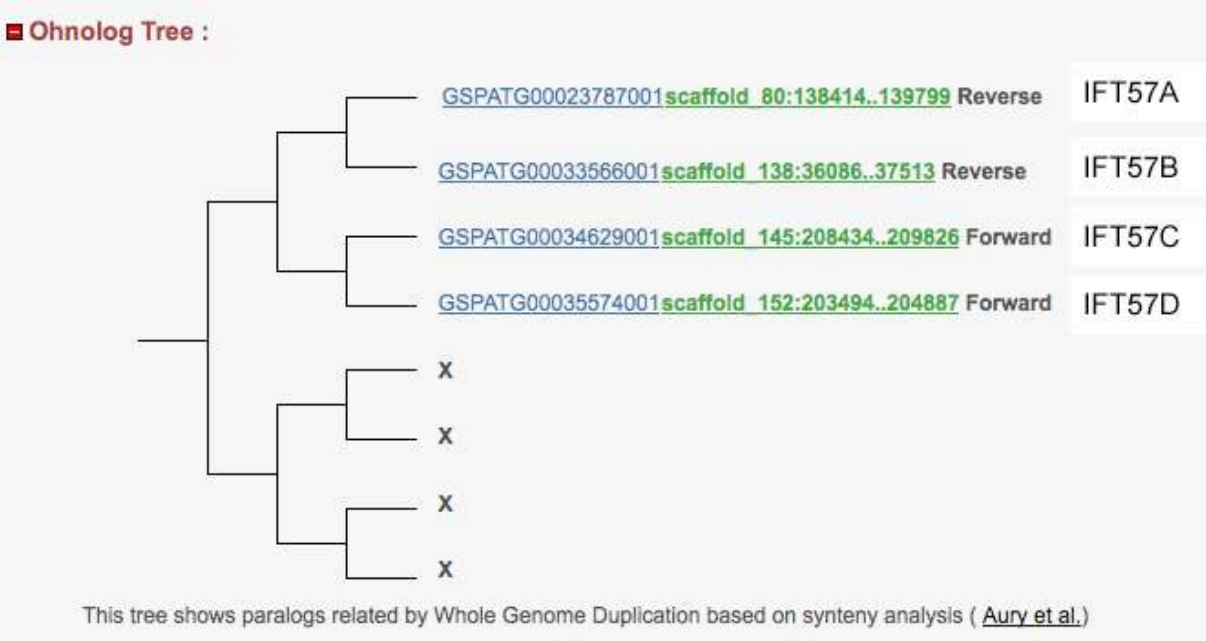

Figure 1-1. Ohnolog tree of IFT57 genes in Paramecium. *Adapted from a screenshot of ParameciumDB*

Sequence comparison at the amino acid level shows that the four proteins are highly similar (Fig. 1-2).

a

b

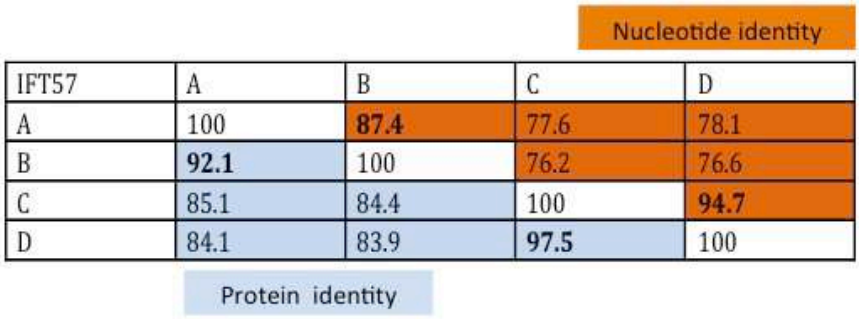

IFT57	A	B	C	D
A	100	**87.4**	77.6	78.1
B	**92.1**	100	76.2	76.6
C	85.1	84.4	100	**94.7**
D	84.1	83.9	**97.5**	100

Figure 1-2. a: Amino acid alignment of the four IFT57 proteins of Paramecium, b: protein identity and nucleotide identity between four IFT57 in Paramecium. *Adapted from Paramecium_DB*

Scanning the different IFT57 genes using the InterproScan software indicated that the whole sequence represents a single domain by itself (Fig. 1-3).

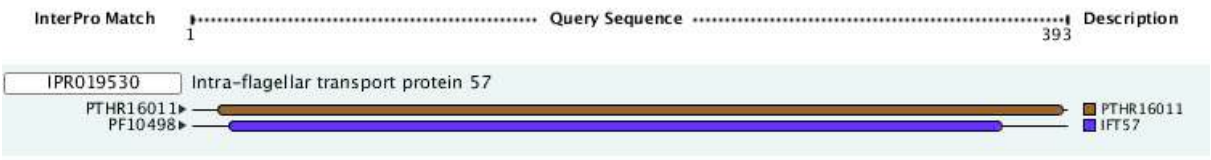

Figure 1-3. Interpro domain match obtained by scanning the IFT57 genes of Paramecium.

Looking now for proteins presenting this domain, another family of three genes appeared, GSPATG00030463001, GSPATG00024566001, GSPATG00024451001, which we called IFT57-like1 to 3 respectively, containing this domain together with a kinase domain (Fig. 1-4).

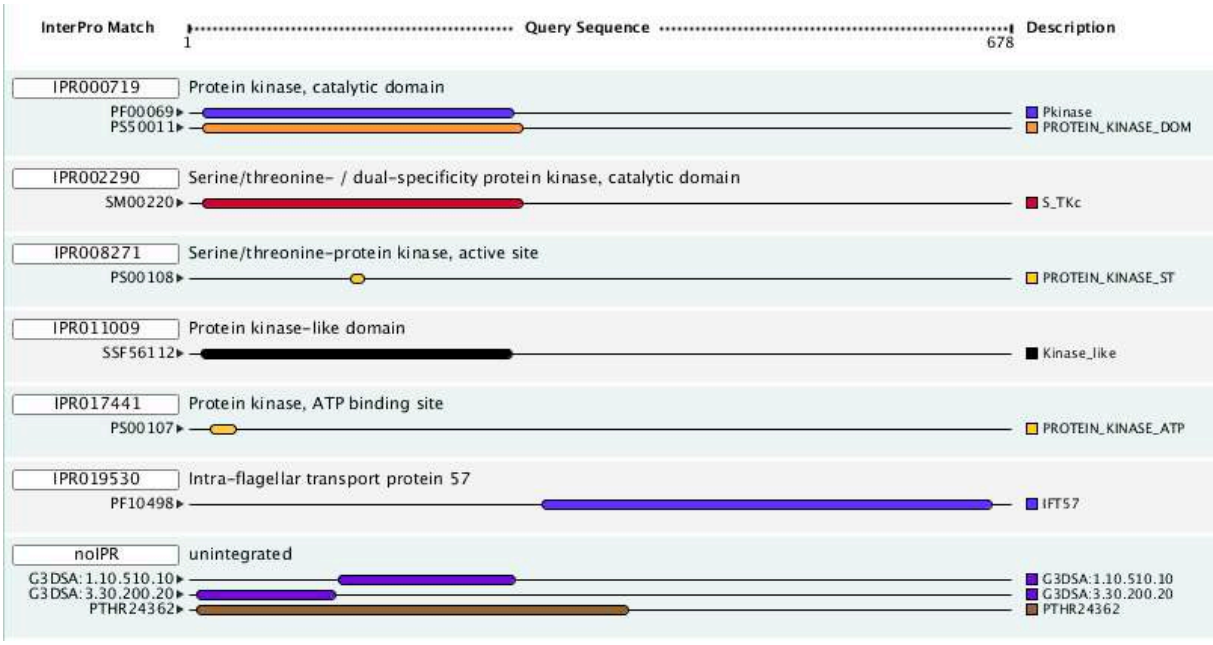

Figure 1-4. Interpro domain match obtained by scanning the IFT57-like genes of Paramecium.

The three IFT57-like genes appear to be ohnologs from the recent and intermediate duplications WGD1 and WGD2 (Fig. 1-5).

a

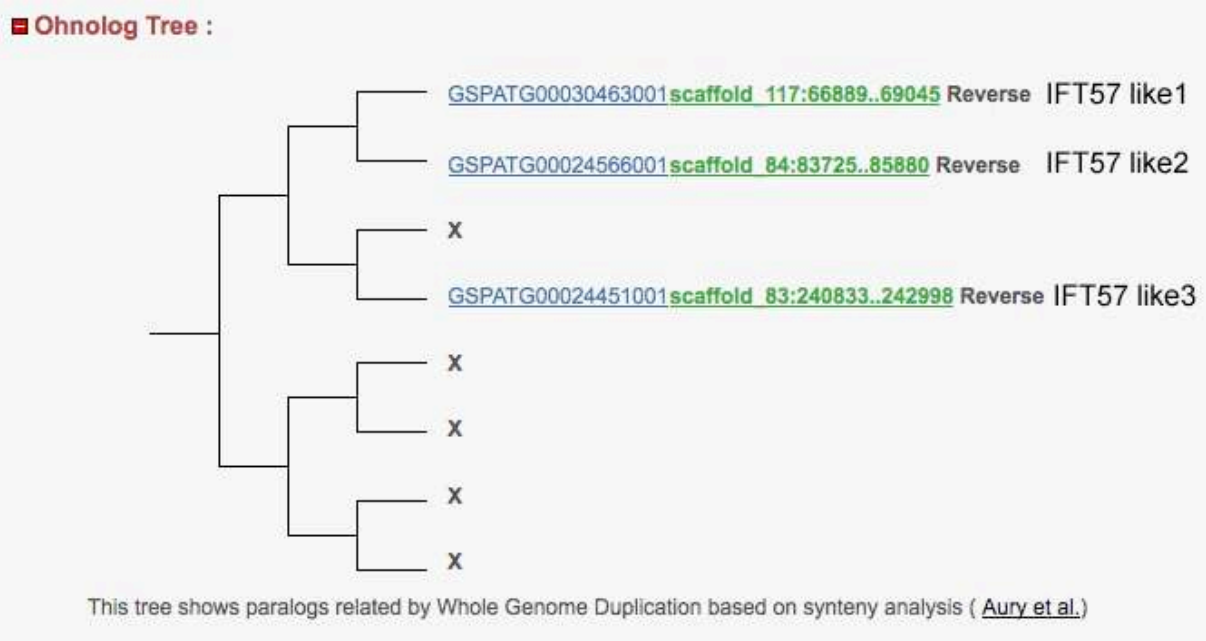

b

		Nucleotide identity	
IFT57-like	A	B	C
A	100	89.9	71.1
B	95.6	100	71.6
C	75.7	75.6	100

Protein identity

Figure 1-5. a:Ohnolog tree of IFT57-like genes in Paramecium, b: protein identity and nucleotide identity between three IFT57-like in Paramecium*. Adapted from ParameciumDB*

In contrast to IFT57, which is well represented among eukaryotes harboring cilia or flagella, we found IFT57-like proteins only in a few species, *Tetrahymena thermophile*, *Albugo laibachii*, *Volvox carteri* and *Chlamydomonas reinhardtii*. The IFT57 domains of these proteins are included in the sequence alignment below (Fig. 1-6), but they were not further studied in this work. It appears from this tree that IFT57 and IFT57-like proteins display a fairly well conserved domain through evolution.

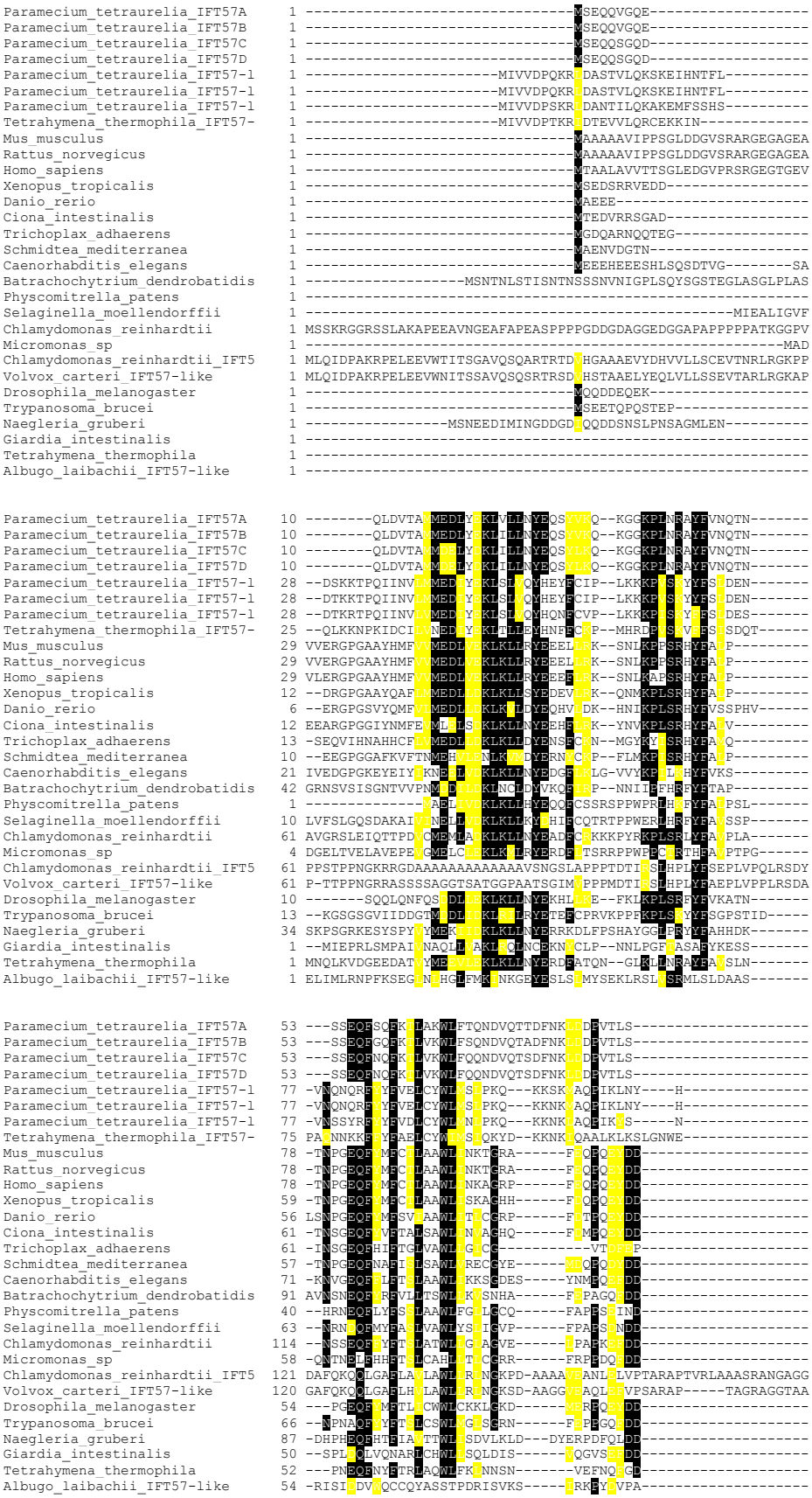
Paramecium_tetraurelia_IFT57A
Paramecium_tetraurelia_IFT57B
Paramecium_tetraurelia_IFT57C
Paramecium_tetraurelia_IFT57D
Paramecium_tetraurelia_IFT57-1
Paramecium_tetraurelia_IFT57-1
Paramecium_tetraurelia_IFT57-1
Tetrahymena_thermophila_IFT57-
Mus_musculus
Rattus_norvegicus
Homo_sapiens
Xenopus_tropicalis
Danio_rerio
Ciona_intestinalis
Trichoplax_adhaerens
Schmidtea_mediterranea
Caenorhabditis_elegans
Batrachochytrium_dendrobatidis
Physcomitrella_patens
Selaginella_moellendorffii
Chlamydomonas_reinhardtii
Micromonas_sp
Chlamydomonas_reinhardtii_IFT5
Volvox_carteri_IFT57-like
Drosophila_melanogaster
Trypanosoma_brucei
Naegleria_gruberi
Giardia_intestinalis
Tetrahymena_thermophila
Albugo_laibachii_IFT57-like

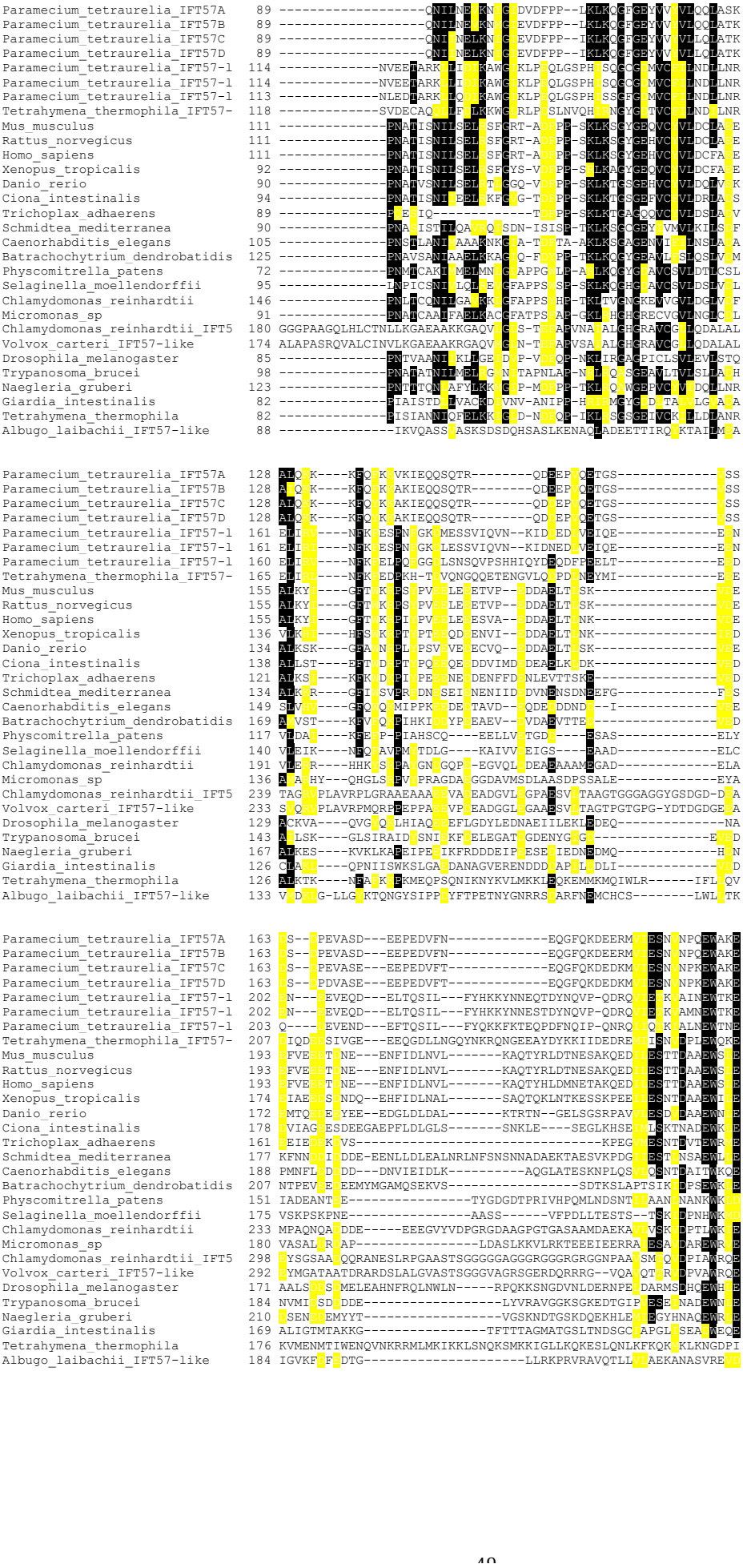
Paramecium_tetraurelia_IFT57A
Paramecium_tetraurelia_IFT57B
Paramecium_tetraurelia_IFT57C
Paramecium_tetraurelia_IFT57D
Paramecium_tetraurelia_IFT57-l
Paramecium_tetraurelia_IFT57-l
Paramecium_tetraurelia_IFT57-l
Tetrahymena_thermophila_IFT57-
Mus_musculus
Rattus_norvegicus
Homo_sapiens
Xenopus_tropicalis
Danio_rerio
Ciona_intestinalis
Trichoplax_adhaerens
Schmidtea_mediterranea
Caenorhabditis_elegans
Batrachochytrium_dendrobatidis
Physcomitrella_patens
Selaginella_moellendorffii
Chlamydomonas_reinhardtii
Micromonas_sp
Chlamydomonas_reinhardtii_IFT5
Volvox_carteri_IFT57-like
Drosophila_melanogaster
Trypanosoma_brucei
Naegleria_gruberi
Giardia_intestinalis
Tetrahymena_thermophila
Albugo_laibachii_IFT57-like

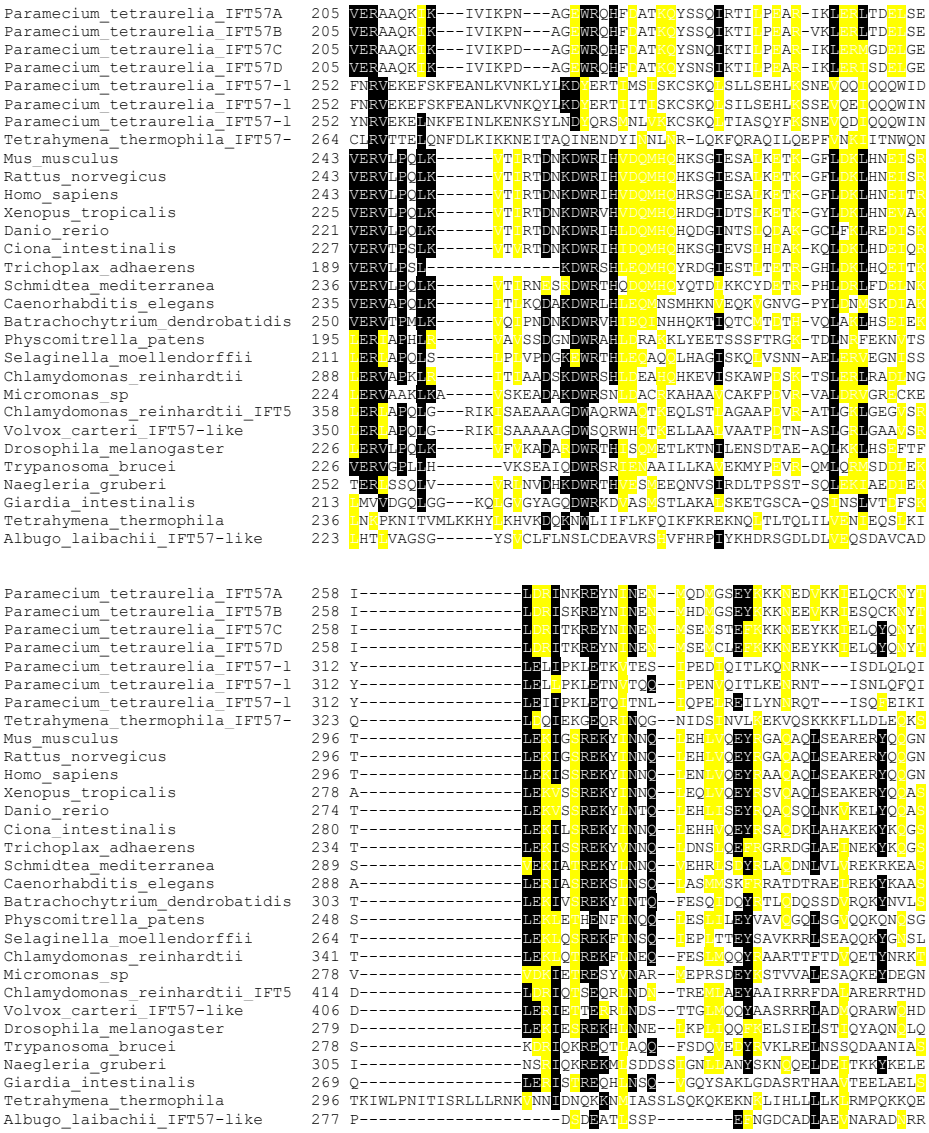
Paramecium_tetraurelia_IFT57A 205
Paramecium_tetraurelia_IFT57B 205
Paramecium_tetraurelia_IFT57C 205
Paramecium_tetraurelia_IFT57D 205
Paramecium_tetraurelia_IFT57-l 252
Paramecium_tetraurelia_IFT57-l 252
Paramecium_tetraurelia_IFT57-l 252
Tetrahymena_thermophila_IFT57- 264
Mus_musculus 243
Rattus_norvegicus 243
Homo_sapiens 243
Xenopus_tropicalis 225
Danio_rerio 221
Ciona_intestinalis 227
Trichoplax_adhaerens 189
Schmidtea_mediterranea 236
Caenorhabditis_elegans 235
Batrachochytrium_dendrobatidis 250
Physcomitrella_patens 195
Selaginella_moellendorffii 211
Chlamydomonas_reinhardtii 288
Micromonas_sp 224
Chlamydomonas_reinhardtii_IFT5 358
Volvox_carteri_IFT57-like 350
Drosophila_melanogaster 226
Trypanosoma_brucei 226
Naegleria_gruberi 252
Giardia_intestinalis 213
Tetrahymena_thermophila 236
Albugo_laibachii_IFT57-like 223
Paramecium_tetraurelia_IFT57A 258
Paramecium_tetraurelia_IFT57B 258
Paramecium_tetraurelia_IFT57C 258
Paramecium_tetraurelia_IFT57D 258
Paramecium_tetraurelia_IFT57-l 312
Paramecium_tetraurelia_IFT57-l 312
Paramecium_tetraurelia_IFT57-l 312
Tetrahymena_thermophila_IFT57- 323
Mus_musculus 296
Rattus_norvegicus 296
Homo_sapiens 296
Xenopus_tropicalis 278
Danio_rerio 274
Ciona_intestinalis 280
Trichoplax_adhaerens 234
Schmidtea_mediterranea 289
Caenorhabditis_elegans 288
Batrachochytrium_dendrobatidis 303
Physcomitrella_patens 248
Selaginella_moellendorffii 264
Chlamydomonas_reinhardtii 341
Micromonas_sp 278
Chlamydomonas_reinhardtii_IFT5 414
Volvox_carteri_IFT57-like 406
Drosophila_melanogaster 279
Trypanosoma_brucei 278
Naegleria_gruberi 305
Giardia_intestinalis 269
Tetrahymena_thermophila 296
Albugo_laibachii_IFT57-like 277
Paramecium_tetraurelia_IFT57A 299
Paramecium_tetraurelia_IFT57B 299
Paramecium_tetraurelia_IFT57C 299
Paramecium_tetraurelia_IFT57D 299
Paramecium_tetraurelia_IFT57-l 350
Paramecium_tetraurelia_IFT57-l 350
Paramecium_tetraurelia_IFT57-l 350
Tetrahymena_thermophila_IFT57- 364
Mus_musculus 337
Rattus_norvegicus 337
Homo_sapiens 337
Xenopus_tropicalis 319
Danio_rerio 315
Ciona_intestinalis 321
Trichoplax_adhaerens 275
Schmidtea_mediterranea 330
Caenorhabditis_elegans 329
Batrachochytrium_dendrobatidis 344
Physcomitrella_patens 289
Selaginella_moellendorffii 305
Chlamydomonas_reinhardtii 382
Micromonas_sp 319
Chlamydomonas_reinhardtii_IFT5 455
Volvox_carteri_IFT57-like 447
Drosophila_melanogaster 320
Trypanosoma_brucei 319
Naegleria_gruberi 348
Giardia_intestinalis 310
Tetrahymena_thermophila 356
Albugo_laibachii_IFT57-like 308

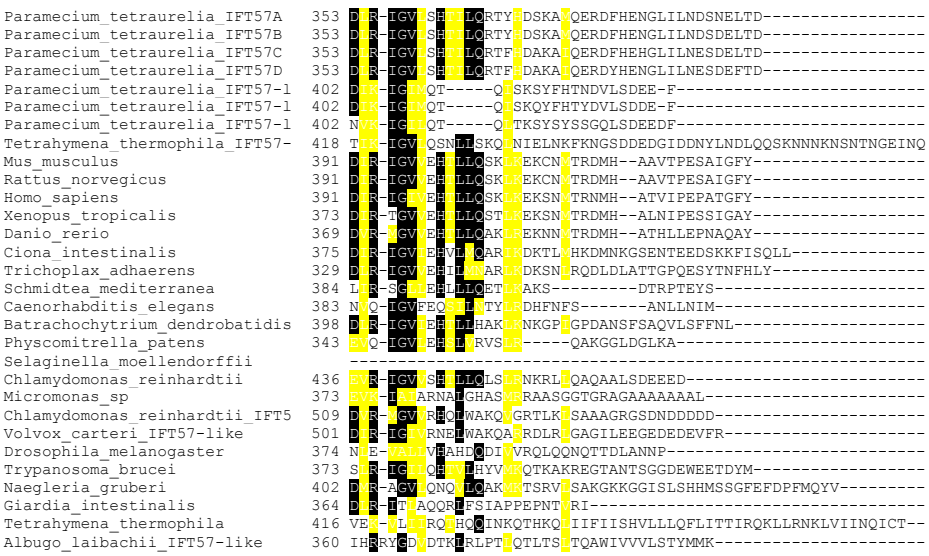

Figure 1-6. Alignment of IFT57-domain-containing proteins.

To see whether the IFT57 genes were related to ciliary function in *Paramecium*, we looked in ParameciumDB for the presence of peptides in the ciliary proteome and for expression changes during ciliary growth, at early stage (30 minutes after deciliation: EARLY-T0) and at late stage (120 minutes after deciliation (LATE-T0). As shown in the table below, one peptide was detected for IFT57A and B, and a weak increase of expression during ciliogenesis for IFT57C and D (Table 1-2).

Locus Symbol	Synonym	Number of different peptides in cilia	Fold Change (reciliation EARLY-T0)	False Discovery Rate (reciliation EARLY-T0)	Fold Change (reciliation LATE-T0)	False Discovery Rate (reciliation LATE-T0)
GSPATG00023787001	IFT57A	**1**	1,05	*0,97*	1,69	*0,14*
GSPATG00033566001	IFT57B	**1**	1,30	*0,75*	1,75	*0,19*
GSPATG00034629001	IFT57C	0	1,54	*0,43*	**2,25**	***0,05***
GSPATG00035574001	IFT57D	0	**3,16**	***0,01***	**3,85**	***0,01***

Table 1-2. Raw data concerning IFT57 genes in proteomics of cilia and messenger expression during reciliation*. Data extracted from ParameciumDB.*

Although at the limit of significance, these observations suggest that IFT57 proteins are indeed involved in ciliary function in *Paramecium*.

We also analyzed the expression of IFT57 genes during autogamy, data from microarray experiments (Arnaiz et al. 2010), as reported in ParameciumDB. No change appeared for any of the four genes during the course of autogamy.

1.3. IFT46 (synonyms: DYF-6; FAP32)

A single IFT46 gene (GSPATG00024708001) is found in the *Paramecium* genome. InterPro scanning revealed that IFT46 is a single domain by itself (Fig. 1-7), and that this domain is found only in IFT46 proteins (in contrast to the situation we described for IFT57).

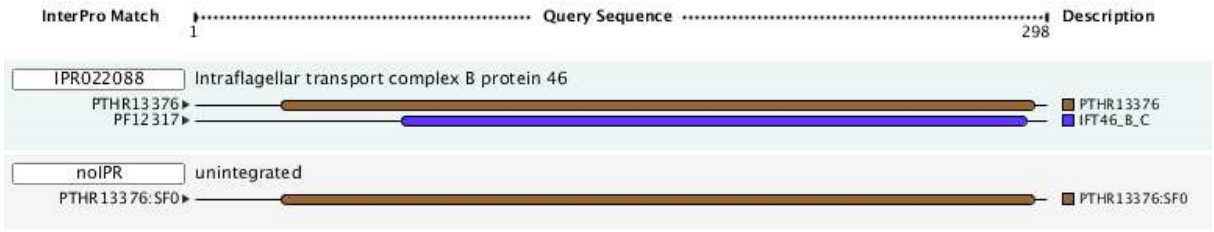

Figure 1-7. Interpro domain match obtained by scanning the IFT46 gene of Paramecium.

The alignment of IFT46 proteins of various species shows that they are highly conserved through evolution, including in *Paramecium* (Fig. 1-8).

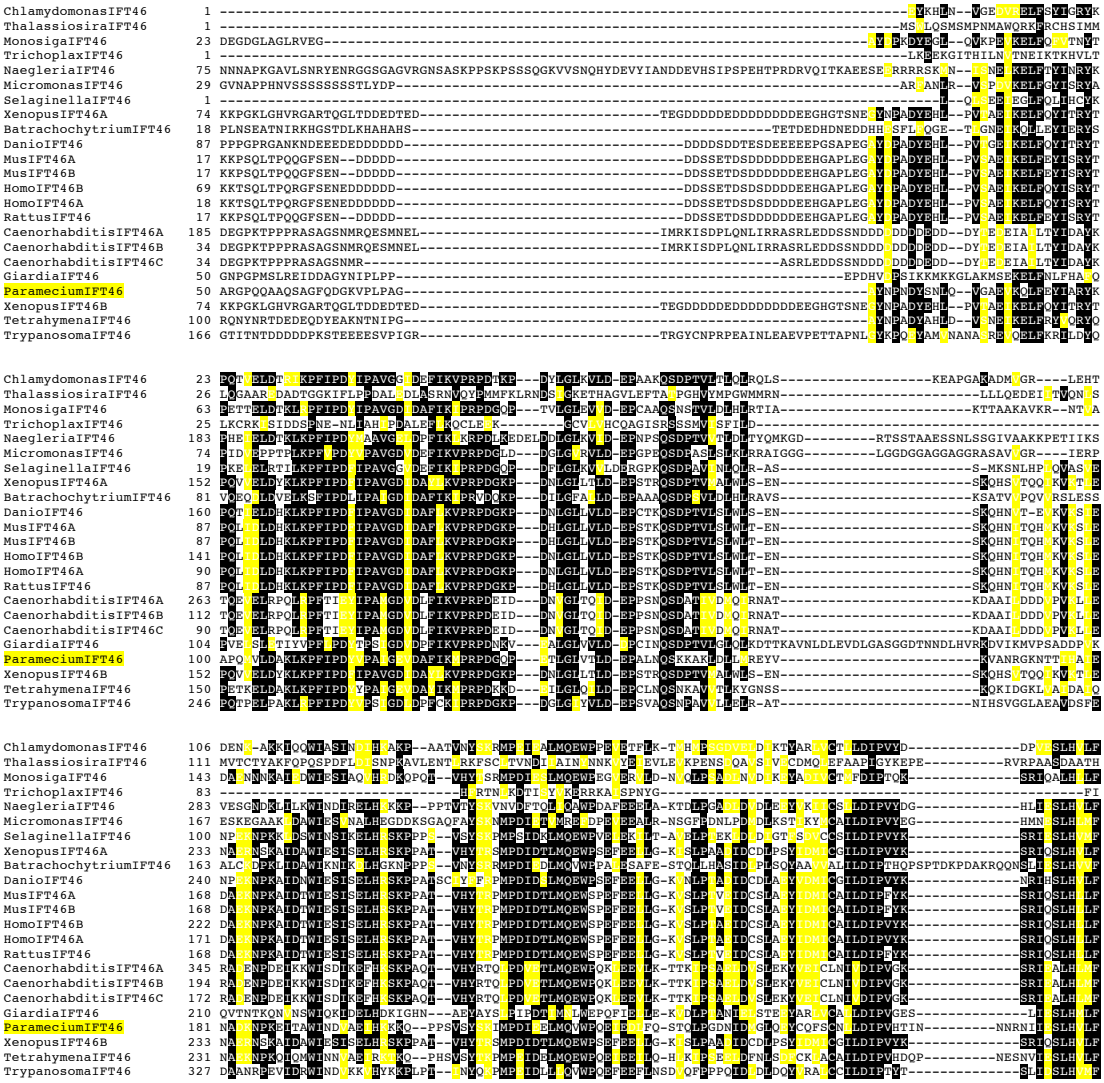

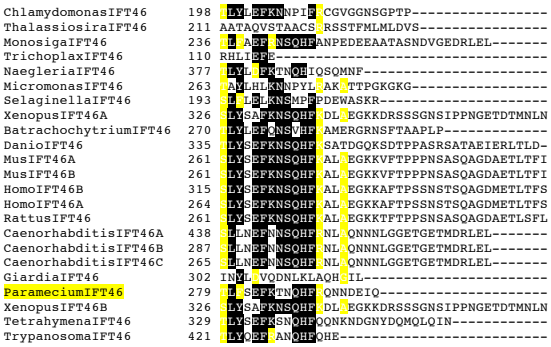

Figure 1-8. Alignment of IFT46-domain-containing proteins.

Post genomic analyses show only little evidence for a ciliary role, with a single peptide found in the ciliary proteomics. This probably means that IFT46 is not very abundant in cilia (Table 1-3).

Locus Symbol	Synonym	Number of different peptides in cilia	Fold Change (reciliation EARLY-T0)	False Discovery Rate (reciliation EARLY-T0)	Fold Change (reciliation LATE-T0)	False Discovery Rate (reciliation LATE-T0)
GSPATG00024708001	IFT46	**1**	1,26	*0,79*	1,93	*0,11*

Table 1-3. Raw data concerning the IFT46 gene in proteomics of cilia and messenger expression during reciliation*. Data extracted from ParameciumDB.*

1.4. IFT139 (synonym: FAP60)

IFT139 matches two ohnolog genes issued from the last genome duplication in *Paramecium*, GSPATG00011236001 and GSPATG00011426001 called IFT139A and B respectively (Fig. 1-9). They are sharing 95.1% identity in nucleotide and 91.7% identity in aminoacid sequence.

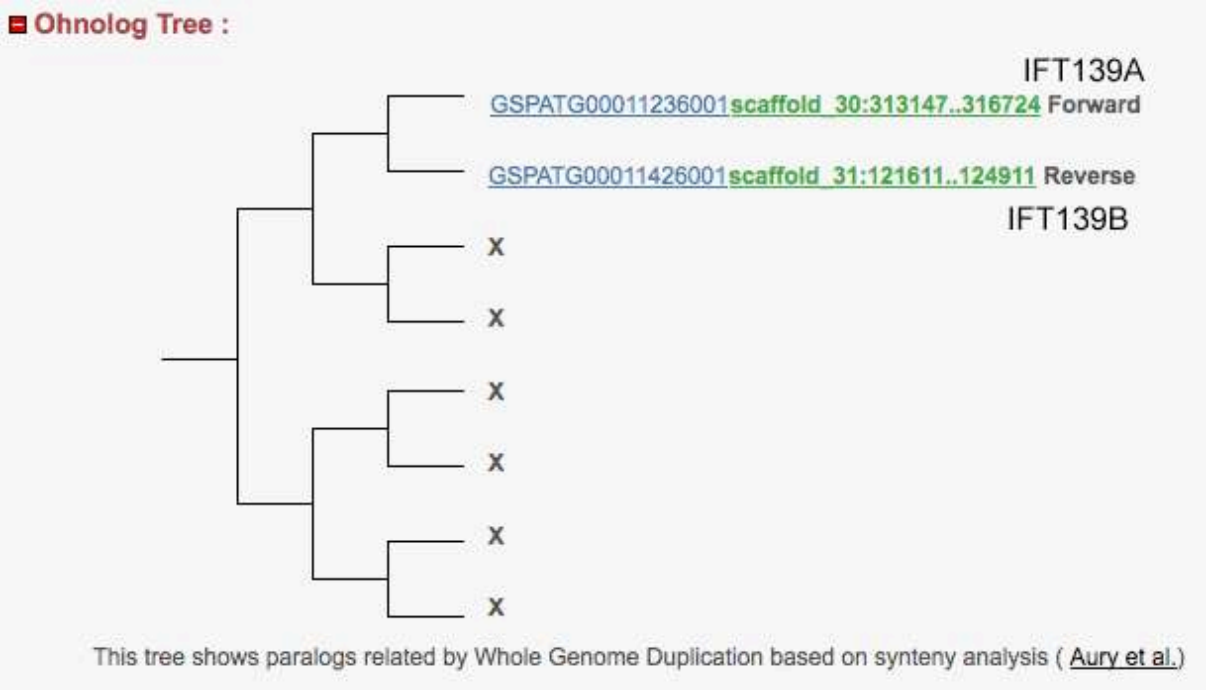

Figure 1-9. Ohnolog tree of IFT139 genes in Paramecium*. Adapted from a screenshot of ParameciumDB*

The InterproScan analysis revealed that the main domain of this IFT139 is a Tetratricopeptide domain, found in many proteins and supposed to be involved in protein-protein interactions (Fig. 1-10).

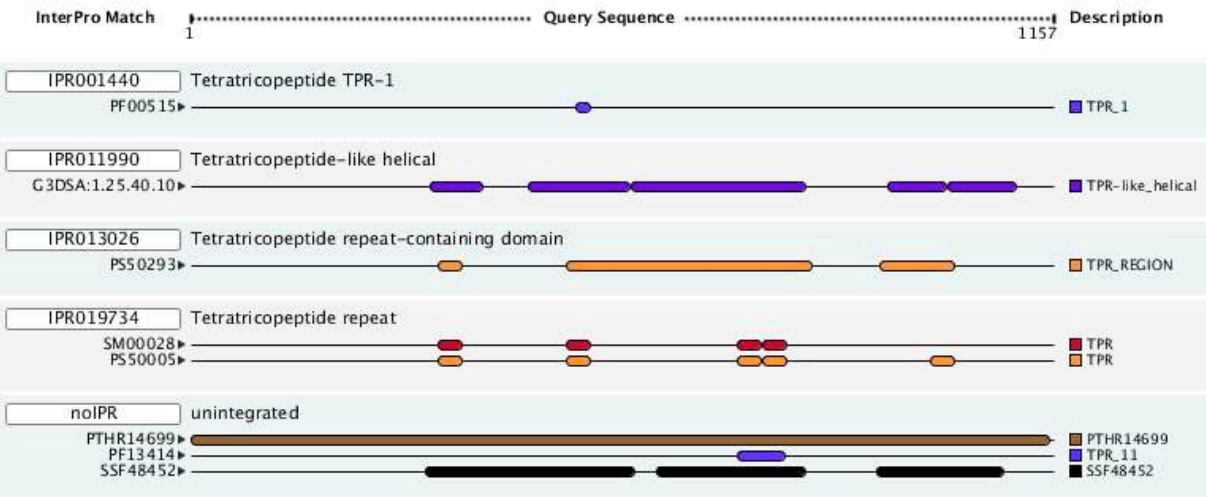

Figure 1-10. Interpro domain match obtained by scanning the IFT139 genes of Paramecium.

Alignment of IFT139 proteins showing the sequence conservation through evolution (Fig. 1-11):

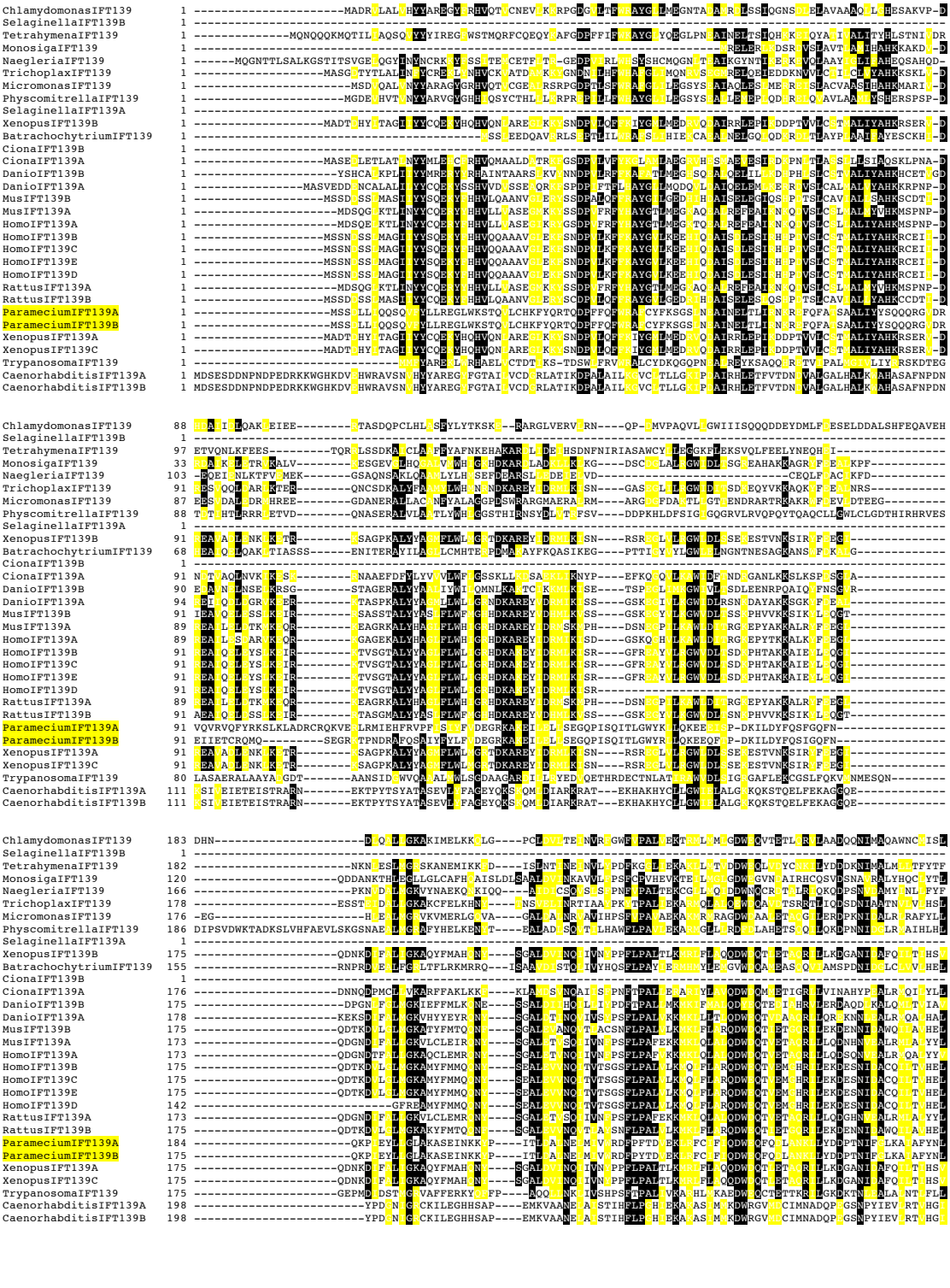

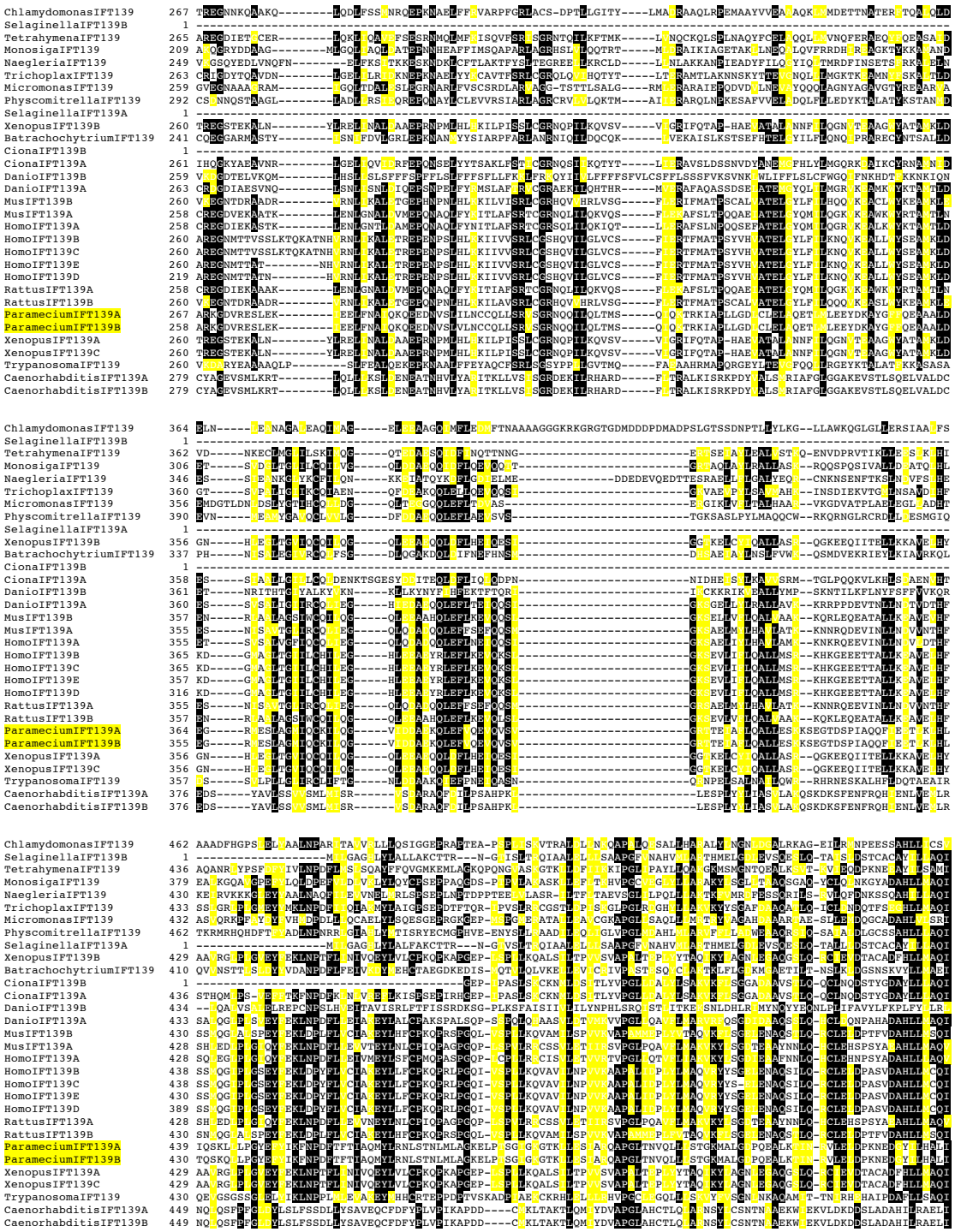

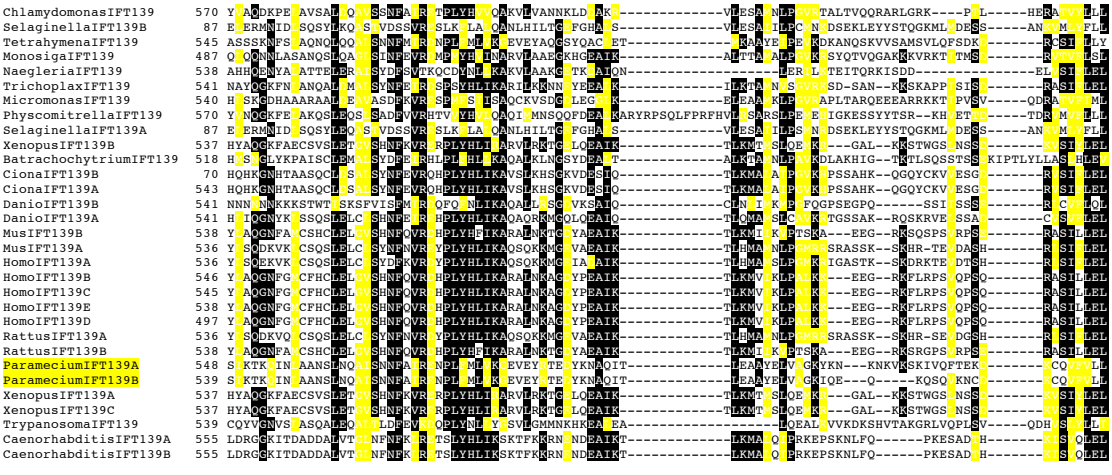

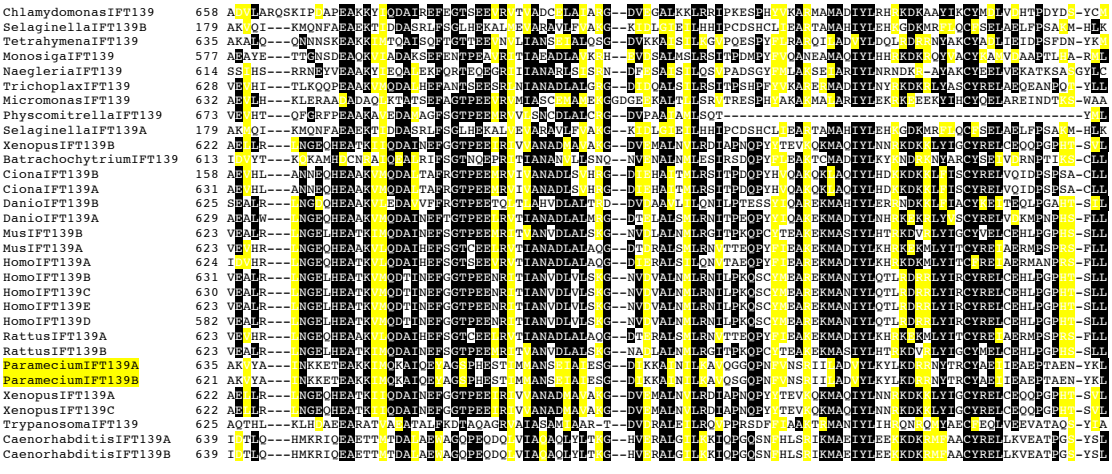

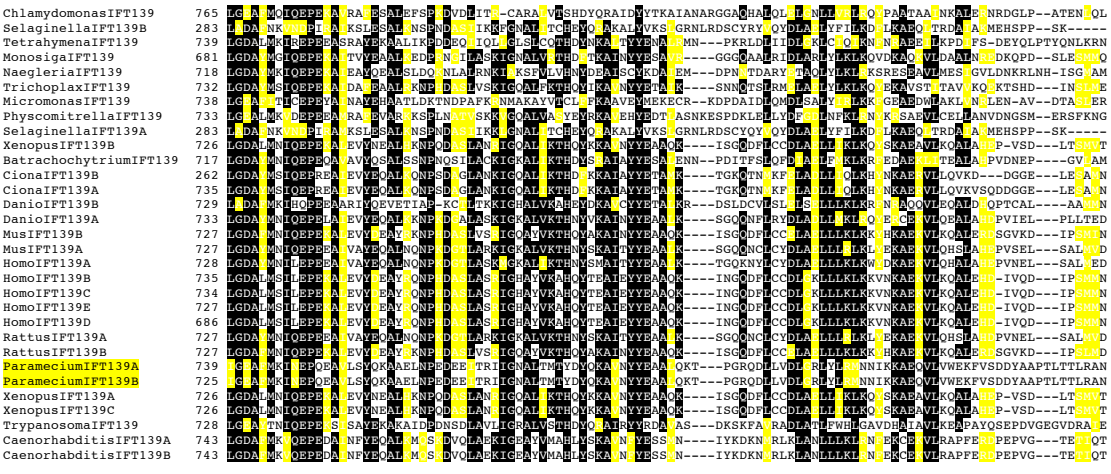

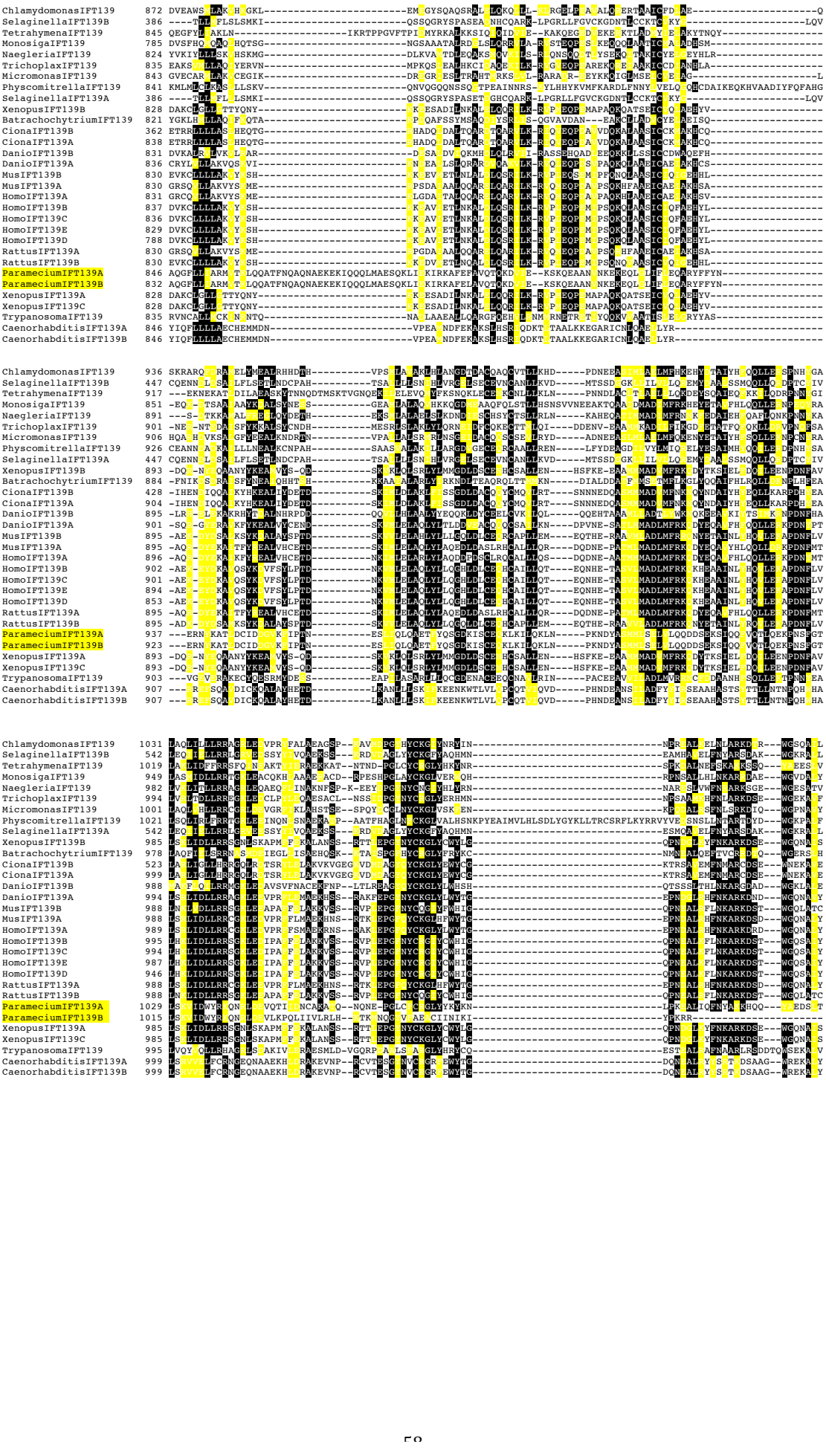
ChlamydomonasIFT139
SelaginellaIFT139B
TetrahymenaIFT139
MonosigaIFT139
NaegleriaIFT139
TrichoplaxIFT139
MicromonasIFT139
PhyscomitrellaIFT139
SelaginellaIFT139A
XenopusIFT139B
BatrachochytriumIFT139
CionaIFT139B
CionaIFT139A
DanioIFT139B
DanioIFT139A
MusIFT139B
MusIFT139A
HomoIFT139A
HomoIFT139B
HomoIFT139C
HomoIFT139E
HomoIFT139D
RattusIFT139A
RattusIFT139B
ParameciumIFT139A
ParameciumIFT139B
XenopusIFT139A
XenopusIFT139C
TrypanosomaIFT139
CaenorhabditisIFT139A
CaenorhabditisIFT139B

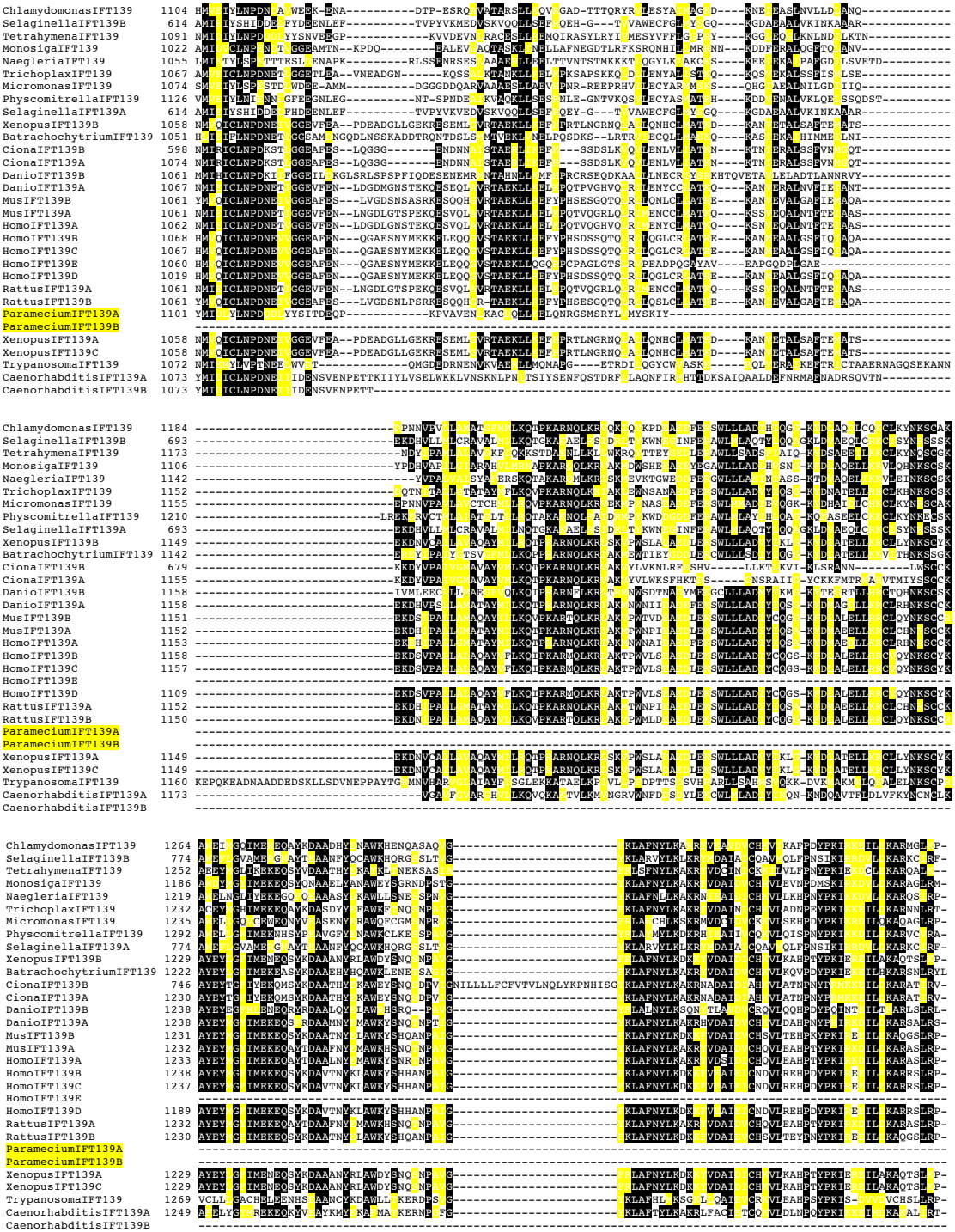

Figure 1-11. Alignment of IFT139-domain-containing proteins.

Post genomic analyses show that 9 peptides of the IFT139 protein can be identified in the ciliary proteomics, an indication of a strong abundance in the cilia, and that a weak upregulation of the genes occurs at late stages after deciliation (Table 1-4).

Locus Symbol	Synonym	Number of different peptides in cilia	Fold Change (reciliation EARLY-T0)	False Discovery Rate (reciliation EARLY-T0)	Fold Change (reciliation LATE-T0)	False Discovery Rate (reciliation LATE-T0)
GSPATG00011236001	IFT139A	**9**	1,86	*0,38*	**2,74**	*0,06*
GSPATG00011426001	IFT139B	**9**	1,74	*0,52*	2,42	*0,13*

Table 1-4. Raw data concerning IFT139 genes in proteomics of cilia and messenger expression during reciliation. *Data extracted from ParameciumDB.*

1.5. IFT172 (synonym: OSM-1)

Three *Paramecium* gene models are detected by BLAST for a IFT172 query. One of them (GSPATG00013914001) matches the full length of IFT172, and is called IFT172A. The two other ones are adjacent gene models (GSPATG00033190001 and GSPATG00033191001) matching each a different part of the molecule, indicating that the annotation split the gene into two. Manual re-annotation with correction of the assembly sequence permitted to build the actual IFT172B gene as PTETG13500002001, the true ohnolog of IFT172A (Fig. 1-12). Since the automatic downstream calculations use only the automatic annotation, the curated gene does not appear in the ohnolog tree nor in the post genomic analyses. They are sharing 94.8% identity in nucleotide and 97.7% identity in aminoacid sequence

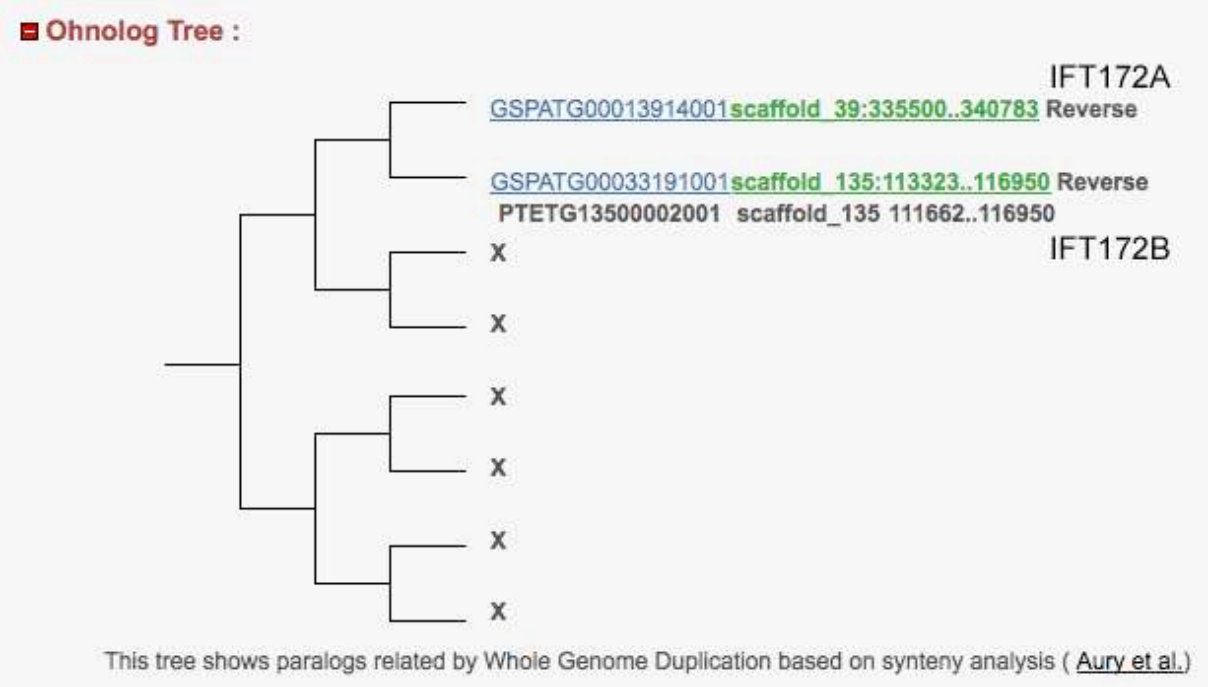

Figure 1-12. Ohnolog tree of IFT172 genes in Paramecium. Adapted from a screenshot of ParameciumDB

The InterproScan analysis revealed that the main domain of this IFT172 is a WD40 repeat domain, found in many proteins and supposed to be involved in protein-protein interactions (Fig. 1-13).

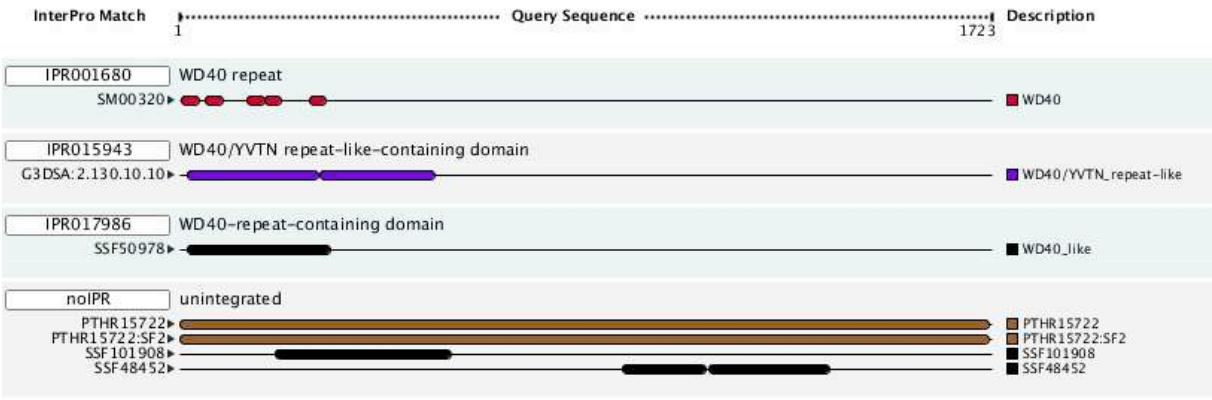

Figure 1-13. Interpro domain match obtained by scanning the IFT172 genes of Paramecium.

Alignment of IFT172 proteins showing the sequence conservation through evolution (Fig. 1-14).

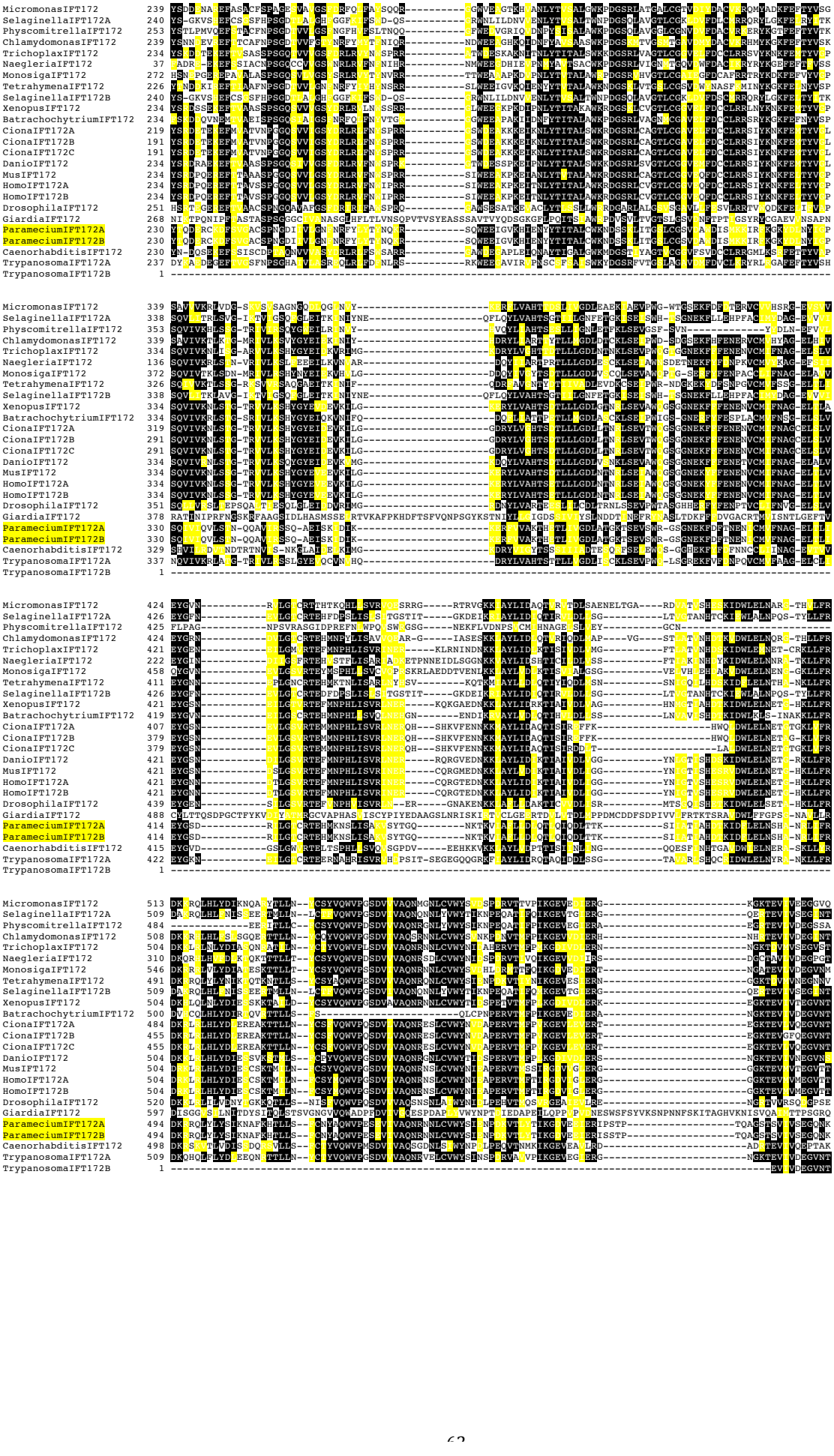
MicromonasIFT172
SelaginellaIFT172A
PhyscomitrellaIFT172
ChlamydomonasIFT172
TrichoplaxIFT172
NaegleriaIFT172
MonosigaIFT172
TetrahymenaIFT172
SelaginellaIFT172B
XenopusIFT172
BatrachochytriumIFT172
CionaIFT172A
CionaIFT172B
CionaIFT172C
DanioIFT172
MusIFT172
HomoIFT172A
HomoIFT172B
DrosophilaIFT172
GiardiaIFT172
ParameciumIFT172A
ParameciumIFT172B
CaenorhabditisIFT172
TrypanosomaIFT172A
TrypanosomaIFT172B

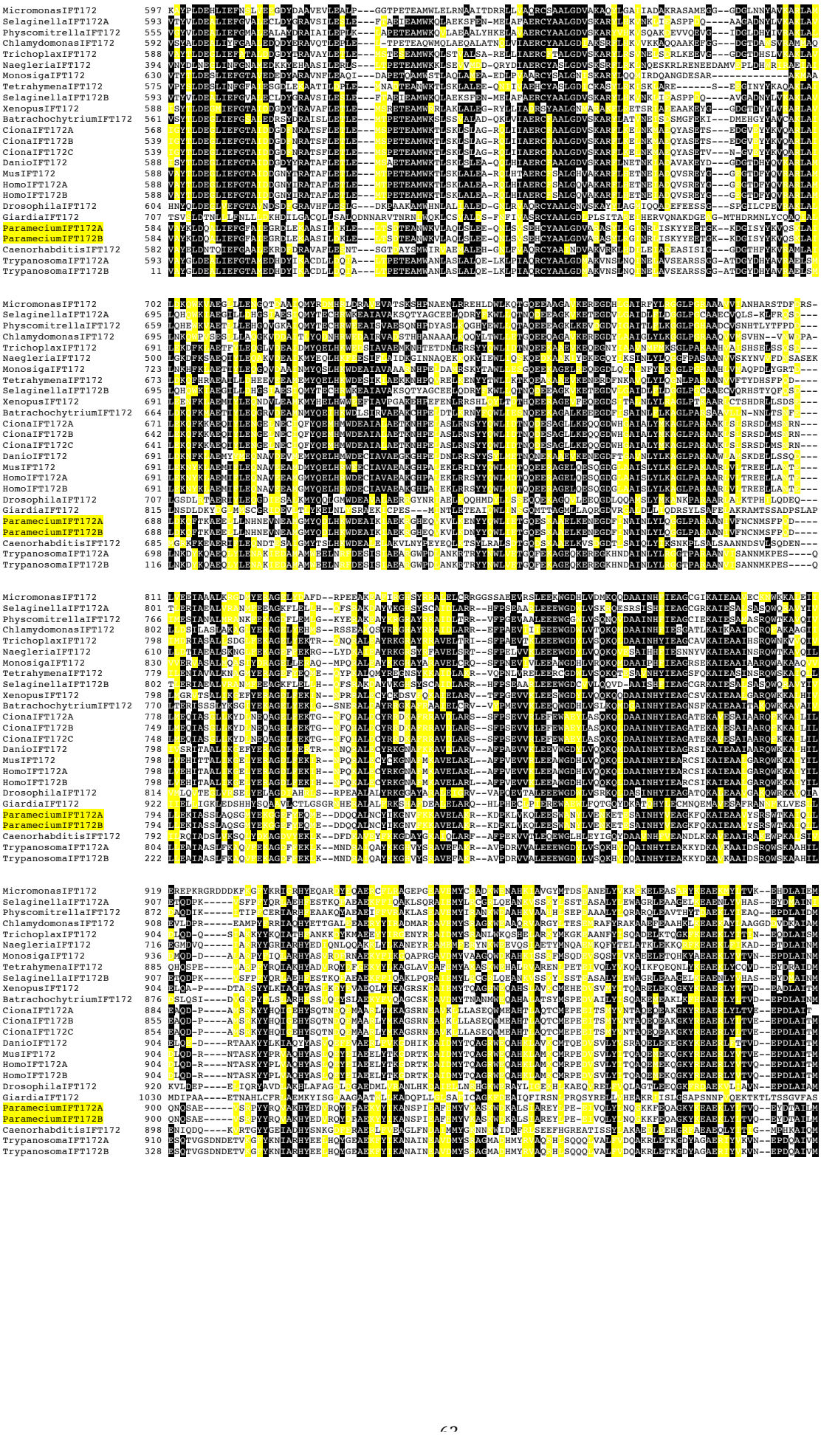

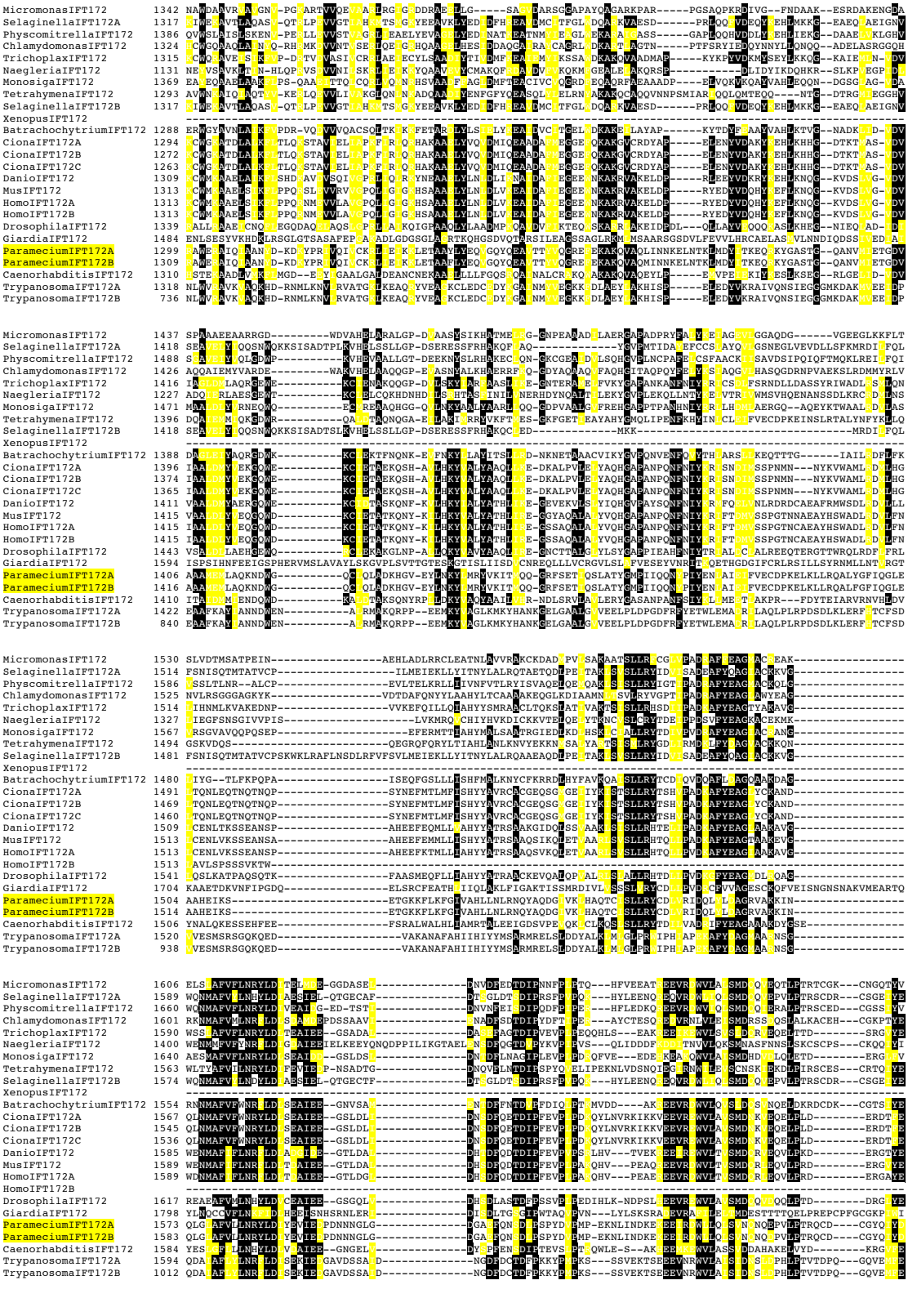

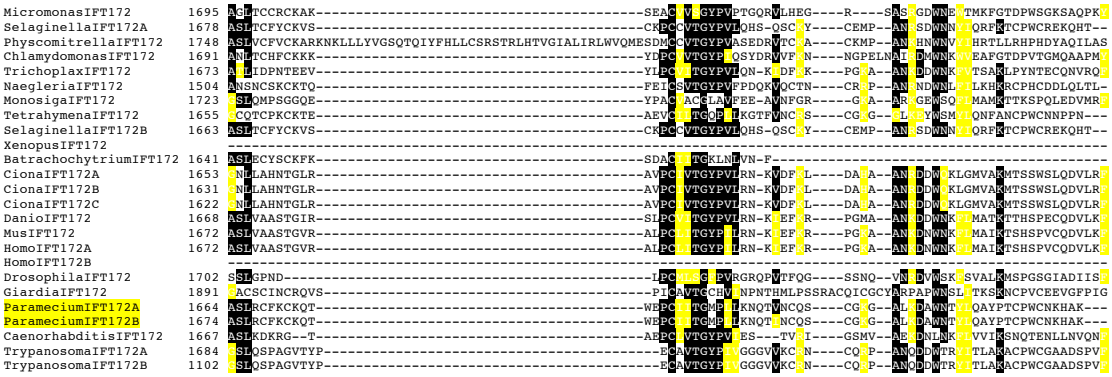

Figure 1-14. Alignment of IFT172-domain-containing proteins.

Post genomic analyses show that at least 2 peptides of the IFT172A and B proteins can be identified in the ciliary proteomics, an indication of a its presence in cilia, and that a weak upregulation of the genes occurs at late stages after deciliation (Table 1-5).

Locus Symbol	Synonym	Number of different peptides in cilia	Fold Change (reciliation EARLY-T0)	False Discovery Rate (reciliation EARLY-T0)	Fold Change (reciliation LATE-T0)	False Discovery Rate (reciliation LATE-T0)
GSPATG00013914001	IFT172A	**2**	1,44	*0,72*	2,50	*0,08*
GSPATG00033190001	IFT172B1	**2**	1,58	*0,54*	**2,54**	*0,06*
GSPATG00033191001	IFT172B2	**1**	1,23	*0,93*	1,88	*0,47*

Table 1-5. Raw data concerning IFT172 genes in proteomics of cilia and messenger expression during reciliation. *Data extracted from ParameciumDB.*

1.6. Qilin (synonyms: CLUAP1; DYF-3; FAP22)

Four ohnologs, GSPATG00001872001, GSPATG00017664001, GSPATG00005213001 and GSPATG00009204001, called respectively qilinA to D, were identified in the *Paramecium* genome (Fig. 1-15).

a

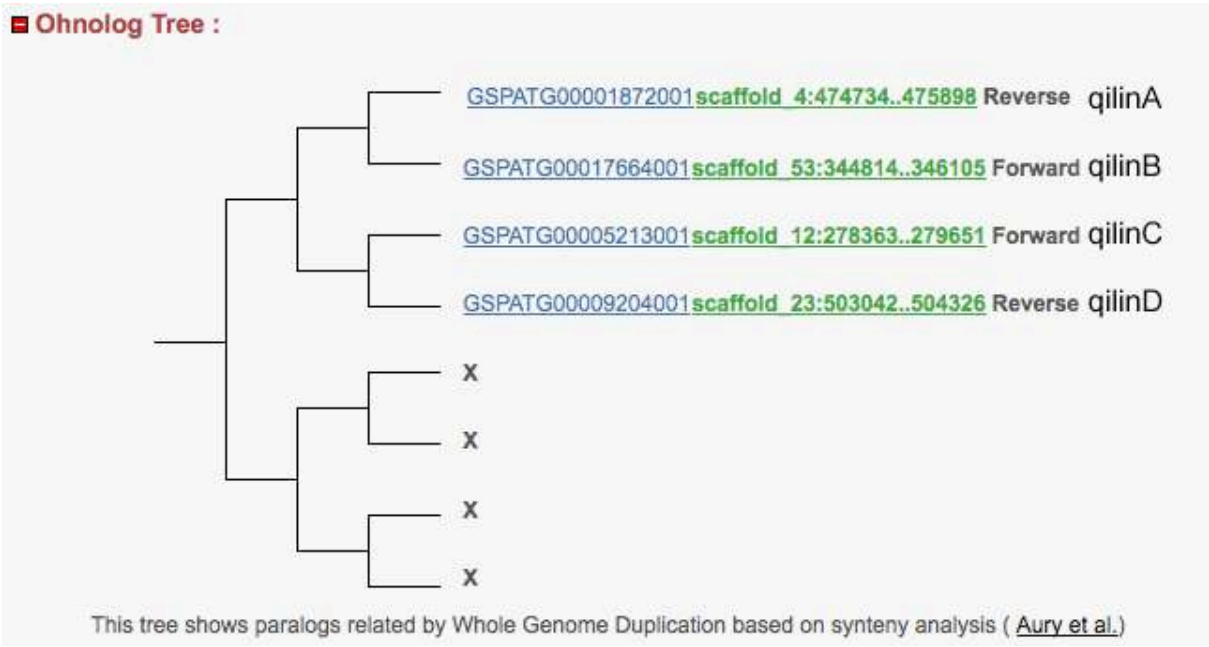

b

Nucleotide identity

Qilin	A	B	C	D
A	100	76.7	70.3	67.6
B	73.2	100	74.2	71.8
C	71.1	82.5	100	83.6
D	64.7	76.4	82.2	100

Protein identity

Figure 1-15.a: Ohnolog tree of qilin genes of paramecium, b: protein and nucleotide identity between four qilin in Paramecium. *Adapted from ParameciumDB*

InterPro scanning revealed that qilin is a single domain by itself, and that this domain is found only in qilins (Fig. 1-16).

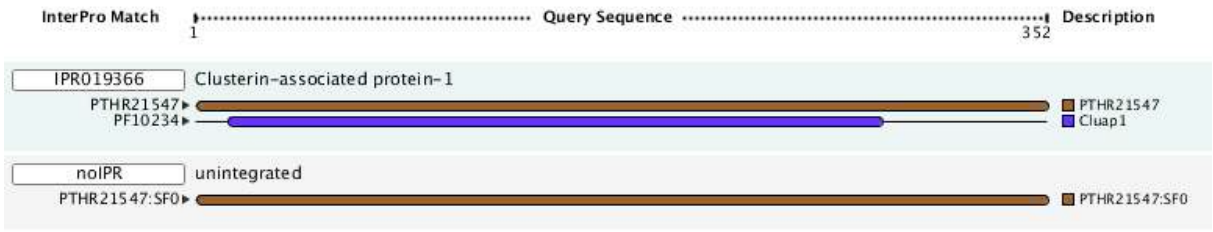

Figure 1-16. Interpro domain match obtained by scanning the qilin genes of Paramecium.

Evolutionary tree of qilins (Fig. 1-17):

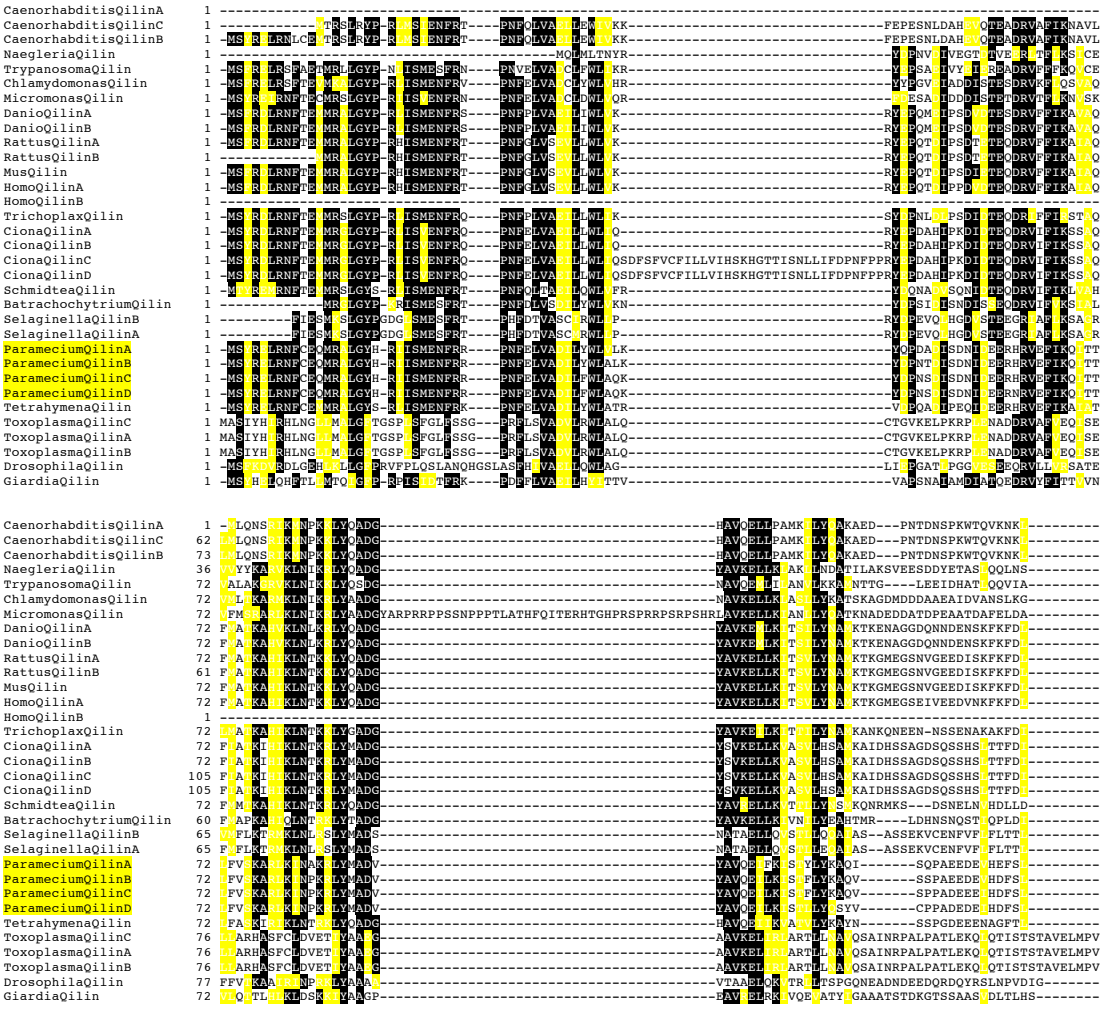

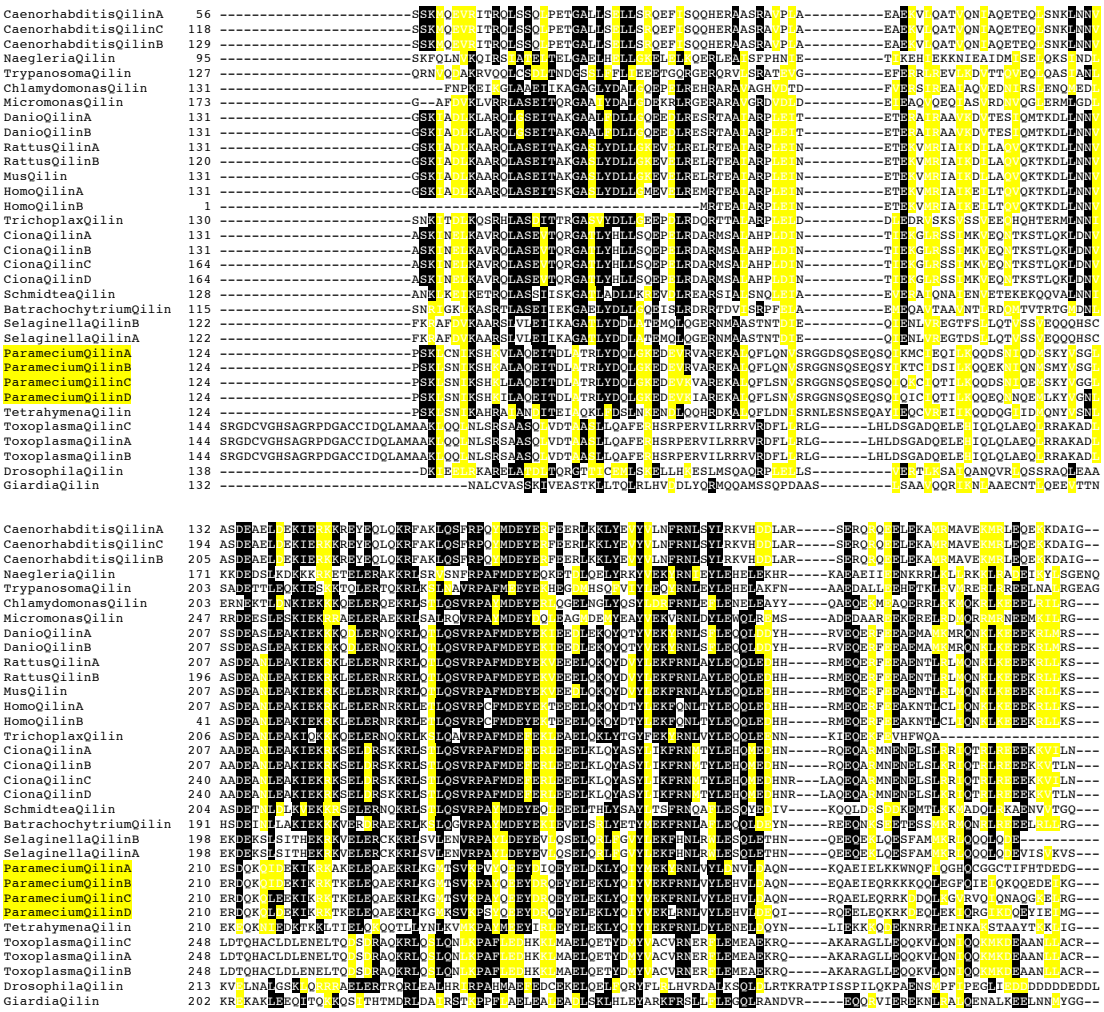

Figure 1-17. Alignment of qilin-domain-containing proteins.

Post genomic analyses show that 2 peptides of the qilinC protein can be identified in the ciliary proteomics and that a weak up-regulation of the qilinA occurs at early stages after deciliation. This indicates a likely presence of qilin in cilia (Table 1-5).

Locus Symbol	Synonym	Number of different peptides in cilia	Fold Change (reciliation EARLY-T0)	False Discovery Rate (reciliation EARLY-T0)	Fold Change (reciliation LATE-T0)	False Discovery Rate (reciliation LATE-T0)
GSPATG00001872001	qilinA	0	**1,96**	***0,04***	1,55	*0,16*
GSPATG00017664001	qilinB	0	0,99	*1,00*	1,07	*0,89*
GSPATG00005213001	qilinC	**2**	1,45	*0,40*	1,83	*0,07*
GSPATG00009204001	qilinD	0	1,71	*0,54*	2,80	*0,08*

Table 1-5. Raw data concerning qilin genes in proteomics of cilia and messenger expression during reciliation. *Data extracted from ParameciumDB.*

A weak increase in qilinA expression was also observed during autogamy compared to vegetative cells.

Conclusion

My main subject on the localization and function of IFT57 will use some molecular tools in the form of other IFT proteins. From overall analyses, these IFT genes appear to be highly conserved in *Paramecium* so that we can attempt to extrapolate biological data obtained in this organism to other systems.

CHAPTER 2

IFT57 IN CILIOGENESIS

PART 2.1. LOCALIZATION STUDY OF IFT57

To study the cellular localization of IFT57 proteins in *Paramecium*, I analyzed the fluorescence in transformed cells expressing IFT57-GFP fusion proteins under control of their endogenous regulator 5' and 3' intergenic regions. Among the four genes arising from genome duplications, I focused on IFT57A and IFT57C as representatives of each gene subfamily. I observed the same labeling whatever the regulator used, so that I present here only results with the endogenous regulators (5' promoter and 3' terminator).

2.1.1. Localization of IFT57A-GFP and IFT57C-GFP proteins in vegetative cells

With both IFT57 fusion proteins and during the interphase of the vegetative cycle, the labeling appears as regular dot alignments likely corresponding to basal bodies and as short segments evoking a subset of cilia In addition, a macronuclear labeling was observed for IFT57A-GFP, but not for IFT57C-GFP (Fig. 2-1) I will focus here on the ciliary aspects of the labeling, the phenomenon about the nucleus will be developed in the next chapter.

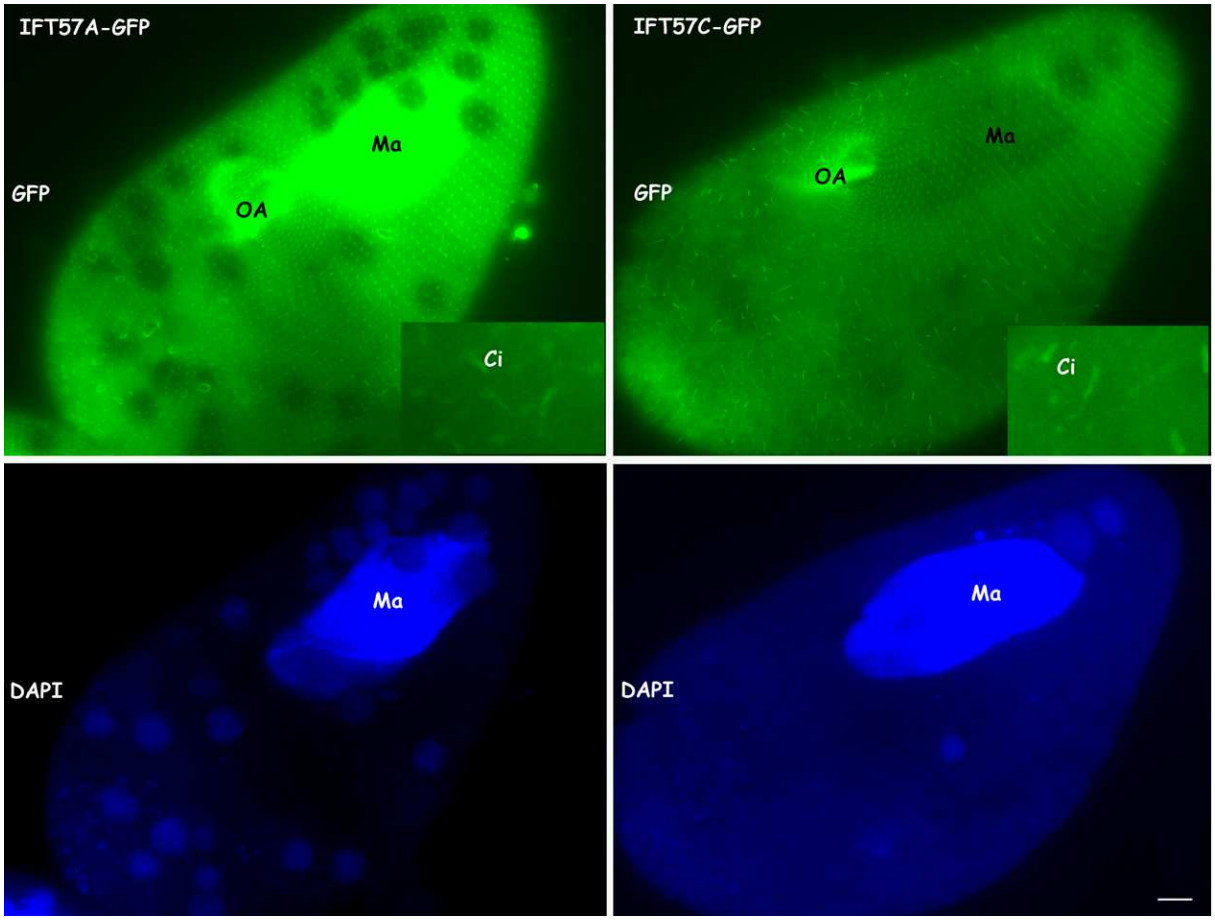

Figure 2-1. Epifluorescence microscopy labeling observed in cells transformed by IFT57A-GFP (left) and IFT57C-GFP (right) after paraformaldehyde fixation*. GFP labeling (top) and DAPI labeling (bottom). Note that the basal bodies are labeled with both fusion proteins and that some short cilia (Ci) can be seen. With IFT57A-GFP, the macronucleus (Ma) appears strongly fluorescent, which is not the case with IFT57C-GFP-labeled cells, in which the macronucleus appears contrasted as dark in the cytoplasm. The stronger fluorescent region seen with both labeling is the oral apparatus (OA), a region dense in basal bodies and cilia. Bar: 10µm.*

In order to confirm the cortical localization of IFT57, I performed immunolabeling on IFT57A-GFP cells with either an antibody directed against *Paramecium* cilia that recognizes polyglycylated tubulin or the anti basal body ID5 monoclonal antibody that recognizes polyglutamylated tubulin). The permeabilization method generally used for immunocytochemistry involve a Triton X100 treatment, but this is too drastic in the case of cells expressing IFT57-GFP and the fluorescent molecules rapidly leak out. To avoid this phenomenon and let the antibody enter the cytoplasm, I used a weak saponin permeabilization, which globally preserves the basal body and ciliary labeling, but however does not prevent some decrease in macronuclear fluorescence (Fig. 2-2).

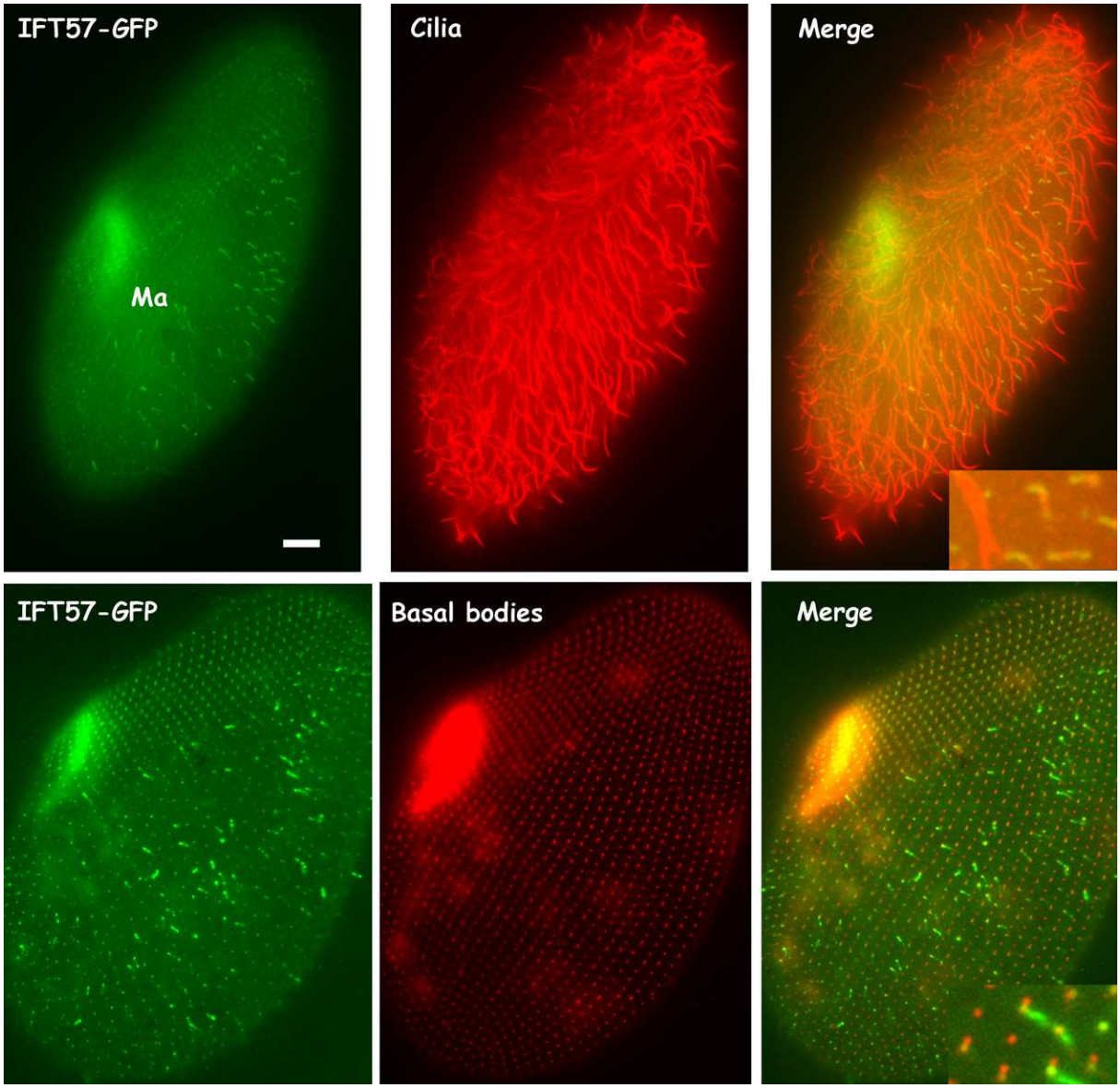

Figure 2-2. Co-localization studies of IFT57A and basal bodies and cilia using ID5 and anti-polyglycylated tubulin antibodies respectively as markers under epifluorescence microscopy*. Top: Short segments of GFP labeling correspond to short, likely growing, cilia, whereas long cilia are not labeled. Bottom: GFP-labeled dots arranged in regular rows correspond to some of the basal bodies. Note that due to permeabilization, the macronucleus (Ma) is only faintly visible in the top cell and not in the bottom one. Bar: 10µm.*

The IFT57-GFP labeling was very visible only on a fraction of cilia, the short ones, likely under growth. The IFT machinery is supposed to have two functions, ciliary biogenesis and ciliary maintenance. Is the absence of labeling in mature cilia an indicator of an active ciliogenesis? In that case, this would mean that IFT57 is involved in ciliogenesis but not in ciliary maintenance. To ascertain the differential localization of IFT57 in steady state and growing cilia, we examined the IFT57-GFP labeling by confocal microscopy (Fig. 2-3)

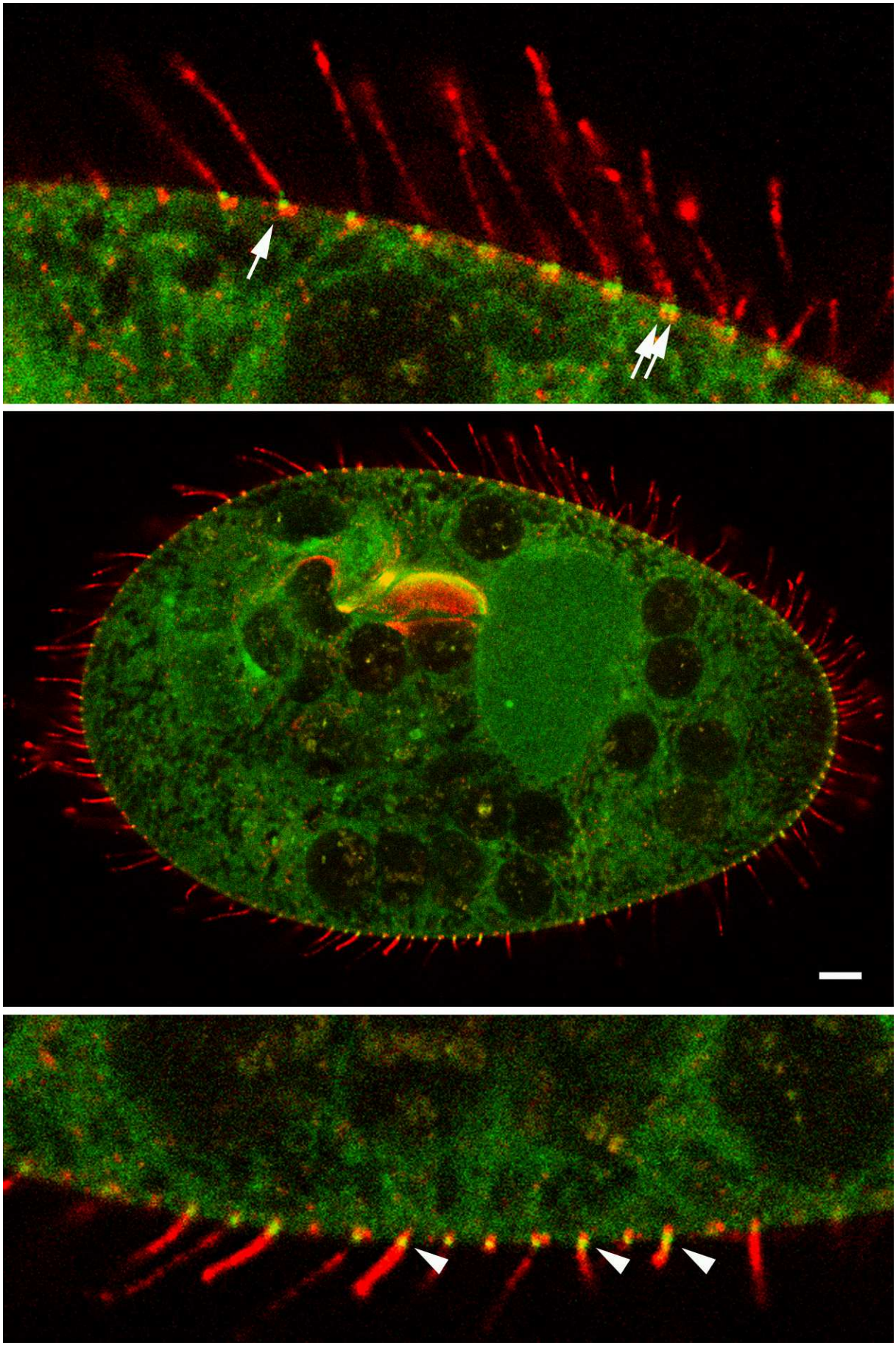

Figure 2-3. Confocal microscopy optical section of an interphase cell expressing IFT57A-GFP. *Cilia are labeled with the anti monoglycylated tubulin monoclonal antibody TPA952 (Callen et al., 1994). Top and bottom are enlarged portions of the middle figure. Arrows point GFP basal body labeling at a distal position, close to the ciliary transition zone. Arrowheads show intra ciliary GFP labeling in short cilia. Bar: 10µm. Photo Anne Aubusson.*

As described in the Introduction (Fig. I-14 and its legend), basal bodies are not homogeneously distributed over the cell surface. Basal bodies can be in pairs (2-bb) or alone (1-bb) in cortical units, and there is a gradient of distribution of 2-bb units versus 1-bb units from the anterior towards the posterior part of the cell. In addition, the two extreme 2-bb unit and 1-bb unit fields at the anterior and the posterior parts of the cells are called invariant fields since their basal body composition do not change over division.
In addition to their non-homogeneity in localization over the cell surface, the basal body can be ciliated or not ciliated (Aubusson-Fleury et al., 2012). Although a thorough study of ciliation during the cell cycle is still to be done, it appears that almost all basal bodies in 1-bb units are ciliated and only one of the two basal bodies in 2-bb units are ciliated, except in the anterior invariant fields where both basal bodies are ciliated. When only one basal body is ciliated, it is always the posterior one, which is the parental basal body.
In IFT57A-GFP expressing cells, the fluorescence exists in some cilia and at the distal part of all basal bodies that are ciliated, be they from 1-bb or 2-bb units.

2.1.2. Localization of IFT57A-GFP in growing cilia

2.1.2.1. Ciliary growth during division

Short cilia labeled all over their length by IFT57-GFP in interphase cells (Fig. 2-2) are likely to correspond to growing cilia. However, we have no direct mean to prove, in interphase, that these short cilia are indeed growing. We therefore checked the IFT57-GFP labeling in two conditions in which we know that cilia are growing: dividing cells (Fig. 2-4, 2-5) and cells recovering cilia after deciliation (Fig. 2-6).

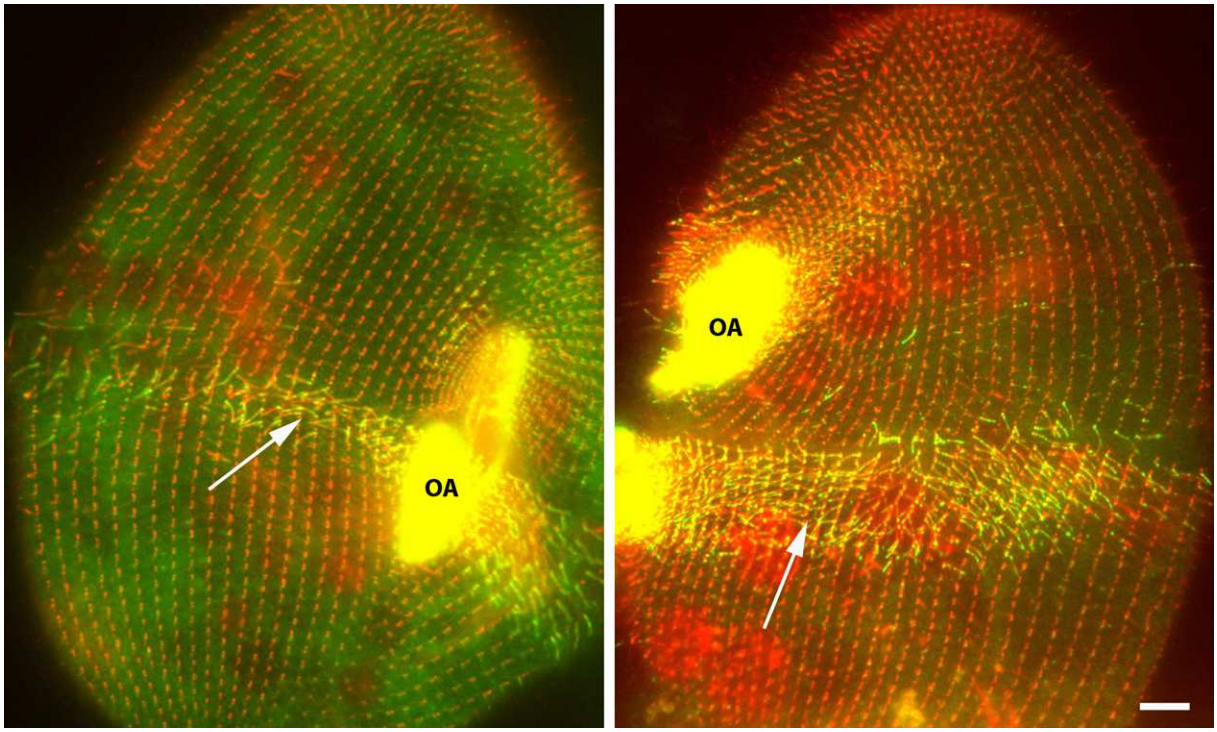

Figure 2-4. Epifluorescence microscopy labeling of dividing cells transformed by IFT57A-GFP after paraformaldehyde fixation. *Top: an early stage in division; bottom: later stages. Highly fluorescent short cilia are clearly seen in regions of active basal body duplication (arrows), as a belt posterior to the fission furrow and in the anterior left field. OA indicates the oral apparatus region, which appears as strongly labeled. Bar: 10µm.*

In dividing cells a zone of active ciliary growth is present at the level of the fission furrow, a zone in which basal bodies actively proliferate (REF). As it can be seen (Fig. 2-4), the fluorescence observed in IFT57A-GFP expressing cells, and identical in IFT57C-GFP (not shown), is in short cilia, predominantly in this zone of active ciliary growth. This is an indication of strong recruitment of IFT57 in growing cilia, as also seen on confocal optical sections of a dividing cell (Fig. 2-5).

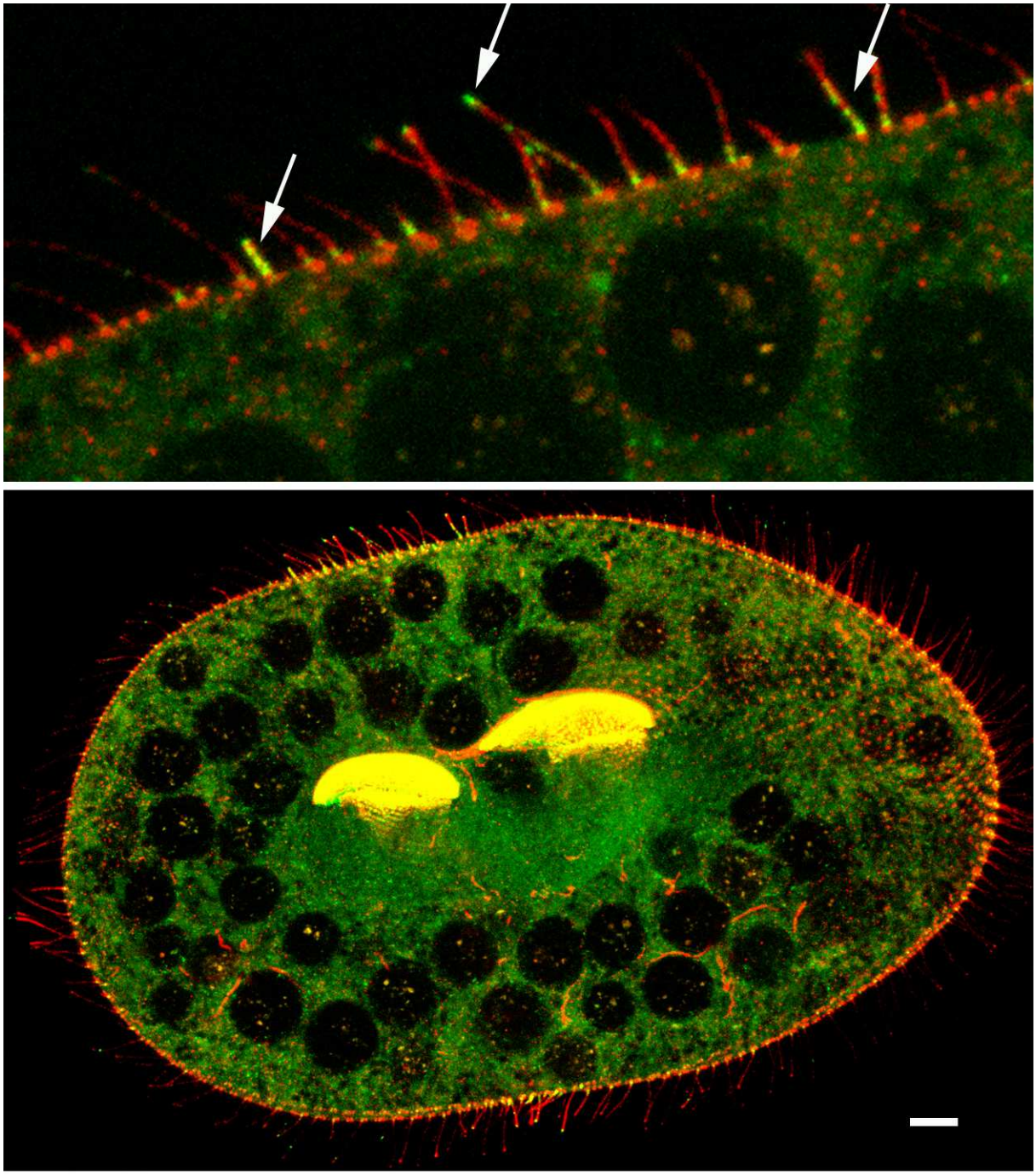

Figure 2-5. Confocal microscopy optical section of a dividing cell expressing IFT57A-GFP and immunolabelled with TAP952 as in Fig. 2-3. *Top: enlargement of a portion of the cell in the region of the fission furrow. Arrows show the intraciliary localization of IFT57-GFP, particularly abundant in a small growing cilium on the left. Bar: 10µm. Photo Anne Aubusson.*

When the detail of the IFT57A-GFP labeling is observed at the confocal microscope level, the fluorescence appears as dots on cilia at various places, including the tip where IFT57 may play a particular role for the shift from IFTB anterograde transport to IFTA retrograde transport, as found in zebra fish in which IFT57 regulates the dissociation between kinesin II and IFT particles at ciliary tips (Krock & Perkins, 2008). Only cilia in the region of active basal body proliferation and ciliary growth are labeled.

2.1.2.2. Ciliary growth after deciliation.

To study ciliary growth under reciliation conditions, IFT57A-GFP expressing cells were first deciliated and three batches were recovered 5, 20 and 40 minutes after deciliation and labeled with ID5, an anti basal body antibody (Fig. 2-6) and with an anti-cilia antibody against polyglycylated tubulin to follow ciliary growth and see the localization of IFT57 (Fig. 2-7).

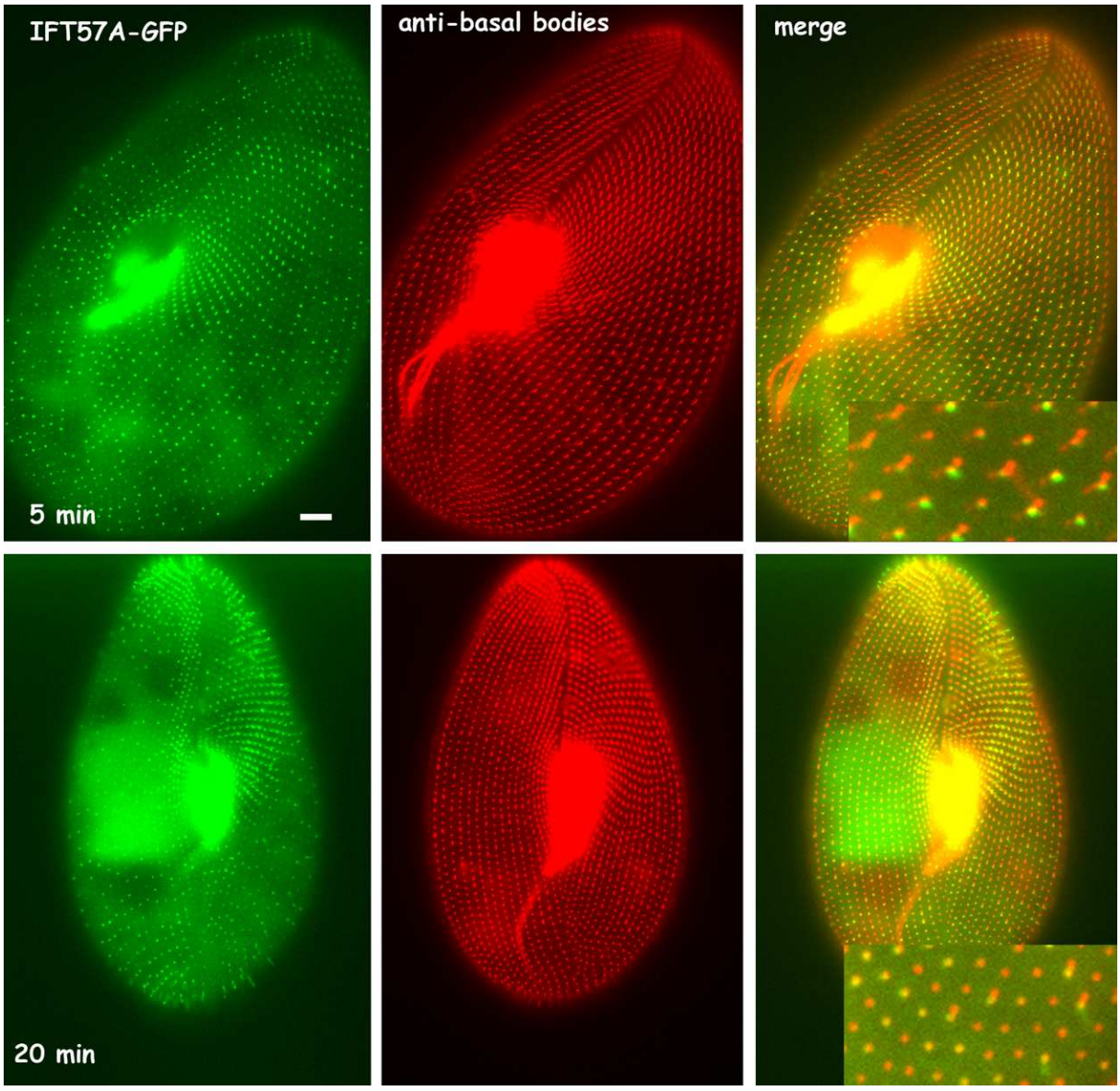

Figure 2-6. IFT57A-GFP localization during ciliary growth after deciliation of Paramecium cells viewed in epifluorescence microscopy. *Cells were labeled with an anti-basal body antibody (in red) to evaluate co-localization with GFP.*

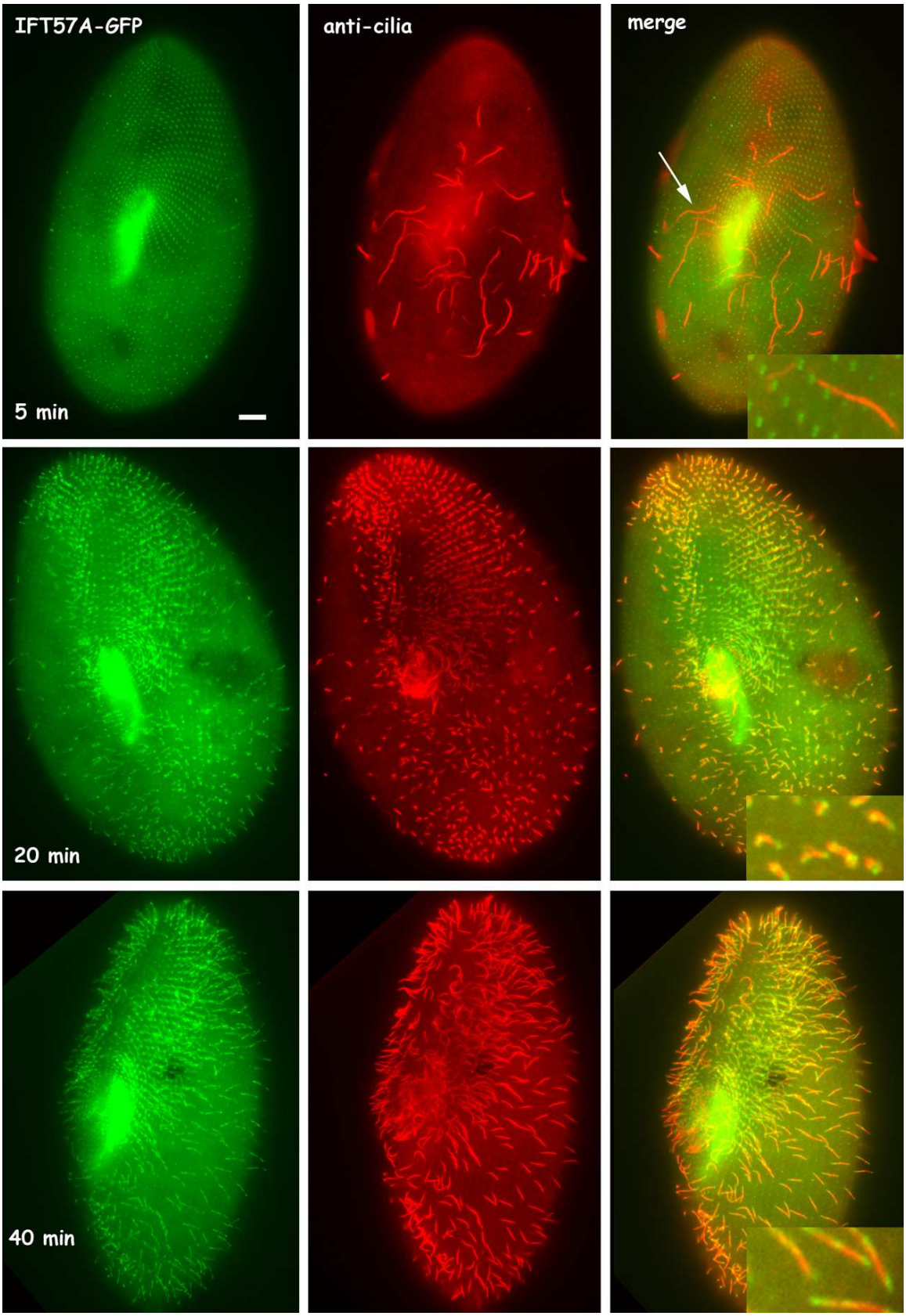
IFT57A-GFP
anti-cilia
merge
5 min
20 min
40 min

Figure 2-7. Epifluorescence microscopy IFT57A-GFP localization during ciliary growth after deciliation of Paramecium cells. *Cells were labeled with an anti-cilia antibody against polyglycylated tubulin (in red) to evaluate co-localization with GFP. Note that deciliation is not perfect in all cells, as shown here for the 5 min. time point in which old cilia without GFP labeling remain (white arrow). Bars: 10µm.*

Five minutes after deciliation, IFT57A-GFP strongly accumulates at the level of some basal bodies, the ones normally ciliated in interphase, in the ones of 1-bb units, the posterior ones in 2-bb units and both in 2-bb units in the anterior invariant field (Fig. 2-6). Some rare cilia can be present, if they escaped the deciliation process, but remain unlabeled (Fig 2-7), an argument in favor of a role of IFT57 in ciliary growing but not maintenance. At 20 and 40 minutes, IFT57A-GFP is clearly visible in all short cilia (Fig. 2-7), showing that they are indeed growing cilia that are labeled by IFT57A-GFP. When cilia reach a certain length, the labeling is visible in more details and appears as discrete dots (Fig. 2-7). In all cases, the GFP labeling is comprised within the red labeling given by the anti-*Paramecium* cilia. Since the antibody is directed against tubulin polyglycylation, and since this phenomenon occurs secondarily in cilia after axonemal elongation (Iftode et al., 2000), IFT57 must be recruited lately in ciliary growth and not as an initial event.
In reciliating cells, IFT57A-GFP (also true for IFT57C-GFP, not shown) is localized in all short growing cilia, a situation different from the one of vegetative cells in which only a minority of cilia is labeled, likely because only a few cilia are growing in steady state.

As we just saw, the IFT57-GFP labeling of growing cilia is not homogeneous along the cilia, as if the fluorescence represented trains of IFT migrating along the cilia. In order to ascertain that interpretation and in order to detect putative movements, as has been shown in *Chlamydomonas* (Diener 2009), I followed living cells during reciliation and I could observe fluorescence train movements along cilia in living cells (Fig. 2-8).

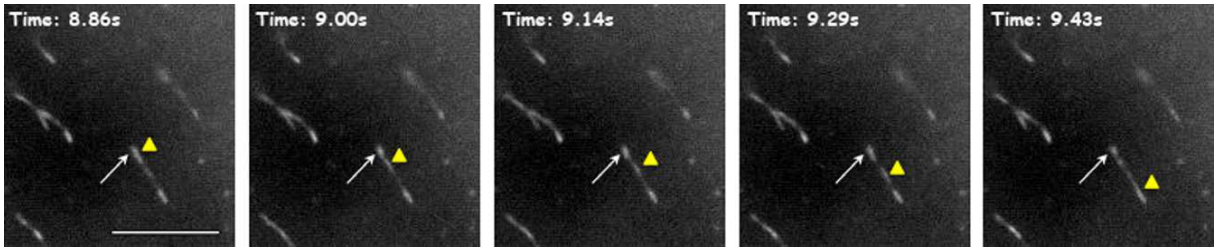

Figure 2-8. Sequential pictures from a movie of ciliary regeneration at 40 minutes post-deciliation in a cell expressing IFT57A-GFP viewed by epifluorescence microscopy*. A train of fluorescent material (yellow arrowhead) is moving from the basal body (white arrow) to the tip of a cilium. Bar: 10µm.*

The non-uniform localization of IFT57 along cilia represents dots under motion, which likely correspond to IFT trains. We tried to detect this labeling at the level of electron microscopy in experiments performed by Michel Lemullois (Fig. 2-9).

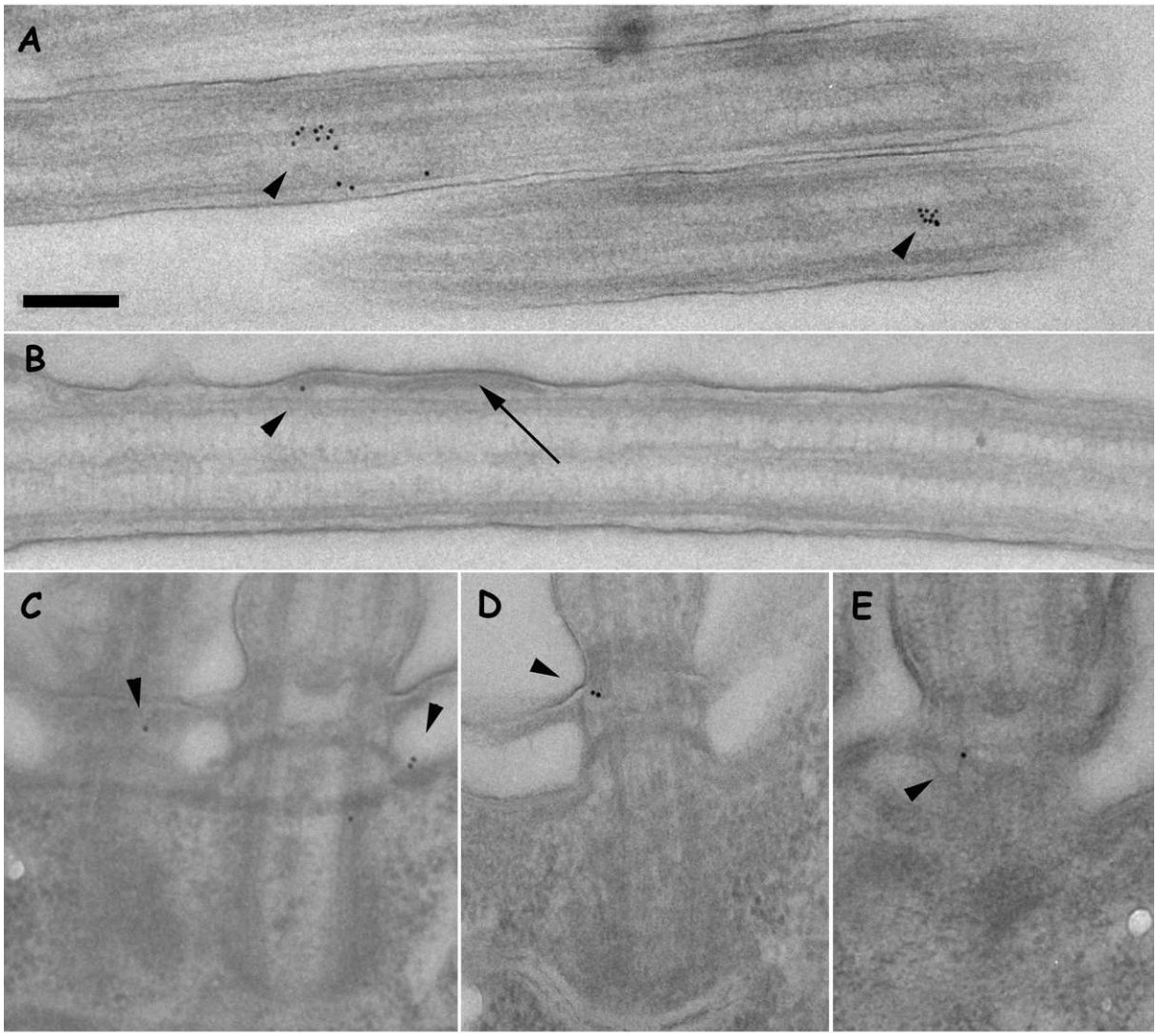

Figure 2-9. Electron micrograph of cilia and basal bodies of cells expressing IFT57A-GFP and labeled with an anti-GFP antibody on ultrathin sections. *The black dots (arrowheads) correspond to gold particles coupled to the secondary antibody and mark the presence of IFT57 accumulation. A: Two cilia showing a labeling. B: A likely IFT train faintly labeled (one gold particle). C-E: Examples of basal bodies harboring a labeling, although most basal bodies of the preparation appear unlabeled. Photo Michel Lemullois.*

The dotty labeling of IFT57A-GFP along cilia confirms its dotty fluorescnece localization and gives one example of a labeled IFT trains (Fig. 2-9B). The basal body labeling viewed in epifluorescence microscopy is much harder to ascertain in electron microscopy, since ca. 80% of the basal bodies seen in the sections are unlabeled. However, when gold particles are visible, they are in majority close to the distal tip of the basal body.

2.1.3. Conclusion of Part 2.1

I examined the localization of IFT57A and IFT57C proteins using GFP fusions using fluorescence microscopy. Except a strong macronuclear labeling obtained with IFT57A-GFP

and not IFT57C-GFP, as described in the next chapter, a recurrent localization of IFT57 was in basal bodies and cilia. IFT57 was easily detected in cilia under growth, in dividing cells and after experimental deciliation. The fact that some short cilia in interphase cells are labeled indicates that a residual activity of ciliary growth exists during interphase. This is a likely indication of ciliary loss and renewal during interphase, or of gradual ciliation after division, some basal bodies being ciliated before others. This point has to be separately addressed and awaits a more thorough study.
Another conclusion is that IFT57 seems to be dispensable in mature cilia, since no fluorescence is seen any more when they have their final length. In contrast to what has been found in *Chlamydomonas* (Dentler et al., 2005; Pan et al., 2005; Wilson et al., 2008; Engel et al., 2009) and in *Trypanosoma* (Absalon et al., 2008; Buisson et al., 2013), do the cilia stay at the surface without maintenance? A possible approach to this phenomenon could be to follow the phenotypes given by gene inactivation, as described in the next part.
I also found that not all basal bodies are labeled with IFT57-GFP. This is in good correlation with the observation that not all basal bodies are ciliated (Aubusson-Fleury et al., 2012) and that only ciliated basal bodies are labeled with IFT57-GFP. This adds a new level in the study of cortical morphogenesis, that is the pattern of ciliary growth in addition to the pattern of basal body proliferation.

PART 2.2. EFFECTS OF INACTIVATION OF IFT57 GENES

To study the function of IFT57 proteins in *Paramecium*, I used the feeding RNAi technique (see Materials and Methods) to inactivate the corresponding genes found in the genome sequence.

2.2.1. Possibilities of co-inactivation within the *Paramecium* IFT57 gene family

There are four IFT 57 genes in *Paramecium* arising from the two last successive whole genome duplications (see Introduction). The result of the last duplication WGD1 gives pairs of genes very similar in sequences, whereas sequences issued form the intermediate WGD2 duplication are more divergent. To make functional analyses, we use an RNAi technique dependent on sequence homology. The presence of common stretches of 23 identical nucleotides, the size of siRNA in *Paramecium* or more can be determined using the "RNAi off-target" tool of *Paramecium*DB and this shows that an IFT57A sequence can co-silence IFT57B and that IFT57C can co-silence IFT57D (Fig. 2-10). The sequence similarity between WGD2 duplicates is not high enough to have a co-silencing using only one of the four sequences, so that two RNAi sequences, IFT57A and IFT57C for example, are needed to inactivate the complete gene family.

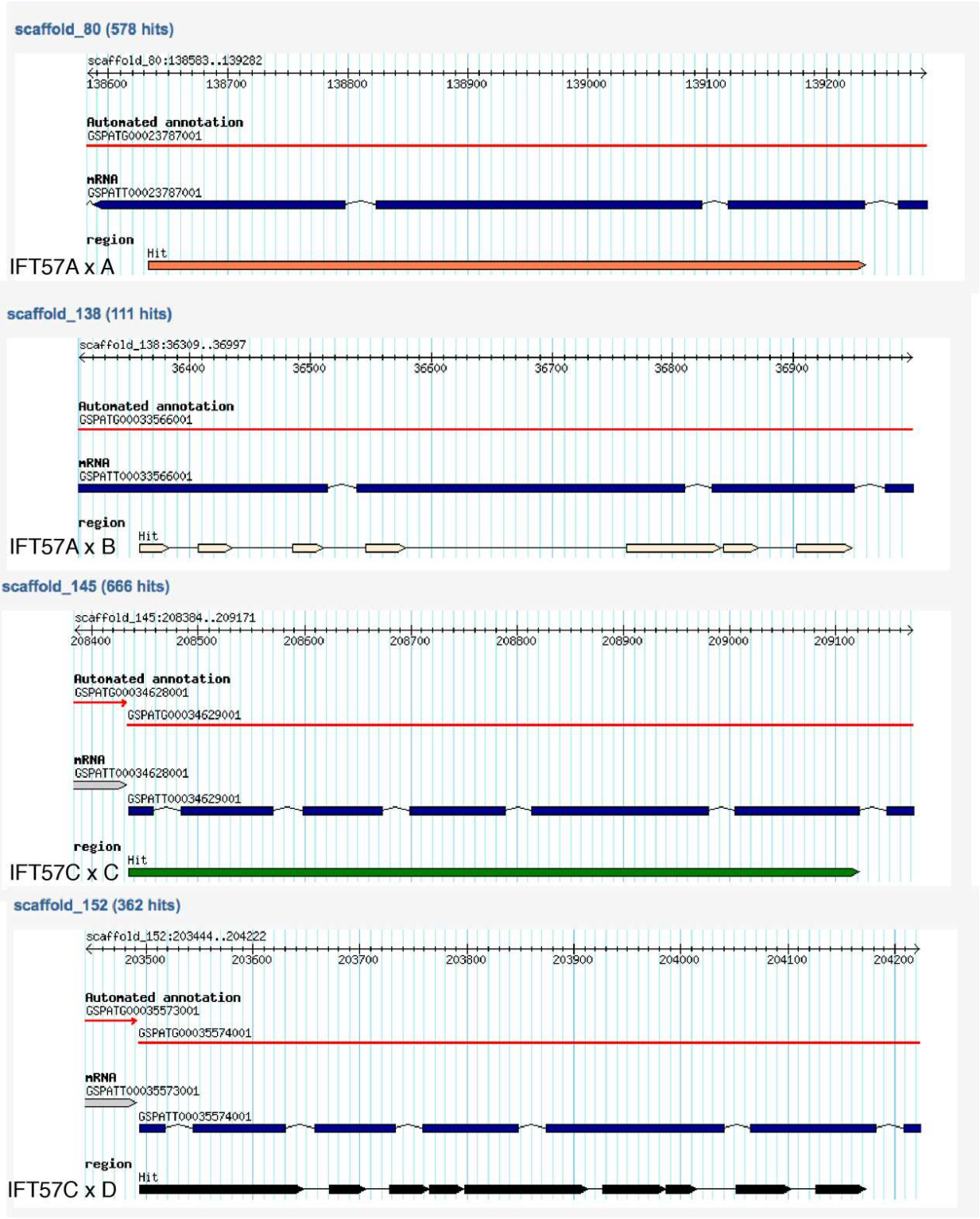

Figure 2-10. Evaluation of co-inactivation of IFT57 genes by RNAi. *The IFT57A and IFT57C sequences used as inserts in the feeding vector was tested using the RNAi off-target tool of ParameciumDB. As shown in screenshots of the results, in addition to the genes corresponding to the input sequences, the ohnolog genes (IFT57B for IFT57A and IFT57D for IFT57C) appeared to be potential targets in RNAi experiments, since they contain long stretches of identical nucleotide sequences. IFT57A RNAi should thus co-inactivate IFT57A and IFT57B, and IFT57C RNAi co-inactivate IFT57C and IFT57D.*

2.2.2. Effect on IFT57 RNAi on *Paramecium* growth rate

Paramecium wild type cells were submitted to RNAi by feeding with bacteria expressing double-strand RNA corresponding to the sequences ND7 (a control that does not affect growth nor swimming but trichocyst discharge), IFT57A or IFT57C. A mixture of bacteria expressing double strand RNA homologous to IFT57A and IFT57C was also used to silence the four IFT genes simultaneously (Table 2-1).

Growth rate (fissions per day)	Day 1	Day 2	Day 3
ND7 (control)	3-4	4	4
IFT57A	2	2-3	2-3
IFT57C	2	2-3	2-3
IFT57A+C	1-2	1-2	**dead**

Table 2-1. Fission rate of wild type cells under IFT7 RNAi.

Separate RNAi experiments using IFT57A or IFT45C have little effect on growth rate, whereas RNAi using both genes has a more dramatic effect, leading to cell death after 3 days. The growth defect is correlated with the decrease of the swimming speed (IFT57A or IFT57C RNAi) and to immobilization after 2 days in the IFT57A+C RNAi mixture (data not shown). I also investigated a possible other phenotype on trichocyst exocytosis, which would be an indicator of an alteration of membrane traffic, but this was normal, as in the wild type untreated control, in contrast to the ND7 RNAi control.

2.2.3. Effect on IFT57 RNAi on *Paramecium* cilia

To see whether the defects in swimming behavior and growth rate observed in RNAi effects were correlated with loss of cilia, I labeled silenced cells with the anti-*Paramecium* cilia antibody (Fig. 2-11).

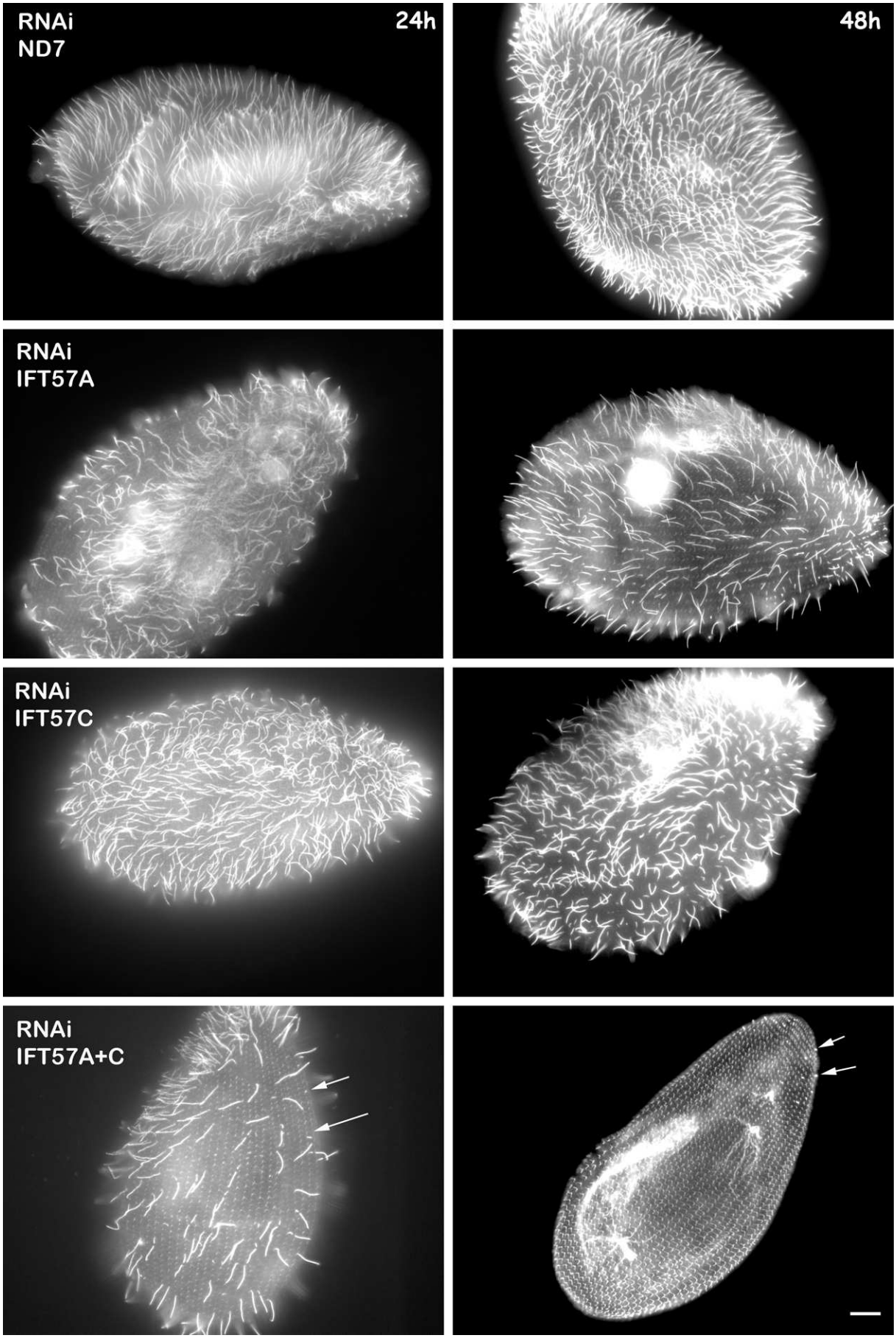
RNAi
ND7
24h
48h
RNAi
IFT57A
RNAi
IFT57C
RNAi
IFT57A+C

Figure 2-11. Labeling with the anti- Paramecium cilia antibody of cells after 24 or 48 hours of RNAi treatment, viewed in epifluorescence microscopy. *ND7 RNAi as a control, IFT51A and IFT57C separately and co-inactivation using the IFT57A and IFT57C RNAi. The number of cilia is a little affected in separate IFT57A or IFT57C RNAi, but progressively decreases in double RNAi till 48 hours. Note that in double RNAi at 24 hours, cilia are either full length or extremely short (white arrows), with no continuous distribution of intermediate lengths. At 48 hours, the cilia completely disappeared, except a few remaining very short cilia (white arrows). Bar: 10µm.*

After 24 hours of RNAi, only weak ciliary depletion is observed on cells under single IFT57A or IFT57C RNAi, whereas double RNAi is much more efficient. In this case, long cilia are still present but "diluted" at the surface, and otherwise, only very short cilia are detected without any cilia of intermediate size. After 48 hours of RNAi, cilia are less numerous but still present in single RNAi and completely lost in double RNAi. These observations are well correlated with the swimming phenotypes. Concerning the growth rate phenotype, it must be directly dependent on cilia, since the cells need swimming to reach and ciliary beating in the oral apparatus to catch their food. The fact that the depletion of IFT57A and IFT57C separately gives only a weak phenotype, whereas the combination of both depletions is drastic, suggests that during vegetative growth each gene product can somehow compensate the depletion of the other.

To investigate the ciliary disappearance under IFT57A+C RNAi, we looked at silenced cells in electron microscopy experiments performed by Michel Lemullois (Fig. 2-13) by comparing the structure of cilia and basal bodies to wild-type ones (Fig. 2-12).

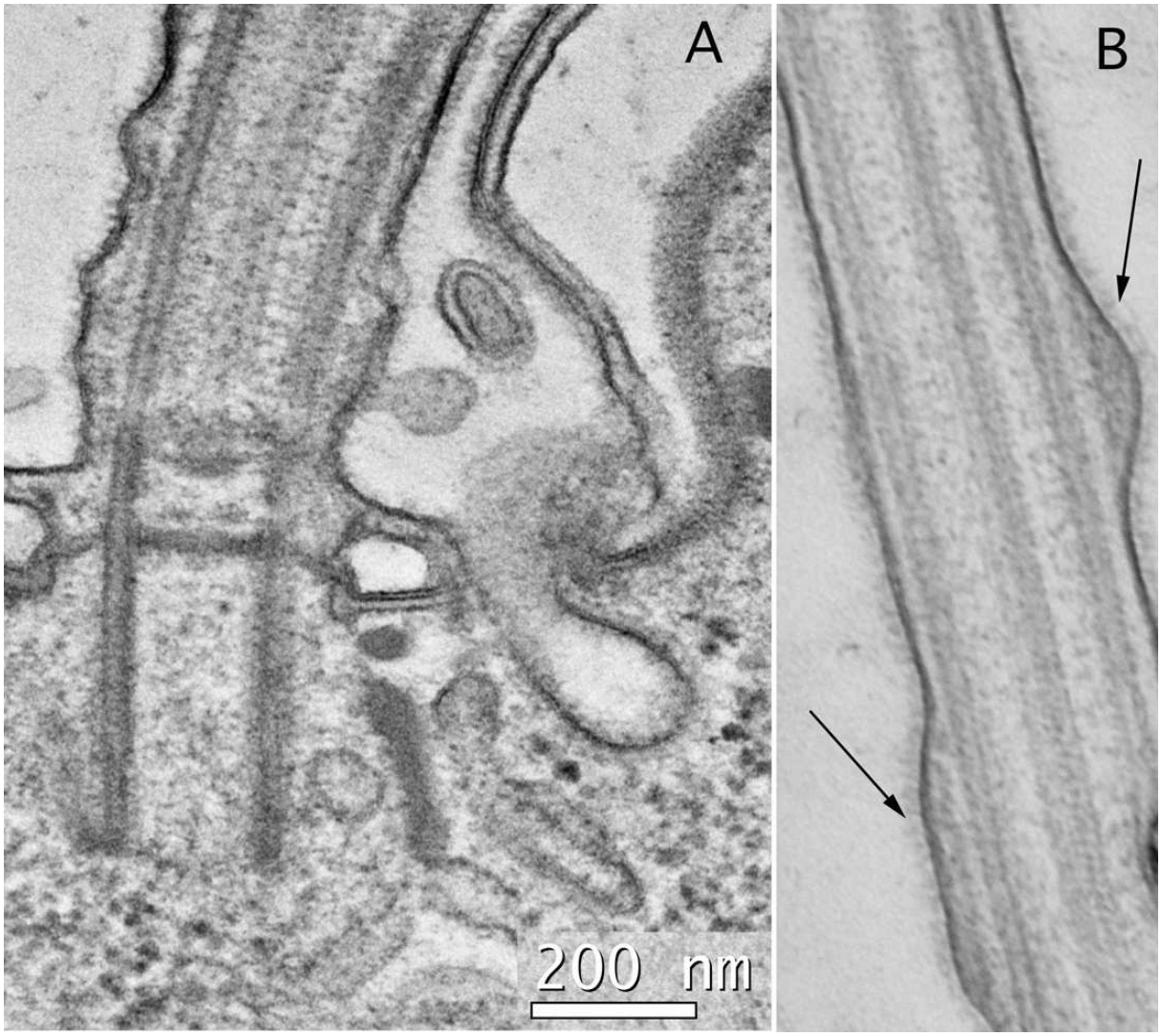

Figure 2-12. Ultrastructure of a Paramecium cilium in electron microscopy*. A. view of the proximal part of a cilium and its basal body anchored at the cell surface, close to coated pit, the parasomal sac, supposed to be involved in membrane traffic from and towards the cilium. B. Longitudinal section of a cilium showing lateral dense protrusions evoking IFT particles (arrows). Photos Michel Lemullois.*

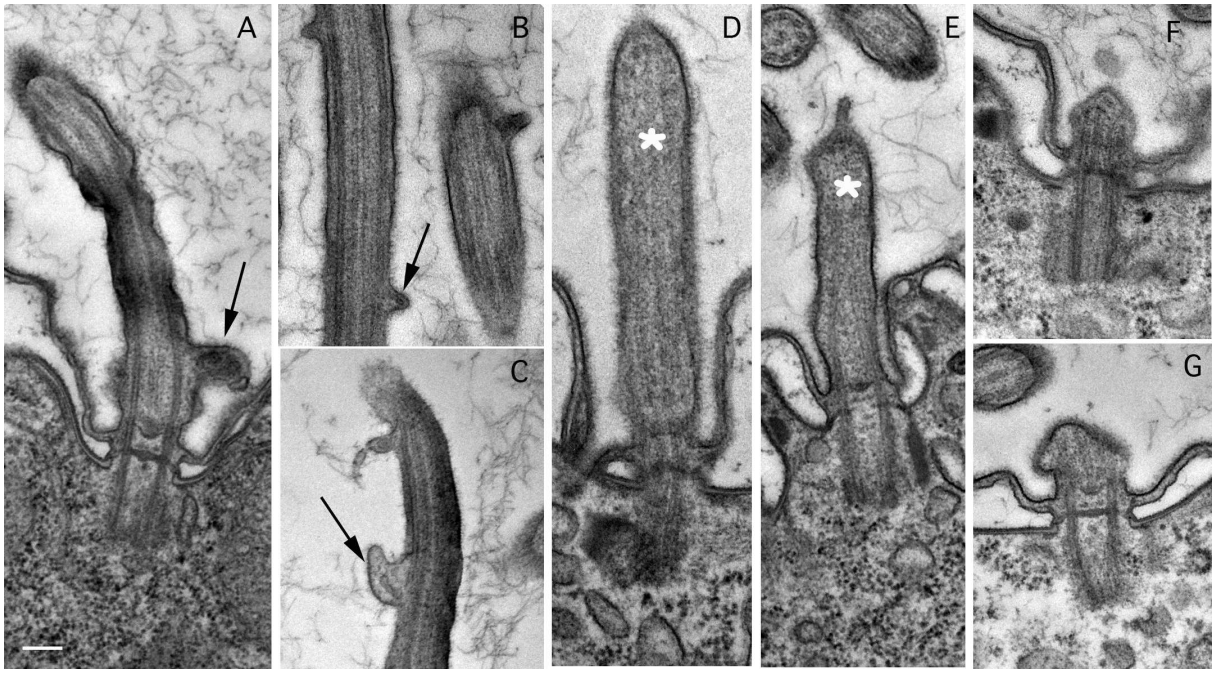

Figure 2-13. Electron micrographs of cells under IFT57A+C RNAi during 24 hours (A-E) and 48 hours (F, G). *During the process of ciliary loss, many cilia display blebs on their side or tip as if material was extruded from them (A-C, arrows). In addition, short cilia seem to contain an axoneme ill structured with disorganization of microtubules (white star). After 48 hours of RNAi (F, G), no cilia or only very small buds of cilia are visible on top of basal bodies. Bar: 200 nm. Photos Michel Lemullois.*

Electron micrographs of sections of cilia after 24 hours of RNAi show frequent blebs containing electron dense material (Fig. 2-13 A-C), which could be assimilated to the material seen along the axoneme (Fig. 2-12 B) that evoke IFT trains. Short cilia are also seen with ill-organized microtubules (Fig. 2-13 D, E), likely corresponding to those detected in fluorescence (Fig 2-11) after 24 hours of double RNAi IFT57A+C. An interesting idea is that IFT57 depletion disturbs normal progression of the IFT particle along cilia so that cilia cannot grow. For example, IFT trains would be secreted in budding vesicles instead of staying along the axoneme for transport. Alternatively, this budding in the absence of IFT57 could reveal that the ciliary membrane has an abnormal membrane composition/rigidity due to lack of normal membrane biogenesis. Whatever the exact mechanisms, such secretory machinery is likely to exist in the cilium in the form of exosome or ectosome secretion, as described in *Chlamydomonas* (Wood et al., 2013) or from mammalian cilia, in the retina or the urinary lumen (reviewed by Avasthi and Marshall, 2013) for instance. Cilia already grown are not affected, as if maintenance was not disturbed by IFT57 depletion. After 48 hours of IFT57A+C RNAi, a few short cilia remain and are extremely abortive and disorganized (Fig. 2-13 F, G).

2.2.4. Effect on IFT57 RNAi on *Paramecium* expressing IFT57A-GFP

To know the significance of single versus double IFT57 A and C RNAi, as well as their specificity, I applied RNAi to cells expressing IFT57A-GFP (Fig. 2-14) and IFT57C-GFP (not shown).

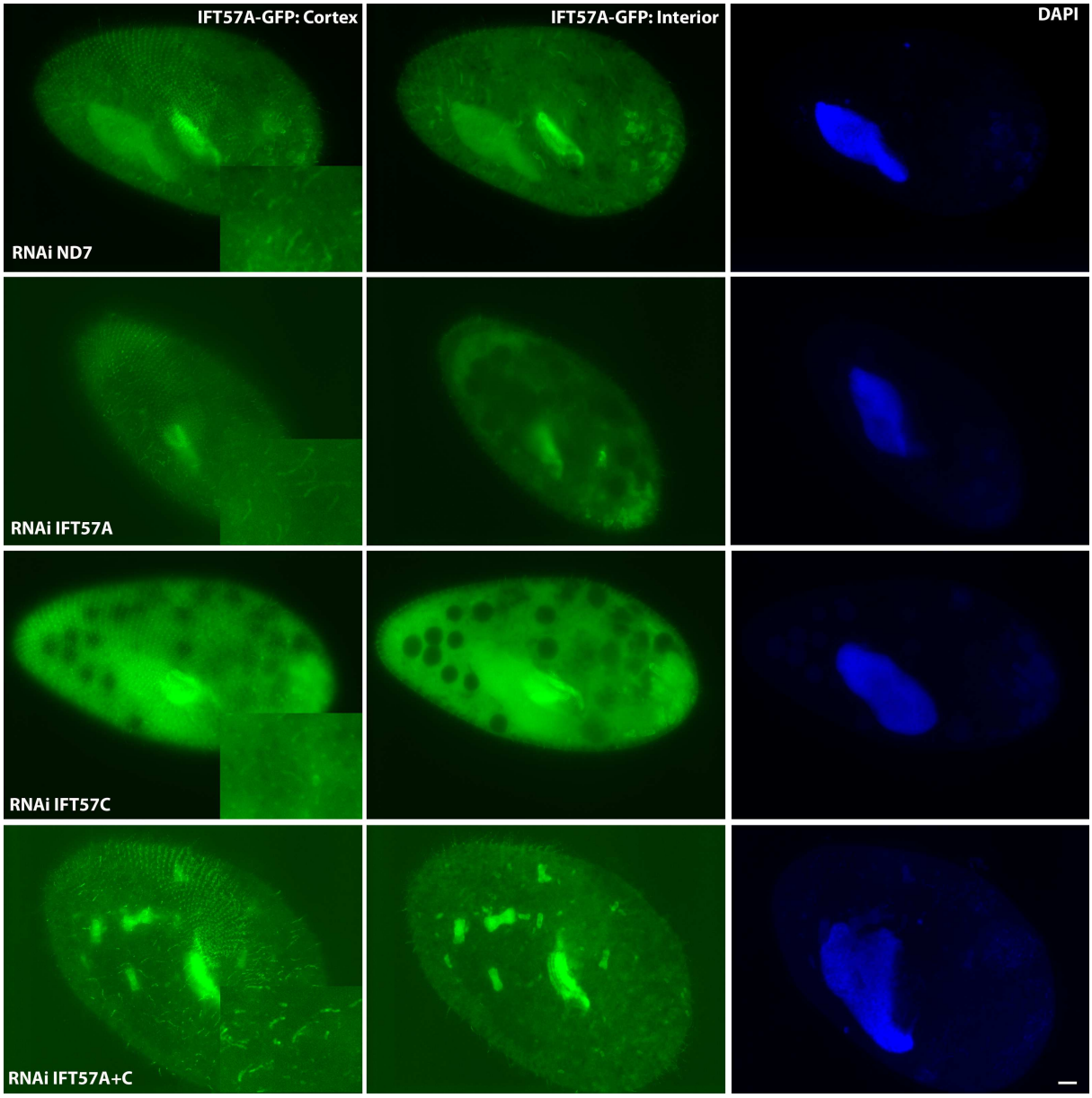

Figure 2-14. Different IFT57 RNAi on vegetative cells expressing IFT57A-GFP viewed by epifluorescence microscopy. *Each line represents a RNAi condition, the first column shows the cortical labeling, the medium column the interior of the cell with the macronucleus on focus ant the third column the DAPI staining of the same cell. The first line is the control ND7 RNAi in which, as in wild type conditions (Fig. 2-1), the fluorescence is localized in a few cilia and in the macronucleus. With IFT57A RNAi, the ciliary fluorescence remains the same, but the macronuclear one disappears. IFT57c RNAi does not prevent ciliary nor nuclear localization of IFT57A, with nevertheless an apparently stronger cytoplasmic fluorescence. The IFT57A+C RNAi was able to abolish the macronuclear labeling of IFT57A-GFP, as did the single IFT57A RNAi, but give systematic stronger ciliary fluorescence, and in more cilia than under control RNAi.*

The first observation of the effect of IFT57A, IFT57C or IFT57A+C RNAi was a less marked alteration of swimming speed and cell growth on IFT57A-GFP or IFT57C-GFP expressing cells than on wild type cells. This is an indication that in the case of (over)expression of the protein fusion, there is a less efficient silencing effect. Concerning the GFP fluorescence

labeling, the ciliary and basal body GFP labeling does not disappear, whatever the RNAi combination. The simplest interpretation is that the IFT57-GFP expression in the cell was too high to be fully antagonized by the RNAi. Nevertheless, the IFT57A RNAi (with or without co RNAi of IFT57C) was able to abolish the IFT57A-GFP fluorescence of the macronucleus, in contrast to IFT57C RNAi alone, which was not. The absence of ciliary labeling decrease, and even possible apparent increase in double RNAi conditions (also true for IFT57C-GFP, not shown) could have another meaning than just moderate effect of RNAi. We can imagine that, since IFT complexes are very stable (Taschner et al., 2011), IFT57-GFP remains trapped and cycles in growing cilia without turnover with the cytoplasmic form, so that cilia can still fluoresce under RNAi conditions.

2.2.5. Conclusion of Part 2.2

The depletion of IFT57A and IFT57C, likely to also provoke the depletion of their respective ohnologs IFT57B and IFT57D, is lethal for *Paramecium*. It progressively decreases the number of cilia on the cortex and presumably also in the oral apparatus, although this is more difficult to document. The way of ciliary disappearance occurs through prevention of ciliary growth and progressive elimination of mature cilia by dilution with cell divisions, and possibly mechanic loss. The absence of intermediate sizes of cilia during the decrease in ciliary numbers pleads against a role in ciliary maintenance, because any deficiency in this mechanism would have lead to ciliary progressive shortening. However, the sequestration of IFT57-GFP fluorescence in cilia under double IFT57 A+C RNAi may reveal a certain insulation of this protein in the cilium, permitting permanent maintenance without new import from the cytoplasm. This aspect will be discussed again later in view of the behavior of other IFT proteins presented in part 2.3.

PART 2.3. IFT57 WITHIN THE INTRAFLAGELLAR TRANSPORT

The IFT57 protein, together with IFT20, is known to be peripheral to the core IFT complex and represents a linker with the kinesin motor (Krock and Perkins, 2008). I tried to have insight into some other IFT proteins to see which of the properties found for IFT57 are specific for this proteins and which one are common to other IFTs.
I first localized some GFP fusion IFT proteins, IFT46, a core IFT protein, and qilin, a protein more loosely associated with the IFT. I studied the effect of silencing some proteins components of the IFTB (anterograde) and IFTA (retrograde) particles on the general phenotype of the cell and on the localization of IFT-GFP fusion proteins.

2.3.1. Localization of IFT46 and qilin GFP fusions.

To study the localization of IFT proteins, I constructed a IFT46-GFP fusion gene and used qilinA-GFP and qilinC-GFP fusion genes (Houssein Chalhoub unpublished data. I observed the fluorescence localization in vegetative growth, in interphase and division, as well as during ciliary growth after deciliation (Fig. 2-15).

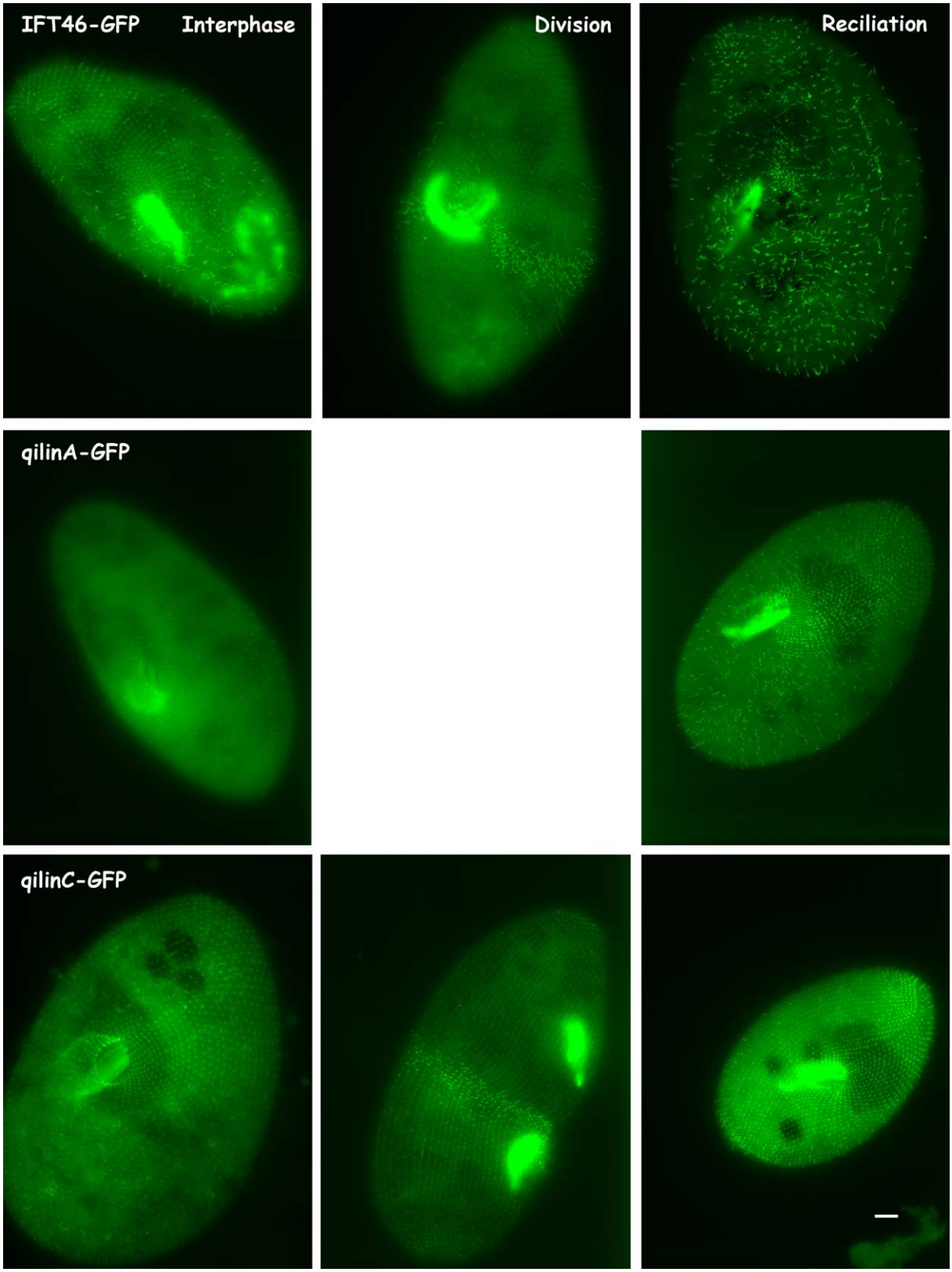
IFT46-GFP
Interphase
Division
Reciliation
qilinA-GFP
qilinC-GFP

Figure 2-15: Localization of IFT46-GFP, qilinA-GFP, qilinC-GFP in vegetative paramecia viewed in epifluorescence microscopy*. Interphase (first column) under division (second column) and under ciliary growth after deciliation (third column) are illustrated. Note that, like in the localization of IFT57 described in Chapter 2, the ciliary localization of IFT proteins is weak in interphase, strongly enhanced in the zones of active ciliary growth under division and in all growing cilia after deciliation. None of the IFT46 and qilin proteins gave a macronuclear labeling. Bar: 10µm.*

As shown in the figure, the characteristic labeling of rare short cilia in interphase, a belt of growing cilia at the fission furrow of dividing cells, and growing cilia during reciliation, already see with IFT57-GFP, is also found for IFT46-GFP and qilin A and C-GFP. The only difference may reside in fluorescence intensity, as far as different transfection experiments can be compared. A slightly more intense labeling is found with IFT46-GFP and less intense with qilinA-GFP, compared to IFT57-GFP.

In addition, a marked difference was observed with IFT46-GFP during reciliation: strongly fluorescent dots appear in the cytoplasm while new cilia are growing (Fig. 2-16).

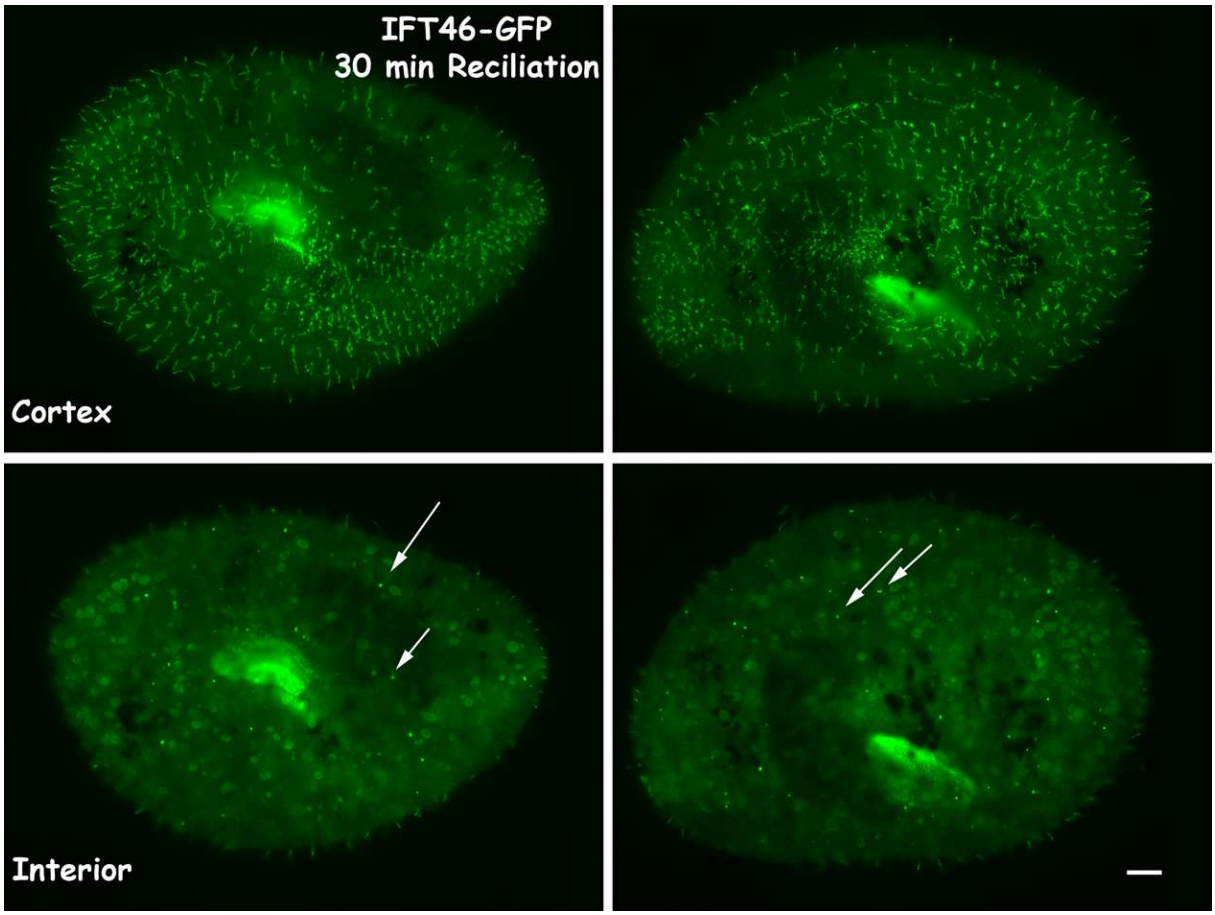

Figure 2-16. Apparition of intracytoplasmic fluorescent dots in cells expressing IFT46-GFP under reciliation, as viewed by epifluorescence microscopy. *Two cells are shown in this figure. White arrows point some of the fluorescent dots. Bar = 10 µm.*

The signification of these dots is not known, but they may represent points of IFT particle assembly in the cytoplasm. IFT20, for instance has a role in membrane traffic at the level of

the Golgi apparatus. IFT57 interacts with IFT20 in the IFT particles. May be an early interaction between these molecules and IFT46 occurs in the cytoplasm.

2.3.2. Effect of the depletion of different IFT proteins.

2.3.2.1. Phenotypes of cells depleted for IFT proteins

To compare the effect of RNAi depletion of IFT57 to other IFT members, I studied the function of four genes, IFT46, IFT172, qilin (components of the IFTB complex) and IFT139 (component of the IFTA complex). The phenotypic results of inactivation by feeding are given in Table 2-2.

Growth rate (fissions per day)	Day 1	Day 2	Day 3
ND7 (control)	3-4	4	4
IFT46	1-2	dead	
IFT172	2-3	1	dead
qilin (A+C)	2-3	1	dead
IFT139	2-3	1	dead

Table 2-2. Effect of IFT protein depletion on cell growth. *In all cases, the RNAi provoked reduction of cell division rate and death in two or three days. This growth arrest was always accompanied by a swimming speed decrease and eventual immobilization.*

As was the case for IFT57 depletion, the depletion of other IFT proteins, be they components of the IFTB or IFTA particles, are rapidly lethal through progressive decrease of division rate and swimming speed. I therefore analyzed the fate of cilia (Fig. 2-17).

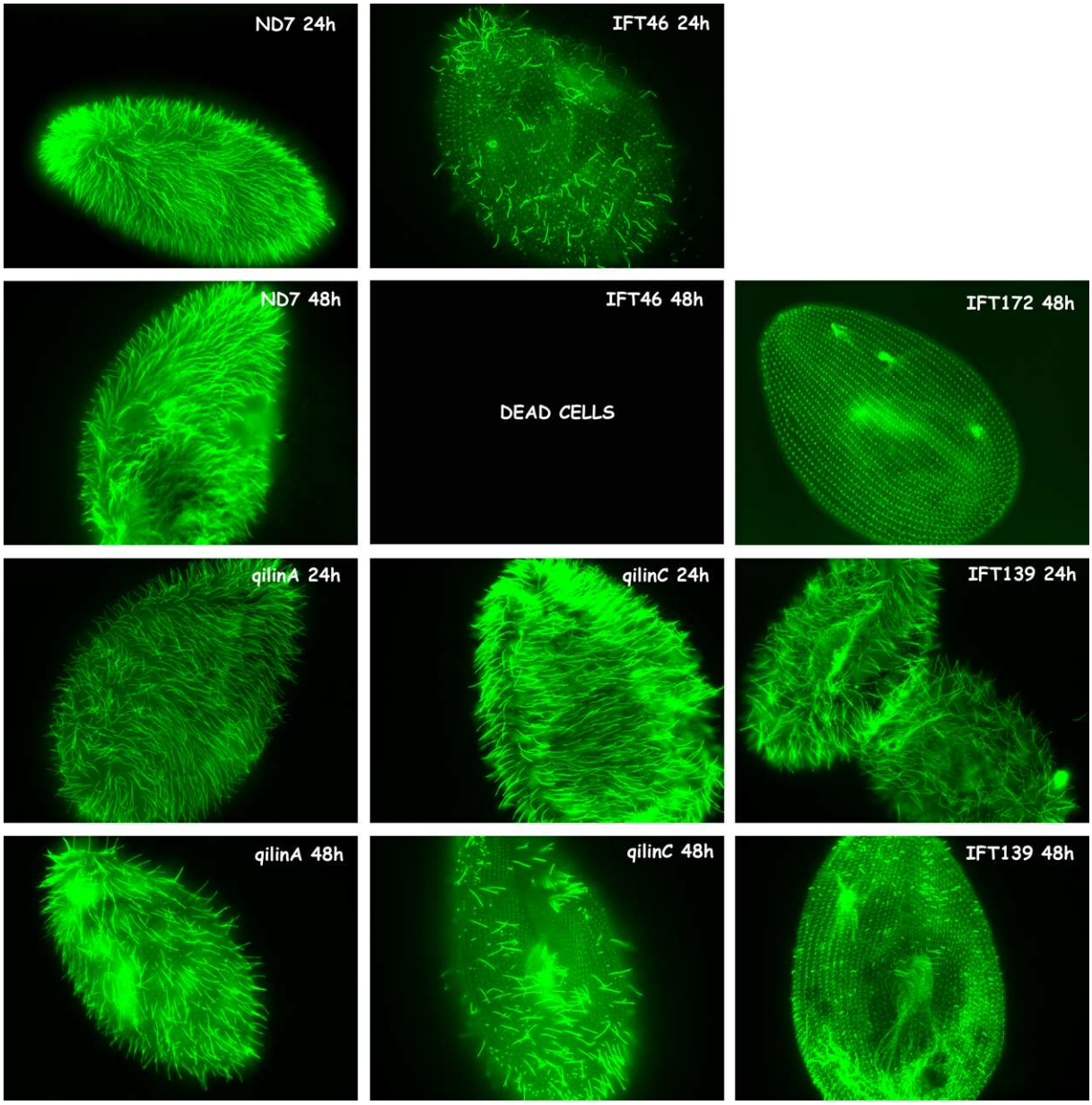

Figure 2-17: Anti-cilia labeling of cells depleted for the control ND7 protein and different IFT proteins IFT46, IFT172, qilinA, qilinC and IFT139 for 24h et 48h RNAi viewed in epifluorescence microscopy. *A progressive ciliary disappearance is observed, correlated with the loss of swimming capacity. IFT172 RNAi provokes a decrease of ciliary number but not length, except very short cilia). IFT46 and qilin RNAi provokes the appearance of short cilia of all sizes. Bar: 10µm.*

The general effect of IFT RNAi is the progressive loss of cilia at the surface. However, the way of ciliary loss is not the same in all cases. For example, there is a progressive dilution of full-length cilia along cell divisions under IFT172 RNAi, like under IFT57 RNAi, but heterogeneous ciliary sizes in IFT46 RNAi and qilin. A comparison of these defects is shown in Fig. 2-18.

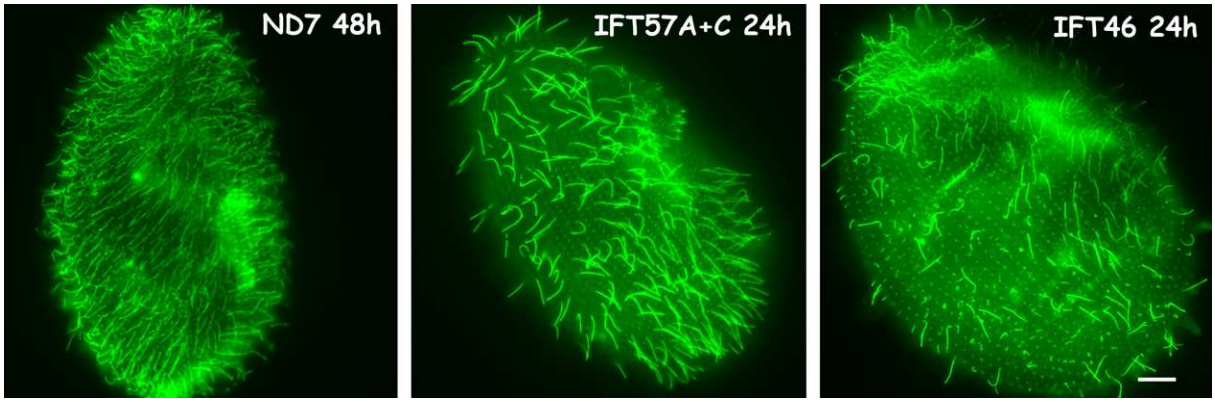

Figure 2-18. Comparison of the mode of ciliary loss under IFT57A+C and IFT46 RNAi. *While cilia appear homogeneous in size when IFT57A+C are depleted, cilia are very heterogeneous under IFT46 RNAi. Bar; 10µm.*

The different ways of loosing cilia under IFT RNAi in *Paramecium* suggests different roles of individual IFT molecules, although they act in the same complexes, or different recycling processes: IFT46 could be necessarily imported from the cytoplasm to be active in ciliary maintenance whereas IFT57 could recycle several time in the cilium and keep its activity even when the cell is deprived of *de novo* synthesis, as it is the case for IFT52 in *Trypanosoma* (Buisson et al., 2013).

2.3.2.2. Effect of IFT46 depletion on IFT46-GFP expressing cells.

Since IFT46 RNAi and IFT57 RNAi have different effects on cells, I wondered whether the effect of IFT46 RNAi on IFT46-GFP expressing cells could be different from the one of IFT57 RNAi on IFT57-GFP expressing cells (Fig. 2-19).

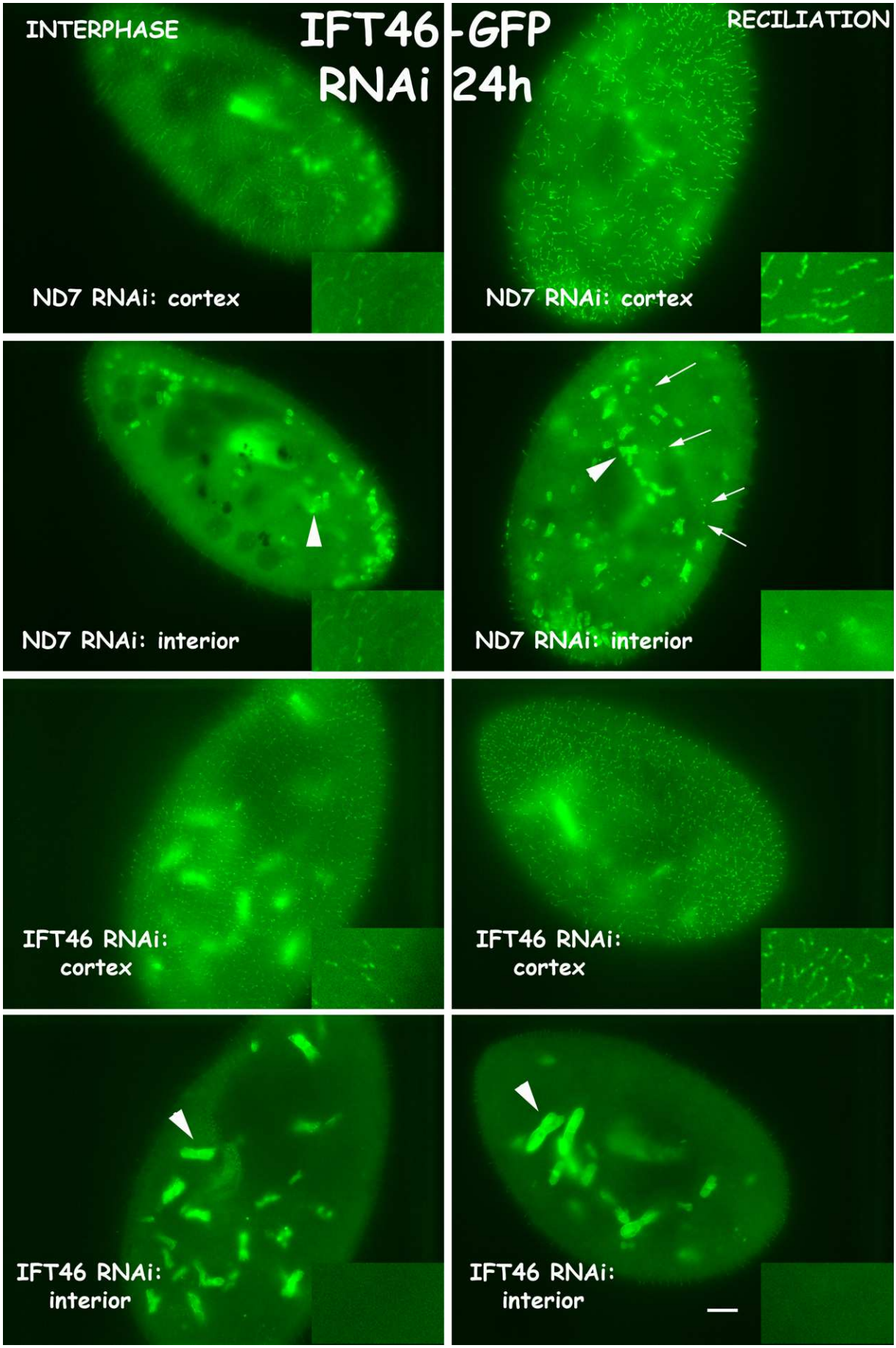
INTERPHASE
IFT46-GFP
RNAi 24h
RECILIATION
ND7 RNAi: cortex
ND7 RNAi: cortex
ND7 RNAi: interior
ND7 RNAi: interior
IFT46 RNAi:
cortex
IFT46 RNAi:
cortex
IFT46 RNAi:
interior
IFT46 RNAi:
interior

Figure 2-19. Epifluorescence microscopy observation of the effect of IFT46 RNAi on IFT46-GFP. *Cells expressing IFT46-GFP were submitted to ND7 (control) RNAi, upper half of the figure, or IFT46 RNAi, lower half of the figure for 24 hours. Left column: interphase cells; right column: cells 30 minutes after deciliation. In each case, a cortical view and an internal view are shown. In ND7 control conditions, a labeling similar to the one described without treatment for interphase cells (Fig 2-14) or reciliating cells (Fig 2-15) was observed, in particular with internal fluorescent dots during reciliation (arrows) The big fluorescent inclusions (white arrowheads) occur for unknown reasons in some cultures, but are not relevant with the GFP fusion protein expressed. Under IFT46 RNAi, the fluorescent signal accumulates preferentially at the tips of cilia. The dots seen under reciliation seem much less numerous. Bar = 10µm.*

When IFT46 RNAi is applied to cells expressing IFT46-GFP, an enhanced labeling was first observed at the tips of cilia at 24 hours of RNAi (Fig 2-19) for unknown reason. The over-expression of IFT46-GFP makes the cells more resistant to IFT46 RNAi than wild type cells they survive another couple of days, but with abnormal divisions that were not seen in RNAi on wild type cells, but that prevent further growth. Interestingly, although we cannot ascertain that in *Paramecium*, IFT46 has been shown to accumulate at the cleavage furrow in *Chlamydomonas* (Wood et al., 2012). A conserved role in cell division could occur. During the time of RNAi, the IFT46-GFP labeling of cilia progressively disappears (not shown). The cytoplasmic dots observed during reciliation also appear to be sensitive to the exposure to IFT46 RNAi for 24 hours. This would lean that the production of cytoplasmic IFT46-GFP induced by deciliation is sensitive to the RNAi, even though the fluorescence is still present in the cell.

2.3.2.3. Cross RNAi depletions of IFT proteins on interphase cells expressing different IFT-GFP.

I applied IFTB protein RNAi (IFT46, IFT57, ITF172 and qilin) and IFTA protein RNAi (IFT139) on cells expressing IFT46-GFP, IFT57A-GFP, IFT57C-GFP, qilinA-GFP and qilinC-GFP. Examples of the effects are presented for interphase cells as inset enlargement of double labeling, GFP and cilia (Fig 2-20).

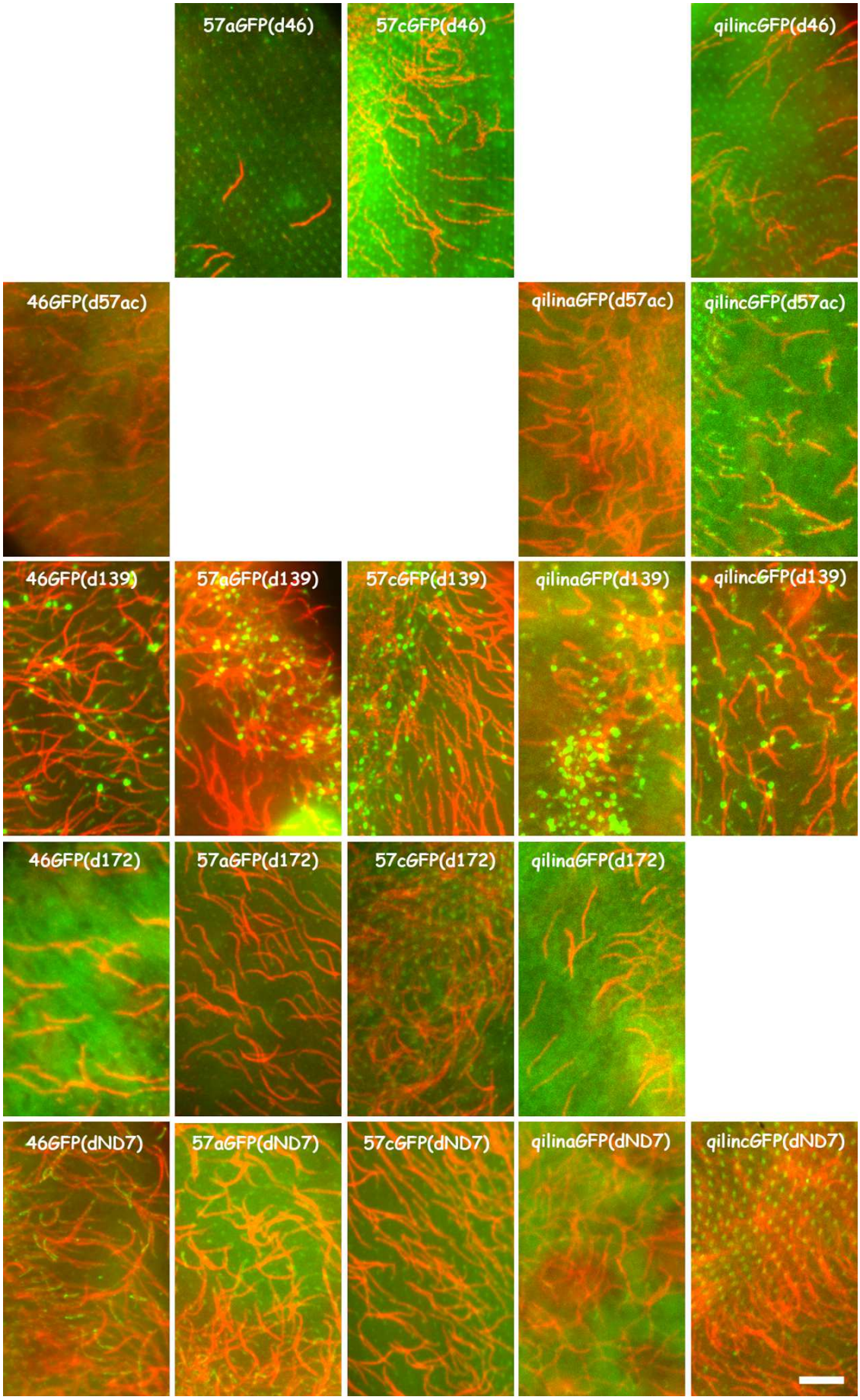
57aGFP(d46)
57cGFP(d46)
qilincGFP(d46)
46GFP(d57ac)
qilinaGFP(d57ac)
qilincGFP(d57ac)
46GFP(d139)
57aGFP(d139)
57cGFP(d139)
qilinaGFP(d139)
qilincGFP(d139)
46GFP(d172)
57aGFP(d172)
57cGFP(d172)
qilinaGFP(d172)
46GFP(dND7)
57aGFP(dND7)
57cGFP(dND7)
qilinaGFP(dND7)
qilincGFP(dND7)

Figure 2-20. Effect of Different IFT RNAi for 24 hours on IFT-GFP expressing cells during interphase viewed by epifluorescence microscopy. *Each panel represents an enlarged inset of a cell labeled with GFP (in green) and with an anti-polyglycylated tubulin (in red). Each column corresponds to an IFT-GFP expression, respectively IFT46, IFT57A, IFT57C, qilinA-GFP, qilinC-GFP. Each row corresponds to an IFT RNAi, respectively IFT46, IFT57A+C, IFT139, IFT172 and the ND7 control. Bar = 10µm.*

When IFTB proteins (IFT46, IFT57, IFT172 and qilin) were depleted by RNAi for 24 hours, a time not sufficient to completely deplete cilia from the surface, all the IFT-GFP labeling disappeared from cilia. In contrast, when the IFTA IFT139 protein was depleted, a strong accumulation of the fluorescence at ciliary tips was observed, confirming that IFT139 has a role in retrograde movement in *Paramecium*. In Fig. 2-20, the basal bodies are less consistently labeled from one cell type to another, but this could be a consequence of the level of expression of each IFT-GFP fusion protein, which has not been controlled.
However, a particular phenomenon was observed at first cell division of cells expressing IFT57A-GFP (or IFT57C-GFP) under IFT46 RNAi (Fig. 2-21).

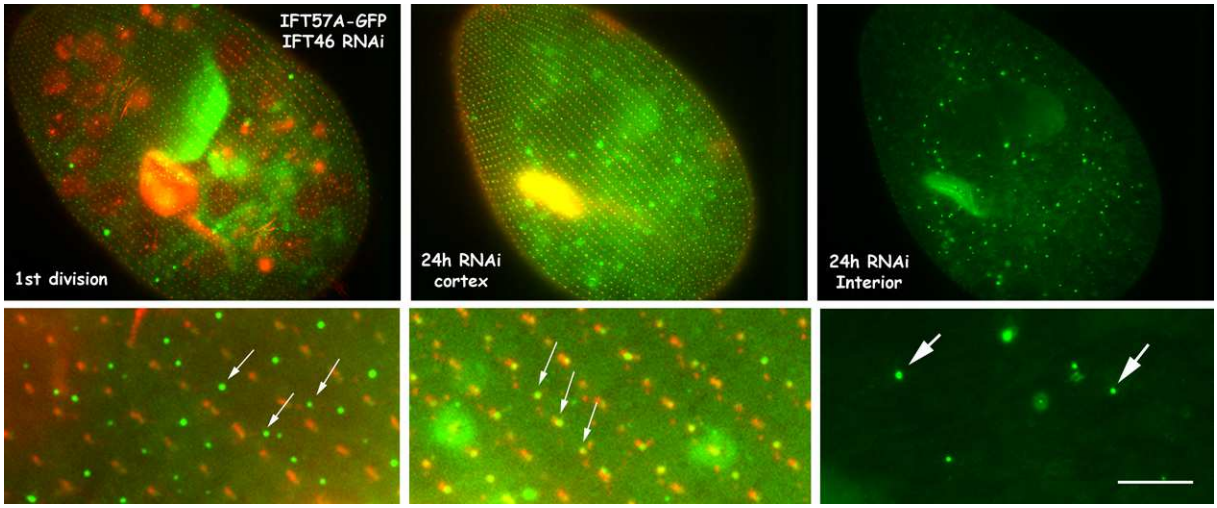

Figure 2-21. Fate of IFT57A-GFP under IFT46 RNAi viewed in epifluorescence microscopy. *Left: cell undergoing its first division since the beginning of RNAi co-labeled with the ID5 antibody against basal bodies. Middle: cortical view of a vegetative cell after 24h of RNAi co-labeled with ID5. Right: internal view the same cell 24h after RNAi. Small arrows: cortical dots; large arrows: internal dots. Bars = 10 µm.*

The depletion of IFT46 in IFT57A-GFP first provokes the apparition of fluorescent GFP dots visible in the cortex between ciliary rows in cells undergoing their first division after RNAi. Later on, while the cilia disappear, the dots are at the level of basal bodies, while small and big dots accumulate within the cytoplasm. This particular sequence of events induced by IFT46 depletion could reveal a pathway for IFT recruitment or recycling otherwise not visible because too rapid. The nature and significance of the fluorescent particles between rows still remain to be elucidated.

2.3.2.4. Cross RNAi depletions of IFT proteins on IFT-GFP localization during reciliation.

Since the ciliary labeling by IFT-GFP fusion proteins is much marked in cells under reciliation, I performed ciliary labeling in IFT-GFP expressing cells during reciliation under different IFT RNAi (Fig. 2-22).

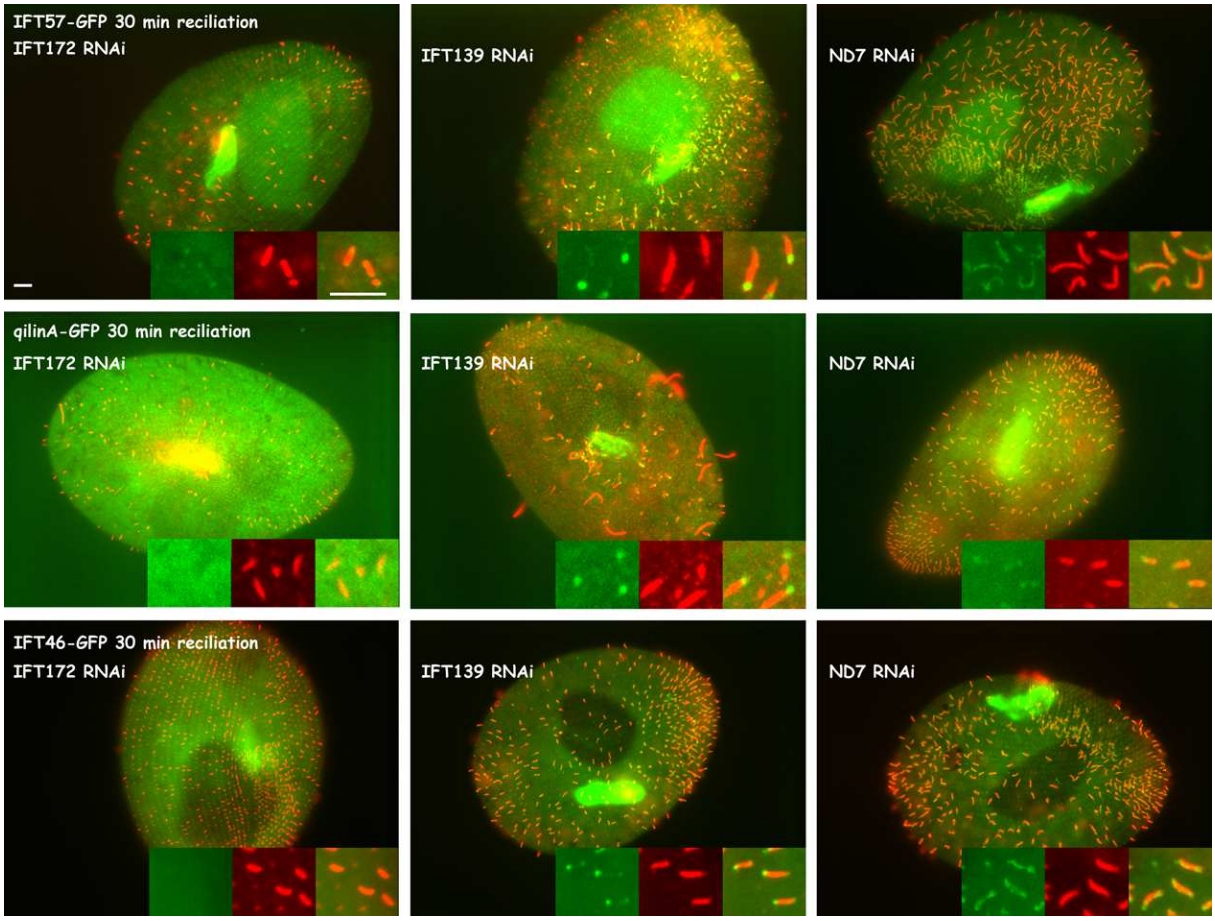

Figure 2-22. Fate of IFT57A-GFP and qilinA-GFP under different IFT RNAi during reciliation viewed in epifluorescence microscopy. *Cells expressing different IFT-GFP fusion proteins were submitted to different IFT RNAi for 24 hours and deciliated. After 30 min of recovery, they were labeled with the anti polyglycylated tubulin that recognizes cilia. Insets show enlargements of nascent cilia with their GFP fluorescence. Note the fluorescence of the macronucleus on the first row (IFT57A-GFP labeling) and a strong labeling of the oral apparatus in all cases. Bar = 10 µm.*

The first observation is that cilia can display residual growth even under IFT RNAi, at least during the first 30 minutes following deciliation, either because the RNAi depletion is not complete, or because even under complete depletion, residual protein already synthesized could work. However, silencing an IFTB partner, IFT172 for example, totally prevents IFT-GFP entry into the nascent cilium (left column of Fig. 2-22). Silencing an IFTA partner, IFT139, does not prevent IFT-GFP entry, but provokes accumulation of the protein at the tip of the growing cilium, as well as at the basis of the cilium, at least for IFT46-GFP (middle column of Fig. 2-22). In the control ND7 RNAi, short growing cilia have an IFT-GFP labeling all over their length (right column of Fig. 2-22). The longer labeling by the green IFT than by the red anti-cilium antibody reflects the fact that the anti-cilium recognizes polyglycylation, a post-translational modification that is delayed compared to ciliary growth.

Concerning IFT46-GFP, since I observed the apparition of cytoplasmic fluorescent dots during reciliation (Fig. 2-19), I analyzed the effect of various IFT RNAi on these fluorescent dots (Fig. 2-23).

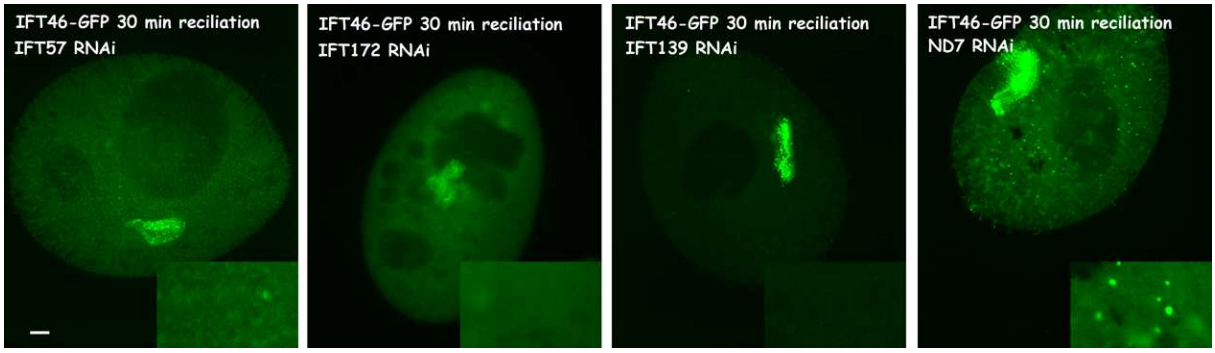

Figure 2-23. Internal views of IFT46-GFP under different IFT RNAi during reciliation viewed in epifluorescence microscopy*. Intra-cytoplasmic IFT46-GFP fluorescent dots induced during reciliation are clearly visible in the ND7 RNAi control, but mainly absent in cells under IFT RNAi. Bar = 10 µm.*

The dots, which appear in IFT46-GFP expressing cells under reciliation, are sensitive to IFT57, IFT172 and IFT139 RNAi. This would mean that either IFT46 expression, or IFT46 accumulation is dependent on other IFT proteins. In the latter case, pre-IFT complexes containing several subunits would assemble in the cytoplasm, or IFT proteins would assemble IFT46 particles trough a catalytic action.

2.3.4. Conclusion of Part 2.3.

The study of other IFT proteins than IFT57 generalizes the observation that the IFT is essential for ciliary biogenesis and cell survival. All IFT-GFP fusion proteins tested localize to the cilia and their depletion yields bald cells in a maximum of two days and subsequent lethality. However, careful examination of ciliary loss suggests that the IFT proteins have not the same role so that their depletion has not the same impact. IFT57 depletion does not induce ciliary regression, in contrast to IFT46 depletion with which shortening cilia are seen. In addition, IFT57-GFP ciliary labeling seems more stable in cilia under IFT57 RNAi than IFT46-GFP, which, under IFT46 RNAi, first accumulates weakly at the ciliary tip, then decreases in intensity.
IFT46 belongs to the core IFTB protein, necessary for its stability (Richey & Qin, 2012), and is in contact with the cargo, whereas IFT57 is a peripheral IFTB protein, linking the core IFTB complex to the motor. The observations made in *Paramecium* would mean that IFT57 could recycle as long as cilia are growing, without renewal, whereas IFT46 would be continuously imported from the cytoplasm. Both IFT proteins could therefore be equally involved in growth and recycling, but one can stay in the cilium while the other one needs to be imported.

Another important observation of this work is the presence of IFT46-GFP dots under certain conditions. When the ciliogenesis is stimulated by deciliation, IFT46-GFP accumulates in growing cilia, but also as cytoplasmic dots in a manner sensitive to the depletion of other IFT proteins. Are the cytoplasmic dots IFT particle precursors? How do they assemble? How do they migrate to reach the basal bodies and the cilium? All these questions are new fields of exploration.
When IFT57-GFP expressing cells are submitted to IFT46 RNAi, cytoplasmic fluorescent dots also appear, first as cortical dots between basal body rows, then at basal bodies and as intra-cytoplasmic dots. There is a clear relationship between IFT46 and IFT57 in the

apparition of these cytoplasmic inclusions. IFT46 RNAi provokes IFT57 dots, whereas IFT57 and other IFT proteins RNAi prevent IFT46 dots induced by reciliation.

CHAPTER 3

POTENTIAL NUCLEAR ROLE OF IFT57

PART 3.1. NUCLEAR TARGETING OF IFT57A

3.1.1. Localization of IFT57A-GFP and IFT57C-GFP proteins in vegetative cells

As already mentioned in Chapter 2, Fig. 2-1, a macronuclear labeling was observed for IFT57A-GFP, but not for IFT57C-GFP. Before addressing the specific differences between these two proteins, we noticed that this labeling was dependent on ciliary stimuli: a strongly enhanced IFT57A-GFP fluorescence of the macronucleus was observed during reciliation (Fig 3-1).

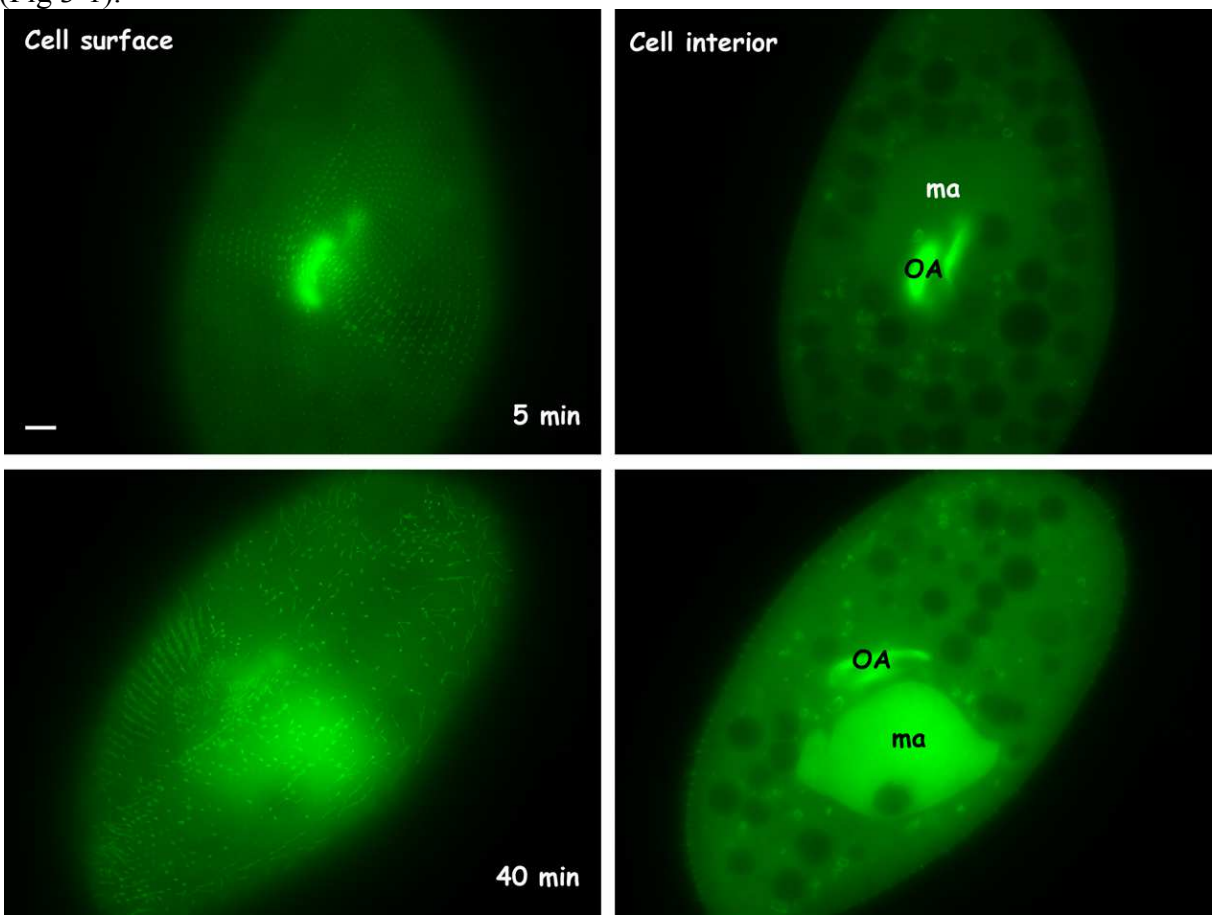

Figure 3-1. IFT57A-GFP accumulation in the macronucleus during reciliation viewed in epifluorescence microscopy*. At 5 and 40 minutes after deciliation, cells were directly fixed in paraformaldehyde without further permeabilization and observed under the fluorescence microscope. OA: oral apparatus, ma: macronucleus. Bar: 10µm.*

A strong macronuclear IFT57A accumulation is visible at 40 minutes post deciliation. This is obvious in this figure and not in previous figures in which the GFP visualization was combined with immunolocalization, because the macronuclear IFT57A-GFP tends to diffuse away under permeabilization. The macronuclear IFT57A accumulation should be due to relocalization from cytoplasm rather than to gene over expression, since microarray data show weak expression stimulation by deciliation only for IFT57C, not IFT57A (see Chapter 1, Table 1-2).

3.1.2. Localization of IFT57A-GFP during autogamy

Since IFT57A-GFP has a macronuclear localization during the vegetative stage, we examined the fate of this labeling during autogamy, a process in which the macronucleus degenerates and new macronuclear anlagen are built from derivatives of the zygotic nucleus (Fig. 3-2).

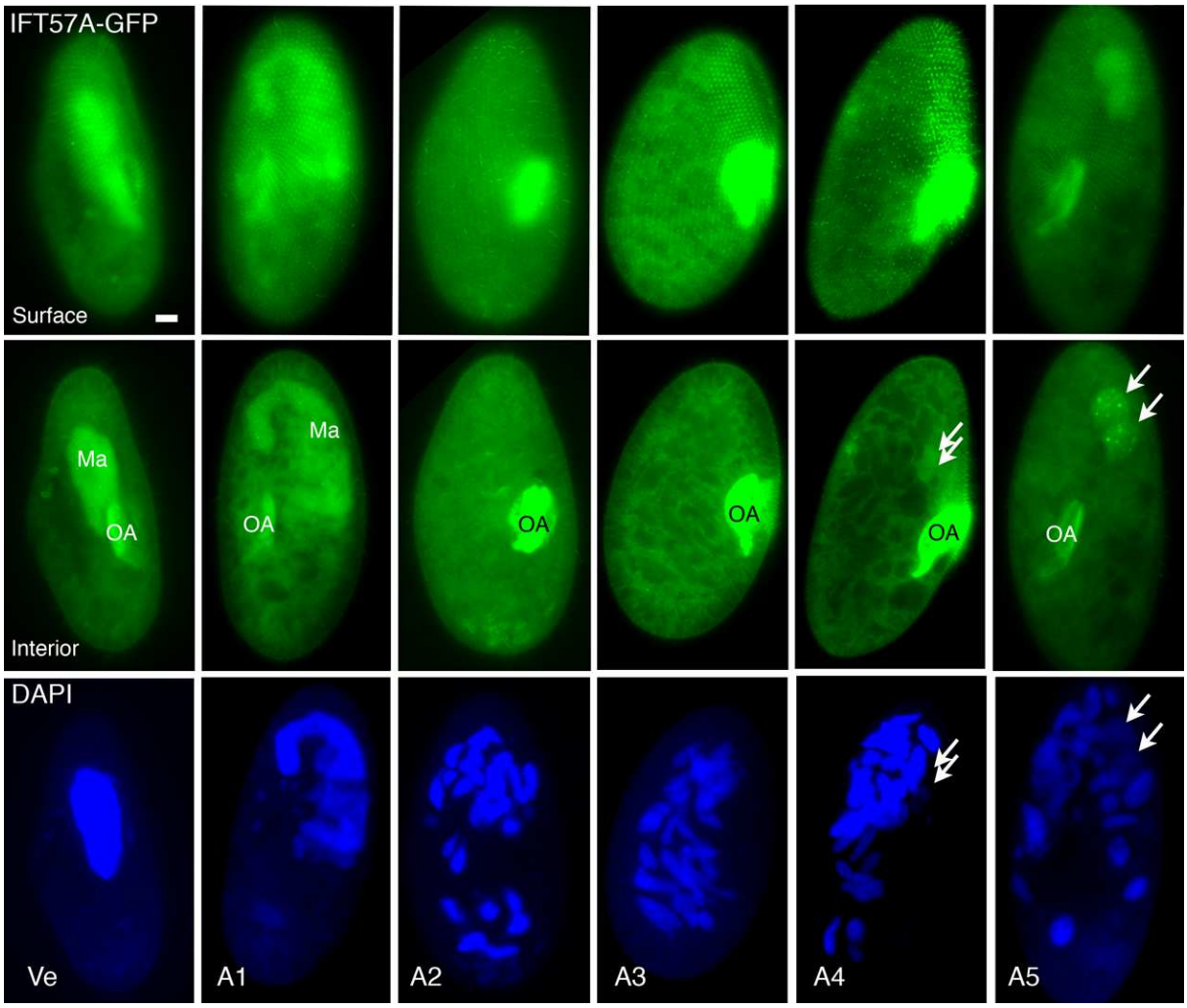

Figure 3-2. IFT57A-GFP localization during autogamy viewed in epifluorescence microscopy. *First column (Ve): vegetative cell. Other columns (A1 to A5): successive stages of Autogamy in which the disorganization and fragmentation of the macronucleus (Ma) occurs and new macronuclear anlagen (arrows) develop. First line: cortical views. Second line: same cells with focus on the interior of the cell. Third line: DAPI staining of the same cells to visualize the nuclei. Note the disappearance of the nuclear GFP labeling from the macronuclear fragments between stages A1 and A2 ant the localization in anlagen at stages A4 and A5 (arrows), with visible foci of accumulation in the stage A5 (see also Fig 3-3). The highly fluorescent object in the middle of the cell is the oral apparatus (OA) undergoing restructuration. Bar = 10 µm.*

It appears that the IFT57-GFP labeling seen in the macronucleus in vegetative cells progressively disappears from the macronuclear fragments to a level where the cytoplasm is more labeled that the fragments, with the oral apparatus reaching a peak of fluorescence (see stages A2 and A3 in figure 3-2), may be at the stage at which the haploid product from the meiosis that will be preserved for caryogamy reaches the paroral cone, close to the oral apparatus. In the mean time, an IFT57-GFP fluorescence concentrates into the macronuclear anlagen that develop. Interestingly, a strong cortical labeling appears in basal bodies and cilia of the anterior left field during the stages of early anlagen development (A4 in Fig. 3-2). Observation of the development of anlagen shows that the labeling increases with anlagen growth in size and concentrate into foci bigger and bigger Fig. 3-3).

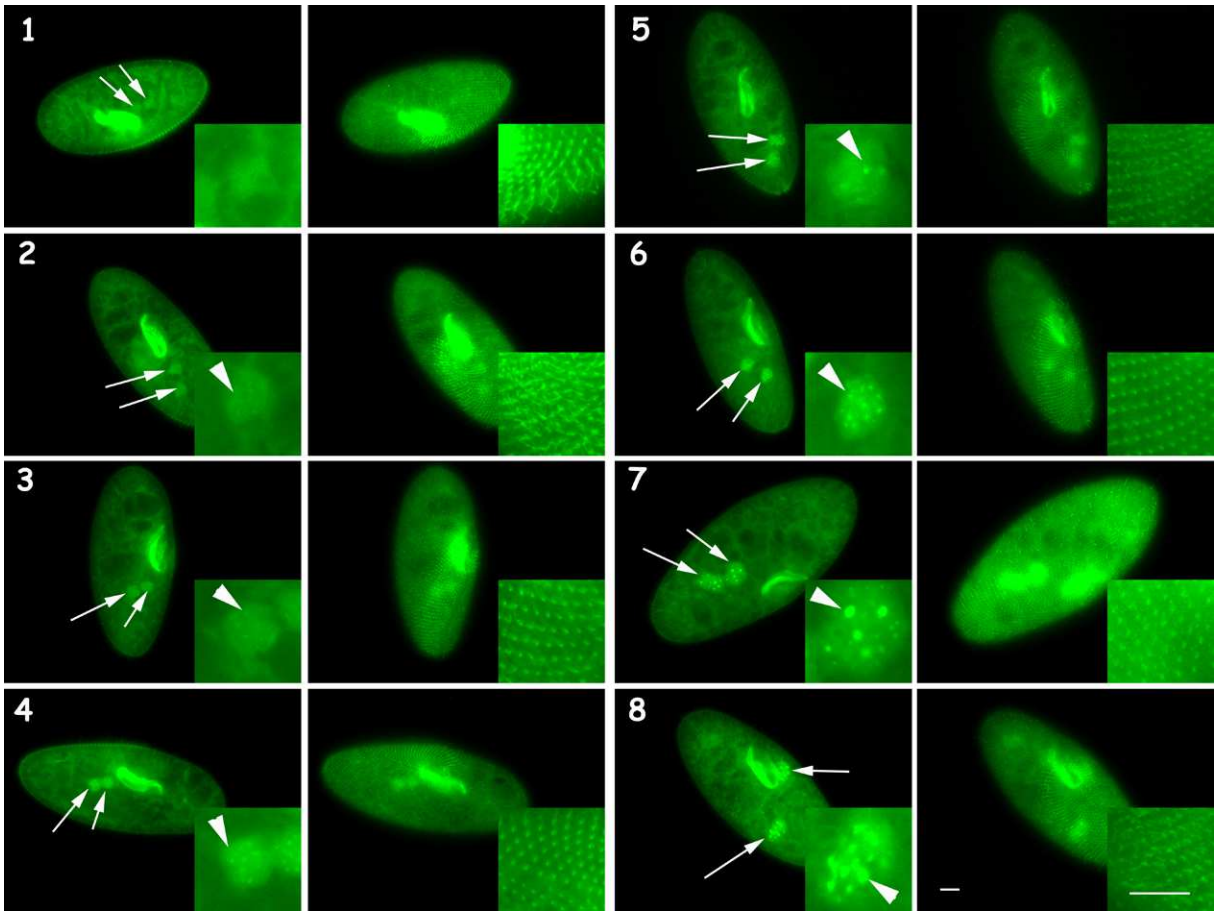

Figure 3-3, IFT57 labeling in the macronuclear anlagen and in the cortex during late stages of autogamy corresponding to panels A4 and A5 of Fig. 3-2 viewed in epifluorescence microscopy. *As anlagen develop (white arrows), the IFT57A-GFP fluorescence accumulates in small foci, which become bigger and bigger (white arrowheads in the insets) while the strong cortical labeling of basal bodies and cilia in the anterior left field of the cortex progressively diminishes. Bars = 10 µm.*

This increase of fluorescence in anlagen is paralleled by a progressive fluorescence decrease first in cilia, and then in basal bodies of the left anterior field. This may reflect either a ciliary reorganization during these stages or a traffic between basal bodies/cilia and nuclei, both phenomena not well documented, but which might be important for signaling during the autogamy processes.

3.1.3. Looking for the signal that targets IFT57A to the macronucleus, compared to IFT57C.

To try to uncover which part of the IFT57A sequence is responsible for its nuclear targeting, compared to IFT57C, I first looked for specific nuclear signals on dedicated servers (http://nls-mapper.iab.keio.ac.jp/cgi-bin/NLS_Mapper_form.cgi for nuclear import signals and http://www.cbs.dtu.dk/services/NetNES/ for nuclear export signal). No striking differences were found between IFT57A and IFT57 sequences, so that I decided to determine the relevant sequence experimentally. I constructed different vectors allowing the expression of chimeric proteins resulting from the fusion of different part of IFT57A and IFT57C (Fig. 3-4).

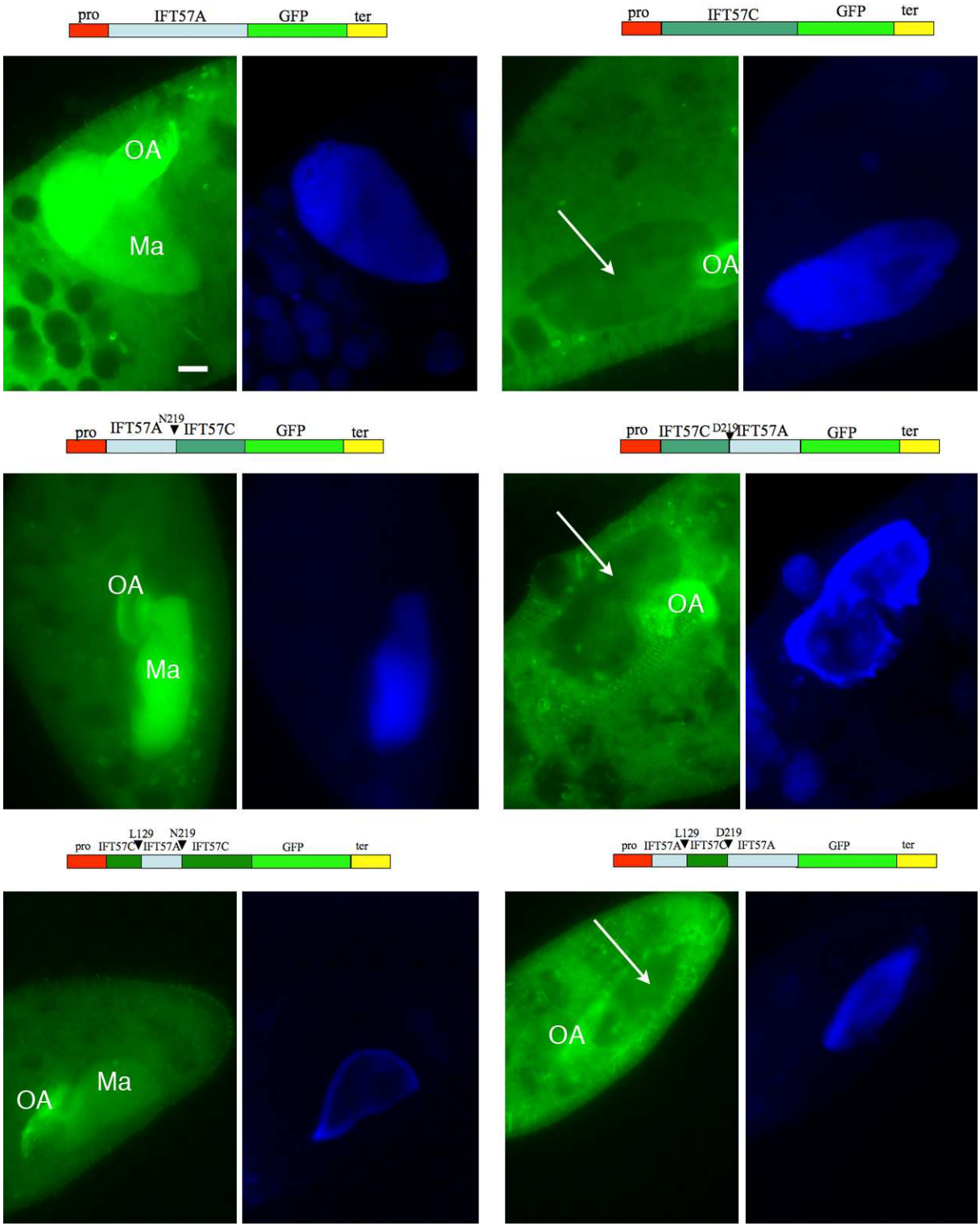
pro
IFT57A
GFP
ter
OA
Ma
pro
IFT57C
GFP
ter
OA
pro
IFT57A N219 IFT57C
GFP
ter
OA
Ma
pro
IFT57C D219 IFT57A
GFP
ter
OA
L129 N219
pro IFT57C IFT57A IFT57C
GFP
ter
OA
Ma
L129 D219
pro IFT57A IFT57C IFT57A
GFP
ter
OA

Figure 3-4. Macronuclear localization of chimeric IFT57A and C proteins tagged with GFP viewed in epifluorescence microscopy. *For each construct, the GFP fluorescence is presented in green and the DAPI labeling of the macronucleus in blue (in some cells like the one presented on the middle left, some food vacuoles take the blue dye). First line, reminder of the macronuclear labeling (Ma) given by IFT57A and the macronuclear exclusion (arrow) given by IFT57C. In the second line, the reciprocal chimaeras with N-ter half of one IFT57 and the C-ter half of the other one shows that the N-ter half of IFT57A contains the macronuclear targeting signal. In the third line, the signal is shown to be more precisely carried by the second N-terminal quarter, the L129-N219 segment, of the molecule. OA: oral apparatus, bar: 10µm.*

First, I fused the N-ter half part of the IFT57A gene encoding amino acid 1 to N219 to the C-ter Half of IFT57C gene encoding amino acid (D219 to stop) and reciprocally. After transformation, I analyzed the localization of the GFP signal. The presence of fluorescence in the nucleus of cells expressing the fusion proteins containing the N-ter half of IFT57A indicates that the signal is present in this part of the protein.. Then, I further manipulated this N-terminus in two pieces and found that the portion of the IFT57A coding L129 to N219 embedded in an IFT57C gene context was sufficient to target the GFP fusion protein to the macronucleus. Reciprocally, the equivalent portion of IFT57C, between L129 and D219 in an IFT57A context was sufficient to exclude the GFP fusion protein from the macronucleus (Fig. 3-4, last line). The macronuclear targeting sequence seems thus to reside between L120-N219 portion of IFT57A, with the precaution that the labeling is neither as strong nor as stable in time as the native IFT57A protein. Indeed, after a few cell divisions, the macronuclear labeling of the chimeric protein disappears.

I wondered whether the L129-N219 macronuclear localization signal was also able to ensure the change of nuclear localization during autogamy. Thus I transformed cells with the chimeric construct at the stage where they are competent for autogamy, to follow the phenomenon right away before the signal vanishes. The resulting transformed cells were then induced for autogamy by starvation and observed (Fig. 3-5).

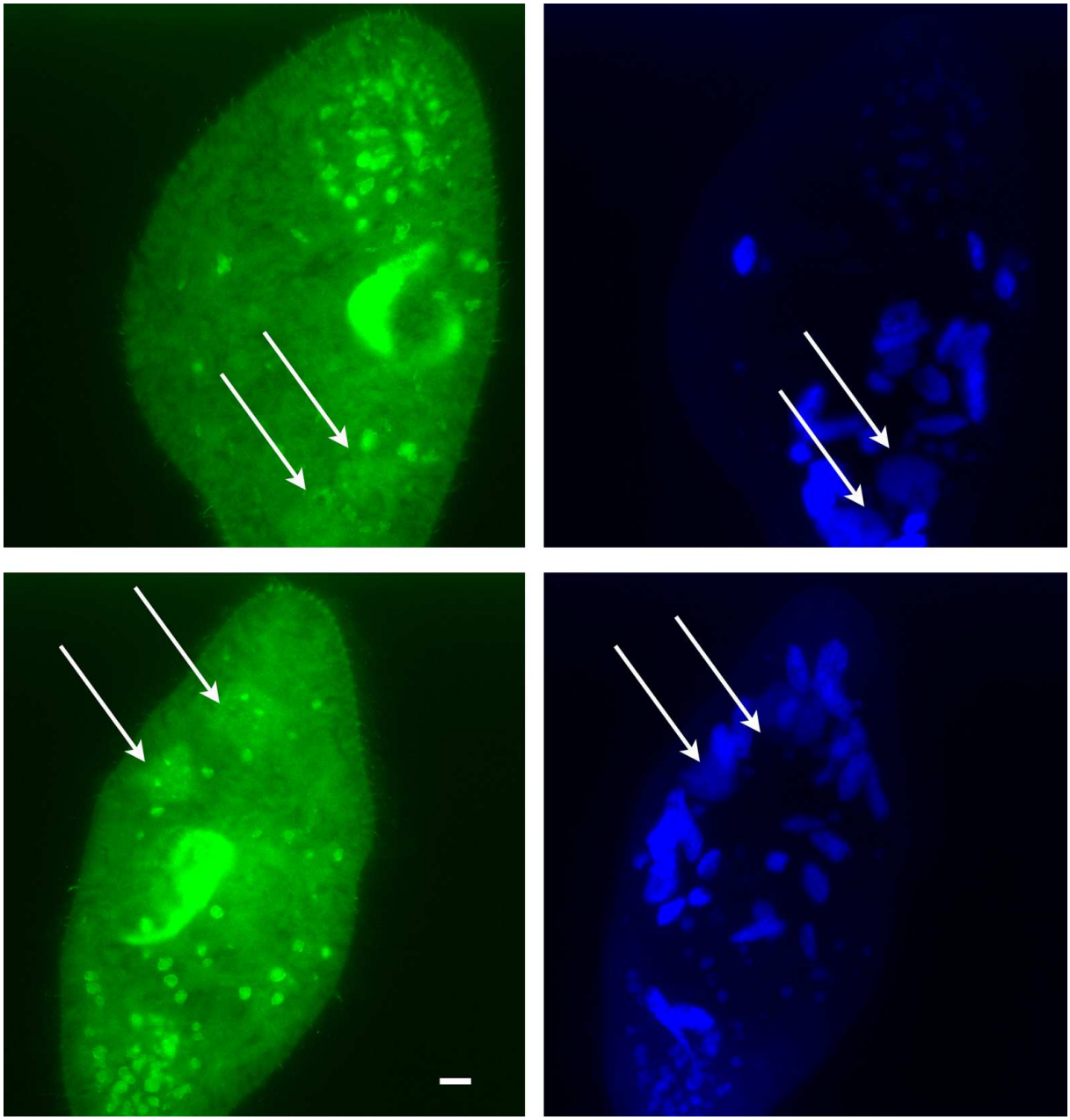

Figure 3-5. Two examples of IFT57-GFP targeting to the developing macronuclear anlagen during autogamy with the shortest IFT57A signal in a chimeric IFT57A+C molecule viewed in epifluorescence microscopy*. Left: GFP labeling, right: DAPI staining. Note that the anlagen are weakly labeled by GFP (arrows), with even a few foci in the anlagen of the bottom cell, whereas the fragments of the old macronucleus (blue in DAPI) are not. Bar: 10µm.*

The IFT57A and IFT57C proteins of *Paramecium* derive from a common ancestor before the occurrence of two successive genome duplications. Their sequences are very similar all over their length, including the L129-N219 region containing a signal experimentally determined for specific macronuclear localization of IFT57A. I summarized all the information about these two sequences in Figure 3-6.

Figure 3-6. Alignment of IFT57A and IFT57C sequences. *Nuclear localization signal sequences (NLS) are highlighted in yellow. Differences appear between the two proteins, but, except the NLS in common which has a medium score (5 on a 1-10 scale), they have a low score around 3. Nuclear export signal sequences (NES) are boxes in black. The NES of IFT57C appears with a higher score than the one of IFT57A, although they have the same sequence. It is likely that amino acid environment influences the prediction algorithm. The L129-N219 sequence determined in this work to target IFT57A to the macronucleus is boxed in blue, and the substitutions pointed by arrowheads.*

Both IFT57A and IFT57C proteins possess a predicted bipartite NLS predicted at positions 109-137 with a score of 5.3 indicative of proteins with dual localizations, in the nucleus and in the cytoplasm. IFT57A possesses other NLSs, one at positions 37-66 with a score of 3.1 and another one at positions 312-339 with a score of 3, both being of low probability. Both proteins also possess the same NES at positions 346-355, but with a probability just above threshold for IFT57A and of twice the threshold for IFT57C. Altogether, this suggests a higher facility for IFT57A than for IFT57C to be nuclear. However, these features do not correspond to the region that I functionally determined by the use of chimeric molecules. This remains mysterious, but will need to examine the substitution between the sequences of the critical region. Apparently, most of the substitutions are conservative. Only V139A, Q199K and N219D (bold arrowheads on Fig. 3-6) could be candidates to be the relevant positions if site-directed mutagenesis is undertaken.

Recently, the laboratory of M. Lynch in Bloomington provided access to the genome sequence of a number of *Paramecium* species they study. These species are *Paramecium caudatum*, *Paramecium multimicronucleatum*, *Paramecium primaurelia*, *Paramecium*

biaurelia and *Paramecium sexaurelia*, which added to the known genome of *Paramecium tetraurelia* make six whole genome sequences for the genus *Paramecium*. I extracted the sequences of IFT57 genes from these genome sequences and performed alignments to see whether inter-species comparison could give clues about the macronuclear targeting (Fig. 3-7).

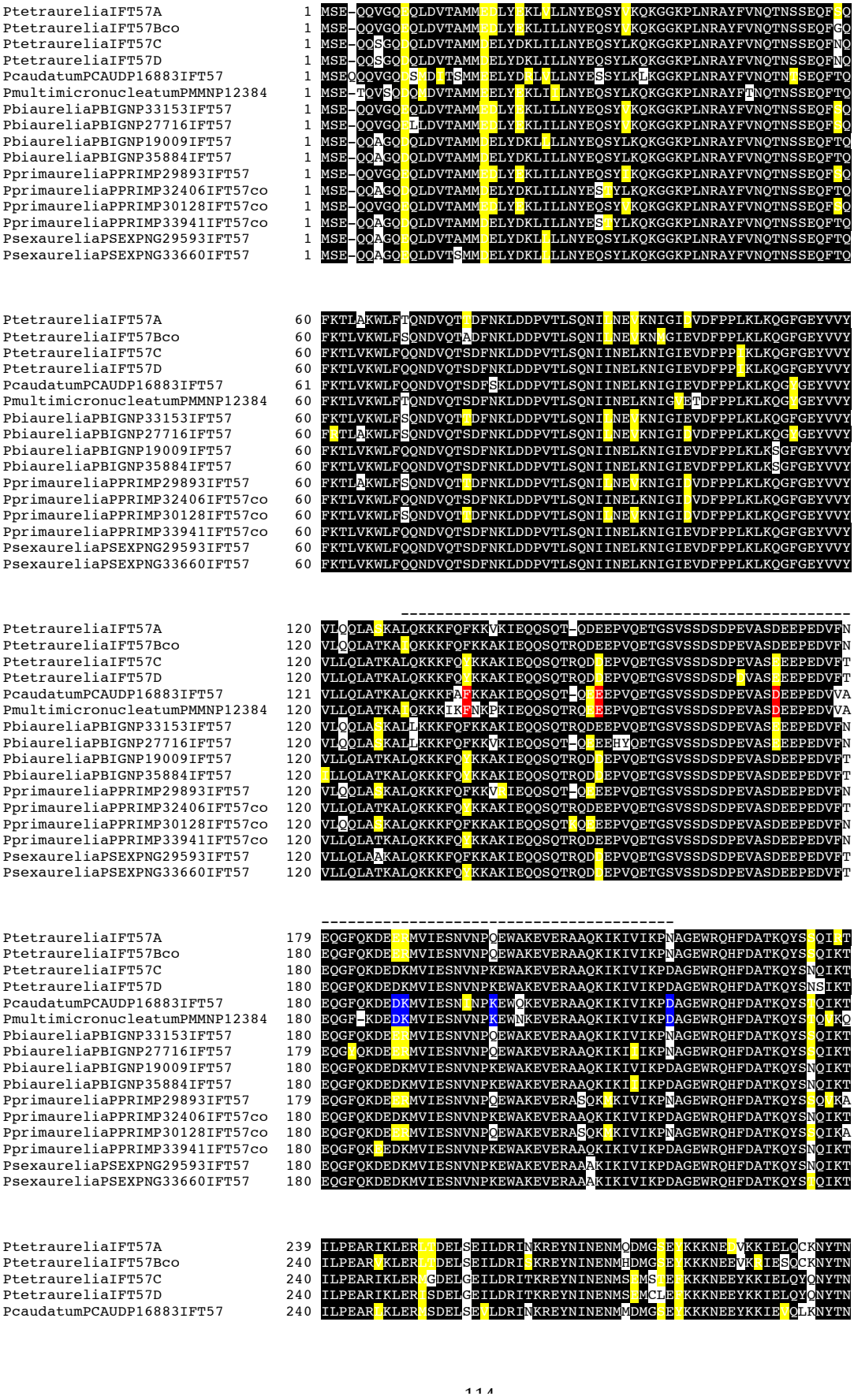

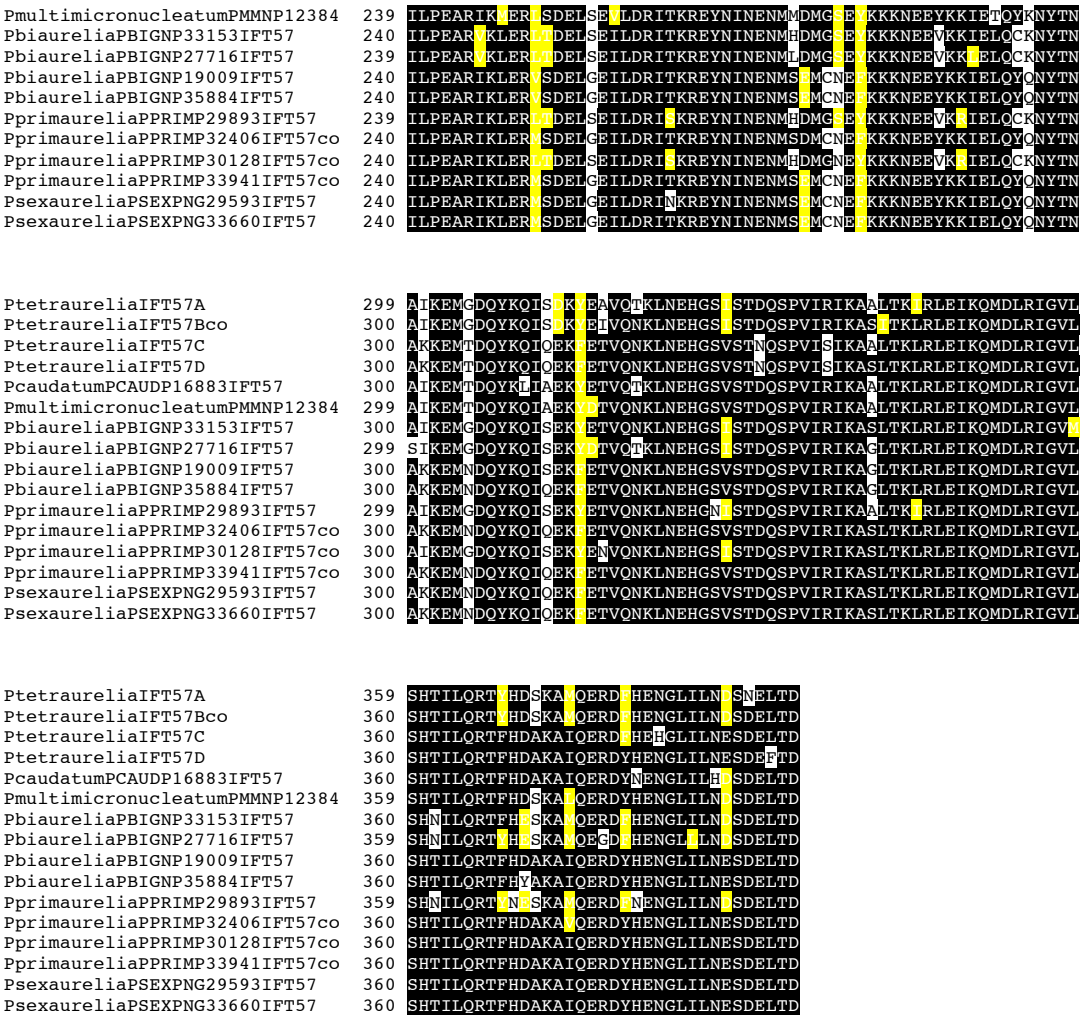

Figure 3-7. Alignment of IFT57 genes from 6 Paramecium species. *In addition to the 4 genes from P. tetraurelia, I found 4 genes in P. primaurelia, 4 genes in P. biaurelia, 2 genes in P. sexaurelia and only a single gene in P. caudatum and in P. multimicronucleatum. These genes come from automatic annotation and I had to manually examine the sequences to correct the gene models (gene name followed by "co" in the alignment). I examined the region corresponding to L129-N219 of tetraurelia in all species. In particular, since P. caudatum and P. multimicronucleatum have only a single IFT57 gene, I compared IFT57A and IFT57C of tetraurelia to these species. In red are positions in P. caudatum and P. multimicronucleatum sequences that correspond to IFT57A-specific substitutions and in blue to IFT57C-specific substitutions.*

In the alignment, both *P. caudatum* and *P. multimicronucleatum* IFT57 unique sequences are identical between them at the positions corresponding to IFT57A versus IFT57C in the critical region. Three positions noted in red in the *P. caudatum* and the *P. micronucleatum* sequences correspond to the IFT57A sequence and four positions, noted in blue, to the IFT57C sequence. If we consider that all of these sequences arise from a common ancestor and that the *P. tetraurelia* duplicate paralogs appeared later, it would be worth knowing whether the ancestral protein had macronuclear localization or not. If it is macronuclear, this would mean that IFT57A has the full function and that IFT57C lost the nuclear function after the duplication that separated the IFT57A from the IFT57C lineages. In such a case, the amino acids highlighted in red would be critical for the nuclear localization. In contrast, if the

ancestral protein is not macronuclear, the macronuclear localization of IFT57A in *P. tetraurelia* would be a gain of function and the positions highlighted in blue, which diverged in IFT57A, would then be critical. I therefore cloned the *P. caudatum* IFT57 sequence in fusion with the GFP gene under its own 5' and 3' regulators and transformed *P. caudatum* cells with this construction (Fig. 3-8).

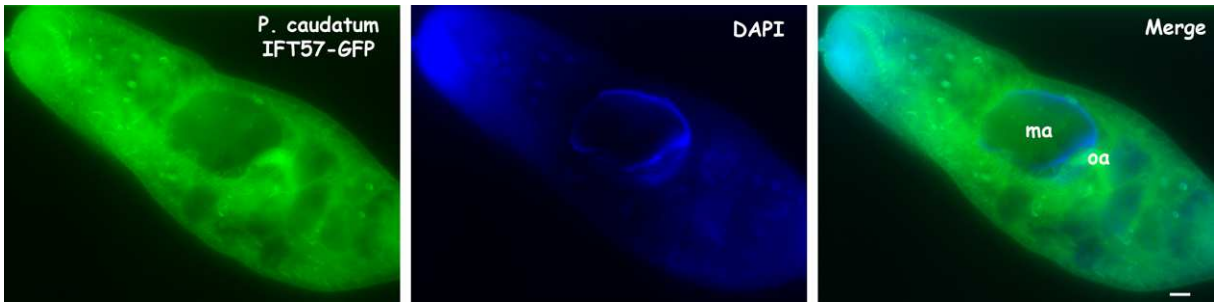

Figure 3-8. Paramecium caudatum expressing endogenous IFT57 fused to GFP. The green fluorescence is clearly excluded from the macronucleus. Bar = 10 µm.

The result of this experiment in *P. caudatum* is that IFT57-GFP localizes, as it does in *P. Aurelia*, in the basal bodies and in growing cilia (not shown), but is excluded from the macronucleus. This would mean that at least one of the four positions noted in blue in the alignment of Figure 3-7 are determinant for localization in or out of the macronucleus. The ancestral sequence DK-x(9)-K-x(19)-D between positions 188 and 219 has been kept in IFT57C after the intermediate whole genome duplication, whereas a shift toward ER-x(9)-Q-x(19)-N occurred in IFT57A that allowed macronuclear localization. The examination of the four mutated positions shows that two of them are conservative D->E, K->R. The two others, K->Q and D->N are therefore more prone to represent the effective positions critical for macronuclear localization/exclusion. This aspect could be addressed by a site-directed mutagenesis approach.

3.1.3. Conclusion of Part 3.1.

IFT57, also known as HIPPI in man, has a nuclear localization in mammalian cells in which it has a role, by interaction with HIP1, in transcription of some caspases. In *Paramecium tetraurelia*, no homologs of HIP1 or of caspases can be found in the genome, but at least one form of the IFT57 molecule can go to the macronucleus and, during autogamy, shift to the developing macronuclear anlagen in which it accumulates in foci. The role of this nuclear localization will be addressed in the next part of this chapter, but I found interestingly that, among the different IFT57 proteins harbored by *Paramecium*, IFT57A could go to the macronucleus whereas IFT57C was excluded from it. Both proteins are very close in amino acid sequences and both display putative NLS. By analyses of chimaeras, I determined the segment L129-N219 as determinant for macronuclear localization or exclusion and, by comparison with the behavior and the sequence of IFT57 in *Paramecium caudatum*, I found that two amino acids might be essential for this localization. However, this region does not overlap with any of the putative NLS of the molecule. The nuclear import should therefore take place through the interaction with another protein travelling to the nucleus. In addition, the particular region containing the two critical amino acids is not conserved in evolution and outside of the regions that can be aligned with the human IFT57/HIPPI amino acid sequence. It should be another region in the human protein that drives its nuclear localization.

Another interesting phenomenon was the changes in localization of IFT57-GFP during the autogamy process, suggesting a strong traffic between cortical elements such as cilia and basal bodies and the nuclei, old macronucleus and developing anlagen.

PART 3.2. LOOKING FOR THE ROLE OF IFT57A IN THE MACRONUCLEUS

The opposite behavior of IFT57A and IFT57C proteins toward nuclear localization asks the question of the role of IFT57A in the macronucleus. Its particular behavior during autogamy, mimicking the behavior of proteins involved in small RNA metabolism responsible for genome rearrangements during macronuclear development (Lepere et al., 2008) leads me to look the effects of its depletion, compared to IFT57C, during sexual events. Indeed, IFT57 has a role of linker between motors and cargo in ciliary transport. An interesting idea to test would be a similar role for cargo transport between old and new macronucleus during sexual events.

3.2.1. Attempts to induce RNAi during autogamy by expression of a hairpin RNA under the NOWA1 promoter.

The lethal effect of IFT57A+C RNAi within two days during vegetative growth prevented the use of the routine feeding protocol carried out to study genes involved in autogamy (Galvani and Sperling 2002). Indeed this protocol requires exponential growth in the silencing bacteria before induction of autogamy as cells reach starvation. I thought that it would be worth to find a way to induce RNAi specifically at autogamy without impairing cell growth. A strategy of expression of hairpin (or sh) RNA under desired promoters is widely used in mammalian cells and has been successfully tried in another ciliate, *Tetrahymena* (Howard-Till & Yao, 2006). Since we know promoters in *Paramecium* that drive gene expression at autogamy (NOWA1, PTIWI09), I decided to develop new tools for inducible hairpin silencing in *Paramecium*.

3.2.1.1. Working out hairpin RNAi in Paramecium.

I started a series of vector constructions to test first the hairpin RNAi principle and second the possibility to have specific induction during autogamy (see Materials and Methods). I used the CAM (calmodulin) promoter for constitutive expression and the NOWA1 promoter for expression as soon as early autogamy. In addition to IFT57A and C, a gene tested was NSF (N-ethylmaleimide sensitive factor) gene is essential in the regulation of the intracellular membrane traffic, especially between the endoplasmic reticulum and the Golgi apparatus (Kissmehl et al., 2002). The turnover of this protein is such as the RNAi by feeding provokes cell lysis within less than 24 hours (Galvani & Sperling, 2002). For this particular gene, I tried two kinds of constructs, a short one of 290 base pairs and a long one of 792 base pairs of the NSF1 sequence, to manipulate possible different lethality effects.

3.2.1.1.1. Efficient hairpin silencing with the NSF gene

The first experiment consisted in transformation of vegetative cells with a hairpin containing 792 base pairs of the NSF gene under the control of the CAM promoter. After injection of the construct into the macronucleus of wild type cells, all the microinjected cells died by lysis (a phenotype characteristic of NSF silencing) between 20 and 24 hours post microinjection. This result indicated that sh RNAi was possible in *Paramecium*.

A second experiment was to co-transform wild type cells with the NSF hairpin vector under control of the NOWA1 promoter and with a vector in which the NOWA1 gene fused to GFP under the control of its own regulators to have a reporter gene for the autogamy process in the transformed cells (Fig. 3-9).

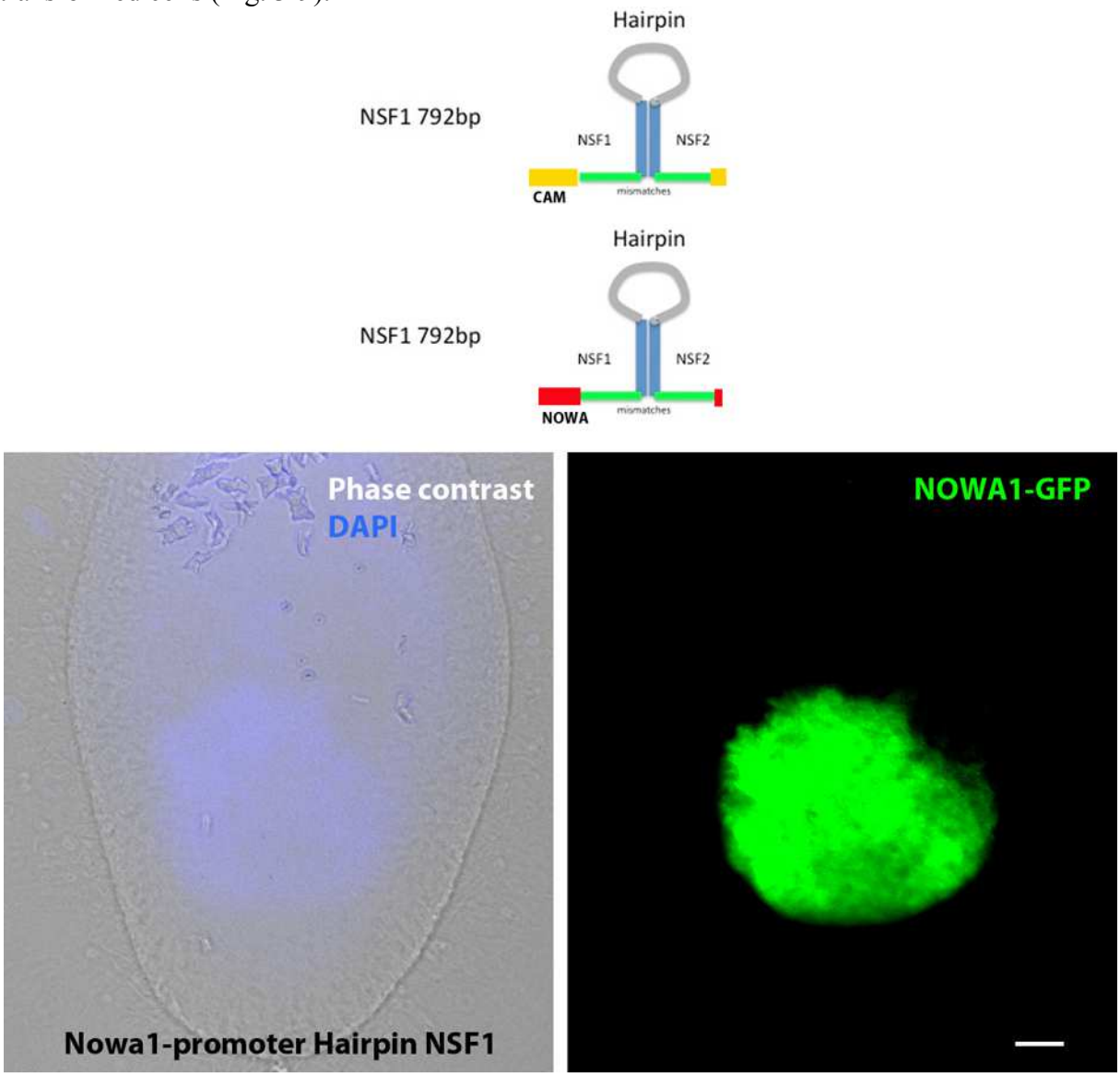

Figure 3-9. Hairpin silencing using NSF as a test gene. *Top- scheme of the constructs used in this experiment: the NSF hairpins were cloned between the CAM regulators (in yellow) or the NOWA1 regulators (in red). Bottom- NSF-hairpin expression during autogamy. Cells were co-microinjected with a NOWA1-GFP fusion under its own regulators and with the NSF hairpin under the same NOWA1 regulators. The NOWA1-GFP was an indicator of the entry into autogamy (right panel) viewed in epifluorescence microscopy. Shortly after autogamy induction, the cells lyzed and died, a process already engaged in the cell of this figure (left panel).*

After co-transformation the non-fluorescent transformants grew perfectly well during the vegetative phase. This growth ability confirms that the under the NOWA promoter, the NSF hairpin in not expressed during vegetative phase. After 25 divisions in log phase after microinjection I induced autogamy in the cells by starvation. As soon as they reached the

plateau, a strong macronuclear fluorescence appeared in the cells, confirming that they were able to enter the autogamy process. A few hours later, they died by lysis indicating that the NSF hairpin is also induced and thus that the RNAi induction specific for autogamy is effective.

3.2.1.1.2. Cycle of Ptiwi09-GFP during autogamy

To avoid any conflicts between the promoters controlling the expression of the hairpin and the reporter gene, I used Ptiwi09 GFP rather GFP Nowa as reporter gene. As Nowa1, Ptiwi09 (Bouhouche et al., 2011) is induced during autogamy. In addition, as does IFT57A, its shift from old to new macronucleus during the autogamy and its presence allowed to test if the IFT57A RNAi has an effect on protein transport from old macronucleus to new anlagen (Fig 3-10).

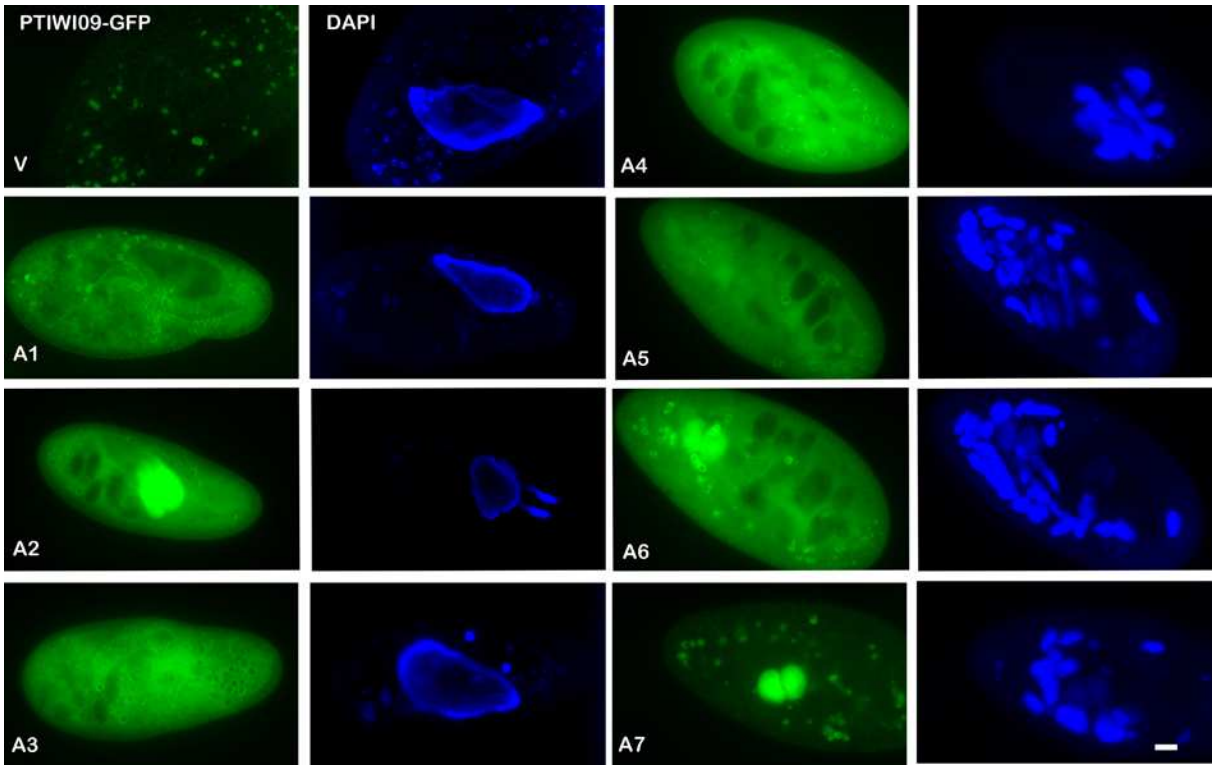

Figure 3-10. Cycle of Ptiwi09-GFP during autogamy viewed in epifluorescence microscopy. *Cells transformed by an expression vector of Ptiwi09-GFP under its own regulators were obtained by DNA microinjection into the macronucleus. After transformation, vegetative cells (V) do not show any GFP fluorescence. When autogamy occurs (stages A1-A7), GFP fluorescence appears. A1: cytoplasmic (and cortical around basal bodies, not shown) fluorescence; A2: strong macronuclear fluorescence; A3-A5: decrease of nuclear fluorescence of the old macronucleus; A6, A7: high fluorescence of the growing anlagen. Bar: 10µm.*

As already described by Bouhouche et al. (2011), I found that Ptiwi09-GFP was specifically expressed during autogamy, first in the cytoplasm and in the cortex in association with basal bodies (not shown), next in the macronucleus, with a final shift to the growing anlagen.

3.2.1.2. Effect of IFT57 RNAi by hairpin expression during sexual events.

To test the effect of IFT57 during autogamy, I undertook the cloning of the hairpin versions of IFT57A and IFT57C under the NOWA1 regulators. If the cloning of the IFT57A hairpin was not problematic, for unknown reasons, the cloning of the IFT57C hairpin did not work despite many attempts.

3.2.1.2.1. Autogamy

I performed the co-transformation of wild type cells with the vectors allowing the expression Ptiwi09-GFP under its own regulators and the IFT57A hairpin under the NOWA1 regulators. (Fig. 3-11). I used the short segment of NSF under the NOWA1 promoter as a non-specific hairpin control. (Fig. 3-12).

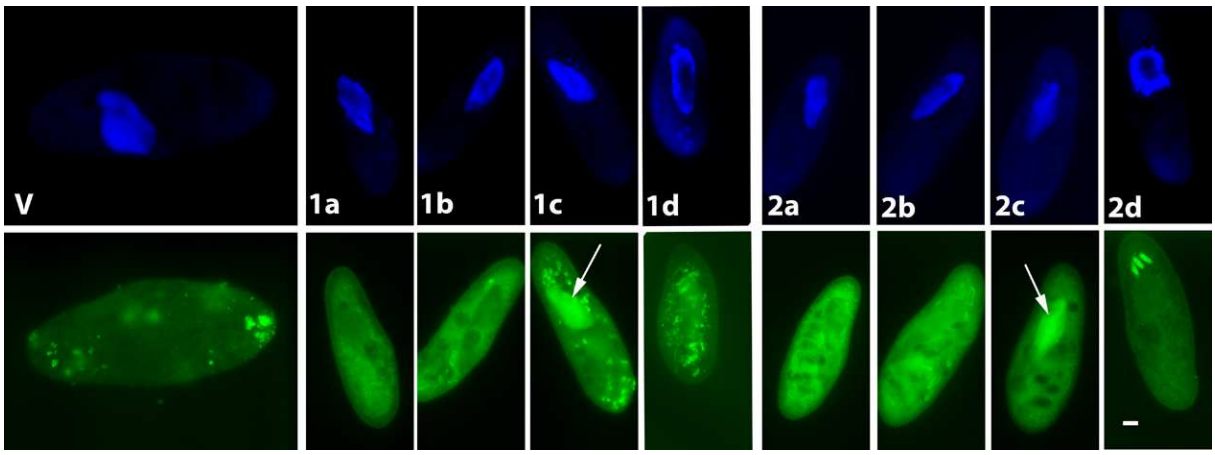

Figure 3-11. Effect of IFT57 hairpin expression during autogamy viewed in epifluorescence microscopy. *Cells co-microinjected with Ptiwi09-GFP and IFT57 hairpin under the NOWA1 promoter (V) become fluorescent first in the cortex (1a, 1b) and then in the macronucleus (1c) under starvation when cells are competent for autogamy. However, autogamy does not proceed further and the macronuclear fluorescence disappears (1d). If cells are put back in growth medium, the fluorescence totally disappears, but reappears as soon as the cells starve, without any incompetence period. The novel "pseudoautogamy" cycle (2a -2d) follows the same scheme as the first one. This has been reproduced for five successive cycles. Bar: 10 µm.*

When autogamy was induced by starvation of the transformed cells, we observed the Ptiwi09-GFP fluorescence deployment in the cortex and in the macronucleus indicating that the early event of autogamy occurred (figure3-11, 1a, 1c), although a small proportion of cells immobilize and die. However, in the bulk of surviving cells, autogamy does not proceed further: the macronuclear fluorescence disappears (1d) but the macronuclear fragmentation does not occurred. If cells are put back in fresh growing medium, they resume a normal growth and could be starved again. At this time fluorescence reappeared indicating they the cells could be competent again for autogamy. But as previously the autogamy did not proceed further. This "pseudoautogamy" process has been reproduced for five successive cycles afterwards the cells were committed to senescence. These observations show that the IFT57A hairpin silencing under the NOWA1 promoter blocks autogamy at a very early stage: (1) autogamy is triggered since Ptiwi09-GFP is up-regulated and localizes to basal bodies and macronucleus; (2) autogamy is blocked at very early stages since no meiotic figures could be detected and the macronucleus never fragments; (3) no sign of hidden autogamy is visible

since, after re-growth in fresh medium, cells display the same early autogamy signs upon starvation, without any immaturity period as should occur if they had completed an autogamy; (4) after a series of growth and starvation period, the clones are committed to senescence, indicating that they never underwent autogamy since the transformation by the hairpin vector.

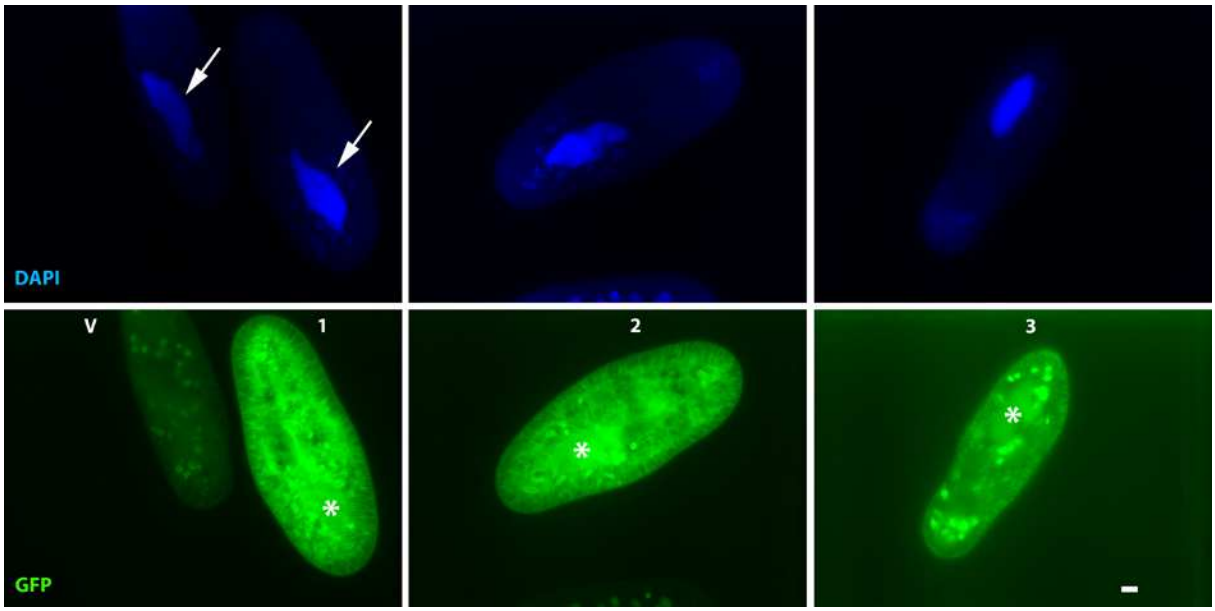

Figure 3-12. Effects on NSF hairpin expression on autogamy viewed in epifluorescence microscopy. *DAPI (top row) and GFP (bottom row) staining of cells expressing both NSF hairpin RNA under the NOWA1 promoter and Ptiwi09-GFP. On the left are presented two cells: one cell noted "v" in vegetative stage (without GFP fluorescence and the other one "1" in early autogamy (both macronuclei are pointed by arrows and the fluorescent macronucleus by a star). Two other cells, "2" and "3" also present a fluorescent macronucleus. Bar: 10µm.*

Using the control induction of NSF short hairpin RNA during autogamy (under the NOWA1 promoter), no lethality was observed, but the same phenotype as the one obtained by IFT57A hairpin induction occurred, i.e. early appearance of Ptiwi09-GFP in the cytoplasm and in the macronucleus, then block of nuclear processes at this stage. The fluorescence diminished with time but the same events can be reproduced after re-growth and starvation.
This last result indicates that the autogamy blockage is a general hairpin effect and not specific to IFT57A silencing. Although very new and interesting, this aspect was not pursued in my thesis because I tried to unravel the nuclear role of IFT57A.

3.2.1.2.2. Conjugation

To try to obtain an information about the transport between the old and new macronuclei I wondered whether this question could be approached during conjugation, because mating with a normal cell could have a compensatory effect and "dilute" the blocking given by the hairpin RNA. Are the hairpin expressing cells able to mate with a wild type partner? Yes they are. I therefore analyzed the course of conjugation between a transformed cell expressing IFT57A hairpin under the NOWA1 promoter and Ptiwi09-GFP and a wild type cell (Fig. 3-13).

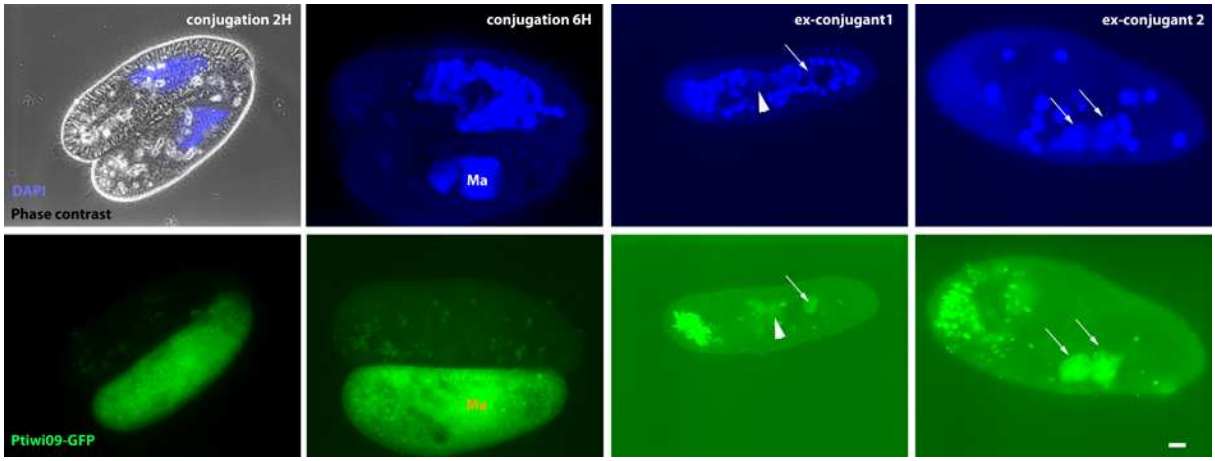

Figure 3-13. Conjugation of cells expressing IFT57A hairpin RNA under the NOWA1 promoter and Ptiwi09-GFP with control cells viewed in epifluorescence microscopy. *From left to right: 1) mating pair after 2 hours of conjugation in which the Ptiwi09-GFP expressing partner is clearly visible; 2) mating pair after 6 hours of conjugation in which a strong asynchrony is seen between the two conjugants, the one expressing Ptiwi09-GFP being delayed in macronuclear fragmentation compared to its mate; 3) and 4) two ex-conjugants from the same pair 16 hours after the end of conjugation. Arrows: anlagen. Arrowhead: putative small anlagen. Ma: macronucleus. Bar: 10µm.*

During conjugation, the first observation is that, as it could be expected, one cell of each pair expresses Ptiwi09-GFP and the other not. Then, the partners expressing Ptiwi09-GFP are delayed in nuclear disorganization compared to the wild type partner. After separation of ex-conjugants and overnight recovery in growth medium, both cells from the pairs are fluorescent, a big cell with fluorescent anlagen and a smaller cell with ill defined weakly fluorescent anlagen. The ex-conjugants from 8 pairs were inoculated in fresh medium, and, for each pair, a cell died and the other gave a growing clone. Although it has not been experimentally followed, it is likely that the small ex-conjugant cells that are also the cells dying at inoculation correspond to Ptiwi09-GFP and IFT57A hairpin expressing parental cells. If yes, this shows that the hairpin RNA does not diffuse to the mating cell in a pair, in contrast to Ptiwi09-GFP, which accumulates in anlagen of both cells.
Whatever the true interpretation, this experiment does not provide evidence that IFT57 RNAi prevents accumulation of Ptiwi09-GFP in anlagen. Although many questions remain unsolved about inducible hairpin RNAi, this was not the way to answer my question of what does IFT57A in the nuclei during autogamy. Therefore, I stopped this part of my research to focus on other means to silence IFT57.

3.2.2. "Regular" IFT57 RNAi during sexual events

The block of autogamy obtained under IFT57A and NSF hairpin silencing does not give any clue to the role of IFT57A in nuclear transport. I therefore decided to go back to regular "feeding" techniques for RNAi during sexual events by ensuring a tight control about the duration and timing of RNAi to avoid vegetative lethality.

3.2.2.1. Effect of IFT57 RNAi during conjugation.

The effects during the first day after conjugation (analysis of DNA rearrangements) and after inoculation into fresh medium (survival) were analyzed (Figure 3-14).

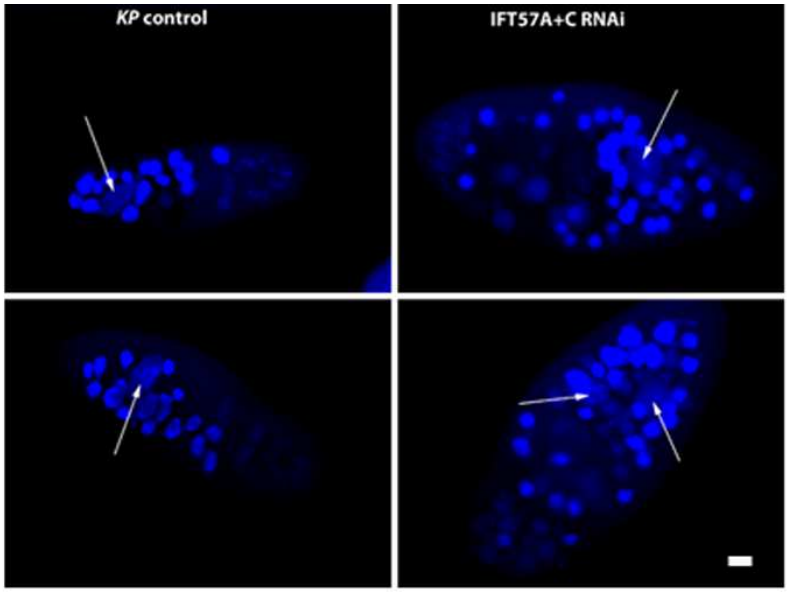
KP control
IFT57A+C RNAi

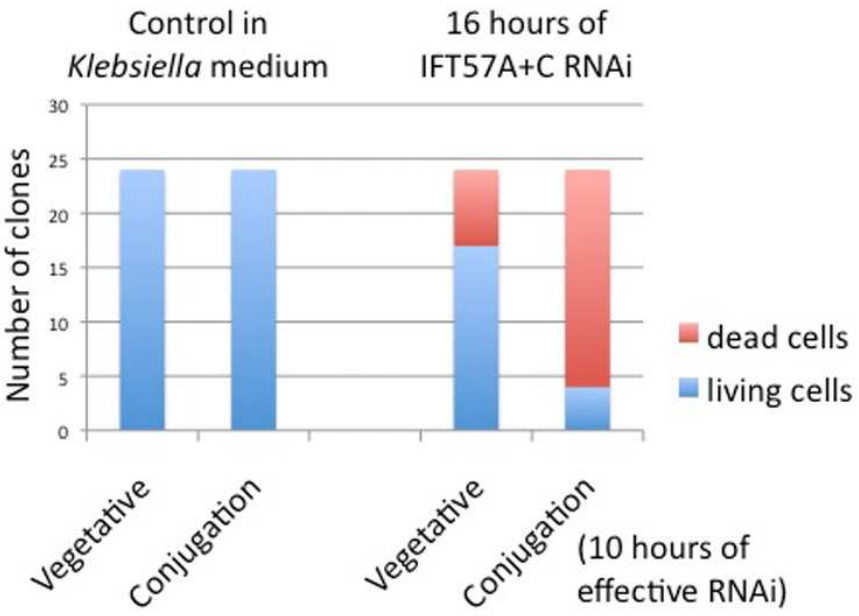
Control in
Klebsiella medium
16 hours of
IFT57A+C RNAi
Number of clones
30
25
20
15
10
5
0
dead cells
living cells
Vegetative
Conjugation
Vegetative
Conjugation
(10 hours of
effective RNAi)

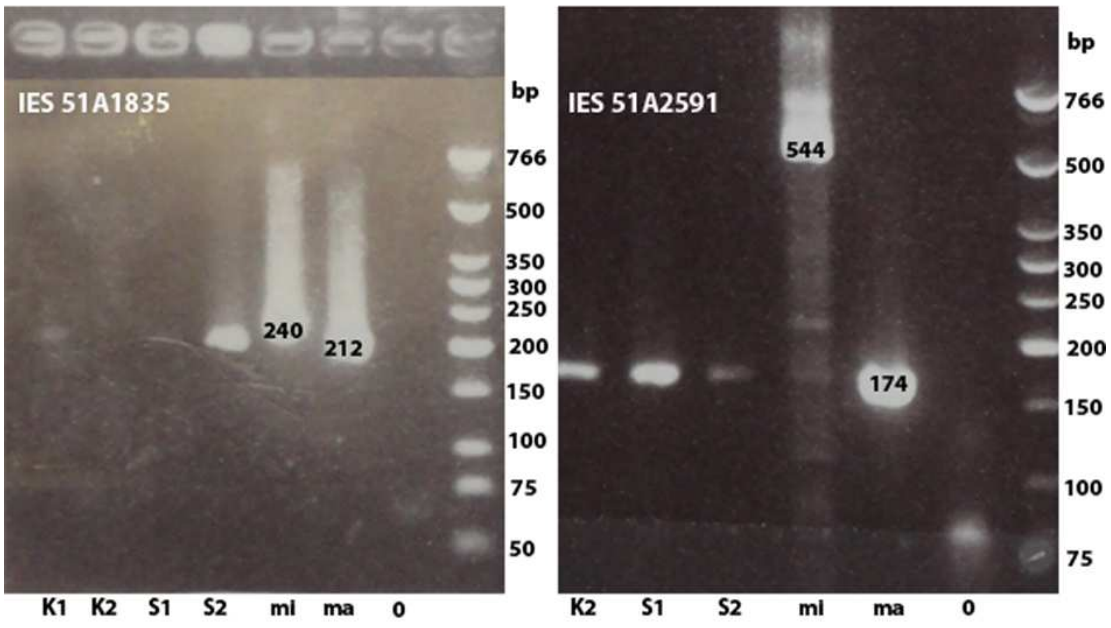
IES 51A1835
bp
766
500
350
300
250
200
150
100
75
50
240
212
K1
K2
S1
S2
mi
ma
0
IES 51A2591
bp
766
500
350
300
250
200
150
100
75
544
174
K2
S1
S2
mi
ma
0

Figure 3-14. Effect of IFT57A+C RNAi on conjugating cells. *Top panel: presence of anlagen (white arrows) in cells issued from conjugation with or without IFT57 RNAi treatment. Bar: 10µm. Middle panel: comparison of clone survival when cells submitted to RNAi are transferred to normal Klebsiella medium (conjugation versus vegetative; IFT57A+C RNAi treatment versus control Klebsiella medium). Bottom panel: evaluation of IES excision by PCR on ~50 cells at the end of the RNAi treatment when anlagen were detectable. K1 and K2: Klebsiella control, S1 and S2: silenced cells using RNAi medium, mi: micronuclear DNA control, ma: macronuclear DNA control, 0: no template DNA. The PCR products in S1 and S2 have the size of the macronuclear versions, i.e. without IES.*

Cells of both mating types were grown and induced to reactivity by starvation in normal *Klebsiella* medium. Reactive cells were mixed and tight pairs were isolated and transferred to IFT57A+C RNAi medium for 16 hours. In parallel, vegetative cells were inoculated in the RNAi medium and left for 16 hours. Conjugating pairs generally separate after 4 to 6 hours, depending on the experiment. Since pairs do not feed, the time of exposure of the cells to the RNAi medium really starts after separation of the conjugants and approximately corresponds to 10 hours. After RNAi treatment, cells are still swimming, however a little slower likely because they start to have a decreased number of cilia. I first checked by DAPI staining the behavior of the nuclei in the ex-conjugants and observed normal macronuclear fragmentation and anlagen development Fig 3-14, top panel).
To test the ability of the inactivated cells to survive I transferred the ex-conjugants and vegetative inactivated cells back to *Klebsiella* medium and I compared their ability to give rise to growing clones. Only 4 over 24 clones were growing among inoculated ex-conjugants after 10 hours of effective IFT57A+C RNAi treatment, compared to the 17 over 24 growing clones from vegetative cells treated for 16 hours (Fig. 3-14, middle panel). Since new anlagen were observed after conjugation, the lethality could be accounted for a defect in a step of the development of the new macronucleus different from DNA amplification.
During the macronuclear development numerous rearrangement of the DNA occurs including transposon and IES elimination. In order to determine if the lethality observed after IFT57A +C RNAi silencing could be correlated with defects in these rearrangements. I tested whether the retention of two IESs of the *A* gene, encoding the A surface antigen, during macronuclear development were normal or not. PCR performed in the regions of these IESs revealed that the excision was normal (Fig. 3-14, bottom panel). The post-conjugation can neither be explained by drastic effect on IES excision.

In conclusion, the lethality observed on ex-conjugants treated by IFT57 suggests a role of IFT57 during the sexual events. However we have no indication on the origin of the post-conjugation lethality.

3.2.2.2. Effect of IFT57 RNAi during autogamy.

To get access to silencing during autogamy, without the equivalent of the RNAi "insulation" period in conjugation in which conjugants do not feed, I worked out another protocol to get efficient silencing by feeding during autogamy. Since the phenotype given by the inactivation IFT57 is clearly visible only after 24 hours in feeding bacteria, I tried another protocol in which the RNAi treatment lasts only 16 hours before introduction into a starvation medium to induce autogamy. Since IFT57A or IFT57C depletions alone do not give strong phenotype, I performed also the double IFT57A + IFT57C RNAi to check whether the particular protocol

used was efficient enough. The answer is yes: cells submitted to the double RNAi become bald after 24 hours of starvation post RNAi. Therefore, the experiment consisted in a first inoculation of log-phase cells competent for autogamy (25 generations from last autogamy = “old” cells) for 16 hours into IFT57A, IFT57C and control ND7 RNAi feeding media at a density of 50 cells/ml to induce inactivation, then in a transfer at a density of 200 cells/ml for 24 hours in exhausted medium in which they cannot divide and are triggered to undergo autogamy. The same protocol was used on control young cells which is this context were not supposed to undergo autogamy after transfer in exhausted medium.

3.2.2.2.1. Effect of IFT57 RNAi on cilia and nuclei during autogamy

Autogamy is supposed to start in old cells as soon as they are in the exhausted medium, but the process lasts a long time and the evolution of anlagen development and genome rearrangements can be followed during several days. In all cases of the experiment, the RNAi treated populations survived, except that a variable proportion (10-20%) of cells depleted for IFT57A were found immobile in the culture and devoid of cilia, about to die. Therefore, for the rest of the experiment, I used samples of well-swimming cells in each culture (the three RNAi conditions on old and young cells). Every day during four days, I fixed and DAPI-stained cells and I extracted genomic DNA. In addition, the first and the fourth day, I immuno-stained the samples with the anti-*Paramecium* cilia and ID5 antibodies, in the presence of DAPI stain, to see any effects of the RNAi on cilia and basal bodies (Fig. 3-15).

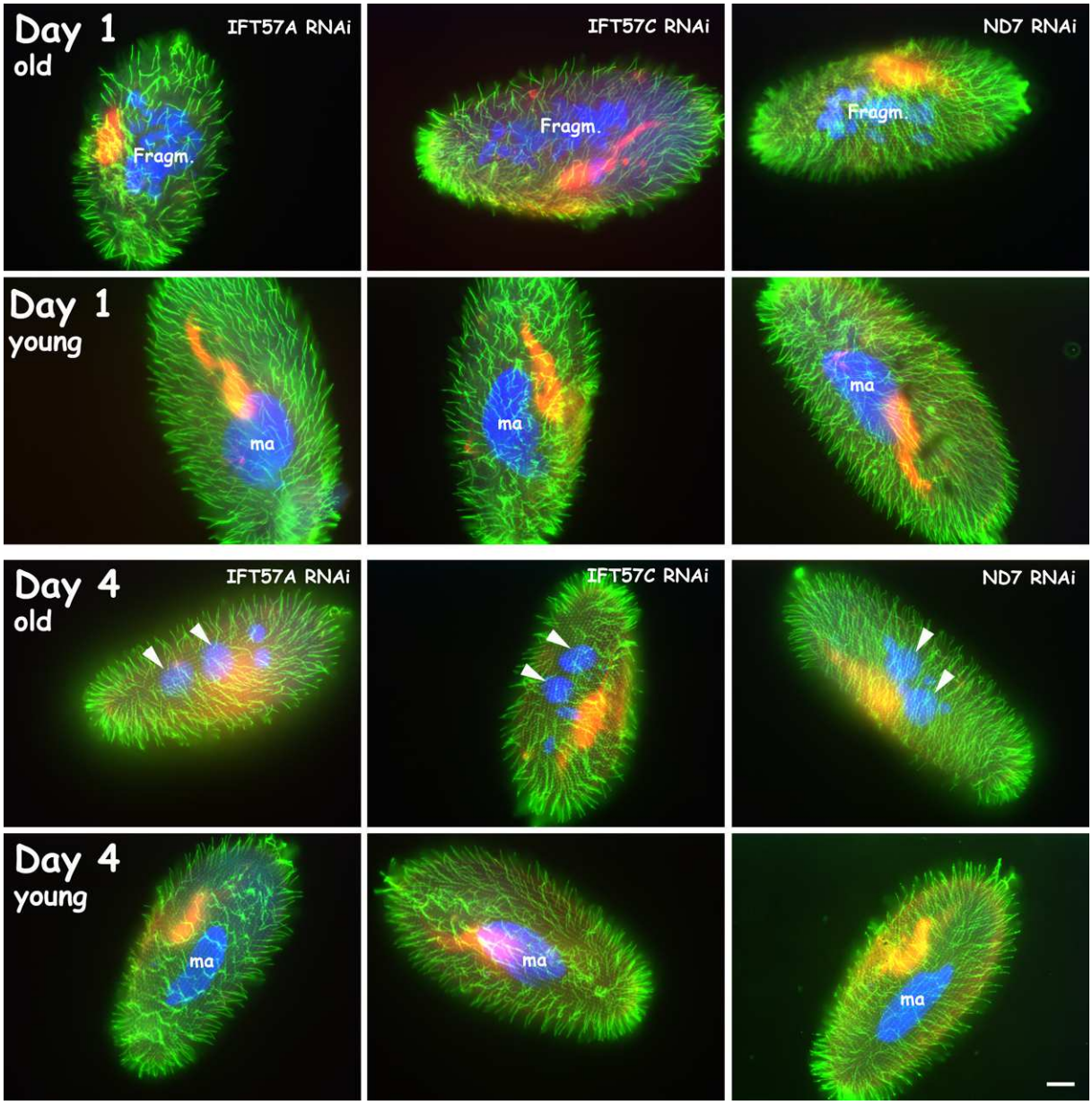

Figure 3-15. Effect of IFT57 RNAi on cilia during autogamy viewed in epifluorescence microscopy. *IFT57A, IFT57C and ND7 were inactivated separately during 16 hours in old and young populations after what cells were transferred in exhausted medium. At days 1 and 4, samples of each conditions were immunolabelled to examine their physiological state, autogamous or not, and the presence of cilia at the surface. At Day 1, old cells have started the autogamy process, as illustrated by the presence of macronuclear fragments (Fragm.). At Day 4, old cells are in late stage of autogamy, in which big anlagen are present (white arrowheads). On both days, young cells have a normal macronucleus (ma), representative of a vegetative stage. Bar: 10µm.*

The DAPI staining confirms that during the treatment the old cells underwent the autogamy process while young cells did not. Concerning the IFT57A and IFT57C silencing, the conclusion is less clear from these pictures, but if we know that in vegetative cells these RNAi treatment are also poorly visible (Fig. 2-11) and that the preliminary experiment of double RNAi under the new protocol was effective, we can conclude that RNAi occurred.

3.2.2.2.2. Effect of IFT57 RNAi on IES excision and clone survival

To test if the IFT57 depletion could give a phenotype linked to a defect in nuclear function during the complex reorganizations that occur during autogamy, I tested the post-autogamous survival by inoculation of 24 individual cells from each sample every day into fresh *Klebsiella* growth medium. The growth capacity of the derived clones is monitored the next day. Only the results for sample inoculated at Day 1 and Day 4 are presented (Fig. 3-16). In parallel, to detect potential defect in IES excision, IES retention at Day 4 was examined by PCR on extracted genomic DNA using primers specific for the region flanking two known IESs (Fig. 3-16).

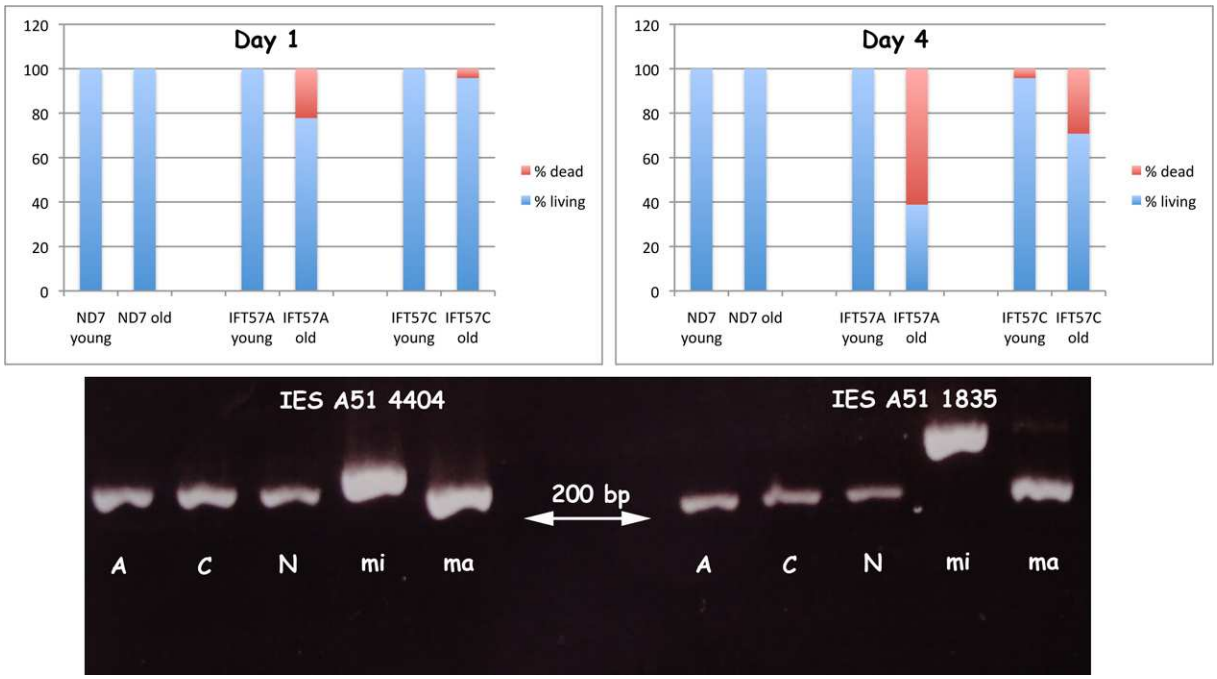

Figure 3-16. Effects of IFT57 RNAi during autogamy. *Top row: summary of clonal survival after the RNAi and starvation medium treatment. Results of Day 1 and Day 4 are presented, in which only old cells, having undergone autogamy, give lethality in IFT57 RNAi media, with a stronger effect in IFT57A RNAi. Number of clones in each sample = 24. Bottom row: Gel of PCR samples produced by amplification of the regions flanking IES 4404 and IES 1835 of the A gene (surface antigen gene) on DNA extracted at Day 4. A: IFT57A RNAi, C: IFT57C RNAi, N: ND7 RNAi, mi: micronuclear DNA control, ma: macronuclear DNA control. RNAi.*

Separate IFT57A and IFT57C RNAi treatment prior to induction of autogamy produce post autogamous lethality. This is specific for autogamy, since young cells that underwent the same treatment did not undergo autogamy and did not produce post-treatment lethality. A simple idea would be that post autogamous lethality comes from anomalies in the new macronuclei that developed in cells loaded with IFT57 siRNA. I therefore checked a simple potential defect, IES excision, but found no retention at Day 4, meaning that the excision process was not altered, as I already found in conjugation with a different RNAi kinetics.
The question is now what gives post autogamous and post-conjugation clonal lethality, if this is not genome rearrangement. A possibility is that this is not a general effect on IES excision but an effect limited to only a few rearrangements that were not examined. Another possibility could be linked to the fact that the cells reorganize their oral apparatus during

sexual events. The lethality effect could be due to inefficient oral apparatus in cells deriving from IFT57 RNAi during the sexual events. This hypothesis would need to carefully follow the oral apparatus reorganization during the treatment.

3.2.2.2.3. Effect of IFT57 RNAi on Ptiwi09-GFP nuclear localization.

Despite the lack of effect of IFT57 RNAi during autogamy on IES excision, I wondered whether an effect could be detected on the transport of some molecules between nuclei. Indeed, IFT57 is known to be associated to transport, at least in the IFT, and itself moves from the old fragmenting macronucleus to new anlagen during autogamy. I applied IFT57A, IFT57C and L4440 (empty vector) RNAi on Ptiwi09-GFP transformed cells competent for autogamy and followed the fluorescence (Fig. 3-17).

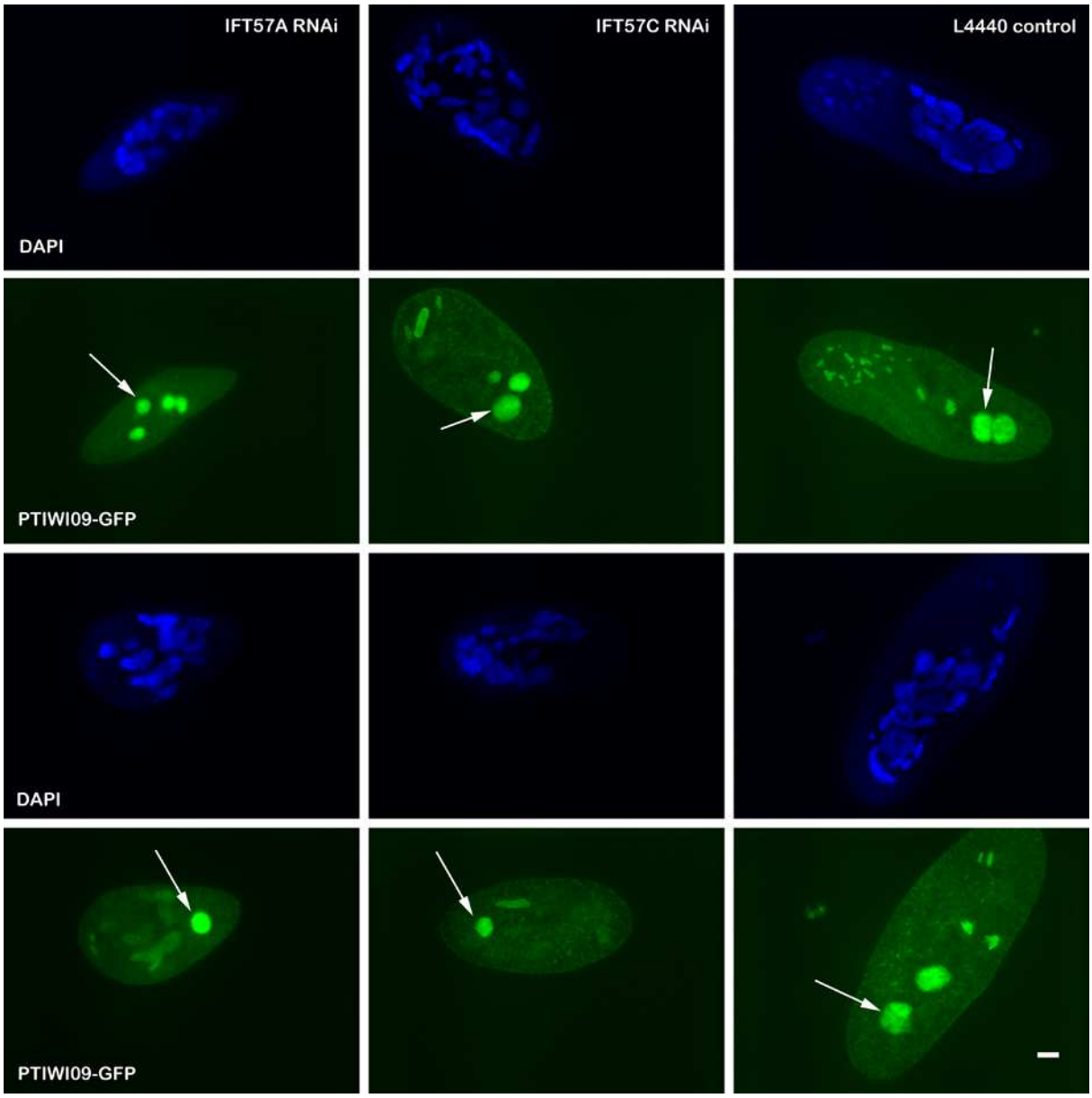

Figure 3-17. Effect of IFT57 RNAi on anlagen localization of Ptiwi09-GFP during autogamy viewed in epifluorescence microscopy. *A clone expressing Ptiwi09-GFP was submitted to IFT57 RNAi before induction of autogamy and the GFP fluorescence was examined at the end of the process. Two cells are presented for each condition: IFT57A RNAi on the left, IFT57C RNAi in the middle, L4440 empty vector on the right. Bar: 10µm.*

As clearly visible after DAPI staining (Fig. 3-17) in all RNAi experiments the cells were able to undergo autogamy and the Ptiwi09-GFP fluorescence concentrated in the new macronuclear anlagen showing that IFT57A or IFT57C proteins were not separately essential for the Ptiwi09-GFP transport. However we sometimes observed anomalies in the number of anlagen developing in post autogamous cells. It is known that the relative number of anlagen/micronuclei after the second post-zygotic division is driven by the position of the nuclei at both poles of the cells (Grandchamp & Beisson, 1981). Indeed, at the second post-zygotic nuclear division, the separation spindle, orient longitudinally so that two daughter nuclei are transiently positioned at the anterior pole of the cell – and are committed to become

micronuclei, while the two other daughter nuclei are positioned at the posterior pole – and are commited to become macronuclei. Possibly, this may mean that IFT57 participates in some way in this positioning.

3.2.3. Conclusion of Part 3.2.

The macronuclear localization of IFT57A and its successive localizations in old and new macronuclei during autogamy address the question of its nuclear function. I tried to deplete the protein during sexual events, conjugation or autogamy, by regular feeding methods or by developing a new way of inducible RNAi by hairpin RNA expression. If some post-sexual events lethality could be observed after IFT57 RNAi treatment, I could not a defect in genome rearrangement, even though I tested only two IESs. Beyond the cause of the post sexual events lethality, which could have a non-nuclear origin and reside in oral apparatus reorganization for instance, the question remains of the role of IFT57 in the nucleus, if there is one. It has to be kept in mind that functional studies during sexual events is a challenge when genes essential for vegetative life are silenced, and a balance has to be found between not too strong exposure to avoid lethality and not too weak to get a phenotype. It is not excluded that the RNAi I applied during sexual events was not strong enough to reach potential functions in the nuclear exchanges.
Another interesting outcome of this work, although it did not help in understanding the nuclear function of IFT57A during autogamy, is the irreversible blocking effect of autogamy by early and massive expression of hairpin RNA under the NOWA1 promoter. Such phenomenon can be exploited in experiments where autogamy has to be avoided.

DISCUSSION

In this work, I approached the ciliary and nuclear role of the IFT57 proteins in *Paramecium* using combinations of GFP-fusion localization and RNAi methods. The ciliary role of IFT57 proteins is obvious since it is essential for correct ciliogenesis. However, the nuclear function is more difficult to decipher: although the nuclear localization of one of the proteins, IFT57A, is striking in vegetative cells as well as during sexual events, no obvious phenotype that could be imputed to nuclear defects has been observed under IFT57 depletion.

The new elements provided by this work and that I will discuss in this chapter concern on the one hand the functional links with other IFT proteins in ciliogenesis and on the other hand the localization changes between the cortex and the various kinds of nuclei during sexual events. I will conclude by the examination of possible functional relationships between cilia and nuclei.

D.1. IFT57 in the IFT system for ciliogenesis.

The first observation made from this work is that the IFT57 proteins, as well as the other IFT proteins that I studied, whose function was extrapolated from sequence homology through evolution, are indeed involved in ciliary transport: the GFP fusions of these proteins localize to basal bodies and growing cilia, the depletion of these proteins give rise to ciliary loss. Moreover, the depletion of one protein of the IFTA complex, IFT139, provokes the accumulation of IFTB components, such as IFT57, IFT46 and qilin, and the depletion of IFTB components, such as IFT57, IFT172, IFT46 or qilin prevent the entry of other IFTB components into the cilium, either at steady state or during ciliary growth.

However, some of the results do not give straightforward interpretation and need more examination.

D.1.1. Ciliary growth and maintenance in relation to IFT recycling.

Cells depleted in IFT57 proteins, as well as the one depleted for IFT172 (both proteins belonging to the peripheral set of IFTB components) display a smaller cilia number over time but without ciliary shortening. In normal conditions, when cells divide, basal bodies are duplicated in an uneven way over the surface, some regions being not duplicating at all and others undergoing one or several rounds of duplications. After division, each cell inherits of a set of old and a set of new basal bodies. Old ciliated basal bodies remain ciliated, whereas some of the new basal bodies nucleate new cilia. Under IFT57 or IFT172 RNAi, cells after division keep the old cilia with normal length and new basal bodies do not grow any cilia or only abortive ones, making the sell surface less dense in cilia. After two or three rounds of divisions, only rare long cilia are detected, unevenly represented on the clonal offspring. The simplest interpretation is that these peripheral IFTB proteins, necessary for ciliary growth, are not involved in ciliary maintenance: once the cilium is made, it is stable and never disappear except by breakage into the medium. However, this is not true when the core IFTB IFT46 protein is depleted and cells with short cilia of any sizes are produced. This would mean that

IFT46 is necessary for ciliary maintenance as well as for ciliary growth. How could we explain this apparent contradiction? Two hypotheses can be imagined:
Firstly, the two IFT proteins do not have the same role in the machinery. IFT46, as a protein necessary for the IFTB complex stability, would also be involved in ciliary maintenance, whereas IFT57, a linker between the kinesin motor and the IFTB core would be dispensable for this maintenance.
Secondly, may be the core and peripheral IFT proteins have not the same fate in the cilium. An argument for this hypothesis is that when IFT57-GFP expression is antagonized by IFT57 RNAi (a condition that may not remove the totality of the IFT over expressed in the cell), cilia remain fluorescent, may be more fluorescent than without RNAi. In contrast, IFT46-GFP expressing cells submitted to IFT46 RNAi do not show the same phenomenon since the fluorescence rather tends to decrease over time. An idea would be that IFT57, at least in IFT57 RNAi conditions, would be trapped in the cilia by exit inhibition and recycle, even in the absence of neo synthesis and import of new protein from the cytoplasm. The intraflagellar recycling of an IFT protein has been recently reported in *Trypanosoma* using the expression of IFT52-GFP and photobleaching and recovery experiments on the flagellum (Boileau et al., 2013), indicating that such phenomenon is conceivable. IFT57 could thus have a role in ciliary maintenance, so that the expression decrease gives no ciliary shortening phenotype. In such a hypothesis, IFT46 could not be trapped under IFT46 RNAi so that its function in maintenance can be revealed by ciliary shortening when it is depleted.
IFT proteins are mobilized during ciliary growth, a phenomenon easily visible after experimental deciliation, which, in addition, offers a way to synchronize the observations. When IFTA (IFT139) or IFTB (IFT46, IFT57, IFT172, and qilin) components have been already depleted for 24 hours at the time of the reciliation experiments, residual ciliary growth occurs. This could be accounted for the fact that the RNAi depletion is not total and trace amount of the depleted IFT remain in the cytoplasm to carry out residual ciliary growth. However, when the depletion concerns an IFTB protein (IFT46, IFT57, IFT172, qilin), no GFP-tagged IFT protein (IFT46, IFT57, qilin) enters the short cilia, as if the residual growth was independent of the IFT, at least of two IFT proteins in each case, the one which is depleted and the one which is tagged with GFP. In the case of IFT139 depletion, the short cilia accumulate GFP-tagged IFT at their tip, in agreement with the observations on vegetative cells. A careful examination of Figure 2-22, middle panel, green enlarged insets, may suggest that, in addition to the ciliary tip labeling, there is a more obvious basal body and ciliary GFP labeling in IFT46-GFP expressing cells than in IFT57-GFP or qilin-GFP expressing cells. If such tiny difference in fluorescence is significant, this could be related to the easier trapping of IFT57 into cilia than IFT46.

D.1.2. Cytoplasmic complexes of IFT proteins

The IFT particles are large complexes of more that 20 subunits. The way of the assembly of these subunits, which has been addressed in *Chlamydomonas* (Richey and Qin, 2012), is stepwise and involves progressive addition of proteins or of pre-complexes. It is admitted that the assembly occurs at the basal body before interaction with the transition zone (Deane et al., 2001; Follit et al., 2006), which enable the entry of the complex into the cilium. Evidences exist that at least some IFT proteins can have a function outside of the cilia (Gervais et al., 2002; Delaval et al., 2011;Finetti et al., 2009), and that IFT proteins can interact together outside of the basal bodies (Finetti et al., 2009). Some experiments of my work are in favor of such extra-basal body interactions.
First, I detected some cytoplasmic foci of IFT46-GFP induced after deciliation. The appearance of these foci is sensitive to the depletion of other IFT proteins (IFT172, 1FT57).

However, such foci do not occur with IFT57-GFP or Qilin-GFP in cells under reciliation. One hypothesis is that some IFT proteins interact with IFT46-GFP to help in generating the foci, but do not accumulate into them. Another hypothesis is that there is a control of gene expression making an IFT46 down-regulation upon IFT57 or IFT172 RNAi.
Second, I detected IFT57-GFP foci in cells under IFT46 RNAi, but only in this condition. The origin of these foci is not clear, since they appear very early in cortical rows between the basal bodies, before accumulating as big inclusions in the cytoplasm. The appearance of IFT57-GFP foci under IFT46 RNAi means that, in untreated cells, IFT46 is necessary for good targeting of IFT57-GFP. Does the IFT46 depletion just slow down a physiological phenomenon normally too fast to be detected (foci between ciliary rows) or does it induce anomalous localization, or both? This remains open, but this is another indication of cytoplasmic interaction between IFT46 and IFT57.

D.2. The presence of IFT57A in the macronucleus, a still unsolved mystery

When tagged with GFP, IFT57A enters the macronucleus while IFT57C is excluded from it. I first tried to understand which part of the molecules make the difference, and then to try to find a role to this macronuclear localization, as discussed below.

D.2.1. Nuclear targeting of IFT57A-GFP

After constructing chimeras between IFT57A and IFT57C fused to GFP, I determined a region (L129-N219) representing ~25% of the sequence in which reside the differences among which should be the signal that targets IFT57A to the macronucleus and excludes IFT57C from it. I took advantage of the recent sequencing of the genomes of other *Paramecium* species, to which I had access before release, to analyze other IFT57 genes in the genus. The *P. aurelia* syngen underwent two whole genome duplications that did not occur in other species such as *P. caudatum* and *P. multimicronucleatum*, so that these species have a single IFT57 gene instead of four in *P. tetraurelia*. The rationale was that the unique IFT57 gene in *P. caudatum* and *P. multimicronucleatum* would behave as the ancestral IFT57 gene in the *P. aurelia* syngen, before the two last whole genome duplications. It was worth to test whether the *P. caudatum* IFT57-GFP fusion could go into the macronucleus or not. The answer is no, meaning that most probably, the nuclear localization of IFT57A in *P. tetraurelia* represents a gain of function after genome duplication. By sequence comparison, this allows to have a more precise idea about the amino acid difference responsible for the different localizations of IFT57A and IFT57C. However, although this is difficult to imagine, it appears that there is no need for nuclear function of IFT57 in *P. caudatum*. To date, I did not demonstrate a function of IFT57A in the nucleus of *P. tetraurelia*. May be the fact that it is dispensable in other *Paramecium* species means that the macronuclear in *P. tetraurelia* localization is fortuitous? However, the homologous molecule in mammals has a nuclear function, what would stimulate further research to identify the actual role of IFT57A in the macronucleus of *P. tetraurelia*.

D.2.2. Possible nuclear roles of IFT57A deduced from its localization.

IFT57A-GFP strikingly localizes in the macronucleus of vegetative cells and, during autogamy, the labeling disappears from the fragmenting macronucleus just before the appearance of new anlagen, which load with fluorescence as they grow in size. In the same time fluorescent foci appear in their nucleoplasm and become more and more intense. Interestingly, similar foci appear at the same stage with at least another protein, piggymac,

which is involved with double strand DNA breaks associated with IES excision (Baudry et al., 2009). It would be interesting to know whether these foci co-localize with the IFT57A foci. Such a co-localization would lead us to search for possible direct or indirect interactions between the two proteins, and in particular to see whether IFT57A drives in any way the entry of piggymac into the anlagen. Seeing functional protein foci into the nucleus is not unique. The protein Spag16, also harboring a ciliary and nuclear localization in mammals, according to its splice variant forms, accumulates as foci called speckles in the nucleus, in which it regulates its own expression (Nagarkatti-Gude et al., 2011). Since IFT57/HIPPI has been shown to participate to the regulation of some caspases in mammalian cells, it may be possible that IFT57A has some role in gene expression in the developing anlagen, however not concerning genome rearrangements. Concerning a possible nuclear role of IFT57A during vegetative life, I wondered whether it could serve in accompanying the nuclear import of some proteins. The rationale would be that their transport could concern ciliary proteins that also have a nuclear function, such as BUG22 (Laligné et al, 2010) or BBS7 (Gascue et al., 2012), already described in *Paramecium* with a ciliary role (Valentine et al., 2012). I showed that IFT57A+C RNAi had no impact on the nuclear localization of BUG22-GFP, and I could not address this question for BBS7-GFP since this construct gave no fluorescence. If the putative function at autogamy is the sole nuclear role, with a neutral nuclear localization in vegetative cells, this could be an explanation why no nuclear function was selected in *P. caudatum*, since this species does not perform autogamy (provided that no special role concerns conjugation, since *P. caudatum* undergoes conjugation).

D.3. IFT57A as a possible revelator of a cross talk between cilia/basal bodies and nuclei at autogamy

The localization of IFT57 proteins, in *Paramecium* as well as in other organisms, is markedly in basal bodies and along cilia. In *Paramecium tetraurelia*, the IFT57A isoform also localizes to the macronucleus. At autogamy, striking IFT57A reorganizations occur, not only between old and new macronuclei, but also in the cortex, in particular in basal bodies and cilia of the anterior left field. Similar dual localizations, in basal bodies and nuclei at autogamy have been already described for other proteins, involved in RNA metabolism, Dicel-like5 (Lepere et al. 2005) and Ptiwi09 (Bouhouche et al., 2011). We do not know the basal body role of such proteins involved in RNA metabolism, but it is striking that, in vertebrates, ciliogenesis is under the control of a micro RNA, miR-449 (Marcet et al., 2011).

The first event seen in autogamy is an increase of IFT57A-GFP cortical fluorescence concomitant with the appearance of Ptiwi09-GFP fluorescence at basal bodies. The IFT57A-GFP fluorescence becomes stronger in the cytoplasm and at the oral apparatus when the fragmenting macronucleus starts to loose its IFT57A-GFP fluorescence (likely with the same timing as for Ptiwi09-GFP loss of fluorescence). The cortex will stay highly fluorescent with both markers until the new anlagen develop, and then its fluorescence will progressively decrease. If we keep in mind that IFT57 can be linked to kinesin motors, its movements can be related to transport of some cargo in the cell, between basal bodies and nuclei, and between nuclei. Since autogamy nuclear processes are accompanied by important short RNA metabolism and that corresponding enzymes seem to co-localize with IFT57 in two different locations (basal body and nuclei), it may be possible that a signal transduction from cilia and a cross-talk involving small RNA specific for autogamy and the associated proteins exist between basal bodies and nuclei, in association with a transporter linked to IFT57 and other transport molecules.

MATERIALS AND METHODS

This work has been conducted on *Paramecium*. Most of the protocols for *Paramecium* are available online at http://paramecium.cgm.cnrs-gif.fr/parawiki/Protocols and in a publication (Beisson et al., 2010). I will detail here the methods specific of y work concerning *Paramecium* culture, transformation and RNA interference, as well as the molecular biology vectors and tools used in this study.

M.1. Strains and culture conditions

Stock d4-2 of *Paramecium tetraurelia*, a derivative of Stock 51, is the wild type strain used for RNAi experiments. The mutant nd7-1, which carries a recessive monogenic mutation preventing trichocyst discharge, a dispensable function under laboratory conditions, was used as a control for transformations. Cells were grown at 27°C in wheat grass infusion, BHB (L'arbre de vie, Luçay Le Mâle, France), inoculated with *Klebsiella pneumoniae* and supplemented with 0.8 µg/ml β-sitosterol according to standard procedures (Sonneborn 1970). The *Paramecium caudatum* strain used for genomic DNA preparation and microinjection was Stock MY43C3a, the one whose genome has been sequenced. Culture conditions and manipulations were the same as the one used for *Paramecium tetraurelia*.

M.2. Physiological manipulations of *Paramecium*

M.2.1. Deciliation

In order to remove cilia from *Paramecium* cells to follow ciliary growth during reciliation, a few hundreds of cells were first collected in a small volume and transferred to a 1.5 ml micro-tube containing 1ml of 5µL Ethanol and 1mM $CaCl_2$. After 30s of vortex and 15s of centrifugation, cells were put back into fresh medium at 27℃ and collected at various times thereafter.

M.2.2. Trichocyst discharge

To monitor the trichocyst exocytosis ability, a few cells are deposited in a small drop of the fixative picric acid and observed under low magnification (10x objective) dark field microscopy. This test was used to evaluate the efficiency of transformation, since the wild type ND7 gene is co-microinjected with any of the constructs into the macronucleus of the nd7-1 mutant, and to monitor the efficiency of control ND7 RNAi.

M.2.3. India ink labeling of food vacuoles

In order to use the same conditions between control and RNAi-treated cells in immunolabeling experiments, cells of the control group were fed with India ink for 10 minutes prior to mixing and processing of the two samples together. This permit to distinguish control from treated cells directly on the slide during observation at the microscope.

M.3. Molecular biology methods

Molecular biology was performed according to standard methods. *Paramecium* genomic DNA was extracted using Nucleospin Tissue XS kit (MACHEREY-NAGEL GmbH& Co.KG). DNA digestion and ligation were performed using New England BioLabs enzymes. PCR products for cloning were amplified using High-Fidelity DNA Polymerase (Phusion, FINNZYMES). Bacterial transformations were performed by electroporation.

M.4. Vectors used

Two kinds of vector have been used or constructed. A series of vector serve for gene expression, and another one for gene silencing by feeding.

M.4.1. GFP-fusion expression vectors

M.4.1.1. pZZ-GFP02

Classically, the expression of GFP fusion in *Paramecium* is carried out in the laboratory by cloning the desired sequence into pPXV-GFP (REF), a plasmid in which the GFP gene is under the promoter and terminator of the *CAM1* calmodulin gene and which possesses endogenous telomeric repeat sequences, which can be freed by enzymatic digestion (*Sfi*I). The qilinA-GFP and qilinC-GFP fusion genes were cloned into pPXV-GFP by Houssein Chalhoub before I started my work (unpublished).
To be able to clone genes under their own regulators, I used the pZZ-GFP02 plasmid designed for this purpose. The vector pZZ-GFP02 is a derivative of pPXV-GFP (Hauser et al., 2000) in which the promoter and terminator regions have been replaced by specific restriction enzyme polylinkers (Fig. M-1).

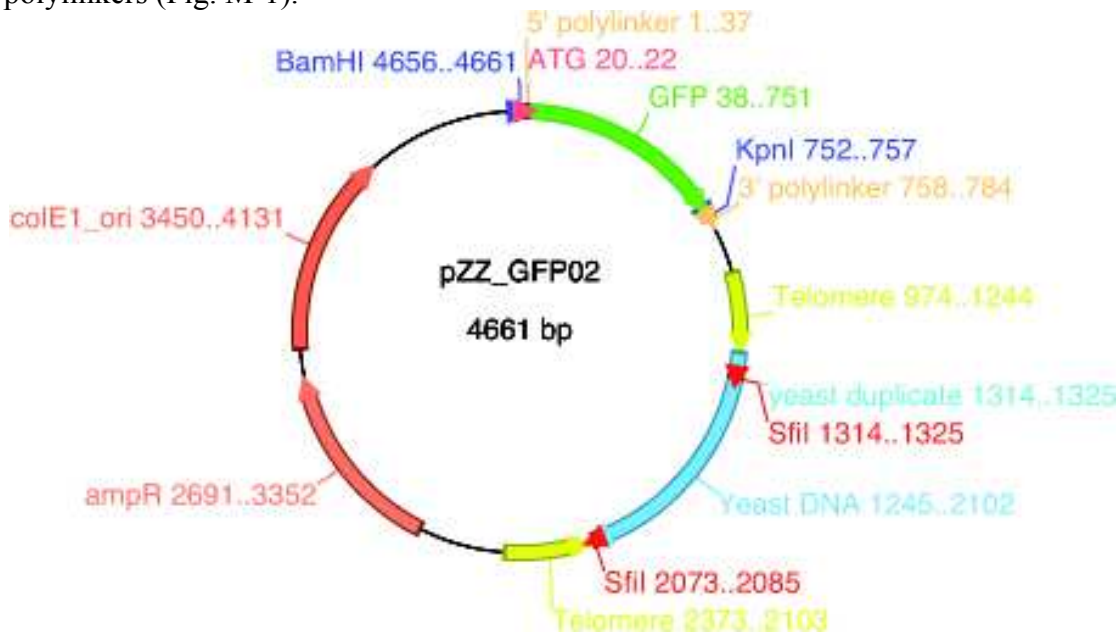

Figure M-1. Graphic map of the pZZ-GFP02 plasmid used for GFP fusion gene cloning and transformation of Paramecium. *This plasmid allows the introduction of GFP at any place within the protein. The 5' polylinker can be used for just promoter cloning (in this case the gene + terminator will be cloned in 3'), clone the promoter +the gene (the terminator will be cloned in the 3' polylinker), or the promoter + a part of the protein (the other part + the terminator being cloned in 3'.*

In addition, the ATG of the GFP is preceded by a sequence of three glycines (necessary for better independent folding of the cloned protein and the GFP) and another ATG encompassed by a *Sph*I site, allowing the junction with any sequence upstream of it, a promoter for instance, without altering the endogenous context (Fig. M-2).

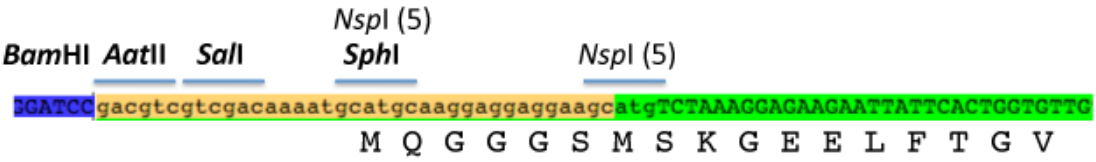

Figure M-2. Polylinker in 5' of GFP in the pZZ-GFP02 plasmid.

M.4.1.2 Construction of IFT57-GFP and IFT46-GFP fusion vectors

The IFT57A gene was amplified from *Paramecium* DNA by PCR using primers 5'-ttattGGATCCaaaaggattaaatatatatctatatgtatttg-3' and 5'-GATTCAAATGAGTTAACAGATgcatgcAACC-3' and cloned between *Bam*HI and *Sph*I sites of pZZ-GFP02. The terminator of IFT57A was obtained by annealing the primers 5'-CtgatatatatatttatatataattaatacaccatttaaattaattaatacacttgtcaC-3' and 5'-GTACCtgatatatatatttatatataattaatacaccatttaaattaattaatacacttgtcaCCCGG-3' and cloning the resulting fragment between *Kpn*I and *Sma*I sites of pZZ-GFP02.
The IFT57C gene was amplified by PCR using primers 5'-ttattGGATCCtgagagaacattaatatatatatatatt-3' and 5'-CCTAAATGAGTCTGATGAATTAACAGATgcatgcAACC-3' and cloned between the *Bam*HI and *Sph*I sites of pPZZ-GFP02. The terminator of IFT57C was amplified from *Paramecium* DNA by PCR using primers 5'-ttattGGTACCtgaaatatatatattaatacgccagtc-3' and 5'-gtagttaaaacaaaattaatacaaaaCCCGGGaacc-3' and cloned between *Kpn*I and *Sma*I sites of pZZ-GFP02

The IFT46 gene was amplified by PCR using primers 5'-atacttggatccTATTTAATATAATTAAATAAATACTGTTATTC -3' and 5'-GACAAAACAATGATGAAATTTAAggcatgcaagtat -3' and cloned between the *Bam*HI and *Sph*I sites of pPZZ-GFP02. The terminator of IFT46 was amplified from *Paramecium* DNA by PCR using primers 5'- atacttggtacctgaATATTCAATAATATAACATTATTTTC-3' and 5'- GGAATATTTATTATAATTATTAA-3' and cloned between *Kpn*I and *Sma*I sites of pZZ-GFP02

M.4.1.3. Construction of Paramecium caudatum IFT57-GFP fusion vectors

The IFT57 gene was amplified from *Paramecium caudatum* DNA by PCR using primers 5'-atacttggatccATGAGTATGTTAAGGAACAAAATATTC -3' and 5'-

GCATGACTCCGATGAACTCACAGATggcatgcaagtat -3' and cloned between the *Bam*HI and *Sph*I sites of pPZZ-GFP02. The terminator *Paramecium caudatum* IFT57 was amplified by PCR using primers 5'- atacttggtacctgaTATAAATTTAATTATATACAC -3' and 5'-CATTTTATTAATTAAATTTTTTACCAA -3' and cloned between *Kpn*I and *Sma*I sites of pZZ-GFP02

M.4.1.4. Construction of chimeric GFP-expression vectors.

Chimeric IFT57**A-C**-GFP and IFT57**C-A**-GFP expression vectors were constructed by reciprocal exchanges of restriction fragments from both IFT57A and IFT57C genes. The IFT57A-GFP expression vector and IFT57C-GFP expression vector were digested by *Bam*HI and *Bsl*I. The N-terminal region of the IFT57A gene, from positions -61 to 826, was replaced by the positions from positions -61 to 826 of the IFT57C gene and reciprocally.
Chimeric IFT57**C-A-C**-GFP and IFT57**A-C-A**-GFP expression vectors were constructed by cloning of PCR fragments between restriction sites. The N-terminal region of IFT57C gene from positions -61 to 480 was amplified by PCR using primers 5'-ttattGGATCCtgagagaacattaatatatatatatatt-3' and 5'-GTTTATGTGTTGCTGTAATTGGCAAGCAaagcttAACC-3' and inserted between the *Bam*HI and *Hind*III sites of the plasmid IFT57**A-C**-GFP to produce the IFT57**C-A-C**-GFP chimera. Reciprocally, the C-terminal region of IFT57A, from the position 813 to the C-terminus was amplified by PCR with primers 5'-TTATTaagcttAAACCAAAGCATTGCAAAAAAAG-3' and 5'-GATTCAAATGAGTTAACAGATAgcatgcAACC-3' using the vector Nter-IFT57**C-A**-GFP-Cter as a template and inserted between the *Sph*I and *Hind*III sites of the plasmid of IFT57A-GFP to produce the IFT57**A-C-A**-GFP chimera.

M.4.2. RNAi vectors.

M.4.2.1. "Feeding" constructs.

The feeding vectors I used in this study were targeted against IFT57A, IFT57C, IFT46, IFT139, IFT172 qilinA and qilinC. The Ift172 vector comes from the work of Chloé Laligné (Laligné et al., 2010), the qilin vector from the work of Houssein Chalhoub (unpublished) and the IFT139 vector from a previous study of France Koll (unpublished).
Part of the IFT57A sequence was amplified from positions 568 to 1168 with the primers 5'-ttattactagtGAAACTGGGAGTGTGTCATC -3' and 5'-CAGATAAGTATGAAGCTGTGCctcgagaacc -3' and cloned into the *Spe*I and *Xho*I sites of L4440 (Kamath et al. 2000).
Part of the IFT57C sequence was amplified from positions 1 to 688 with the primers 5'-ttattaagcttTAGTAATCAGGTTAAgtaatc-3' and 5'-GTATTTACTGAATAGGGATTCctcgagaacc-3' and cloned into the *Spe*I and *Xho*I sites of L4440,
Part of the IFT46 sequence was amplified from positions 199 to 793 with the primers 5'-ttattactagtGCTGGAGCTAGAGGACCCCAATAAGC-3' and 5'-GGTGTGGCCACAAGAGATTGAAGctcgagaacc-3' and was cloned into the *Spe*I and *Xho*I sites of L4440.

M.4.2.2. Vectors for "hairpin" silencing.

The idea for hairpin silencing was to introduce double strand RNA within *Paramecium* by expression of complementary sequences into its macronucleus after transformation. The preparation of such a vector is a two-step procedure. First, a *Paramecium* sequence has to be cloned in both orientations into the forward and reverse HP cloning sites of the pZHP vector (Fig. M-3).

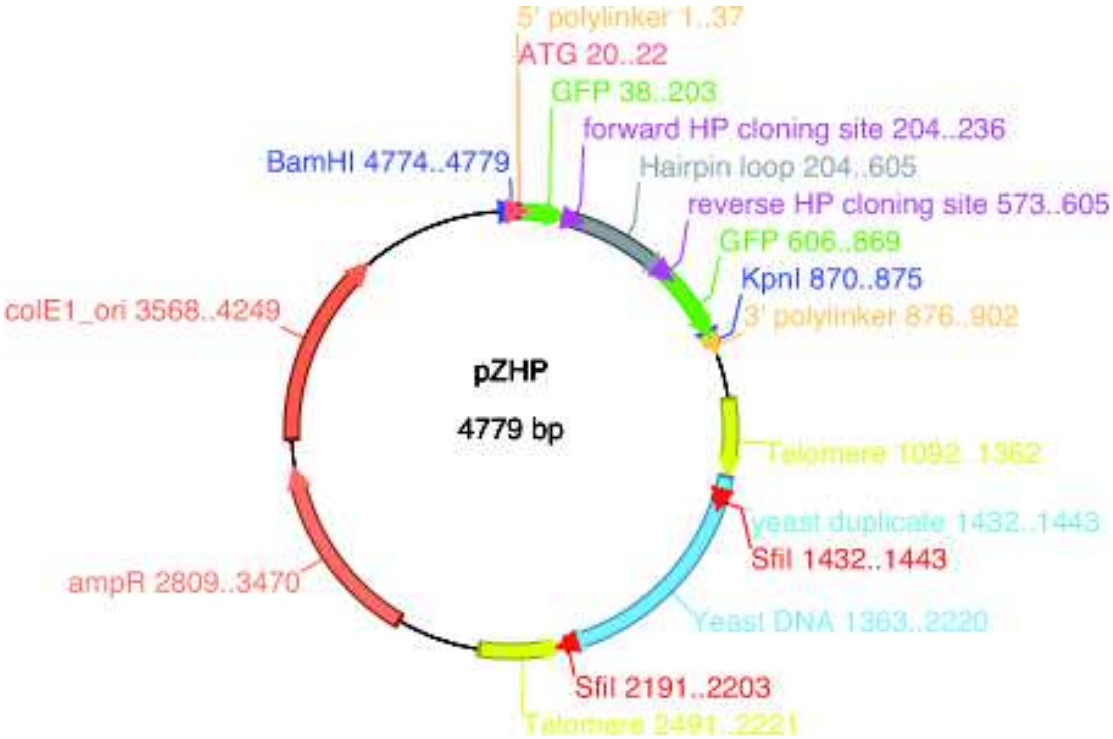

Figure M-3. Grafic map of the pZHP vector designed for cloning hairpin constructs*. pZHP is a derivative of pZZ-GFP02 in which the NcoI-BstZ17I internal fragment of the GFP gene has been replaced by a "loop" sequence flanked by polylinkers for forward and reverse cloning of the hairpin fragments. The loop is needed because direct hairpins are very unstable in E. coli. The loop has been chosen as the TA-indel 4356, because as a TA-indel (micronuclear sequence found in the macronucleus with a lox frequency) it is likely not coding, but is accommodated in the macronucleus without damage. It could then be used for expression of the hairpin.*

The cloning into the hairpin vector consisted in PCR amplification of a sequence with two different pairs of oligonucleotides: the 5' part of the fragment was amplified with either of the forward (F) or reverse (R) oligonucleotides, F incorporating a *Apa*I restriction site and R a *Mlu*I restriction site. In both PCR, the 3' median (M) oligonucleotides had no restriction site to allow blunt end cloning. The PCR fragments were respectively cloned into the *Apa*I and *Pme*I restriction sites of the Forward HP cloning site and into the *Nru*I and *Mlu*I restriction sites of the reverse HP cloning site.

The sequences to be cloned as hairpin in pZHP were:
NSF1 long (792bp) : covering the amino acid region 125-381 of NSF1.
F: gaaatggGCCCCATTCTTGAAAAGAG
M:CAATTAAGTCTTTTCTATTAG
R: gaaatacgcgtGCCCCATTCTTGAAAAGAG

NSF1 short (290 bp) : covering the amino acid region 125-214 of NSF1.
F and R: same as for NSF1 long.
M: GTCCTCTCTAAATATACTAGC

IFT57A (580 bp) : covering the amino acid region 149-325 of IFT57A .
F: gaaatgggcccGATGAAGAACCTGTTTAGG
M: ACCATGTTCATTTAATTTGG
R: gaaatacgcgtGATGAAGAACCTGTTTAGG

IFT57C (686 bp) : covering the amino acid region 1-185 of IFT57C.
F: gaaatgggcccATGTCTGAATAGTAATCAGG
M: TTTTTGGAATCCCTATTCAG
R: gaaatcgcgtATGTCTGAATAGTAATCAGG

Second, a portion of the pZHP vector containing the full hairpin is transferred to another plasmid containing the desired 5' and 3' expression regulators, for example CAM1 for constitutive expression or NOWA1 for expression early in autogamy. Such vectors have been previously constructed as the pZX family, derivatives of the pZZ-GFP02 in which the desired promoters are cloned directly at the ATG using the *Sph*I site and the terminator at the 3' *Kpn*I site of the GFP.

Three of these four cloning succeeded: NSF1 short, NSF1 long and IFT57A. However, surprisingly, the reverse gene portion was not the same as the forward one, NSF2 was apposed to NSF1 and IFT57B to IFT57A. The first step of the hairpin cloning of IFT57C succeeded, but, as a true hairpin, could never be transferred to the pZX plasmid containing the NOWA1 promoter. It is possible that such long hairpins are very unstable in *E. coli* so that only hairpins with a few mismatches could be maintained. Anyway, the sequence identity of these ohnologs is important enough to produce sufficient amount of double strand RNA and siRNA.

M.5. Transformation of *Paramecium*.

DNA (5µg/ml) containing a mixture at a ratio of 10:1 of the plasmids of interest (GFP fusion genes, hairpin silencing vector) and a plasmid directing the expression of the ND7 gene was microinjected into the macronucleus of nd7-1 cells. Microinjection was performed under a Nikon phase-contrast inverted microscope, using a Narishige micromanipulation device and an Eppendorf air pressure microinjector. Successfully transformed cells were screened for their ability to discharge trichocysts on picric acid stimulation and were further analyzed.

M.6. Immunofluorescence microscopy.

Immunostaining of cells was carried out using the polyclonal anti-*Paramecium* ciliary tubulin antibody raised in the laboratory (Cohen et al., 1982) at a 1:400 dilution, the monoclonal TAP952 antibody again monoglycylated tubulin (Callen et al., 1994) at the 1:10 dilution and the monoclonal ID5 antibody against polyglutamylated tubulin at the 1:50 dilution. Appropriate anti rabbit IgG or anti mouse IgG fluorescent secondary antibodies were applied

at 1:500 dilutions and nuclei were stained with Hoechst-33258. As the fluorescence of GFP-fusion protein is not very stable when cells are permeabilized by Triton-X100, different treatments were used according to the antibody: with the polyclonal anti-*Paramecium* ciliary tubulin antibody, GFP-fusion cells were firstly fixed by paraformaldehyde for 30s, and then treated by Triton-X100 0.5% for 30 minutes; when the TAP952 or ID5 monoclonal antibodies were used, GFP-fusion cells were treated by saponins for 2 minutess first till they become transparent, and then fixed by paraformaldehyde for 10 minutes. Slides were mounted in Citifluor (London). Preparations were observed under a Zeiss Axioskop 2-plus fluorescence microscope equipped with a Roper Coolsnap-CF intensifying camera with GFP filters. Images were processed with Metamorph software (Universal Imaging). Alternatively, they were observed with the help of Anne Aubusson in the laboratory, under a Confocal Nikon eclipse TE 2000-U microscope equipped with argon and Helium-Neon lasers using the EZ-C1 3.30 software for acquisitions.

M.7. Electron microscopy.

Electron microscopy was performed by Michel Lemullois in the laboratory. For morphological observations, cell pellets were fixed in 1% (v/v) glutaraldehyde and 1% OsO4 (v/v) in 0.05M cacodylate buffer for 30 min. After rising and dehydration in ethanol and propylene oxide series, they embedded in Epon resin. For post embedding immunolocalization, cell pellets were fixed in 3% paraformaldehyde and 0.15% glutaraldehyde in 0.05M cacodylate buffer for 60 min. After washes and dehydration in ethanol they embedded in LR White (London Resin). Thin sections were collected on nickel grids and treated with double-distilled water then 0.1 M NH4Cl in 0.1 M PBS and then saturated and processed with 3% BSA and 0.1M glycine in PBS. Sections were incubated with anti-GFP polyclonal antibodies anti-GFP diluted 1:500 for 45 min. After several washes in PBS, a gold-labeled anti-rabbit IgG (GAR G10, aurio) diluted 1:25 for 30 min. The grid were rinsed in PBS and distilled water. All ultrathin sections were contrasted with uranyl acetate and lead citrate. The sections were examined with a Jeol 1400 (120 kV) transmission electron microscope.

M.8. RNAi by the “feeding” method.

M.8.1. RNAi by feeding during vegetative growth.

RNAi gene knockdown was performed according to the method of Galvani and Sperling (2002). HT115, an RNase III-deficient strain of *Escherichia coli* with an isopropyl-β-D-thiogalactopyranoside (IPTG)-inducible T7 polymerase, was transformed by the desired constructs into L4440 plasmids. Wild-type paramecia were incubated in these transformed bacteria expressing double-stranded-RNA (dsRNA) and were transferred daily into fresh feeding medium. Control cells were fed with bacteria expressing double strand RNA corresponding to the complete coding region of the ND7 gene.

M.8.2. RNAi by feeding during autogamy

RNAi was performed following the feeding method used for vegetative cells. Old cells that already fulfill more than 20 divisions (competent for autogamy) and young cells as a control,

were separately fed with feeding bacteria overnight at the concentration 50 cells/mL and then transferred to exhausted medium for 24 hours at the concentration 500 cells/mL to induce autogamy. Autogamy occurrence was checked by DAPI staining of the cells and observation at the fluorescence microscope.

M.8.3. RNAi by feeding during conjugation

For conjugation, mating-reactive *Paramecium* cells were mixed at a density of >2,000 cells/ml and incubated at 27°C. After 1h30-2h, individual mating-pairs were transferred into fresh feeding medium and left there overnight.

BIBLIOGRAPHY

Absalon S, Blisnick T, Kohl L, et al. Intraflagellar transport and functional analysis of genes required for flagellum formation in trypanosomes. *Mol Biol Cell*. 2008; 19(3): 929-44

Absalon S, Blisnick T, Bonhivers M, et al. Flagellum elongation is required for correct structure, orientation and function of the flagellar pocket in Trypanosoma brucei. *J Cell Sci*. 2008; 121:3704-16

Adhiambo C, Blisnick T, Toutirais G, et al. A novel function for the atypical small G protein Rab-like 5 in the assembly of the trypanosome flagellum. *J Cell Sci*. 2009; 122:834-41

Ahmed NT, Gao C, Lucker BF, et al. ODA16 aids axonemal outer row dynein assembly through an interaction with the intraflagellar transport machinery. *J Cell Biol*. 2008; 183(2): 313-22

Ashe A, Butterfield NC, Town L, et al. Mutations in mouse Ift144 model the craniofacial, limb and rib defects in skeletal ciliopathies. *Hum Mol Genet.* 2012 Apr; 21(8): 1808-23

Arnaiz O, Cain S, Cohen J, et al. ParameciumDB: a community resource that integrates the Paramecium tetraurelia genome sequence with genetic data. Nucleic Acids Res. 2007;35:D439-44.

Arnaiz O, Goût JF, Bétermier M, et al. Gene expression in a paleopolyploid: a transcriptome resource for the ciliate Paramecium tetraurelia. *BMC Genomics*. 2010;11:547

Arnaiz O, Sperling L. ParameciumDB in 2011: new tools and new data for functional and comparative genomics of the model ciliate Paramecium tetraurelia. *Nucleic Acids Res*. 2011; 39:D632-6

Arts HH, Bongers EM, Mans DA, et al. C14ORF179 encoding IFT43 is mutated in Sensenbrenner syndrome. *J Med Genet*. 2011; 48(6): 390-5

Aubusson-Fleury A, Lemullois M, de Loubresse NG, et al. The conserved centrosomal protein FOR20 is required for assembly of the transition zone and basal body docking at the cell surface. *J Cell Sci*. 2012; 125:4395-404.

Aury JM, Jaillon O, Duret L, et al. Global trends of whole-genome duplications revealed by the ciliate Paramecium tetraurelia. *Nature*. 2006; 444(7116): 171-8

Avasthi P, Marshall W. Ciliary secretion: switching the cellular antenna to 'transmit'. *Curr Biol*. 2013;23(11):R471-3.

Avidor-Reiss T, Gopalakrishnan J. Building a centriole. *Curr Opin Cell Biol*. 2013;25(1):72-7

Azimzadeh J, Marshall WF. Building the centriole. *Curr Biol*. 2010;20(18):R816-25

Baker SA, Freeman K, Luby-Phelps K, et al. IFT20 links kinesin II with a mammalian intraflagellar transport complex that is conserved in motile flagella and sensory cilia. *J Biol Chem*. 2003; 278(36): 34211-8

Banerjee M, Datta M, Majumder P, et al. Transcription regulation of caspase-1 by R393 of HIPPI and its molecular partner HIP-1. *Nucleic Acids Res*. 2010; 38(3): 878-92

Baudry C, Malinsky S, Restituito M, et al. PiggyMac, a domesticated piggyBac transposase involved in programmed genome rearrangements in the ciliate Paramecium tetraurelia. *Genes Dev*. 2009; 23(21): 2478-83

Beales PL, Bland E, Tobin JL, et al. IFT80, which encodes a conserved intraflagellar transport protein, is mutated in Jeune asphyxiating thoracic dystrophy. *Nat Genet*. 2007; 39(6): 727-9

Behal RH, Miller MS, Qin H, et al. Subunit interactions and organization of the Chlamydomonas reinhardtii intraflagellar transport complex A proteins. J *Biol Chem*. 2012; 287(15): 11689-703

Bell LR, Stone S, Yochem J, et al. The molecular identities of the *Caenorhabditis elegans* intraflagellar transport genes dyf-6, daf-10 and osm-1. *Genetics*. 2006; 173(3): 1275-86

Benmerah A. The ciliary pocket. *Curr Opin Cell Biol*. 2013; 25(1): 78-84

Bhattacharyya NP, Banerjee M, Majumder P. Huntington's disease: roles of huntingtin-interacting protein 1 (HIP-1) and its molecular partner HIPPI in the regulation of apoptosis and transcription. *FEBS J*. 2008;275(17):4271-9

Bisgrove BW, Yost HJ. The roles of cilia in developmental disorders and disease. *Development*. 2006;133(21):4131-43

Blacque OE, Perens EA, Boroevich KA, et al. Functional genomics of the cilium, a sensory organelle. *Curr Biol*. 2005; 15(10):935-41

Blacque OE, Li C, Inglis PN, et al. The WD repeat-containing protein IFTA-1 is required for retrograde intraflagellar transport. *Mol Biol Cell*. 2006; 17(12): 5053-62

Blacque OE, Reardon MJ, Li C, et al. Loss of C. elegans BBS-7 and BBS-8 protein function results in cilia defects and compromised intraflagellar transport. *Genes Dev.* 2004; 18(13): 1630-42

Bloodgood RA. Directed movements of ciliary and flagellar membrane components: a review. *Biol Cell*. 1992; 76(3): 291-301

Boldt K, Mans DA, Won J, et al. Disruption of intraflagellar protein transport in photoreceptor cilia causes Leber congenital amaurosis in humans and mice. *J Clin Invest*. 2011; 121(6): 2169-80

Borg CL, Wolski KM, Gibbs GM, et al. Phenotyping male infertility in the mouse: how to get the most out of a 'non-performer'. *Hum Reprod Update*. 2010;16(2):205-24

Bouhouche K, Gout JF, Kapusta A, et al. Functional specialization of Piwi proteins in Paramecium tetraurelia from post-transcriptional gene silencing to genome remodelling. *Nucleic Acids Res*. 2011; 39(10): 4249-64

Brand M, Heisenberg CP, Warga RM, et al. Mutations affecting development of the midline and general body shape during zebrafish embryogenesis. *Development*. 1996;123:129-42

Brazelton WJ, Amundsen CD, Silflow CD, et al. The bld1 mutation identifies the Chlamydomonas osm-6 homolog as a gene required for flagellar assembly. *Curr Biol*. 2001; 11(20): 1591-4

Bredrup C, Saunier S, Oud MM, et al. Ciliopathies with skeletal anomalies and renal insufficiency due to mutations in the IFT-A gene WDR19. *Am J Hum Genet.* 2011; 89(5): 634-43

Brent W. Bisgrove and H. Joseph Yost The roles of cilia in developmental disorders and disease. *Development*. 2006; 133, 4131-4143

Brust-Mascher I, Ou G, Scholey JM. Measuring Rates of Intraflagellar Transport Along Caenorhabditis elegans Sensory Cilia Using Fluorescence Microscopy. *Methods Enzymol*. 2013; 524:285-304

Buisson J, Chenouard N, Lagache T, et al. Intraflagellar transport proteins cycle between the flagellum and its base. *J Cell Sci*. 2013;126:327-38

Callen AM, Adoutte A, Andrew JM, et al. Isolation and characterization of libraries of monoclonal antibodies directed against various forms of tubulin in Paramecium. *Biol Cell*. 1994;81(2):95-119

Chang P, Giddings TH Jr, Winey M, et al. Epsilon-tubulin is required for centriole duplication and microtubule organization. *Nat Cell Biol*. 2003; 5(1): 71–76

Chang P, Stearns T. Delta-tubulin and epsilon-tubulin: two new human centrosomal tubulins reveal new aspects of centrosome structure and function. *Nat Cell Biol.* 2000; 2(1): 30–35

Cohen J, Adoutte A., Grandchamp S, et al. Immunocytochemical study of microtubular structures throughout the cell cycle of Paramecium. *Biol. Cell*. 1982; 44: 35-44

Cole DG, Diener DR, Himelblau AL, et al. Chlamydomonas kinesin-II-dependent intraflagellar transport (IFT): IFT particles contain proteins required for ciliary assembly in Caenorhabditis elegans sensory neurons. *J Cell Biol*. 1998; 141(4): 993-1008

Collet J, Spike CA, Lundquist EA, et al. Analysis of osm-6, a gene that affects sensory cilium structure and sensory neuron function in *Caenorhabditis elegans*. *Genetics*. 1998; 148(1): 187-200

Corbit KC, Shyer AE, Dowdle WE, et al. Kif3a constrains beta-catenin-dependent Wnt signalling through dual ciliary and non-ciliary mechanisms. *Nat Cell Biol*. 2008; 10(1): 70-6

Craige B, Tsao CC, Diener DR, et al. CEP290 tethers flagellar transition zone microtubules to the membrane and regulates flagellar protein content. *J Cell Biol*. 2010; 190(5): 927-40
Datta M, Choudhury A, Lahiri A, et al. Genome wide gene expression regulation by HIP1 Protein Interactor, HIPPI: prediction and validation *BMC Genomics*. 2011a; 12:463

Datta M, Bhattacharyya NP. Regulation of RE1 protein silencing transcription factor (REST) expression by HIP1 protein interactor (HIPPI). *J Biol Chem*. 2011b; 286(39): 33759-69

Dave D, Wloga D, Sharma N, et al. DYF-1 is required for assembly of the axoneme in *Tetrahymena thermophila*. *Eukaryot Cell*. 2009; 8(9): 1397-406

Davey MG, James J, Paton IR, et al. Analysis of talpid3 and wild-type chicken embryos reveals roles for Hedgehog signalling in development of the limb bud vasculature. *Dev Biol*. 2007; 301(1): 155-65

Deane JA, Cole DG, Seeley ES, et al. Localization of intraflagellar transport protein IFT52 identifies basal body transitional fibers as the docking site for IFT particles. *Curr Biol.* 2001; 11(20): 1586-90

De Bono M, Tobin DM, Davis MW, et al. Social feeding in Caenorhabditis elegans is induced by neurons that detect aversive stimuli. *Nature*. 2002; 419(6910): 899-903

Delaval B, Bright A, Lawson ND, et al. The cilia protein IFT88 is required for spindle orientation in mitosis. *Nat Cell Biol*. 2011; 13(4): 461-8

Delmas P, Hao J, Rodat-Despoix L. Molecular mechanisms of mechanotransduction in mammalian sensory neurons. *Nat Rev Neurosci.* 2011; 12(3): 139-53

Dentler WL, Rosenbaum JL Flagellar elongation and shortening in Chlamydomonas. III. structures attached to the tips of flagellar microtubules and their relationship to the directionality of flagellar microtubule assembly. *J Cell Biol.* 1977;74(3):747-59

Dentler WL. Structures linking the tips of ciliary and flagellar microtubules to the membrane. *J Cell Sci*. 1980; 42:207-20

Dentler W. Intraflagellar transport (IFT) during assembly and disassembly of Chlamydomonas flagella. *J Cell Biol.* 2005;170(4):649-59

Detraves C, Mazarguil H, Lajoie-Mazenc I, et al. Protein complexes containing gamma-tubulin are present in mammalian brain microtubule protein preparations. *Cell Motil Cytoskeleton*. 1997; 36(2): 179-89

Diener D. Analysis of cargo transport by IFT and GFP imaging of IFT in Chlamydomonas. *Methods Cell Biol*. 2009;93:111-9

Dishinger JF, Kee HL, Jenkins PM, et al. Ciliary entry of the kinesin-2 motor KIF17 is regulated by importin-beta2 and RanGTP. *Nat Cell Biol.* 2010; 12(7): 703-10

Drummond IA, Majumdar A, Hentschel H, et al. Early development of the zebrafish pronephros and analysis of mutations affecting pronephric function. *Development*. 1998; 125(23): 4655-67

Dupuis-Williams P, Fleury-Aubusson A, de Loubresse NG, et al. Functional role of epsilon-tubulin in the assembly of the centriolar microtubule scaffold. *J Cell Biol*. 2002; 158(7): 1183–1193

Dutcher SK, Trabuco EC. The UNI3 gene is required for assembly of basal bodies of Chlamydomonas and encodes delta-tubulin, a new member of the tubulin superfamily. *Mol Biol Cell.* 1998; 9(6): 1293-308

Dutcher. Long-lost relatives reappear: identification of new members of the tubulin superfamily. *Curr Opin Microbiol*. 2003; 6(6):634-40

Dutcher SK, Morrissette NS, Preble AM, et al. Epsilon-tubulin is an essential component of the centriole. *Mol Biol Cell*. 2002; 13(11): 3859–3869

Eddé B, Rossier J, Le Caer JP, et al. Posttranslational glutamylation of alpha-tubulin. *Science*. 1990; 247(4938): 83-5

Engel BD, Ludington WB, Marshall WF. Intraflagellar transport particle size scales inversely with flagellar length: revisiting the balance-point length control model. *J Cell Biol*. 2009;187(1):81-9

Fan ZC, Behal RH, Geimer S, et al. Chlamydomonas IFT70/CrDYF-1 is a core component of IFT particle complex B and is required for flagellar assembly. *Mol Biol Cell.* 2010; 21(15): 2696-706

Field MC, Carrington M. The trypanosome flagellar pocket. *Nat Rev Microbiol*. 2009 Nov;7(11):775-86.

Finetti F, Paccani SR, Riparbelli MG, et al. Intraflagellar transport is required for polarized recycling of the TCR/CD3 complex to the immune synapse. *Nat Cell Biol*. 2009; 11(11): 1332-9

Fisch C, Dupuis-Williams P. Ultrastructure of cilia and flagella - back to the future! *Biol Cell*. 2011;103(6):249-70

Follit JA, Tuft RA, Fogarty KE, et al. The intraflagellar transport protein IFT20 is associated with the Golgi complex and is required for cilia assembly. *Mol Biol Cell.* 2006; 17(9): 3781-92

Follit JA, San Agustin JT, Xu F, et al. The Golgin GMAP210/TRIP11 anchors IFT20 to the Golgi complex. *PLoS Genet*. 2008; 4(12): e1000315

Follit JA, Xu F, Keady BT, et al. Characterization of mouse IFT complex B. *Cell Motil Cytoskeleton*. 2009; 66(8): 457-68

Franklin JB, Ullu E. Biochemical analysis of PIFTC3, the Trypanosoma brucei orthologue of nematode DYF-13, reveals interactions with established and putative intraflagellar transport components. *Mol Microbiol*. 2010; 78(1):173-86

Fujiwara M, Ishihara T, Katsura I. A novel WD40 protein, CHE-2, acts cell-autonomously in the formation of C. elegans sensory cilia. *Development*. 1999; 126(21):4839-48

Gadelha C, Wickstead B, Gull K. Flagellar and ciliary beating in trypanosome motility. *Cell Motil Cytoskeleton*. 2007;64(8):629-43

Gaertig J, Wloga D. Ciliary tubulin and its post-translational modifications. *Curr Top Dev Biol*. 2008; 85:83-113

Galvani A, Sperling L. RNA interference by feeding in Paramecium. *Trends Genet*. 2002; 18(1):11-2

Garnier O, Serrano V, Duharcourt S, et al. RNA-mediated programming of developmental genome rearrangements in Paramecium tetraurelia. *Mol Cell Biol.* 2004; 24(17): 7370-9

Garreau de Loubresse N, Ruiz F, Beisson J, et al. Role of delta-tubulin and the C-tubule in assembly of Paramecium basal bodies. *BMC Cell Biol*. 2001; 2:4.

Gascue C, Tan PL, Cardenas-Rodriguez M, et al. Direct role of Bardet-Biedl syndrome proteins in transcriptional regulation. *J Cell Sci*. 2012 Jan 15;125(Pt 2):362-75

Gerdes JM, Davis EE, Katsanis N. The vertebrate primary cilium in development, homeostasis, and disease. *Cell*. 2009;137(1):32-45

Gervais FG, Singaraja R, Xanthoudakis S, et al. Recruitment and activation of caspase-8 by the Huntingtin-interacting protein Hip-1 and a novel partner Hippi. *Nat Cell Biol*. 2002; 4(2): 95-105

Gibbons BH, Asai DJ, Tang WJ, et al. Phylogeny and expression of axonemal and cytoplasmic dynein genes in sea urchins. *Mol Biol Cell*. 1994; 5(1):57-70

Gilissen C, Arts HH, Hoischen A, et al. Exome sequencing identifies WDR35 variants involved in Sensenbrenner syndrome. *Am J Hum Genet*. 2010; 87(3): 418-23

Gilley D, Preer JR Jr, Aufderheide KJ, et al. Autonomous replication and addition of telomerelike sequences to DNA microinjected into Paramecium tetraurelia macronuclei. *Mol Cell Biol*. 1988;8(11):4765-72

Giorgio G, Alfieri M, Prattichizzo C, et al. Functional characterization of the OFD1 protein reveals a nuclear localization and physical interaction with subunits of a chromatin remodeling complex. *Mol Biol Cell*. 2007;18(11):4397-404

Gogendeau D, Hurbain I, Raposo G, et al. Sas-4 proteins are required during basal body duplication in Paramecium. *Mol Biol Cell*. 2011; 22(7): 1035-44

Grandchamp S, Beisson J. Positional control of nuclear differentiation in Paramecium. *Dev Biol.* 1981;81(2):336-41.

Guichard P, Chrétien D, Marco S, Tassin AM. Procentriole assembly revealed by cryo-electron tomography. *EMBO J*. 2010;29(9):1565-72

Harris PC, Torres VE. Polycystic kidney disease. *Annu Rev Med*. 2009; 60:321-37

Hatch EM, Kulukian A, Holland AJ, et al. Cep152 interacts with Plk4 and is required for centriole duplication. *J Cell Biol.* 2010;191(4):721-9.

Hauser K, Haynes WJ, Kung C, et al. Expression of the green fluorescent protein in Paramecium tetraurelia. *Eur J Cell Biol.* 2000;79(2):144-9

Haycraft CJ, Schafer JC, Zhang Q, et al. dentification of CHE-13, a novel intraflagellar transport protein required for cilia formation. *Exp Cell Res*. 2003; 284(2): 251-63

Howard-Till RA, Yao MC. Induction of gene silencing by hairpin RNA expression in Tetrahymena thermophila reveals a second small RNA pathway. *Mol Cell Biol.* 2006;26(23):8731-42

Houde C, Dickinson RJ, Houtzager VM, et al. Hippi is essential for node cilia assembly and Sonic hedgehog signaling. *Dev Biol*. 2006; 300(2): 523-33

Hou Y, Pazour GJ, Witman GB. A dynein light intermediate chain, D1bLIC, is required for retrograde intraflagellar transport. *Mol Biol Cell*. 2004; 15(10):4382-94

Hou Y, Qin H, Follit JA, et al. Functional analysis of an individual IFT protein: IFT46 is required for transport of outer dynein arms into flagella. *J Cell Biol*. 2007; 176(5): 653-65

Hu Q, Milenkovic L, Jin H, et al. A septin diffusion barrier at the base of the primary cilium maintains ciliary membrane protein distribution. *Science*. 2010; 329(5990): 436-9

Huangfu D, Liu A, Rakeman AS, et al. Hedgehog signalling in the mouse requires intraflagellar transport proteins. *Nature*. 2003; 426(6962):83-7

Huitorel P. From cilia and flagella to intracellular motility and back again: a review of a few aspects of microtubule-based motility. *Biol Cell*. 1988; 63(2): 249-58

Hurd TW, Hildebrandt F. Mechanisms of nephronophthisis and related ciliopathies. *Nephron Exp Nephrol*. 2011; 118(1): e9-14

Iftode F, Cohen J, Ruiz F, et al. Development of surface pattern during division in Paramecium. I. Mapping of duplication and reorganization of cortical cytoskeletal structures in the wild type. *Development. 1989; 105, 191-211*

Iftode F, Clérot JC, Levilliers N, Bré MH. Tubulin polyglycylation: a morphogenetic marker in ciliates. *Biol Cell*. 2000;92(8-9):615-28

Iftode F, Fleury-Aubusson A. Structural inheritance in Paramecium: ultrastructural evidence for basal body and associated rootlets polarity transmission through binary fission. *Biol Cell*. 2003; 95(1):39-51

Inglis PN, Blacque OE, Leroux MR. Functional genomics of intraflagellar transport-associated proteins in C. elegans. *Methods Cell Biol*. 2009;93:267-304

Insinna C, Besharse JC. Intraflagellar transport and the sensory outer segment of vertebrate photoreceptors. *Dev Dyn*. 2008; 237(8): 1982-92

Iomini C, Li L, Esparza JM, et al. Retrograde intraflagellar transport mutants identify complex A proteins with multiple genetic interactions in Chlamydomonas reinhardtii. *Genetics*. 2009; 183(3): 885-96

Iomini C, Babaev-Khaimov V, Sassaroli M, et al. Protein particles in Chlamydomonas flagella undergo a transport cycle consisting of four phases. *J Cell Biol.* 2001; 153(1): 13-24

Ishikawa H, Marshall WF. Ciliogenesis: building the cell's antenna. *Nat Rev Mol Cell Biol*. 2011; 12(4): 222-34

Ishikawa H, Thompson J, Yates JR 3rd, et al. Proteomic analysis of mammalian primary cilia. *Curr Biol.* 2012;22(5):414-9

Jarrett SG, Novak M, Dabernat S, et al. Metastasis suppressor NM23-H1 promotes repair of UV-induced DNA damage and suppresses UV-induced melanomagenesis. *Cancer Res*. 2012; 72(1): 133-43

Jekely Arendt. Evolution of intraflagellar transport from coated vesicles and autogenous origin of the eukaryotic cilium. *Bioessays*. 2006;28(2):191-8

Jerka-Dziadosz M, Gogendeau D, Klotz C, et al. Basal body duplication in Paramecium: the key role of Bld10 in assembly and stability of the cartwheel. *Cytoskeleton*. 2010;67(3):161-71

Jerka-Dziadosz M, Beisson J. Genetic approaches to ciliate pattern formation: from self-assembly to morphogenesis. *Trends Genet.* 1990;6(2):41-5

Jonassen JA, SanAgustin J, Baker SP, et al. Disruption of IFT complex A causes cystic kidneys without mitotic spindle misorientation. *J Am Soc Nephrol*. 2012 23(4): 641-51

Keady BT, Le YZ, Pazour GJ. IFT20 is required for opsin trafficking and photoreceptor outer segment development. *Mol Biol Cell*. 2011; 22(7): 921-30

Khan ML, Ali MY, Siddiqui ZK, *et* al. C. elegans KLP-11/OSM-3/KAP-1: orthologs of the sea urchin kinesin-II, and mouse KIF3A/KIFB/KAP3 kinesin complexes. *DNA Res*. 2000; 7(2): 121-5

Kim S, Dynlacht BD. Assembling a primary cilium. *Curr Opin Cell Biol*. 2013. doi:pii: S0955-0674(13)00074-4. 10.1016/j.ceb.2013.04.011

Kissmehl R, Froissard M, Plattner H, NSF regulates membrane traffic along multiple pathways in Paramecium. *J Cell Sci.* 2002;115:3935-46

Klink VP, Wolniak SM. Centrin is necessary for the formation of the motile apparatus in spermatids of Marsilea. *Mol Biol Cell*. 2001; 12(3): 761-76

Koblenz B, Schoppmeier J, Grunow A, et al. Centrin deficiency in Chlamydomonas causes defects in basal body replication, segregation and maturation. *J Cell Sci*. 2003; 116:2635-46

Kozminski KG, Johnson KA, Forscher P, et al. A motility in the eukaryotic flagellum unrelated to flagellar beating. *Proc Natl Acad Sci U S A*. 1993;90(12):5519-23

Kozminski KG, Beech PL, Rosenbaum JL. The Chlamydomonas kinesin-like protein FLA10 is involved in motility associated with the flagellar membrane. *J Cell Biol*. 1995; 131:1517-27

Krock BL, Perkins BD. The intraflagellar transport protein IFT57 is required for cilia maintenance and regulates IFT-particle-kinesin-II dissociation in vertebrate photoreceptors. *J Cell Sci*. 2008; 121:1907-15

Kulaga HM, Leitch CC, Eichers ER, et al. Loss of BBS proteins causes anosmia in humans and defects in olfactory cilia structure and function in the mouse. *Nat Genet.* 2004; 36(9): 994-8

Kunitomo H, Iino Y. Caenorhabditis elegans DYF-11, an orthologue of mammalian Traf3ip1/MIP-T3, is required for sensory cilia formation. *Genes Cells*. 2008; 13(1): 13-25

Lechtreck KF, Luro S, Awata J, et al. HA-tagging of putative flagellar proteins in Chlamydomonas reinhardtii identifies a novel protein of intraflagellar transport complex B. *Cell Motil Cytoskeleton*. 2009; 66(8): 469-82

Lepère G, Bétermier M, Meyer E, et al. Maternal noncoding transcripts antagonize the targeting of DNA elimination by scanRNAs in Paramecium tetraurelia. *Genes Dev.* 2008; 22(11): 1501-12

Lin J, Heuser T, Song K, Fu X, Nicastro D. One of the nine doublet microtubules of eukaryotic flagella exhibits unique and partially conserved structures. *PLoS One*. 2012;7(10):e46494

Liu A, Wang B, Niswander LA. Mouse intraflagellar transport proteins regulate both the activator and repressor functions of Gli transcription factors. *Development*. 2005; 132(13): 3103-11

Loktev AV, Zhang Q, Beck JS, et al. A BBSome subunit links ciliogenesis, microtubule stability, and acetylation. *Dev Cell*. 2008;15(6):854-65

Lucker BF, Behal RH, Qin H, et al. Characterization of the intraflagellar transport complex B core: direct interaction of the IFT81 and IFT74/72 subunits. *J Biol Chem*. 2005; 280(30): 27688-96

Lucker BF, Miller MS, Dziedzic SA, et al. Direct interactions of intraflagellar transport complex B proteins IFT88, IFT52, and IFT46. *J Biol Chem*. 2010; 285(28): 21508-18

Majumder P, Choudhury A, Banerjee M, et al. Interactions of HIPPI, a molecular partner of Huntingtin interacting protein HIP1, with the specific motif present at the putative promoter sequence of the caspase-1, caspase-8 and caspase-10 genes. *FEBS J*. 2007a; 274(15): 3886-99

Majumder P, Chattopadhyay B, Sukanya S, et al. Interaction of HIPPI with putative promoter sequence of caspase-1 in vitro and in vivo. *Biochem Biophys Res Commun*. 2007b; 353(1): 80-5

Majumder P, Chattopadhyay B, Mazumder A, et al. Induction of apoptosis in cells expressing exogenous Hippi, a molecular partner of huntingtin-interacting protein Hip1. *Neurobiol Dis*. 2006; 22(2): 242-56

Manisha Banerjee, Pritha Majumder, Nitai P. et al. Cloning, expression, purification, crystallization and preliminary crystallographic analysis of pseudo death-effector domain of HIPPI, a molecular partner of Huntingtin-interacting protein HIP-1. *Acta Crystallogr Sect F Struct Biol Cryst Commun*. 2006; 62:1247-50

Manning DK, Sergeev M, van Heesbeen RG, et al. Loss of the ciliary kinase Nek8 causes left-right asymmetry defects. *J Am Soc Nephrol*. 2013; 24(1): 100-12

Mans DA, Voest EE, Giles RH. All along the watchtower: is the cilium a tumor suppressor organelle? *Biochim Biophys Acta*. 2008; 1786(2): 114-25

Marcet B, Chevalier B, Luxardi G, et al. Control of vertebrate multiciliogenesis by miR-449 through direct repression of the Delta/Notch pathway. *Nat Cell Biol*. 2011;13(6):693-9

Marshall WF, Rosenbaum JL. Intraflagellar transport balances continuous turnover of outer doublet microtubules: implications for flagellar length control. *J Cell Biol*. 2001; 155(3): 405-14

Meyer E, Duharcourt S. Epigenetic programming of developmental genome rearrangements in ciliates. *Cell*. 1996; 87(1): 9-12

McEwen DP, Koenekoop RK, Khanna H, et al. Hypomorphic CEP290/NPHP6 mutations result in anosmia caused by the selective loss of G proteins in cilia of olfactory sensory neurons. *Proc Natl Acad Sci U S A*. 2007; 104(40): 15917-22

McGrath J, Somlo S, Makova S, et al. Two populations of node monocilia initiate left-right asymmetry in the mouse. *Cell*. 2003; 114(1): 61-73

Middendorp S, Küntziger T, Abraham Y, et al. A role for centrin 3 in centrosome reproduction. *J Cell Biol*. 2000; 148(3): 405-16

Mizuno N, Taschner M, Engel BD, et al. Structural studies of ciliary components. *J Mol Biol.* 2012;422(2):163-80

Molla-Herman A, Ghossoub R, Blisnick T, The ciliary pocket: an endocytic membrane domain at the base of primary and motile cilia. *J Cell Sci.* 2010;123:1785-95

Moritz M, Zheng Y, Alberts BM, et al. Recruitment of the gamma-tubulin ring complex to Drosophila salt-stripped centrosome scaffolds. *J Cell Biol*. 1998; 142(3): 775-86

Morris RL, Scholey JM. Heterotrimeric kinesin-II is required for the assembly of motile 9+2 ciliary axonemes on sea urchin embryos. *J Cell Biol*. 1997; 138(5): 1009-22

Morris RL, English CN, Lou JE, et al. Redistribution of the kinesin-II subunit KAP from cilia to nuclei during the mitotic and ciliogenic cycles in sea urchin embryos. *Dev Biol*. 2004; 274(1): 56-69

Mukhopadhyay A, Deplancke B, Walhout AJ, et al. C. elegans tubby regulates life span and fat storage by two independent mechanisms. *Cell Metab*. 2005; 2(1): 35-42

Murayama T, Toh Y, Ohshima Y, et al. The dyf-3 gene encodes a novel protein required for sensory cilium formation in Caenorhabditis elegans. *J Mol Biol*. 2005; 346(3):677-87

Nachury MV, Loktev AV, Zhang Q, et al. A core complex of BBS proteins cooperates with the GTPase Rab8 to promote ciliary membrane biogenesis. *Cell*. 2007;129(6):1201-13

Nachury MV, Seeley ES, Jin H. Trafficking to the ciliary membrane: how to get across the periciliary diffusion barrier? *Annu Rev Cell Dev Biol*. 2010; 26:59-87

Nagarkatti-Gude DR, Jaimez R, Henderson SC, et al. Spag16, an axonemal central apparatus gene, encodes a male germ cell nuclear speckle protein that regulates SPAG16 mRNA expression. *PLoS One.* 2011; 6(5): e20625.

Nakazawa Y, Hiraki M, Kamiya R, et al. SAS-6 is a cartwheel protein that establishes the 9-fold symmetry of the centriole. *Curr Biol*. 2007;17(24):2169-74

Nicastro D, Schwartz C, Pierson J, et al. The molecular architecture of axonemes revealed by cryoelectron tomography. *Science.* 2006;313(5789):944-8.

Nonaka S, Tanaka Y, Okada Y, et al. Randomization of left-right asymmetry due to loss of nodal cilia generating leftward flow of extraembryonic fluid in mice lacking KIF3B motor protein. *Cell*. 1998; 95(6): 829-37

Nowacki M, Shetty K, Landweber LF. RNA-Mediated Epigenetic Programming of Genome Rearrangements. *Annu Rev Genomics Hum Genet*. 2011;12:367-89

Nowacki M, Zagorski-Ostoja W, Meyer E. Nowa1p and Nowa2p: novel putative RNA binding proteins involved in trans-nuclear crosstalk in Paramecium tetraurelia. *Curr Biol*. 2005; 15(18): 1616-28

Nowak JK, Gromadka R, Juszczuk M, et al. Functional study of genes essential for autogamy and nuclear reorganization in Paramecium. *Eukaryot Cell.* 2011; 10(3): 363-72

Nozawa YI, Lin C, Chuang PT. Hedgehog signaling from the primary cilium to the nucleus: an emerging picture of ciliary localization, trafficking and transduction. *Curr Opin Genet Dev*. 2013. pii: S0959-437X(13)00062-2. doi: 10.1016/j.gde.2013.04.008

Oakley CE, Oakley BR. Identification of gamma-tubulin, a new member of the tubulin superfamily encoded by mipA gene of Aspergillus nidulans. *Nature*. 1989; 338(6217): 662–664

Obado SO, Rout MP. Ciliary and nuclear transport: different places, similar routes? *Dev Cell*. 2012;22(4):693-4

Oegema K, Wiese C, Martin OC, et al. Characterization of two related Drosophila gamma-tubulin complexes that differ in their ability to nucleate microtubules. *J Cell Biol.* 1999; 144(4): 721-33

Oishi I, Kawakami Y, Raya A, et al. Regulation of primary cilia formation and left-right patterning in zebrafish by a noncanonical Wnt signaling mediator, duboraya. *Nat Genet.* 2006; 38(11):1316-22

Omori Y, Zhao C, Saras A, et al. Elipsa is an early determinant of ciliogenesis that links the IFT particle to membrane-associated small GTPase Rab8. *Nat Cell Biol*. 2008; 10(4): 437-44

Ou G, Qin H, Rosenbaum JL, et al. The PKD protein qilin undergoes intraflagellar transport. *Curr Biol*. 2005; 15(11): R410-1

Ou G, Blacque OE, Snow JJ, et al. Functional coordination of intraflagellar transport motors. *Nature*. 2005; 436(7050): 583-7

Pan J, Snell WJ. Chlamydomonas shortens its flagella by activating axonemal disassembly, stimulating IFT particle trafficking, and blocking anterograde cargo loading. *Dev Cell.* 2005;9(3):431-8

Pan X, Ou G, Civelekoglu-Scholey G, et al. Mechanism of transport of IFT particles in C. elegans cilia by the concerted action of kinesin-II and OSM-3 motors. *J Cell Biol*. 2006;174(7):1035-45

Paprocka J, Jamroz E. Joubert syndrome and related disorders. *Neurol Neurochir Pol*. 2012; 46(4): 379-83

Pathak N, Obara T, Mangos S, et al. The zebrafish fleer gene encodes an essential regulator of cilia tubulin polyglutamylation. *Mol Biol Cell.* 2007;18(11):4353-64

Pazour GJ, Wilkerson CG, Witman GB. A dynein light chain is essential for the retrograde particle movement of intraflagellar transport (IFT). *J Cell Biol.* 1998; 141(4):979-92

Pazour GJ, Dickert BL, Vucica Y, et al. Chlamydomonas IFT88 and its mouse homologue, polycystic kidney disease gene tg737, are required for assembly of cilia and flagella. *J Cell Biol*. 2000; 151(3): 709-18

Pazour GJ, Baker SA, Deane JA, et al. The intraflagellar transport protein, IFT88, is essential for vertebrate photoreceptor assembly and maintenance. *J Cell Biol*. 2002; 157(1): 103-13

Pazour GJ, Dickert BL, Vucica Y, Seeley ES, Rosenbaum JL, Witman GB, Cole DG. Chlamydomonas IFT88 and its mouse homologue, polycystic kidney disease gene tg737, are required for assembly of cilia and flagella. *J Cell Biol*. 2000;151(3):709-18

Perrault I, Saunier S, Hanein S, et al. Mainzer-Saldino syndrome is a ciliopathy caused by IFT140 mutations. *Am J Hum Genet*. 2012; 90(5): 864-70

Pedersen LB, Geimer S, Sloboda RD, et al. The Microtubule plus end-tracking protein EB1 is localized to the flagellar tip and basal bodies in Chlamydomonas reinhardtii. *Curr Biol*. 2003;13(22):1969-74

Pedersen LB, Miller MS, Geimer S, et al. Chlamydomonas IFT172 is encoded by FLA11, interacts with CrEB1, and regulates IFT at the flagellar tip. *Curr Biol*. 2005; 15(3): 262-6

Pedersen LB, Rosenbaum JL. Intraflagellar transport (IFT) role in ciliary assembly, resorption and signalling. *Curr Top Dev Biol*. 2008;85:23-61

Perrone CA, Tritschler D, Taulman P, et al. A novel dynein light intermediate chain colocalizes with the retrograde motor for intraflagellar transport at sites of axoneme assembly in chlamydomonas and Mammalian cells. Mol Biol Cell. 2003 May;14(5):2041-56

Pigino G, Cantele F, Vannuccini E, et al. Electron tomography of IFT particles. *Methods Enzymol*. 2013;524:325-42

Piperno G, Mead K, Henderson S. Inner dynein arms but not outer dynein arms require the activity of kinesin homologue protein KHP1(FLA10) to reach the distal part of flagella in Chlamydomonas. *J Cell Biol*. 1996; 133(2): 371-9

Piperno G, Siuda E, Henderson S, et al. Distinct mutants of retrograde intraflagellar transport (IFT) share similar morphological and molecular defects. *J Cell Biol*. 1998; 143(6): 1591-601

Plotnikova OV, Golemis EA, Pugacheva EN. Cell cycle-dependent ciliogenesis and cancer. *Cancer Res.* 2008; 68(7): 2058-61

Poole CA, Flint MH, Beaumont BW. Analysis of the morphology and function of primary cilia in connective tissues: a cellular cybernetic probe? *Cell Motil*. 1985; 5(3): 175-93

Porter ME, Bower R, Knott JA, Cytoplasmic dynein heavy chain 1b is required for flagellar assembly in Chlamydomonas. *Mol Biol Cell*. 1999; 10(3):693-712

Qin H, Wang Z, Diener D, et al. Intraflagellar transport protein 27 is a small G protein involved in cell-cycle control. *Curr Biol*. 2007; 17(3): 193-202

Qin J, Lin Y, Norman RX, et al. Intraflagellar transport protein 122 antagonizes Sonic Hedgehog signaling and controls ciliary localization of pathway components. *Proc Natl Acad Sci U S A*. 2011; 108(4): 1456-61

Qin L, Smant G, Stokkermans J, et al. Cloning of a trans-spliced glyceraldehyde-3-phosphate-dehydrogenase gene from the potato cyst nematode Globodera rostochiensis and expression

of its putative promoter region in Caenorhabditis elegans. *Mol Biochem Parasitol*. 1998; 96(1-2): 59-67

Rajagopalan V, Corpuz EO, Hubenschmidt MJ, et al. Analysis of properties of cilia using Tetrahymena thermophila. *Methods Mol Biol*. 2009; 586:283-99

Reiter JF, Blacque OE, Leroux MR. The base of the cilium: roles for transition fibres and the transition zone in ciliary formation, maintenance and compartmentalization. *EMBO Rep.* 2012;13(7):608-18

Richey EA, Qin H. Dissecting the sequential assembly and localization of intraflagellar transport particle complex B in Chlamydomonas. *PLoS One*. 2012;7(8):e43118

Rompolas P, Pedersen LB, Patel-King RS, et al. Chlamydomonas FAP133 is a dynein intermediate chain associated with the retrograde intraflagellar transport motor. *J Cell Sci*. 2007; 120:3653-65

Robert A, Margall-Ducos G, Guidotti JE, et al. The intraflagellar transport component IFT88/polaris is a centrosomal protein regulating G1-S transition in non-ciliated cells. *J Cell Sci.* 2007; 120:628-37

Ruiz F, Beisson J, Rossier J, et al. Basal body duplication in Paramecium requires gamma-tubulin. *Curr Biol*. 1999; 9(1): 43-6

Ruiz F, Krzywicka A, Klotz C, et al. The SM19 gene, required for duplication of basal bodies in Paramecium, encodes a novel tubulin, eta-tubulin. *Curr Biol.* 2000; 10(22): 1451-4

Ruiz F, Dupuis-Williams P, Klotz C, et al. Genetic evidence for interaction between eta- and beta-tubulins. *Eukaryot Cell*. 2004; 3(1): 212-20

Ruiz F, Garreau de Loubresse N, Klotz C, et al. Centrin deficiency in Paramecium affects the geometry of basal-body duplication. *Curr Biol*. 2005; 15(23): 2097-106

Salisbury JL, Baron A, Surek B, et al. Striated flagellar roots: isolation and partial characterization of a calcium-modulated contractile organelle. *J Cell Biol*. 1984; 99(3): 962-70

Salisbury JL, Suino KM, Busby R, et al. Centrin-2 is required for centriole duplication in mammalian cells. *Curr Biol*. 2002; 12(15): 1287-92

Sarpal R, Todi SV, Sivan-Loukianova E, et al. Drosophila KAP interacts with the kinesin II motor subunit KLP64D to assemble chordotonal sensory cilia, but not sperm tails. *Curr Biol.* 2003;13(19):1687-96

Schafer JC, Winkelbauer ME, Williams CL et al. IFTA-2 is a conserved cilia protein involved in pathways regulating longevity and dauer formation in Caenorhabditis elegans. *J Cell Sci*. 2006; 119: 4088-100

Schmidt KN, Kuhns S, Neuner A, et al. Cep164 mediates vesicular docking to the mother centriole during early steps of ciliogenesis. *J Cell Biol*. 2012 24;199(7):1083-101

Schrick JJ, Onuchic LF, Reeders ST, et al. Characterization of the human homologue of the mouse Tg737 candidate polycystic kidney disease gene. *Hum Mol Genet*. 1995; 4(4): 559-67

Selvapandiyan A, Debrabant A, Duncan R, et al. Centrin gene disruption impairs stage-specific basal body duplication and cell cycle progression in Leishmania. *J Biol Chem*. 2004; 279(24): 25703-10

Shang Y, Tsao CC, Gorovsky MA. Mutational analyses reveal a novel function of the nucleotide-binding domain of gamma-tubulin in the regulation of basal body biogenesis. *J Cell Biol*. 2005; 171(6): 1035-44

Shiba D, Yokoyama T. The ciliary transitional zone and nephrocystins. *Differentiation*. 2012; 83(2): S91-6

Signor D, Wedaman KP, Orozco JT, et al. Role of a class DHC1b dynein in retrograde transport of IFT motors and IFT raft particles along cilia, but not dendrites, in chemosensory neurons of living Caenorhabditis elegans. *J Cell Sci*. 2007;120:3653-65

Silva DA, Huang X, Behal RH, et al. The RABL5 homolog IFT22 regulates the cellular pool size and the amount of IFT particles partitioned to the flagellar compartment in Chlamydomonas reinhardtii. *Cytoskeleton*. 2012; 69(1): 33-48

Sloboda RD. Posttranslational protein modifications in cilia and flagella. *Methods Cell Biol*. 2009; 94:347-63

Sloboda RD, Howard L. Localization of EB1, IFT polypeptides, and kinesin-2 in Chlamydomonas flagellar axonemes via immunogold scanning electron microscopy. *Cell Motil Cytoskeleton*. 2007;64(6):446-60

Snow JJ, Ou G, Gunnarson AL, et al. Two anterograde intraflagellar transport motors cooperate to build sensory cilia on C. elegans neurons. *Nat Cell Biol*. 2004; 6(11): 1109-13

Sonneborn TM. Gene action in development. *Proc R Soc Lond B Biol Sci*. 1970;176(44):347-66

Sperling L. Remembrance of things past retrieved from the Paramecium genome. *Res Microbiol*. 2011;162(6):587-97

Starich TA, Herman RK, Kari CK, et al. Mutations affecting the chemosensory neurons of *Caenorhabditis elegans*. *Genetics*. 1995; 139(1): 171-88

Stemm-Wolf AJ, Morgan G, Giddings TH Jr, et al. Basal body duplication and maintenance require one member of the Tetrahymena thermophila centrin gene family. *Mol Biol Cel*l. 2005; 16(8): 3606-19

Stephen LA, Davis GM, McTeir KE, James J, McTeir L, Kierans M, Bain A, Davey MG. Failure of centrosome migration causes a loss of motile cilia in talpid(3) mutants. *Dev Dyn*. 2013. doi: 10.1002/dvdy.23980

Stottmann RW, Tran PV, Turbe-Doan A, et al. Ttc21b is required to restrict sonic hedgehog activity in the developing mouse forebrain. *Dev Biol*. 2009; 335(1): 166-78

Sui H, Downing KH. Molecular architecture of axonemal microtubule doublets revealed by cryo-electron tomography. *Nature*. 2006;442(7101):475-8

Sukumaran S, Perkins BD. Early defects in photoreceptor outer segment morphogenesis in zebrafish ift57, ift88 and ift172 Intraflagellar Transport mutants. *Vision Res.* 2009; 49(4): 479-89

Sun Z, Amsterdam A, Pazour GJ, et al. A genetic screen in zebrafish identifies cilia genes as a principal cause of cystic kidney. *Development.* 2004; 131(16): 4085-93

Takahashi M, Lin YM, Nakamura Y, et al. Isolation and characterization of a novel gene CLUAP1 whose expression is frequently upregulated in colon cancer. *Oncogene*. 2004; 23(57): 9289-94

Tammachote R, Hommerding CJ, Sinders RM, et al. Ciliary and centrosomal defects associated with mutation and depletion of the Meckel syndrome genes MKS1 and MKS3. *Hum Mol Genet*. 2009; 18(17): 3311-23

Taschner M, Bhogaraju S, Vetter M, et al. Biochemical mapping of interactions within the intraflagellar transport (IFT) B core complex: IFT52 binds directly to four other IFT-B subunits. *J Biol Chem*. 2011; 286(30): 26344-52

Teglund S, Toftgård R. Hedgehog beyond medulloblastoma and basal cell carcinoma. *Biochim Biophys Acta*. 2010;1805(2):181-208

Thauvin-Robinet C, Thomas S, Sinico M, et al. OFD1 mutations in males: phenotypic spectrum and ciliary basal body docking impairment. *Clin Genet*. 2013;84(1):86-90

Thazhath R, Jerka-Dziadosz M, Duan J, et al. Cell context-specific effects of the beta-tubulin glycylation domain on assembly and size of microtubular organelles. *Mol Biol Cell*. 2004; 15(9): 4136-47

Tran PV, Haycraft CJ, Besschetnova TY, et al. THM1 negatively modulates mouse sonic hedgehog signal transduction and affects retrograde intraflagellar transport in cilia. *Nat Genet*. 2008; 40(4): 403-10

Tsao CC, Gorovsky MA. Tetrahymena IFT122A is not essential for cilia assembly but plays a role in returning IFT proteins from the ciliary tip to the cell body. *J Cell Sci*. 2008a; 121:428-36

Tsao CC, Gorovsky MA. Different effects of Tetrahymena IFT172 domains on anterograde and retrograde intraflagellar transport. *Mol Biol Cell*. 2008b; 19(4): 1450-61

Tsujikawa M, Malicki J. Intraflagellar transport genes are essential for differentiation and survival of vertebrate sensory neurons. *Neuron*. 2004; 42(5): 703-16

van Breugel M, Hirono M, Andreeva A, et al. Structures of SAS-6 suggest its organization in centrioles. *Science.* 2011;331(6021):1196-9

Valentine MS, Rajendran A, Yano J, et al. Paramecium BBS genes are key to presence of channels in Cilia. *Cilia*. 2012;1(1):16

Valente EM, Silhavy JL, Brancati F, et al. Mutations in CEP290, which encodes a centrosomal protein, cause pleiotropic forms of Joubert syndrome. *Nat Genet*. 2006; 38(6): 623-5

Vincensini L, Blisnick T, Bastin P. 1001 model organisms to study cilia and flagella. *Biol Cell*. 2011; 103(3): 109-30

Walther Z, Vashishtha M, Hall JL. The Chlamydomonas FLA10 gene encodes a novel kinesin-homologous protein. J Cell Biol. 1994; 126(1): 175-88

Wang Z, Fan ZC, Williamson SM, et al. Intraflagellar transport (IFT) protein IFT25 is a phosphoprotein component of IFT complex B and physically interacts with IFT27 in Chlamydomonas. *PLoS One*. 2009; 4(5): e5384

Weatherbee SD, Niswander LA, Anderson KV. A mouse model for Meckel syndrome reveals Mks1 is required for ciliogenesis and Hedgehog signaling. *Hum Mol Genet*. 2009; 18(23): 4565-75

Whitfield TT, Granato M, van Eeden FJ, et al. Mutations affecting development of the zebrafish inner ear and lateral line. *Development*. 1996; 123:241-54

Wicks SR, de Vries CJ, van Luenen HG, et al. CHE-3, a cytosolic dynein heavy chain, is required for sensory cilia structure and function in Caenorhabditis elegans. *Dev Biol*. 2000; 221(2):295-307

Wick MJ, Ann DK, Loh HH. Molecular cloning of a novel protein regulated by opioid treatment of NG108-15 cells. *Brain Res Mol Brain Res.* 1995; 32(1): 171-5

Williams CL, Li C, Kida K, et al. MKS and NPHP modules cooperate to establish basal body/transition zone membrane associations and ciliary gate function during ciliogenesis. *J Cell Biol.* 2011;192(6):1023-41

Williamson SM, Silva DA, Richey E, et al. Probing the role of IFT particle complex A and B in flagellar entry and exit of IFT-dynein in Chlamydomonas. *Protoplasma.* 2012; 249(3): 851-6

Wilson NF, Iyer JK, Buchheim JA, et al. Regulation of flagellar length in Chlamydomonas. *Semin Cell Dev Biol*. 2008;19(6):494-501

Wood CR, Wang Z, Diener D, et al. IFT proteins accumulate during cell division and localize to the cleavage furrow in Chlamydomonas. *PLoS One*. 2012;7(2):e30729

Wood CR, Huang K, Diener DR, et al.. The cilium secretes bioactive ectosomes. *Curr Biol*. 2013;23(10):906-11

Xia L, Hai B, Gao Y, et al. Polyglycylation of tubulin is essential and affects cell motility and division in Tetrahymena thermophila. *J Cell Biol*. 2000; 149(5):1097-106

Yang Z, Roberts EA, Goldstein LS. Functional analysis of mouse kinesin motor Kif3C. *Mol Cell Biol*. 2001a; 21(16): 5306-11

Yang Z, Roberts EA, Goldstein LS. Functional analysis of mouseC-terminal kinesin motor KifC2. *Mol Cell Biol*. 2001b; 21(7): 2463-6

Yang P, Yang C, Wirschell, et al. Novel LC8 mutations have disparate affects on the assembly and stability of flagellar complexes. *J Bio Chem*. 2009; 284(45): 31412-21

Zhang Q, Nishimura D, Vogel T, et al. BBS7 is required for BBSome formation and its absence in mice results in Bardet-Biedl syndrome phenotypes and selective abnormalities in membrane protein trafficking. *J Cell Sci*. 2013;126:2372-80

Zhao C, Malicki J. Genetic defects of pronephric cilia in zebrafish. *Mech Dev*. 2007; 124(7-8): 605-16

Mon travail de thèse a porté sur l'étude chez la paramécie d'une protéine à localisation à la fois ciliaire et nucléaire. Les cils sont des organites conservés chez la plupart des eucaryotes qui pointent à la surface cellulaire vers le milieu extérieur. Leur squelette microtubulaire est nucléé par la structure centriolaire sous jacente, le corps basal, qui transmet sa structure à symétrie 9. Une parenté évolutive lointaine existe entre le compartiment cil, isolé du cytoplasme par un filtre moléculaire appelé zone de transition, et les noyaux dont les contacts avec le cytoplasme sont réduits aux pores nucléaires. Cette homologie fonctionnelle est soutenue par l'existence de mécanismes et de partenaires apparentés dans la communication avec le cytoplasme. Les dysfonctionnements des cils conduisent à des maladies graves appelées ciliopathies.

La croissance des cils est réalisée au moyen de complexes protéiques appelés IFT (intraflagellar transport) qui incluent au moins 17 protéines regroupés en deux sous complexes, IFTB, lié au moteur kinésine pour le mouvement antérograde vers la pointe du cil et IFTA lié au moteur dynéine pour le mouvement rétrograde vers la base du cil.

L'objet principal de ma thèse, dans le cadre de l'étude de l'IFT chez la paramécie, a porté sur la protéine IFT57, aussi connue sous le nom de HIPPI chez l'homme, où elle assure, en plus de sa fonction ciliaire, une fonction d'activateur transcriptionnel associé à l'apoptose dans la maladie de Huntington. Chez la paramécie, il y a quatre gènes codant IFT57 provenant de duplications globales de génome, IFT57A et B d'une part et IFT57C et D d'autre part, suffisamment proches deux à deux pour que l'inactivation d'un gène puis éteindre également l'autre.

Dans un premier temps, j'ai étudié la fonction ciliaire d'IFT57 et j'ai montré qu'il était nécessaire à la croissance ciliaire, mais apparemment pas à sa maintenance, contrairement à d'autres protéines de l'IFT telles qu'IFT46. L'action croisée d'inactivation d'une IFT sur la localisation d'une autre IFT fusionnée à la GFP on permis de suggérer des interactions entre IFT 46 et IFT57 dans le cytoplasme, en amont de leur site habituel d'interaction que représente le corps basal.

Je me suis ensuite intéressé à la localisation nucléaire d'IFT57. La protéine IFT57A-GFP entre dans le macronoyau, en plus de sa localisation ciliaire, alors que IFT57C-GFP en est exclue. J'ai essayé de déterminer la différence de séquence qui permet de distinguer ces deux molécules proches pour en envoyer une dans le noyau et pas l'autre. L'aspect le plus marquant de la localisation nucléaire d'IFT57A est le changement de localisation au cours des événements sexuels, où le marquage quitte l'ancien macronoyau pour rejoindre les nouveaux macronoyaux en formation. Cette relocalisation évoque celle observée avec des protéines impliquées dans le métabolisme de petits ARN importants pendant les événements sexuels.

Une idée est que IFT57A, protéine associée au transport, puisse gouverner ces mouvements internucléaires et j'ai entrepris d'analyser l'effet de l'inactivation de cette protéine sur les événements sexuels. La difficulté qui est apparue est que l'extinction d'IFT57A est rapidement létale. J'ai réalisé plusieurs approches méthodologiques pour contourner ce problème, dont la mise au point d'une nouvelle méthode d'inactivation par ARN en épingle à cheveux, mais sans pouvoir répondre à la question.

En utilisant des constructions chimères entre les deux protéines, puis en comparant les séquences au sein du genre *Paramecium*, j'ai déterminé une région de 90 acides aminés, L129-N219, avec deux positions critiques pour distinguer fonctionnellement ces deux protéines.

Mots-clés: *Paramecium*, IFT, IFT57/hippi, cil, noyau